Microstructural considerations on the propagation of waves in layered structures

A Thesis

submitted in partial fulfillment of the requirements for the award of the degree of

Doctor of Philosophy

in

School of Mathematics

by

Vanita Sharma

Registration No.: 901811011

under the supervision of

Dr. Satish Kumar

Associate Professor

School of Mathematics

THAPAR INSTITUTE
OF ENGINEERING & TECHNOLOGY
(Deemed to be University)

THAPAR INSTITUTE OF ENGINEERING AND TECHNOLOGY

PATIALA-147004, Punjab, India

January, 2022

Certificate

I hereby certify that the work, which is being presented in the thesis entitled **Microstructural considerations on the propagation of waves in layered structures**, in partial fulfillment of the requirements for the award of the degree of **Doctor of Philosophy** and submitted to the institution is an authentic record of my own work carried out during the period **July 24, 2018** to **January, 2022** under the supervision of **Dr. Satish Kumar**, Associate Professor, School of Mathematics, Thapar Institute of Engineering and Technology, Patiala. It is certified that the matter presented in this thesis has not been submitted elsewhere for the award of any other degree or diploma from any institution.

Date: 03-02-2022

Vanita Sharma

(**Vanita Sharma**)
Candidate

It is certified that the above statement made by the candidate is correct to the best of my knowledge.

Date: 03-02-2022

Satish

(**Dr. Satish Kumar**)
Supervisor
Associate Professor
School of Mathematics
TIET, Patiala-147004, India

Dedicated to the love of

My husband

and

My son

Acknowledgements

I owe to the grace almighty, whose divine light provided me the perseverance, guidance, enormous patience, inspiration, faith, and strength to carry out this work.

Firstly, I wish to express my sincere and genuine thanks to my research supervisor **Dr. Satish Kumar** (Associate Professor, School of Mathematics, Thapar Institute of Engineering and Technology, Patiala) for his cooperation, inspiration, suggestions, understanding, and patience which added considerably to my research experience. He put a tremendous amount of effort into every aspect of my thesis.

I would like to thank the authorities of the Thapar Institute of Engineering and Technology, Patiala for giving prominent research facilities. I also express my sincere thanks to Prof. Mahesh Kumar Sharma (Head, School of Mathematics), Doctoral committee members, and Prof. Rafat Siddique (Dean of Research and Sponsored Project) for encouraging me to carry out the research work.

I would like to thank the Council of Scientific and Industrial Research (CSIR), New Delhi, for providing me the opportunity to work on the research project under grant no. (CSIR/25(0289)/18/EMR-II) and helping me with financial assistance.

I express my most profound appreciation and thanks to my husband Dr. Munish Kansal for his unconditional love, support, and encouragement. I will forever be grateful for everything he has done for me. Thanks to my son 'Armaan' for being my driving force and helping me emerging as a strong person. My sincere thanks extend to my parents and brothers for their blessings and encouragement to endure the research work.

Finally and most importantly, I would like to thank Almighty, whose blessing gave me the motivation, patience, confidence, and power to complete this work.

Vanita Sharma

Vanita Sharma

Abstract

Classical continuum mechanics has widespread applications in solving problems encountered in many aspects of physics and numerous fields of engineering. Despite being a successful theory its anticipation is not always correct for experimental phenomena observed in both natural and man-made materials as it cannot predict accurately the physical phenomena that is exhibited by the long-range interactions in the material medium. Mechanical modeling of matter under the impression of classical continuum mechanics ignores the fact that the material is made up of atoms and hence, it cannot be applied to analyze the discrete nature of matter. Furthermore, due to the absence of any length scale parameter, the theory of classical elasticity is invariant w.r.t the length scale and thus, unable to predict the size-dependency effect exhibited by mechanical properties of nanostructures and microstructures. These constraints led to the motivation to evolute various continuum mechanics approaches accounting for size dependency that includes couple stress, micropolar, micromorphic, nonlocal, and high order strain gradient theories. The motivation behind these approaches was to develop such continuum-based theories that can accurately predict the physical phenomena on the micro/nano-scales. It was Cosserat brothers in 1909 who first developed the size-dependent continuum approach. For almost half a century their work was not considered significant and hence, didn't get recognition. Later in 1955, the Cosserat theory was invoked and protracted by many research groups. In the recent years, these size-dependent theories are appeared to be practical for much explained mathematical representations of the physical world. Several modifications and recommendations for improving the size-dependent continuum theories are formulated. These size-dependent theories are the modifications of classical continuum theories that can predict the material size effect exhibited at an atomic scale accurately. Couple stress, micropolar, strain gradient, and nonlocal theory of elasticity are some of the widely known size-dependent continuum theories which have been successfully applied to many physical problems of engineering.

The prime objective and motivation in carrying out the proposed study are to highlight the microstructural size dependency which significantly effects the behavior of surface wave propagation phenomenon through various layered structured models comprising of material layers viz. elastic, piezoelectric, piezomagnetic, functionally graded piezo material. To capture the microstructural effects the microcontinuum theories such as couple stress theory, micropolar theory, and nonlocal theory of elasticity have been utilized. The whole work has been divided into six chapters.

Chapter 1 comprises of historical overview and evolution of the theory of continuum elasticity. The impact and applications of microcontinuum theories are discussed. The basic governing equations and constitutive relations of microcontinuum theories such as couple stress theory, micropolar theory, and nonlocal theory of elasticity (in piezoelectric material) are provided in this chapter. The characteristics of smart materials viz. piezoelectric, piezomagnetic, and functionally graded piezo materials along with their basic governing equations and constitutive relations are discussed in this chapter. Recent investigations of wave propagation phenomena through these said materials are also presented.

Chapter 2 deals with the propagation of Love-type waves in an elastic layer sandwiched between viscous liquid half-space and size-dependent couple stress substrate. To grab the size dependency effect couple stress theory is used. The viscous liquid loading effect on the wave propagation is also analyzed. Dispersion curve is obtained for the considered structure which is further scrutinized in the absence of viscous liquid layer and then further deduced for the isotropic elastic case to validate the obtained result with the well-known dispersion relation for Love waves in the classical structure. The graphical illustrations showing dimensionless phase velocity against dimensionless wave number for characteristic length parameter, the thickness of the elastic layer, and the density and coefficient of viscosity parameter associated with viscous liquid layer are presented. The microstructural size dependency effect is found to be significant and it enhances the phase velocity of the wave. It has been observed that viscous liquid loading has a suppressing effect on the phase velocity of the propagating wave. This study may be used significantly for designing Love-type wave based devices in liquid-phase environments-a situation typical of biosensors.

Chapter 3 is devoted to the study of microstructural and viscous liquid loading effects on the propagation of Love waves in smart materials. For this purpose piezomagnetic smart material layer is considered. Couple stress theory is used to grab the microstructural size dependency effect. Dispersion equations for magnetically open and short conditions are derived. Possible particular cases such as dispersion equations in the absence of viscous liquid layer, or in the absence of piezomagneticity and then in the absence of couple stress effect, are deduced. The obtained dispersion relation is reduced to match with the classical Love wave equation for the sake of validation of results. To exhibit the analytical outcomes graphically Cobalt ferrite material as piezomagnetic material and Dionysos marble as a couple stress substrate are considered. The influence of various affecting parameters viz. coefficient of viscosity, liquid mass density, length scale parameter, the thickness of the viscous liquid layer, and piezomagnetic parameters, viz. piezomagnetic constant, magnetic permeability, elastic constant, and thickness on the phase velocity of Love-type waves are

analyzed. The magnetic permeability and the elastic constant have an increasing effect while the piezomagnetic constant has a decreasing effect on the phase velocity of the wave. It has been observed that the phase velocity of the Love-type wave in the considered structure for the magnetically open condition is greater than the magnetically short condition. As it is a well-established fact that perception of surface acoustic wave (SAW) devices confides on phase delay, the piezomagnetic properties related to the piezomagnetic material confine the wave for a longer duration, which reduces the phase velocity of the propagating wave and thus enhancing the sensitivity of Love-type wave sensors. The salient feature of the study in this chapter is to optimize the efficiency of Love-type wave sensors working in liquid media.

Chapter 4 is concerned with the study of the effect of the material gradient parameter which is responsible for functional gradedness in the material on the propagation of Love-type surface waves in functionally graded piezoelectric smart material. PZT-5H ceramic material layer as functionally graded piezoelectric material with exponential variation, when the electrical and mechanical constants vary distinctively, is considered. The effect of microstructural size dependency is captured by taking a couple stress substrate, where the length scale parameter is explicitly present in the formulation. The effect of material gradient factor on electromechanical coupling factor, which is an essential parameter in the design of acoustic sensors and is related to sensor efficiency, is also explored in this chapter. Dispersion equations for electrically open and short conditions are obtained. Possible particular cases are discussed. The dispersion relation is reduced to the classical Love wave equation to validate the results. The emphatic influence of microstructural parameter, electromechanical coupling factor, thickness, functional gradedness, and material parameters of functionally graded piezoelectric material stratum on the phase velocity of the Love-type wave has been scrutinized and illustrated through graphical representations for both the cases of electrically open and short conditions. The material gradient parameter has a substantial effect on the phase velocity of the wave. It favors the phase velocity of the wave for both electrically open and short conditions. The elastic constant and piezoelectric constant associated with the FGPEM stratum disfavors the phase velocity of the wave while dielectric constant favors the phase velocity of the wave for both electrically open and short conditions. The relation of the electromechanical coupling factor with the material gradient factor is graphically shown and it is concluded that the value of the electromechanical coupling factor increases moderately as the material gradient factor increases. As phase velocity is always greater than the group velocity in the considered structure so the dispersion relation appears 'normal'. The obtained results may be useful for attaining better performance in Love-type wave based surface acoustic devices.

In **Chapter 5** the theory of micropolar continua has been employed to study the microscale size effects on the propagation of SH-waves (horizontally polarized shear waves) in two distinct models i.e. functionally graded piezomagnetic material (FGPMM) layer overlying the micropolar substrate (Model I) and functionally graded piezoelectric material (FGPEM) layer overlying the micropolar substrate (Model II). The focus of the present work is to reveal how the inhomogeneity of the functionally graded layers and the microscale size effects exhibited by the half-space substrate affect the dispersion behavior of the SH-waves. Dispersion equations for two different circuit conditions associated with Model I (i.e., magnetically open and short cases) and Model II (i.e., electrically open and short cases) are obtained. Particular cases are derived and the results are observed to be in well-agreement with the classical case of dispersion equation of Love wave. Emphatic influence of affecting parameters, viz. material gradient factors, characteristic length, micropolarity, and thickness of piezo material layers on the phase velocities of SH-waves has been analyzed through graphical illustrations. The mechanical coupling factors viz. magnetomechanical coupling factor associated with Model I and electromechanical coupling factor associated with Model II along with the group velocity of the propagating wave in the considered structures are also investigated and the results are demonstrated graphically. Micropolar constant and characteristic length parameter pertinent with the micropolar half-space substrate bearing microscale structures favors the phase velocity of the SH-wave. Micropolar constant and characteristic length parameter encourages the mechanical coupling factors. The material gradient factors associated with the functionally graded piezo material layers have an enhancing effect on the phase velocity of the SH-wave. In the absence of functional gradedness, the mechanical coupling factors reduce.

Chapter 6 is concerned with manifesting the piezoelectric and nonlocal effects on the propagation of surface waves in nanoscale smart structures, which can provide some new insights for the designs and applications of the nanoscale wave devices. Taking the nanoscale size effect into consideration based on the nonlocal theory of elasticity, the propagation of Bleustein-Gulyaev (BG) wave in a nonlocal piezoelectric layer overlying a nonlocal piezoelectric half-space, is investigated. Bleustein-Gulyaev wave is a promising candidate over other surface waves to be employed for sensors and acoustic devices. The dispersion relations and particular cases are derived for the open and short circuit conditions. For the sake of validation of the results, the obtained dispersion relation is reduced to match with the classical BG wave equation. The results show that wave propagation is highly affected by nanoscale size effects due to the nonlocality present in the media. The main intent of the present work is to analyze the effect of nonlocality on the propagation of BG waves in the piezoelectric layered structure. Appropriate boundary conditions are employed at the free surface and at the interface between the layer and the half-space to obtain the disper-

sion relations for both open and short circuit conditions. It is found that BG waves are dispersive in nature and are affected by nonlocality. The nonlocality parameter is present in both open and short circuit conditions. Furthermore, it has been observed that for both cases the wave ceases to propagate beyond the critical frequencies. The variation of phase velocities with frequency has been numerically studied and graphically illustrated. The effects of piezoelectric material parameters, nonlocality parameter, and electromechanical coupling coefficient, on the phase velocity of BG wave, have been shown graphically. Nonlocality has a decaying effect on the critical frequency. In the absence of nonlocality in the media there do not exist critical frequency and the phase velocity attains a constant value for high frequency range. Elastic stiffness constant and piezoelectric constant has enhancing effect on the phase velocity and the dielectric constant have a decaying effect on the phase velocity of the BG wave. The electromechanical coupling coefficient has an enhancing effect on the phase velocity of the BG wave. Phase velocity for an electrically open case is observed to be greater than that of an electrically shorted case through graphical representations. The dispersion relation appears 'normal' as the phase velocity of the wave is greater than the group velocity in the considered structure. Nonlocality parameter disfavors the group velocity of the BG wave. An increase in nonlocal parameter leads to a decrease in the group velocity of the BG wave. The considered structure studied in the present work can be utilized in the field of acoustic devices having numerous applications in nanoscale engineering.

List of Publications

1. Vanita Sharma and Satish Kumar, Modelling of Love-type waves in an elastic layer sandwiched between viscous liquid half-space and size dependent couple stress substrate, Journal of Theoretical and Applied Mechanics, 57(4), 1009-1019, 2019.
   DOI:10.15632/jtam-pl/112457
   (SCIE, I.F. = 0.927)

2. Vanita Sharma and Satish Kumar, Microstructural and viscous liquid loading effects on the propagation of love waves in a piezomagnetic layered structure, Mechanics of Advanced Materials and Structures, 28(16), 1703-1713, 2021.
   DOI:10.1080/15376494.2019.1702235
   (SCIE, I.F. = 4.030)

3. Vanita Sharma and Satish Kumar, Analysis of size dependency on Love-type wave propagation in a functionally graded piezoelectric smart material, Mathematics and Mechanics of Solids, 25(8), 1517-1533, 2020.
   DOI:10.1177/1081286520909522
   (SCIE, I.F. = 2.341)

4. Vanita Sharma and Satish Kumar, Comparative study of micro-scale size effects on mechanical coupling factors and SH-wave propagation in functionally graded piezoelectric/ piezomagnetic structures, Waves in Random and Complex Media, 2020.
   DOI:10.1080/17455030.2020.1851068
   (SCIE, I.F. = 4.853)

5. Vanita Sharma and Satish Kumar, Bleustein-Gulyaev wave in a nonlocal piezoelectric layered structure, Mechanics of Advanced Materials and Structures, 2020.
   DOI:10.1080/15376494.2020.1854907
   (SCIE, I.F. = 4.030)

Contents

List of Figures

List of Tables

Chapter 1

Introduction

1.1 Preliminaries

Continuum mechanics is that branch of mechanics which is concerned with the mechanical behavior of the solids and fluids (liquids and gases). It assumes matter to be continuously distributed throughout regions of space by ignoring the fact that matter is of discrete nature, resulting in defining physical quantities such as density, displacement, velocity, etc. as continuous functions of the position. This measure is proved to be satisfactory if, on the microscopic scale, the material bodies under consideration are having large dimensions as compared to the characteristic lengths (for example, interatomic spacings in a crystal, or mean free paths in a gas). Modern-day physical theories implicate that matter is discontinuous on the microscopic scale, it consists of minute particles such as molecules, atoms, and even smaller particles. However, compared with these particles usually the large pieces of matter are considered in nearly all engineering applications of mechanics. So the consideration is not with the motion of individual atoms and molecules, but only with their behavior in some average sense. Conventionally, if the behavior of matter on the microscopic scale is known it would be possible to predict the material behavior on the macroscopic scale. The microscopic scales must not be of atomic dimensions, for example, continuum mechanics can be applied to a granular material such as sand, provided the dimensions of the considered region are very large as compared to that of individual grain. The theory of continuum mechanics assumes that a particle of matter is associated with each and every point of the region of space possessed by a body and the field quantities viz. density, velocity, etc. are ascribed to these particles. Up to some extent this is a justifiable approach that describes and predicts the mechanical behavior of the material in bulk. In the theory of continuum mechanics, the considered variables are related to forces (usually force per unit area or per unit volume, rather than force itself) and kinematic variables such as displacement, velocity, and acceleration. There are two main kinds of equations of continuum mechanics. Firstly, there are equations that are equally applicable to all materials. Universal physical laws, such as conservation of mass and energy are described by them. Secondly, there are equations that characterize the mechanical behavior of specific

materials referred as constitutive equations.

Elasticity is the ability of the body to regain its original configuration after the removal of the deforming force. A force that produces a change in configuration (size or shape) of the object on applying it, is called a deforming force. On removal of the deforming force if the body regains its original shape then it is called an elastic body. On the other hand, if the deformations remain in the body, it is called a plastic body. The theory of elasticity is concerned with resolving intrinsic forces such as stress, strain and finding displacement distribution in elastic solids concealed by applied extrinsic forces. It establishes a mathematical model that provides a solution to various problems having applications in civil, mechanical, geomechanics, material engineering, and scientific fields. It offers significant contributions to deflection and stress analysis of structures viz. beams, plates, rods, and shells encountered in civil engineering fields. It has vast applications including general or thermal stress analysis, fracture mechanics, and fatigue while analyzing and designing machine elements in mechanical engineering. This theory is useful in determining the stress fields and displacement distributions, in crystalline solids or materials with microstructures. Analysis of stress, fracture, and fatigue in aerostructures encountered in aeronautical and aerospace engineering are some additional applications. In geomechanics, this theory helps in the determination of stresses in materials viz. rock, soil, concrete, and asphalt. A mathematical model of the deformation problems is established in elasticity theory. Using basic principles of continuum mechanics, the governing partial differential field equations are formulated in vector and tensor forms. These field equations are solved using various techniques. The historic background of the study related continuum mechanics can be found through the texts ([205], [203], [166]).

1.1.1 Generalized form of Hooke's law

In almost all solids, it was experimentally observed that strains are linearly proportional to the applied load, provided that the extrinsic load does not surpass a given value, known as the elastic limit. Another speck on stress-strain curve which demarcate the initiation of large plastic deformation, is attributed as the yield point. From many experimental studies it can be remarked that a broad range of real materials exhibits linear elastic behavior subjected to small deformations. Thereby, proposing a linear relation for the axial loading (1-dim) case as $\sigma = E\epsilon$, where σ, ϵ, and E are the stress, strain, and the slope of the specified curve, respectively. This approach laid the foundation to establish the general (3-dim) forms of the linear constitutive model of elasticity. Robert Hooke in 1678 was the first to develop and propose the idea of force-deformation relation. This relation mathematically states that "Each components of stress at any point is a linear

function of all strain components at that point." In standard tensor notation it can be written as [166]

$$\sigma_{ij} = c_{ijkl}\epsilon_{kl}, \quad (i, j, k, l = 1, 2, 3), \tag{1.1.1}$$

where c_{ijkl} is a fourth order tensor known as stiffness tensor comprising of all the material parameters that are required to characterize the material. σ_{ij} and ϵ_{kl} are second order tensors known as stress and strain tensors, respectively.

The stiffness tensor has 81 elastic constants for the most general case. The well-known law of reciprocity without changing the constant of proportionality sought us to interchange the directions of force and displacement hence, resulting in the reduction of elastic constants from 81 to 36. The material is said to be triclinic if all of 36 elastic constants are independent. For adiabatic and isothermal system, the existence of strain energy density function reduces the elastic constants from 36 to 21. Such a material is called an anisotropic material. Monoclinic materials are materials with one plane of elastic symmetry and have 13 number of independent constants. Orthotropic materials exhibit symmetry about three diagonal planes. These materials have different properties in all three orthogonal directions. It can be easily observed that if two orthogonal planes are planes of material symmetry, then the third mutually orthogonal plane is also a plane of material symmetry. For orthotropic materials, the number of elastic constants is further reduced to 9. Transversely isotropic materials are a special class of orthotropic materials having the similar properties in one plane (e.g. the $x - y$ plane) and distinct properties in the direction normal to this plane (e.g. the z-axis). Transverse isotropy can be observed in sedimentary rocks where each layer has approximately the same properties in-plane but different properties through the thickness. For transversely isotropic material case the independent elastic constants are reduced to 5. Finally, for isotropic elastic materials the elastic properties are independent of orientation of axis and the number of independent elastic constants are reduced to 2 i.e. λ and μ, known as Lam*é* constants that completely characterizes the elastic behavior of an isotropic solid.

For homogeneous isotropic elastic body, the generalized Hooke's law can be expressed as [166]

$$\sigma_{ij} = \lambda\delta_{ij}\Delta + 2\mu\epsilon_{ij}, \quad (i, j = 1, 2, 3). \tag{1.1.2}$$

Here

$$\delta_{ij} = \begin{cases} 1, \text{if } i = j \\ 0, \text{if } i \neq j \end{cases}$$

is called Kronecker's delta function and $\Delta = \epsilon_{xx} + \epsilon_{yy} + \epsilon_{zz} = \epsilon_{ii}, \ (i = 1, 2, 3)$: this is called dilatation and $\epsilon_{ij} = \frac{1}{2}(u_{i,j} + u_{j,i})$: is called strain tensor. Here u_i are the displacement components in i^{th} direction.

It is to be noted that isotropic elastic media involves exactly two independent elastic constants i.e., Lam*é* constants. To attain a broad overview of physical importance of elastic constants, that characterizes the behavior of material, elastic solid subjugated to simple tension, pure shear, and hydrostatic pressure is considered. Usually, four elastic constants are used for this viz. Young's modulus E, Poisson's ratio ν, the bulk modulus k, and the modulus of rigidity, or the shear modulus which is identical with Lam*é* constant μ.
Poisson's ratio- It is defined as the ratio between the lateral contraction and the longitudinal extension of the specimen denoted by $\nu = \frac{\lambda}{2(\lambda+\mu).}$
Young's modulus-It is defined as the ratio of tensile stress and the axial extension produced by the tensile stress and is denoted by $E = \frac{\mu(3\lambda+2\mu)}{(\lambda+\mu)}$.
Bulk modulus-It is defined as the ratio between the applied pressure and the fractional change in volume when the solid is subjected to uniform hydrostatic compression and is denoted by $k = \lambda + \frac{2\mu}{3}$.
Finally, the **modulus of rigidity**, or the shear modulus of elasticity denoted by μ, corresponds to the ratio between the shear stress and the shear strain. It is eminent that other elastic constants are expressible in terms of these Lam*é* constants.

1.1.2 Equations of motion in an isotropic elastic medium

Considering a continuous medium enclosed within a volume σ, to be in equilibrium. Then, the consequent force acting on the media within σ must vanish. For a homogeneous isotropic elastic solid the equation of equilibrium is given as [203]

$$\sigma_{ij,j} = -F_i, \quad (i,j = 1,2,3), \tag{1.1.3}$$

where F_i are the components of body forces and the functions σ_{ij} and their first partial derivatives $\sigma_{ij,k} \equiv \frac{\partial \sigma_{ij}}{\partial x_k}$ are continuous and single-valued in σ.
Using the constitutive stress-displacement relation

$$\sigma_{ij} = \lambda \delta_{ij} u_{i,i} + \mu(u_{i,j} + u_{j,i}), \tag{1.1.4}$$

in Eq. (1.1.3), we get

$$\mu u_{i,jj} + (\lambda + \mu) u_{j,ji} + F_i = 0, \tag{1.1.5}$$

In vector form, above Eq. (1.1.5) can be written as

$$\mu \nabla^2 \overrightarrow{u} + (\lambda + \mu) \nabla(\nabla . \overrightarrow{u}) + \overrightarrow{F} = 0, \tag{1.1.6}$$

where $\nabla = \hat{i}\frac{\partial}{\partial x} + \hat{j}\frac{\partial}{\partial y} + \hat{k}\frac{\partial}{\partial z}$; $\quad \nabla^2 = \frac{\partial^2}{\partial x^2} + \frac{\partial^2}{\partial y^2} + \frac{\partial^2}{\partial z^2}$.
If $\varrho(x, y, z)$ is the density of the continuous medium, then components of the force of inertia acting on the mass contained within the volume element $d\sigma$ are $-\varrho\frac{\partial^2 u_i}{\partial t^2}d\sigma$, $(i = 1, 2, 3)$. Hence, adding the components of the force of inertia per unit volume to the components F_i of the body force $\overrightarrow{F}$ in Eq. (1.1.3) gives the dynamical equation of motion

$$\sigma_{ij,j} + F_i = \varrho\frac{\partial^2 u_i}{\partial t^2}, \quad (i, j = 1, 2, 3) \tag{1.1.7}$$

The displacements u_i are functions of the space variables x_i and time t. Thus, from the equation of equilibrium defined in Eq. (1.1.6), the dynamical equation of an isotropic elastic solid can be asserted as

$$\mu\nabla^2\overrightarrow{u} + (\lambda + \mu)\nabla(\nabla.\overrightarrow{u}) + \overrightarrow{F} = \varrho\frac{\partial^2\overrightarrow{u}}{\partial t^2}. \tag{1.1.8}$$

1.1.3 Waves in elastic medium

All material medium comprises of atoms, that can be forcibly indulged in vibrational motion about their equilibrium or mean positions. Within the elastic limit, the individual material particles exhibit elastic oscillations under an external applied force. As external force is applied to the material, the particles gets displaced from their mean positions resulting in the rising of intrinsic restoring forces. These intrinsic forces along with the inertia of the particles results in oscillatory motion of the particles. In an isotropic, homogeneous medium, waves are simply a periodic molecular disturbance, dependent on both time and position that carries energy through matter or space in the medium from one point to another point. This phenomenon is known as the wave propagation phenomenon. This phenomena can be divided into two categories i.e. Body waves and Surface waves. Body waves can travel in the interior of a medium while surface waves can travel along the free surface of the medium. Acoustic waves in the air and electromagnetic waves in the vacuum are examples of body waves. Rayleigh waves and Love waves are the examples of surface waves. In an elastic solid, two types of wave motion are possible. In the first case, the motion of the particles at their mean positions are in the same direction as that of the propagating wave and hence termed as longitudinal waves while for the second case, the motion of the particles at their mean positions are in normal direction to the direction of the wave propagation and are termed as transverse waves.
In the absence of body forces the Eq. (1.1.8) results in

$$\mu\nabla^2\overrightarrow{u} + (\lambda + \mu)\nabla(\nabla.\overrightarrow{u}) = \varrho\frac{\partial^2\overrightarrow{u}}{\partial t^2}. \tag{1.1.9}$$

Using the vector identity $\nabla^2\overrightarrow{u} = \nabla(\nabla.\overrightarrow{u}) - \nabla\times(\nabla\times\overrightarrow{u})$ in Eq. (1.1.9) results in

$$(\lambda+2\mu)\nabla(\nabla.\overrightarrow{u}) - \mu\nabla\times(\nabla\times\overrightarrow{u}) = \varrho\frac{\partial^2\overrightarrow{u}}{\partial t^2}. \tag{1.1.10}$$

By using Helmholtz decomposition,

$$\overrightarrow{u} = \nabla\Phi + \nabla\times\overrightarrow{\Psi}, \quad \nabla.\overrightarrow{\Psi} = 0 \tag{1.1.11}$$

where Φ is a scalar potential function and $\overrightarrow{\Psi}$ is a vector potential function.
Substituting (1.1.11) into (1.1.10) we get

$$\nabla\{(\lambda+2\mu)\nabla^2\Phi - \varrho\ddot{\Phi}\} + \nabla\times(\mu\nabla^2\overrightarrow{\Psi} - \varrho\ddot{\overrightarrow{\Psi}}) = 0. \tag{1.1.12}$$

This equation will be satisfied if each bracketed term vanishes, thus giving

$$(\lambda+2\mu)\nabla^2\Phi = \varrho\ddot{\Phi}, \tag{1.1.13}$$

$$\mu\nabla^2\overrightarrow{\Psi} = \varrho\ddot{\overrightarrow{\Psi}}. \tag{1.1.14}$$

Thus, it can be observed that waves may be propagated with two different velocities within the elastic solid. The waves traveling with no rotation propagates with velocity $\left[\frac{(\lambda+2\mu)}{\rho}\right]^{\frac{1}{2}} = \widetilde{c_1}$ (say) and are termed as irrotational or dilatational or longitudinal waves. While the other waves which involve no dilatation travel with velocity $\left[\frac{\mu}{\rho}\right]^{\frac{1}{2}} = \widetilde{c_2}$ (say) and are termed as distortional or equivoluminal or transverse waves. The ratio of the respective velocities may be expressed as

$$\widetilde{k} = \frac{\widetilde{c_1}}{\widetilde{c_2}} = \left(\frac{\lambda+2\mu}{\mu}\right)^{\frac{1}{2}} = \left(\frac{2-2\nu}{1-2\nu}\right)^{\frac{1}{2}}. \tag{1.1.15}$$

Since $0 \le \nu \le \frac{1}{2}$ always, we see that $\widetilde{c_1} > \widetilde{c_2}$. These waves have variety of terminology. Dilatational waves are also called primary (P) waves and the distortional waves are also called secondary (S) waves. These designations have been arisen from seismology. Since $\widetilde{c_1} > \widetilde{c_2}$, so primary (P) waves appear first than secondary (S) waves on the seismograms. When body waves propagate towards the surface, they come in contact with the surface rocks resulting in the generation of a new set of waves termed as Surface waves. These waves are the last to report on the seismograph. These travel adjacent to the earth's surface and are very destructive. These waves have a high amplitude and long wavelength. Rayleigh waves, Love waves are the type of surface waves. When the solid has a free

surface or where there exist a surface boundary amid two solids, the waves identical to gravitational surface waves were first observed by Lord Rayleigh [161]. He demonstrated that their impact decreases promptly with depth, and their propagation speed is smaller than that of body waves. These waves involve both longitudinal and transverse motion and the particles at the surface exhibit elliptic motion in planes normal to the surface and parallel to the direction of the transference-the major axis of the ellipse is vertical. These can propagate in homogeneous half-space and layered ones. There is one more type of wave that can propagate in the presence of a superficial layer of finite thickness embedded on a half-space medium, called Love waves. These waves are horizontally polarized shear (SH) waves, named after British mathematician, A.E.H. Love in 1911 [127]. Love [128] was the first to examine the SH-wave in an isotropic composite structure comprising of a homogeneous isotropic layer of finite thickness over a homogeneous isotropic half-space. This SH-wave is referred as Love wave and specified as shear wave that is horizontally polarized and propagates at the surface of the medium. These waves can exist only in the presence of a waveguide, i.e. softer superficial layer above stiffer material, and can be generated by multiple reflections of energy trapped in this layer. During an earthquake, these waves cause horizontal shifting of the earth. These waves travel with a lower velocity than P and S-waves but faster than Rayleigh waves.

1.1.3.1 Love waves in a layered half-space

Considering the SH-waves propagating through the isotropic layer of finite thickness h overlying homogeneous isotropic semi-infinite medium. The wave is propagating in the direction of y-axis, displacement is along z-axis and x-axis is taken positive in vertically downward direction perpendicular to the wave propagation direction as shown in Fig. 1.1

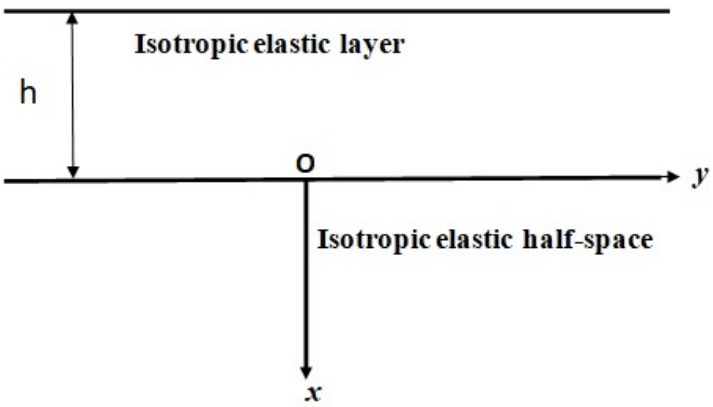

Figure 1.1: Schematic illustration

Governing equation of motion

The governing equation of motion in the absence of body forces obtained from Eqn. (1.1.7) is

$$\sigma_{ij,j} = \varrho \frac{\partial^2 u_i}{\partial t^2}, \quad (i, j = 1, 2, 3), \tag{1.1.16}$$

where σ_{ij} are stress sensors, ϱ is a density of elastic medium, and u_i are displacement components.

Constitutive relation

The constitutive relation obtained from Eqn. (1.1.2) is expressed as

$$\sigma_{ij} = \lambda \delta_{ij} \Delta + 2\mu \epsilon_{ij}, \tag{1.1.17}$$

where λ and μ are Lam*é* constants. ϵ_{ij} are strain tensors. Δ is called cubical dilatation. δ_{ij} is a Kronecker delta function.

As Love wave is propagating along y-direction inducing displacement along z-direction, we assume

$$u_1 = u_2 = 0, \ u_3 = u_3(x, y, t) \text{ and } \frac{\partial}{\partial z} \equiv 0. \tag{1.1.18}$$

Substituting the above values in Eq. (1.1.17) we get

$$\begin{aligned} \sigma_{xx} = \sigma_{yy} = \sigma_{zz} = \sigma_{xy} = 0, \\ \sigma_{xz} = \mu \frac{\partial u_3}{\partial x}, \quad \sigma_{yz} = \mu \frac{\partial u_3}{\partial y}. \end{aligned} \tag{1.1.19}$$

Substituting Eqs. (1.1.18) and (1.1.19) in Eq. (1.1.16), the governing equation becomes

$$\nabla^2 u_3 = \frac{1}{{c_{sh}}^2} \frac{\partial^2 u_3}{\partial t^2}. \tag{1.1.20}$$

Here $c_{sh} = \sqrt{\frac{\mu}{\varrho}}$ is the shear wave velocity.

Considering time harmonic solution of (1.1.20) we assume that

$$u_3(x, y, t) = \widetilde{U_3}(x) e^{ik(y - ct)}, \tag{1.1.21}$$

where k is a wave number and c is a phase velocity of the wave. Putting the above solution in (1.1.20) we get

$$\widetilde{U_3}''(x) - k^2 \left(1 - \frac{c^2}{c_{sh}^2}\right) \widetilde{U_3}(x) = 0. \tag{1.1.22}$$

On solving above differential equation for isotropic elastic layer under the assumption that $c > c_{s_1}$, we get the displacement component as

$$u_3^L(x, y, t) = (\cos(km_1 x)A_1 + \sin(km_1 x)A_2)e^{ik(y-ct)}, \tag{1.1.23}$$

where $m_1 = \sqrt{\frac{c^2}{{c_{s_1}}^2} - 1}$ and $c_{s_1} = \sqrt{\frac{\mu^L}{\varrho^L}}$. Here superscript '$L$' denotes the entities in isotropic elastic layer. A_1 and A_2 are arbitrary constants.
Under the assumption that $c < c_{s_2}$ for isotropic elastic half-space, we get the displacement component as

$$u_3^H(x, y, t) = e^{-km_2 x}\overline{A_1}e^{ik(y-ct)}, \tag{1.1.24}$$

where $m_2 = \sqrt{1 - \frac{c^2}{{c_{s_2}}^2}}$ and $c_{s_2} = \sqrt{\frac{\mu^H}{\varrho^H}}$. Here superscript '$H$' denotes the entities in isotropic elastic half-space. $\overline{A_1}$ is an arbitrary constant.

Boundary conditions
Following are the boundary conditions in the considered model.

- The top surface is free of stress.

$$\sigma_{zx}^L = 0 \quad \text{at } x = -h. \tag{1.1.25}$$

- Continuity of the displacement components at the interface.

$$u_3^L = u_3^H \quad \text{at } x = 0. \tag{1.1.26}$$

- The magnitude of shear component of the stress tensors should be equal at the interface.

$$\sigma_{zx}^L = \sigma_{zx}^H \quad \text{at } x = 0. \tag{1.1.27}$$

Derivation of dispersion relation
Using above mentioned boundary conditions from Eqs. (1.1.25) to (1.1.27), we obtain the following equations in terms of three unknown coefficients $A_1,\ A_2,$ and $\overline{A_1}$ as

$$\sin(km_1 h)A_1 + \cos(km_1 h)A_2 = 0, \tag{1.1.28}$$

$$A_1 - \overline{A_1} = 0, \tag{1.1.29}$$

$$\mu^L m_1 A_2 + \mu^H m_2 \overline{A_1} = 0. \tag{1.1.30}$$

To obtain a non-trivial solution, determinant of the coefficients of the unknowns $A_1,\ A_2,$ and $\overline{A_1}$ should vanish. By solving the determinant, we get the following dispersion relation for Love wave in an isotropic elastic layer overlying isotropic elastic half-space.

$$\tan\left(kh\sqrt{\frac{c^2}{{c_{s_1}}^2}-1}\right) = \frac{\mu^H}{\mu^L}\frac{\sqrt{1-\frac{c^2}{{c_{s_2}}^2}}}{\sqrt{\frac{c^2}{{c_{s_1}}^2}-1}}. \tag{1.1.31}$$

This is the classical case of Love wave [128] under the assumption $c_{s_1} < c < c_{s_2}$.

1.1.4 Applications of wave phenomena

Wave phenomena can be observed in wide variety of physical settings for example quantum mechanics, electrodynamics, plasmas, fluids, seismology etc. This phenomena has various practical applications in science and industry [82]. Mathematical equations are used for modeling of water in unsaturated oils, gas dynamics, heat conduction, elasticity, static of flow problem, cosmology, seismology etc [36]. In the structural engineering, the main interest lies in observing the behavior of structural materials under loads. Under transient loads of bearable strength, completely elastic conditions abound the structure and elastic theory can be utilized to predict all aspects of the response. Permanent deformation, perforation, and fracture of the structure may occur under severe loadings. Still elastic wave theory finds application pertaining to such conditions and predict the response away from the area of impact [116]. It is of great interest to the researchers to examine the behavior of structural materials under severe loadings which may cause permanent damage. Various techniques used to study such structural materials employ elastic waves to test the strength of materials under loadings. It has numerous applications are in military and space technology. Another area concerning with study of structures that involves wave phenomena is to analyze crack propagation, dynamic stress fields interaction with existing voids, cracks, or inclusions in a material. Problems arising in this area are analogous of problems arising in acoustics and electromagnetics dealing with scattering and diffraction phenomena. Wave phenomena finds its another application in the field of ultrasonics. It involves the introduction of high frequency stress pulse with low energy level into a material and the subsequent reflection and propagation of the energy is observed. The motivation for introducing and detecting the stress waves in the structure is based on the piezoelectric (PE) effect that can be observed in certain crystals and ceramics. Piezoelectricity is the electric charge that is generated in response to applied mechanical stress or the inverse effect where

an electric field applied to the material causes a mechanical strain. Thus this motivates the viewpoint that an electrical pulse is capable of generating a mechanical pulse. When a mechanical pulse hit a PE crystal and generates an electrical signal, detection process is completed.

Numerous applications are based on the reverse effect exhibited by PE crystals. For instance, many fundamental properties of materials such as elastic constants and damping characteristics can be determined by scrutinizing the propagation, attenuation, and reflection of ultrasonic pulses. These ultrasonics have wide use in detection of defects in materials in the field of non-destructive testing (NDT) techniques. By introducing a pulse into a solid, it is possible to identify defects by observing the pulse energy reflected by the defect in the same manner as observed underwater SONAR detection. Longitudinal waves, shear waves, or surface waves are widely used in various detection applications.

In the field of electronics, ultrasonic delay lines have wide applications. As depicted by signal processing considerations, the main objective of these devices is to inculcate a means to delay an electrical signal for a short interval of time. To accomplish such a delay in electrical signals which are propagating with extremely high velocity through purely electronic components is impractical. Such time delays can be easily obtained by mechanical disturbances moving with relatively slow velocity. This can be accomplished by converting the electrical signal to a mechanical pulse using a PE transducer and forcing the signal to propagate in some type of solid media and then recovering it using another transducer after a specified time. There exist a wide variety of delay lines. Some of them are based on the propagation of torsional or longitudinal waves through thin wires, some are based on the shear waves propagating in thin strips, others are the longitudinal waves propagting in bulk solids, and some along the surface.

Many interesting wave propagation phenomena can be observed from the waves propagating in the earth [117]. Waves with extreme high velocities that can travel thousands of miles are generated by earthquakes. The knowledge about earth's interior is accomplished through study of wave propagation phenomena of such waves. Wave propagating in earth has other aspects in oil and gas exploration [37]. To locate the possible oil-bearing deposits the refelection of waves are observed from underground discontinuities. The application of waves in rocks pertains to mining and quarrying. The blastings done in these operations are attained by introducing intense stress waves. The interactions of waves with boundaries and with each other, are responsible for the fracture, thus removing large quantities of rocks. This application includes many interesting problems pertaining to reflection and transmission of waves at the discontinuities. Thus, wave phenomena has many and widespread applications from practical considerations ([13], [199]).

1.2 Microcontinuum Theories of Elasticity

Classical continuum mechanics [29] deals with those materials, in which the matter is assumed to be continuously distributed throughout the body. In this theory, the behavior of the materials is analyzed at a macro-scale by neglecting the molecular structure of the material. The material particles considered as geometrical points are described by a scalar quantity, called the density of the material. The displacement vector characterizes the deformation of the body and a force called stress vector, uniquely determines the transmission of loads across a surface element. Thus, the symmetric tensors of stress and strain ascribe the deformation of the body. Some materials such as aluminium, steel, concrete, etc. manifest results that fairly coincide with those of experimentally observed results, within the elastic limits. However, the results delivered by classical elasticity showed certain disagreements in comparison to experimentally observed results in many materials such as asphalt, fibrous, polymers, etc. These disagreements are due to the influence of atomic structures of the material which is ignored in the classical theory of elasticity. Such disagreements arise in dynamical problems which deals with elastic vibrations involving high frequencies and short wavelengths. The classical theory of elasticity eventually fails when encountered with the vibrations of granular and multimolecular bodies because the inherent motion of microelements remarkably affects the transferring wave at high frequencies. When sectioned, polished and suitably etched, nearly all engineering materials will be found to exhibit structural features that are characteristics of the material. Almost all engineering materials are found to exhibit structural features that are characteristics of the material and hence, are structurally sensitive. Microstructure analysis can reveal the relationship between a specific microstructural characteristic and a particular physical, chemical, or engineering property. The granular structure or microstructure is a very minute form of material. These can vigorously influence hardness, toughness, corrosion resistance, high/low temperature behavior, ductility, or wear resistance. Microstructure covers the scale of structural phenomena most commonly of concern to the materials scientist and engineers, namely grain and particle sizes, dislocation densities and particle volume fractions, microcracking, and microporosity [25]. These properties consecutively govern the applications of these materials in chemical engineering and industrial practices. Hence, an urgent need to develop consistent size-dependent continuum mechanics was there, which addresses the microstructure of materials. This theory must account for many scales and definitely reduce to classical continuum mechanics at macro-scales.
To complete continuum theory, deformation which is length related is addressed with a new measure such as curvature tensor. Consequently, the introduction of couple-stresses is also required. Voigt [222] was the first who introduced the idea of couple stresses in

addition to force stresses to overcome the shortcomings of the classical theory of elasticity. He interpreted that each element or grain of microstructure rotates about its center of gravity in addition to translation assumed in classical theory of elasticity which demarcated the idea of "Couple Stress (CS) theory". However, to analyze materials with couple-stresses the mathematical model was first developed by Cosserat and Cosserat [38]. In the original Cosserat theory, they considered that the deformation of the medium is described by displacement vector and an independent rotation vector. At each material point, the additional degrees of freedom of rotation were assumed and consequently led to the asymmetry of stress and strain tensors. Despite the originality of the theory, their work did not capture significant attention by the researchers of that time and the theory remained futile during their lifetime. After half century, their research work was rediscovered and captured the glance of many researchers. These theories were advanced by many researchers ([84], [133], [215], [56], [103], [146], [142]) etc. Toupin's theory [216] was termed as "Cosserat theory with constrained rotation", Koiter's theory [103] was termed "CS theory", Eringen's theory [57]- [58] was termed "Indeterminate CS theory", Mindlin theory [133] was termed "strain gradient theory", Nowacki's theory [142] was termed "Cosserat pseudo-continuum theory" etc. The generalized Cosserat continuum theory was referred as "Micropolar (MP) continuum theory" following Eringen [60]. He proposed the MP theory of elasticity by considering three rotational degrees of freedom in addition to three classical displacement degrees of freedom. He established the generalized interpretation of this theory which illuminates the deformation of elastic media with oriented particles. Each microstructural component in addition to displacement rotates about its center of gravity. If the micro-motion of inner structure and macro-motion of particle are not distinguished then MP theory reduces to CS theory. The general theory of non-linear and linear microelastic continua was asserted by Eringen and Suhubi ([57]- [58]) and referred as "Indeterminate CS theory". An another complex generalization of the continuum with microstructures, micromorphic theory is also proposed by Eringen [59].

1.2.1 Couple stress (CS) theory

The consistent CS theory was developed which accounts for size-dependent effects of materials and used to explore various types of problems arising due to elastic vibrations through a material medium [6]. The influence of couple stresses on stress concentration was explored by Mindlin [134]. An experimental study of MP and CS elasticity was performed by Yang and Lakes [230] in compact bone in bending. Bardet and Vardoulakis [14] examined the definition of stress in granular materials and established the conditions under which there may be couple stresses and asymmetric stresses. A modified CS theory showing strain energy to be a quadratic function of symmetric strains, symmetric curvatures, and

involving a single length scale parameter was developed by Yang *et al.* [231]. Akgoz and Civalek [5] used modified CS theory and Kirchhoff plate theories to study the micro-sized plates resting on elastic medium. Using Hamilton's principles the equations for bending, buckling and vibration were derived and also illustrated the effect of length scale parameter on these properties. Hadjesfandiari and Dargush [87] have developed the consistent CS theory by taking into account true continuum kinematical displacement and rotation. They depicted the CS tensor to be skew-symmetric and the consistent curvature tensor be the skew-symmetric part of the gradient of the rotation tensor. This theory may be considered as the modification of the developments accomplished by Mindlin and Tiersten [133] and Koiter [103]. For isotropic materials, it concluded the existence of two Lam*é* parameters and one length scale parameter η^c, which completely characterizes the behavior of the material. CS effect for isotropic solids was accounted by this length scale parameter which is further associated with characteristic material length parameter l^c, which was absent in Cauchy's theory of elasticity [29]. This type of length scale parameter was also predicted by Lakes [110] which may be considered comparable to the average cell size of the material in cellular solids.

Basic governing equations and constitutive relations

(A) **Equations of motion**

The basic governing equation of motion of CS theory for isotropic material in vector form, in the absence of body forces proposed by Hadjesfandiari and Dargush [87] is given by

$$(\lambda^c + \mu^c + \eta^c\nabla^2)\nabla(\nabla.\overrightarrow{U^c}) + (\mu^c - \eta^c\nabla^2)\nabla^2\overrightarrow{U^c} = \rho^c\frac{\partial^2\overrightarrow{U^c}}{\partial t^2}, \tag{1.2.1}$$

Here superscript 'c' denotes the entities in CS substrate. λ^c and μ^c are Lam*é* constants. $\eta^c = \mu^c(l^c)^2$ is CS coefficient. l^c is the characteristic length. $\overrightarrow{U^c} = (u_1^c, u_2^c, u_3^c)$ are the displacement components.ρ^c is density of the material, and $\nabla^2 = \frac{\partial^2}{\partial x^2} + \frac{\partial^2}{\partial y^2} + \frac{\partial^2}{\partial z^2}$.

(B) **Constitutive relations**

The constitutive relations of CS theory are given by

$$\begin{aligned} \sigma_{ji}^c &= \lambda^c u_{k,k}^c\delta_{ij} + \mu^c(u_{i,j}^c + u_{j,i}^c) - \eta^c\nabla^2(u_{i,j}^c - u_{j,i}^c), \\ \mu_{ji}^c &= 4\eta^c(\varpi_{i,j}^c - \varpi_{j,i}^c), \quad \varpi_i^c = \frac{1}{2}\epsilon_{ijk}u_{k,j}^c, \quad (i,j,k = 1,2,3), \end{aligned} \tag{1.2.2}$$

where σ^c_{ji} are the non-symmetric stress tensor. δ_{ij} is Kronecker's delta. ϖ^c_i is a rotation vector. μ^c_{ji} is skew-symmetric CS tensor and

$$\epsilon_{ijk} = \begin{cases} +1, & \text{if ijk is an even permutation of 1, 2, 3} \\ -1, & \text{if ijk is an odd permutation of 1, 2, 3} \\ 0, & \text{otherwise} \end{cases}$$

is a permutation tensor.

Many researchers have employed consistent CS theory of elasticity in various layered structures. Sharma and Kumar [181] utilized CS theory of elasticity to capture the size effects on the propagation of Lamb waves in an elastic plate having mechanical properties typically used for bones with microstructure. Later on, they [182] investigated the effect of size dependency accounted by the characteristic length on the phase velocity of Lamb waves in the plate for various modes in the presence of liquid loadings. The study of leaky Rayleigh waves generated at the interface of solid half-space with liquid layer is of great importance for quick scanning and imaging of large civil engineering structures hence, Sharma and Kumar ([183], [184]) derived the dispersion relations for the problem of leaky Rayleigh waves under liquid loading using consistent CS theory of elasticity. Wide variations of rocks erupted from volcanoes and scattering of high frequency seismic waves support the existence of small scale heterogeneity in the earth's lithosphere. Hence, heterogeneity and viscoelasticity are to be considered for real characterisation of internal microstructure of solid earth. Thus, Sharma and Kumar [185] analyzed the propagation of SH waves in a viscoelastic layer over a CS substrate with imperfect bonding at the interface. Sharma and Sharma [186] modeled the earth's complex structure with fiber-reinforced layer lying over a CS half-space. Dispersion and damping equations are derived for the propagation of Love waves in the considered model. The study of Love waves in a sinusoidal corrugated elastic layer with void pores attached to a microstructural half space described using consistent CS theory is done by Sharma *et al.* [187]. The propagation of Love type waves is investigated by Deep and Sharma [41] in a geometrical configuration which is composed of a viscoelastic layer sandwiched between fiber-reinforced layer and a substratum that is modeled using size-dependent consistent CS theory. Shear wave based acoustic devices are being used in gaseous and liquid environments because of their high-sensitivity so the theoretical study of horizontally polarized shear (SH) waves in a layered structure consisting of a PE ceramic material overlying a CS substrate is done by Goyal *et al.* [75]. Furthermore, Goyal and Kumar [78] considered a theoretical model consisting of a heterogeneous viscoelastic layer sandwiched between a finite layer of PE medium and size-dependent couple stress sub-

strate to manifest the propagation of Love-type wave in multilayered structures that plays a vital role for designing of Love wave-based devices. Kumari and Singh [105] discussed the propagation of a horizontally polarized shear wave in a layered composite structure consisting of CS stratum over a functionally graded orthotropic viscoelastic substrate due to the point source existing at an imperfect interface of the stratum and substrate. Because of the CS effect in the stratum, the existence of the second kind of dispersive (shear) wave is established along with conventional first kind of a shear wave.

1.2.2 Micropolar (MP) theory

Eringen [60] proposed the MP theory of elasticity by considering three rotational degrees of freedom in addition to three classical displacement degrees of freedom. Each microstructural component in addition to displacement rotates about its center of gravity. This theory grabbing the size effects have numerous applications in many physical substances e.g., material particles having rigid directors, anisotropic fluids, bones, cellular solids, platelet composites, chopped fiber composites, aluminium epoxy, polymers, liquid crystal with side chains, a large class of substances like liquid crystals with rigid molecules, rigid suspensions, clouds with dust, magnetic fluids, animal blood with rigid cells, foams, porous materials, concrete with sand, muddy fluids, and many other complex microstructures ([109], [73]).

Basic governing equations and constitutive relations

(A) **Equations of motion**

Following are the equations of motion as proposed by Eringen [60] for semi-infinite MP elastic substrate in the absence of body forces in vector form

$$\begin{aligned}(\lambda^m+\mu^m)\nabla(\nabla.\overrightarrow{U^m})+(\mu^m+\kappa^m)\nabla^2\overrightarrow{U^m}+\kappa^m(\nabla\times\overrightarrow{M^m})=\rho^m\frac{\partial^2\overrightarrow{U^m}}{\partial t^2},\\ (\alpha^m+\beta^m+\gamma^m)\nabla(\nabla.\overrightarrow{M^m})-\gamma^m\nabla\times(\nabla\times\overrightarrow{M^m})+\kappa^m(\nabla\times\overrightarrow{U^m})-2\kappa^m\overrightarrow{M^m}=\jmath^m\rho^m\frac{\partial^2\overrightarrow{M^m}}{\partial t^2}.\end{aligned} \tag{1.2.3}$$

Here superscript 'm' denotes the entities in MP substrate. λ^m and μ^m are Lam$\acute{e}$ constants. ρ^m is density of MP elastic material. α^m, β^m, γ^m, κ^m are the additional MP elastic constants. $\jmath^m$ is the micro inertia. $\overrightarrow{U^m}=(u_1^m,u_2^m,u_3^m)$ are the displacement components and $\overrightarrow{M^m}=(M_1^m,M_2^m,M_3^m)$ are the microrotational components.

(B) **Constitutive relations**

The constitutive relations of MP theory are given by

$$\begin{aligned}\sigma_{ij}^m&=\lambda^m u_{k,k}^m\delta_{ij}+\mu^m(u_{i,j}^m+u_{j,i}^m)+\kappa^m(u_{j,i}^m-\epsilon_{ijk}^m M_k^m),\\ \mu_{ij}^m&=\alpha^m M_{k,k}^m\delta_{ij}+\beta^m M_{i,j}^m+\gamma^m M_{j,i}^m,\quad (i,j,k=1,2,3),\end{aligned} \tag{1.2.4}$$

where σ_{ij}^m and μ_{ij}^m are the force stress tensors and the CS tensors, respectively of the semi-infinite MP elastic substrate. δ_{ij} is kronecker delta. ϵ_{ijk} is a permutation tensor.

Many researchers have employed the MP theory of elasticity to capture the microstructural characteristics of the material. This study will aid researchers to delve into the relationship between the engineering properties of the materials and their microstructural characteristics. The propagation of plane waves in a three-dimensional MP elastic solid was discussed by Parfitt and Eringen [151]. Nowacki and Nowacki [140] have discussed the propagation of a longitudinal monochromatic wave in an infinite MP cylinder and derived the transcendental equations giving the phase speeds of propagating waves. Later, Nowacki and Nowacki [141] have explored the propagation of torsional waves in an infinite MP cylinder and obtained the characteristic transcendental equation determining the phase speed of the propagating waves in the cylinder. Ariman [10] analyzed the wave propagation and reflection phenomenon of a longitudinal displacement wave from a fixed flat surface of a MP elastic half-space. Vasudeva and Bhaskara [219] asymptotically analyzed the frequency spectrum of vibrations of a homogeneous, isotropic, MP elastic cylinder. Gauthier [69] performed experimental investigations on MP media. Surface waves in MP thermoelas-

ticity under the influence of gravity were examined by Das and Sengupta [40]. Nonlinear modulation of transverse waves propagating in an infinite MP elastic medium were studied by Erbay *et al.* [54] and it was shown that the slowly varying complex amplitudes of the transverse (displacement or microrotation) waves are governed by two coupled nonlinear Schrödinger equations. Tomar and Gogna ([207]- [209]) studied the problems dealing with the transmission phenomenon through the plane interface. They derived the reflection and refraction coefficients using the potential method and the relation between angles of various reflected and transmitted waves with the angle of incidence. They found that these coefficients depend on the angle of incidence, elastic properties of the half-spaces and frequency of the incident wave. Later, Tomar and Kumar [210] discussed the reflection and refraction of longitudinal displacement wave at a liquid-MP solid interface and extended their work [211] in analysis of wave propagation at liquid-MP elastic solid interface. Tomar and Singh [212] have considered a spherical cavity in a uniform MP elastic medium, in which the boundary of the cavity is subjected to time dependent force and couple simultaneously. They used Laplace transform technique to obtain radial-displacement and radial-microrotation fields in closed form at any point of the host medium. Frequency equations are obtained by Tomar [213] for Rayleigh–Lamb wave propagation in a plate of MP elastic material with voids. Symmetric and antisymmetric modes of propagation are obtained for frequency equations. Later Tomar [214] studied the wave propagation in a MP elastic layer sandwiched between liquid half-space and MP solid half-space. Singh and Tomar [192] investigated transmission of longitudinal elastic wave at a plane interface between a homogeneous MP fluid half-space and a MP solid half-space. Magneto-thermoelastic surface waves in MP elastic media are investigated by Nath *et al.* [137]. Midya [132] explored the Love-type wave propagation in homogeneous MP isotropic elastic media consisting of a layer of finite thickness lying over a semi-infinite medium. The Eringen's theory on MP continua [60] was summarized and reviewed on MP solids and liquids by Pabst [145]. He presented the nonlinear and linear constitutive relations for anisotropic and isotropic solids, as well as for anisotropic and isotropic fluids, respectively. Lamb waves in MP thermoelastic solid plates immersed in liquid with varying temperature are studied by Sharma and Kumar [180]. Reflection of MP elastic waves at the non-free surface of a MP elastic half-space was investigated by Zhang *et al.* [240]. Then, Zhang *et al.* [241] explored the wave propagation through a MP slab sandwiched by two elastic half-spaces. Later on they [242] studied the reflection of longitudinal displacement wave at the visco-elastically supported boundary of MP half-space. Eremeyev *et al.* [55] applied MP theory to strength analysis of bioceramic materials for bone reconstruction. A mathematical model is developed by Kaur *et al.* [97] in which the effect of imperfect bonding between the constituents of layer and half-space on the phase velocity and damped velocity of SH-wave is discussed.

The model consists of a MP elastic half-space bonded imperfectly with a heterogeneous viscoelastic layer. Rayleigh wave on transversely isotropic MP elastic solid half-space are studied by Singh and Sindhu [193] and later the exploration of Rayleigh wave in a MP elastic medium with impedance boundary conditions are carried out by Singh [194]. As linear theory of MP elasticity has potential applications in exploration of materials made from bar-like molecules with micro-rotational effects, Singh and Kaur [198] employed this theory to investigate the Rayleigh surface waves in an incompressible MP solid half-space whose surface is subjected to the Tiersten's impedance boundary conditions. Kundu *et al.* [108] studied the impact of heterogeneity on propagation of Love wave in a heterogeneous MP layer over an elastic inhomogeneous stratum, when both rigidity and density are assumed to vary linearly with depth. Analytical solution for the dispersion equation was obtained using method of separation of variables by means of the Airy function and Whittaker function. The propagation characteristics of SH-type wave and a new type of dispersive surface wave in an irregular composite structure comprised of a layer overlying a half-space, both constituted by distinct homogeneous MP isotropic elastic materials are provided by Singh *et al.* [190].

1.3 Smart materials

Smart materials are designed materials that comprise of certain properties that can be managed in a controlled way by varying external stimuli like pressure, temperature, electric field, magnetic field, etc. These smart materials with specific properties are extremely relevant materials in sensing technologies. Additionally, these materials provide appropriate working conditions when combined with other distinguished materials with better characteristics in the form of toughness or thermal resistance.

1.3.1 Piezoelectric (PE) material layer

During 18^{th} century Carlous Linnaeus and Franz Aepinus observed that certain materials such as crystals and ceramics, with the temperature change, generate an electric charge. In 1880, the Curie brothers, Pierre and Jacques were the first to prove the direct PE effect ([42], [232]). An unusual characteristic of certain crystalline materials such as tourmaline, topaz, quartz, cane sugar, and Rochelle salt was discovered by them. It was detected that proportional to the applied load, the tension and compression generated voltages of opposite polarity. Hankel called this the piezoelectric (PE) effect. Piezoelectricity is the electric charge that is generated in response to applied mechanical stress in certain classes of crystalline materials. Later on, at the end of 18^{th} century, the existence of the converse of PE

effect was predicted by Lippman which was confirmed by the Curie brothers. They observe that the exposure of voltage generating crystals to electric fields results in their lengthening and shortening according to the polarity of the field, and in proportion to its strength. PE materials are natural as well as man-made. The crystals like quartz, Rochelle salt, topaz, tourmaline, and some organic substances such as silk, wood, enamel, hair, rubber, tendon, collagen, etc. are natural PE materials. Certain crystals that are quartz analogs (Langasite, $La_3Ga_5SiO_{14}$ and Gallium orthophosphate $GaPO_4$), composites, ceramics (Barium Titanate, $BaTiO_3$; Lead Titanate, $PbTiO_3$; Lead Zirconate Titanate, PZT; Lithium Niobate, $LiNbO_3$), and polymers, are man-made crystals showing PE effect. PE materials have a unique atomic structure containing positive and negative ions in the form of pairs called unit cells. In most cases, the PE materials show a crystal structure with symmetry of hexagonal 6 mm class [131]. PE materials got recognition for their role in the first world war when quartz was used as resonators in SONAR (Sound Navigation and Ranging). During the period of the second world war, synthetic PE material was discovered, which later led to the development of various PE devices.

Basic governing equations and constitutive relations

(A) **Equations of motion**

The basic governing equations of motion of the PE layer in the absence of body forces are given by [143]

$$\begin{aligned} &\sigma^e_{ij,j} = \rho^e \ddot{u}^e_i, \\ &D^e_{i,i} = 0, \quad (i,j = 1,2,3). \end{aligned} \tag{1.3.1}$$

Here superscript 'e' denotes the entities in PE medium. ρ^e is the mass density of PE material. σ^e_{ij} is the stress tensor. u^e_i and D^e_i are the mechanical and electrical displacement components in the PE medium. The dot (.) denotes time (t) differentiation, the comma followed by the subscript (i) indicates space coordinate differentiation with respect to the corresponding coordinate, and the repeated subscript implies summation with respect to that index.

(B) **Constitutive relations**

The constitutive relations can be written as

$$\begin{aligned} &\sigma^e_{ij} = c^e_{ijkl} S^e_{kl} - d^e_{kij} E^e_k, \\ &D^e_j = d^e_{jkl} S^e_{kl} + \epsilon^e_{jk} E^e_k, \quad (i,j,k,l = 1,2,3). \end{aligned} \tag{1.3.2}$$

Here S^e_{kl} are the strain tensors. c^e_{ijkl}, d^e_{kij}, ϵ^e_{jk}, and E^e_k are the elastic constants, PE constants, dielectric constants, and electric field respectively.

(C) **Strain-displacement relation**

$$S^e_{ij} = \frac{1}{2}(u^e_{i,j} + u^e_{j,i}) \quad (i, j = 1, 2, 3). \tag{1.3.3}$$

(D) **Relation between electric field and the electric potential function**
Let ϕ^e be the electric potential function then

$$E^e_i = -\phi^e_{,i} \quad (i = 1, 2, 3). \tag{1.3.4}$$

It is a well established fact that surface avoustic waves (SAWs) are widely used in sensors and transducers. PE materials are extensively used in SAW devices. A structure comprising of thin film embedded on a substrate is adopted to achieve high performance. Numerous investigations have been performed for scrutinizing the characteristics of SAWs in layered PE structures by various researchers in different disciplines due to its wide and important applications in SAW devices. The propagation of SAWs through PE materials usually exhibits dispersion behavior i.e., the phase velocity is dependent on the wave number. The dispersion relation so obtained is a significant factor affecting the performances of SAW sensors ([12], [158], [217]). Thus, these dispersion relations catches the focus of attention of the researchers working in this area. The study of direct PE coupling effect to surface elastic waves was carried out by White and Voltmer [227]. A solution for dispersion relations of Love waves in a PE material and existence conditions for various modes were proposed by Curtis and Redwood [39]. The circulation of shear harmonic waves around a long metallic cylinder covered with a PE layer was illustrated by Wang *et al.* [224]. Propagation behavior of horizontally polarized shear waves (SH-waves) in a periodic PE–polymeric layered structure consisted of PE thin films bonded perfectly with polymeric thin films alternately is accomplished by Qian *et al.* [153]. The effect of initial stress on the propagation behavior of SH waves in PE coupled plates is examined by Son and Kang [204]. The study of reflection and refraction of plane waves at interface between two PE media is explored by Yuan *et al.* [236]. Borodina *et al.* [23] carried out the study of acoustics wave in a structure carrying two PE plates separated by an air (vaccum) gap. Properties of Love waves in a PE layered structure with a viscoelastic guiding layer were examined by Liu *et al.* [123] and later Liu [124] carried out a theoretical study on Love wave sensors in a structure with multiple viscoelastic layers on a PE substrate. Effect of initial stress on the propagation behavior of SAW in a layered PE structure comprising

of ZnO/Al_2O_3 is manifested by Mseddi *et al.* [136]. Ebrahimi and Dabbagh [49] analyzed the wave propagation in smart rotating porous heterogeneous PE nanaobeams. Transference of SH waves through irregular interface between corrugated PE layer and pre-stressed viscoelastic layer is examined by Chaudhary *et al.* [31] and later Chaudhary *et al.* [32] proposed an analytic model for Rayleigh wave propagation in PE layer overlaid orthotropic substratum. Singh *et al.* [189] used Green's function approach to study the propagation of SH-wave in PE layer influenced by a point source. In-plane elastic wave propagation in nanoscale periodic layered PE structures was observed by Yan *et al.* [229]. For designing highly sensitive microacoustic devices for sensing applications the propagation characteristics of Love wave form an essential basis. The propagation of Love wave in a MP-PE structure is investigated by Goyal *et al.* [76] with the objective of enhancing the performance of Love wave based devices. The dispersion properties of Love waves are utilized for the fabrication of sensor devices in the different material environments. For this Goyal and Kumar [77] studied the propagation of Love wave in a double-layered structure consisting of two finite layers of viscoelastic and PE material lying over the semi-infinite size-dependent MP substrate. Reflection and transmission of elastic waves at an interface between two MP-PE half-spaces are analyzed by Singh *et al.* [196]. The investigation of wave characteristics in PE-coupled laminated fiber-reinforced composite cylindrical shells is carried out by Bisheh *et al.* [20], by considering the transverse shear effects, rotary inertia, and different polarizations of the piezoelectricity. Comparative study of the flexoelectricity effect with a highly/weakly interface in distinct PE materials is done by Singhal *et al.* [201].

1.3.2 Piezomagnetic (PM) material layer

In the present scenario, there are laudable applications of magnetic materials in piezocomposites due to their potential for multi-functional device applications, including magnetic sensors, energy harvesters, tunable microwave devices, magnetoelectric (ME) random access memory and logic devices, and ME antenna. These composites have undoubtedly made their presence felt in this cutting-edge technology and have many future perspectives and engineering applications ([33], [35], [102]). From physical consideration, the magnetostriction phenomenon is associated with a strong coupling between the magnetic and mechanical properties of materials. PM materials are smart materials that induce spontaneous magnetic moment by application of mechanical strain and vice versa. One of the finest features of these materials is their nature to exhibit reversibility, i.e. internal generation of magnetic charge on the application of applied mechanical force and also the generation of a mechanical strain in response to the magnetic field. Piezomagneticity is the magnetic charge that is generated in response to applied mechanical stress. This can be ascribed by the dependence of the stress tensor σ^p and the magnetic field H^p towards the

magnetic induction B^p and the strain tensor S^p. The PM effect depends on various parameters of the material such as density, elastic constant, permeability, PM coefficients, etc. Some common examples of PM materials are uranium dioxide, terfenol-D, ferromagnetic materials, etc. Among magnetostrictive phases, $CoFe_2O_4$ stands out because of its very high magnetostriction which is due to high magneto-crystalline anisotropy and coercive field.

Piezomagnetism is a phenomenon similar to the formerly considered piezoelectricity [42]. Just in this case, elastic distortions turn out to be coupled with magnetic, instead of an electric field. Accordingly, all the theory can be almost identically repeated with some necessary replacements: Electric field E^e by magnetic field H^p, electric displacement D^e by magnetic induction B^p, electrical permittivity ϵ^e_{jk} by magnetic permeability m^p_{jk}, PE constant d^p_{kij} by PM constant h^p_{kij}, etc.

Basic governing equations and constitutive relations

(A) **Equations of motion**

The basic governing equations of motion of the PM layer in the absence of body forces are given by [143]

$$\begin{aligned} \sigma^p_{ij,j} &= \rho^p \ddot{u}^p_i, \\ B^p_{i,i} &= 0, \qquad (i,j=1,2,3). \end{aligned} \tag{1.3.5}$$

Here the superscript 'p' denotes the entities in PM medium. ρ^p denotes the mass density, σ^p_{ij} is the stress tensor, u^p_i are the mechanical displacement components, and B^p_i are the magnetic inductions in PM medium. The dot (.) denotes time (t) differentiation, the comma (,) followed by the subscript indicates space coordinate differentiation with respect to the corresponding coordinate, and the repeated subscript implies summation with respect to that index.

(B) **Constitutive relations**

The constitutive relations can be written as

$$\begin{aligned} \sigma^p_{ij} &= c^p_{ijkl} S^p_{kl} - h^p_{kij} H^p_k, \\ B^p_j &= h^p_{jkl} S^p_{kl} + m^p_{jk} H^p_k, \qquad (i,j,k,l=1,2,3). \end{aligned} \tag{1.3.6}$$

Here S^p_{kl} are the strain tensors. c^p_{ijkl}, h^p_{kij}, m^p_{ij}, and H^p_i are the stiffness, PM constants, magnetic permeability, and magnetic field in PM material, respectively.

(C) **Strain-displacement relation**

$$S_{ij}^{p} = \frac{1}{2}(u_{i,j}^{p} + u_{j,i}^{p}), \quad (i,j = 1,2,3). \tag{1.3.7}$$

(D) **Relation between magnetic field and the magnetic potential function**
Let ϕ^{p} be the magnetic potential function then

$$H_{i}^{p} = -\phi_{,i}^{p} \quad (i = 1,2,3). \tag{1.3.8}$$

Many researchers have transmitted numerous informative facts and figures through the study of wave propagation in smart structures to the scientific community which are engaged in revealing characteristics of the waves propagating through such structures. Alshits *et al.* [8] investigated the existence of surface waves in semi-infinite anisotropic elastic media with PE and PM properties. Propagation of Rayleigh type surface waves in a transversely isotropic PE layer on a PM half-space are explored by Pang *et al.* [147]. Wei *et al.* [226] examined SH-waves in a PE-PM coupled layered half-space. Reflection and transmission of plane waves at an imperfectly bonded interface between PE and PM media are studied by Pang *et al.* [148]. SH-wave propagation in the imperfect interface of PE-PM bilayer system was examined by Nie *et al.* [138]. Theoretical study of SH-wave propagation in periodically-layered PM structure is done by Liu *et al.* [125]. Pang *et al.* [149] analyzed the propagation of SH waves in an infinite/semi-infinite PE/PM periodically layered structure. A theoretical approach is taken into consideration by Ezzin *et al.* [66], to investigate Love wave propagation in a transversely isotropic PE layer on a PM half-space. The magneto-electrically open and short conditions are applied to solve the problem. Further, they [67] explored propagation of SH-waves in laminated PM/PE plates using the ordinary differential equation and stiffness matrix methods. Propagation of two transverse surface waves i.e., Love-type wave and BG type wave in a three-layer system consisting of a PE/PM bi-layer bonded on an elastic half-space is theoretically investigated by Nie *et al.* [139]. Scattering phenomena of shear waves by a two-phase multiferroic sensor embedded in a PE/PM medium is explored by Hashemi [89]. SH wave propagation in a PE/PM plate with an imperfect magnetoelectroelastic interface is observed by Pang *et al.* [150]. Li *et al.* [115] theoretically investigated the propagation characteristics of SH wave in PM-PE structures. Sahu *et al.* [168] explored polarized shear waves in functionally graded PE material layer sandwiched between corrugated PM layer and elastic substrate. Further, Sahu and Baroi [169] analyzed the behavior of surface waves in corrugated PM layer resting on inhomogeneous half-space. Modeling of Love-type wave propagation in a PM layer

of Terfenol-D over a lossy viscoelastic substrate was consummated by Goyal *et al.* [80]. Further, an analytical study of the transference of wave in piezo-composite layer lying over an elastic substrate is performed by Goyal and Sahu [81]. The interface of the geometry is assumed to be imperfect where imperfection is characterized by Linear Spring Model. Ray *et al.* [159] used Green's function technique to model Love type wave propagation due to an impulsive point source in a PM layered structure. The study encapsulating the reflection/refraction phenomenon of quasi-pressure waves when they strike the imperfect corrugated interfaces of PE and PM half-spaces is carried out by Ray and Singh [160].

1.3.3 Functionally graded materials

Composite material is an advanced material made from two or more constituent materials combined in solid states with remarkably different physical and chemical properties. These materials grant an excellent combination of properties that are distinct from the individual parent material. Wood is an example of natural composite material. In the mid-1980s, researchers in Japan faced this challenge in a spaceplane project which required a thermal barrier with an outside temperature of 2000 K and inside temperature of 1000 K across less than 10 mm thickness. Under extreme conditions, composite materials fail to perform [223]. To solve this limitation, researchers came up with a novel concept in the structural design of materials called functionally graded materials (FGMs) [177]. These are revolutionary materials, belonging to a class of advanced materials with material properties varying over a changing dimension [11]. Examples of naturally occurring FGMs are bones, teeth, bamboo, human skin, etc. Nature has designed these to meet the expected service requirements. To solve many engineering problems this idea is emulated from nature. FGMs eliminate the failure due to sharp interfaces existing in composite materials by replacing the sharp interface with the gradient interface resulting in the smooth transition from one material to another. Thus, FGMs are superior to conventional laminated materials. For specific functions and applications, FGMs can be designed. The graded characteristics of such materials is usually established and restrained using powder metallurgy, centrifugal casting, and chemical vapor deposition. The analytical studies of these materials typically assumes linear, exponential, and power law variation in elastic moduli of the form

$$\begin{aligned} \tilde{c_{ij}}(x) &= c_{ij}^0(1+ax) \\ \tilde{c_{ij}}(x) &= c_{ij}^0 e^{ax} \\ \tilde{c_{ij}}(x) &= c_{ij}^0 x^a \end{aligned} \tag{1.3.9}$$

where c_{ij}^0 is the value of $\tilde{c_{ij}}(x)$ at $x = 0$, a is prescribed constant responsible for functional gradedness in the material, and x is the spatial coordinate [166].

These materials have numerous applications in aircraft, aerospace engineering, the automotive industry, biomedical implants, etc. Non-destructive testing (NDT) is a wide group of analysis techniques used in the science and technology industry to evaluate the properties of a material, component, or system without causing damage. NDT methods rely upon the use of surface waves and other signal conversions to examine a wide variety of articles (metallic and non-metallic, food-product, artifacts and antiquities, infrastructure) for integrity, composition, or condition with no alteration of the article undergoing examination. Surface wave propagation phenomena in functionally graded piezo material received significant attention due to their extensive engineering applications such as surface acoustic wave (SAW) sensors, filters, and delay lines [24]. This motivates the researchers to investigate the surface wave propagation in a system involving FGMs to attain more effective usage of piezo materials in sensors and acoustic devices. Rabin and Shiota [157] were the first to suggest the concept of functionally graded materials. Ichinose [90] fabricated ultrasonic transducers with functionally graded PE ceramics. Liu and Tani [118] investigated surface waves in functionally gradient PE plates. Han and Liu [88] analyzed elastic wave propagation in a functionally graded PE cylinder. Dispersion of waves and characteristic wave surfaces in functionally graded PE plates are studied by Liu *et al.* [119]. Li *et al.* [111] investigated the features of Love waves in a layered functionally graded PE structure. The mathematical model was established based on the elastic wave theory, and the Wentzel–Kramers–Brillouin (WKB) method was applied to solve the coupled electromechanical field differential equation. Du *et al.* [44] used an exact approach to investigate the Love waves in functionally graded PE material layer bonded to a semi-infinite homogeneous solid. The propagation of Love waves in a smart functionally graded PE structure was analyzed by various researchers ([26], [27], [120], [121], [122]). Cao *et al.* [28] theoretically studied the propagation of Love waves in a functionally graded PE material layer lying in between two different homogeneous PE materials, as an upper layer and a substrate by employing the power series technique. They investigated the influence of the gradient coefficients of FGPEM, the electromechanical coupling factor, stress distributions, and the layer thickness on the phase velocity of Love waves in the considered structure. The problem of Love waves in functionally graded PE material with elastic properties having quadratic variation is discussed by Eskandari and Shodja [65]. Propagation behavior of Love waves in a functionally graded half-space with initial stress is examined by Qian *et al.* [154]. Du *et al.* [46] examined the properties of SH surface acoustic wave propagation in layered functionally graded PE material structures loaded with viscous liquid (VL). Love-type waves in functionally graded PE material sandwiched between initially

stressed layer and the elastic substrate is investigated by Saroj *et al.* [171]. Size-dependent thermo-electrical buckling analysis of functionally graded PE nanobeams is discussed by Ebrahimi and Salari [48]. Propagation of surface waves in a homogeneous layer of finite thickness over an initially stressed functionally graded magneto-electric-elastic half-space is studied by Li and Wei [114]. An analytical solution for surface wave propagation in functionally graded PE material is derived by Sahu et al. [167]. Then, Sahu *et al.* [168] explored SH waves in functionally graded PE material layer sandwiched between corrugated PM layer and elastic substrate. Furthermore, Sahu and Nirwal [170] proposed an asymptotic approximation solution for the propagation of Love-type surface waves in a smart composite structure involving functionally graded PE material. Singhal *et al.* [200] investigated the propagation of Love-type wave in functionally graded PE material layer bonded between PM plate and pre-stressed PE half-space. Spatial varying WKB method is used to obtain an analytical solution for functionally graded PE layer. in which material gradients vary exponentially in the direction of layers width. Gupta and Bhengra [86] studied the surface wave vibrations in a functionally graded material layered structure using the WKB approach. Mondal *et al.* [135] studied transference of Love-type waves in a bedded structure containing a functionally graded material and a porous PE medium. Singh *et al.* [191] analyzed the propagation behavior of Love-type wave in an exponentially graded piezoelectric-viscoelastic material stratum lying over a functionally graded piezoelectric-viscoelastic material substrate due to an impulsive point source at its interfacial surface. The electro-visco-mechanical field equations are laid down for the piezoelectric-viscoelastic medium using an analytical solution procedure that involves the use of suitable Green's function and admissible boundary conditions. Mahanty *et al.* [129] discussed the characteristics of shear acoustic waves propagating in an imperfectly bonded functionally graded PE layer over a PE cylinder. Love-type wave propagation in functionally graded PM material resting on PE half-space are examined by Baroi and Sahu [16]. Goyal and Kumar [79] investigated Love-type wave propagation in functionally graded orthotropic material layer bonded imperfectly over MP elastic substrate. Dispersion curves are plotted to illustrate the influence of imperfectness of interface, microstructure of the substrate, thickness as well as heterogeneity involved in functionally graded layer on the phase velocity of Love-type wave.

1.4 Nonlocal (NL) theory of elasticity in PE media

During the last decade, the nanoscale structures have received considerable attention from researchers ([9], [126], [178], [202]), due to their potential applications of nanoelectromechanical systems (NEMSs) like beams, plates, shells, gears, etc., in engineering fields.

These nanoscale structures have been employed in many areas like bio-engineering, actuators, nanocomposite, and nanoelectromechanical (NEM) devices. With the advancement in nanoscience and nanotechnology, NEMSs have been fabricated and employed in several industries for their superior features and promising applications in different nanodevices such as nanoresonators, nanosensors, and nanogenerators. In the NEMSs, the nanoscale size effect plays an important role. Some studies have reported that the NEMSs at nanoscale show a size-dependent manner. Overlooking the size-effect in designing of NEMSs may lead to completely incorrect predictions and hence inaccurate designs and irreparable damages. Hence, for the realistic designing of NEMSs comprising of PE materials, the size effect should be taken into account to achieve reliable results with appropriate accuracy. To achieve high performance various SAW devices and sensors are comprised of layered structures with a PE material layer deposited on the substrate. It is to be noted that the mechanical properties of PE materials are also size-dependent. Focussing on the PE effects, the band structures of elastic waves in nanoscale smart periodic structures can be tuned actively which can provide some new instincts for the designs and applications of the nanoscale wave devices [34]. Recent investigations in the nanoscale field reveal that the materials are not continuous at the nanoscale. Therefore, a mathematical model based on the classical theory of elasticity is incapable to investigate this behavior. The experimental analysis also indicates that materials in nanostructures do not obey the continuum theory [173]. For this reason, new theories are developed to account for nanoscale effects in small structures. One of the well-known theory which is used in the nanoscale analysis is Eringen's nonlocal (NL) theory ([61]- [64]). The NL solutions of the dispersion curves for time-harmonic waves (e.g. plane, Rayleigh, and other surface waves) perfectly fit with the atomic dispersion curves throughout the entire Brillouin zone obtained by lattice dynamic computations [62]. The NL theory of elasticity has been studied by many researchers ([52], [53]). In the NL theory of elasticity, the stress at any reference point within a continuous body is not only a function of strain at that point but also the function of the strain fields at all other points of the body. Thus, the NL stress forces act as remote action forces. Such types of forces are intermittently confronted in the atomic theory of lattice dynamics. The distinctive features of NL theory may fall in the materials with microstructures, where the internal characteristic length (e.g. grain size) may be considered as comparable with an external characteristic length (e.g. wavelength). The NL theory help to explain and predict the physical phenomena at small length scales i.e. at nanoscales, by employing NL parameter $\Upsilon = e_0 l^n$ in the formulation. l^n being the internal characteristic length and e_0 is a material constant. The internal characteristic length l^n is the interatomic distance e.g. length of C-C bond (0.142 mm in Carbon nanotube) [195].

Basic governing equations and constitutive relations

(A) **Equations of motion**

The basic governing equations of motion in nonlocal PE medium can be expressed as [34]

$$\begin{aligned} \sigma^n_{ij,j} &= \rho^n \ddot{u^n_i}, \\ D^n_{i,i} &= 0, \quad (i,j=1,2), \end{aligned} \tag{1.4.1}$$

where ρ^n is the density of the PE material. A comma $(,)$ in the subscript denotes the differentiation with respect to some spatial coordinates while a superposed dot notation signifies time (t) derivative.

(B) **Constitutive relations**

The constitutive relations for the PE material based on NL elasticity theory can be written as

$$\begin{aligned} (1-\Upsilon^2\nabla^2)\sigma^n_{ij} &= c^n_{ijkl}S^n_{kl} - d^n_{kij}E^n_k, \\ (1-\Upsilon^2\nabla^2)D^n_j &= d^n_{jkl}S^n_{kl} + \epsilon^n_{jk}E^n_k, \quad (i,j,k,l=1,2,3), \end{aligned} \tag{1.4.2}$$

where σ^n_{ij} and S^n_{kl} are the stress and strain tensors, respectively. D^n_i and E^n_i are the components of electric displacement vector and electric field vector, respectively. c^n_{ijkl}, d^n_{kij}, and ϵ^n_{jk} are the elastic stiffness constants, PE constants, and dielectric constants, respectively. ∇^2 denotes the Laplace operator. $\Upsilon = e_0 l^n$ is the NL parameter which denotes the small scale effect. Here e_0 is the material constant and l^n is the internal characteristic length.

(C) **Strain-displacement relations**

$$S^n_{ij} = \frac{1}{2}(u^n_{i,j} + u^n_{j,i}) \quad (i,j=1,2,3). \tag{1.4.3}$$

At a glance, it can be seen that in the absence of nonlocality, the constitutive equations (1.4.2) reduce to those for local PE medium [147].

Various problems concerned with surface wave propagation using NL theory of elasticity have been attempted by many researchers ([93], [144], [162], [165]). In NL visco-elastic solids, Acharya and Mondal [3] deduced the Rayleigh surface wave propagation with small wavelength. Later, using NL theory of elasticity they [4] studied the effect of rotation on Rayleigh surface waves. In general anisotropic medium, Chakraborty [30] scrutinized the effect of NL elasticity on wave propagation. The non-locality effect on the dispersion relation is compared with its local (classical) effect on the wave response. The work done by

Gopalakrishnan and Narender [74] on application of NL elastic models pertaining to wave propagation in nano-structure is significant in the research area. Reflection of plane longitudinal waves from the stress-free boundary of a (nonlocal micropolar) NLMP solid half-space are explored by Khurana and Tomar [98]. They showed four dispersive waves namely, an independent longitudinal displacement wave, an independent longitudinal micro-rotational wave and two sets of coupled transverse waves, propagating in NLMP elastic solid medium. Later they [99] examined Rayleigh-type waves in NLMP solid half-space. The propagation of time-harmonic plane waves in an infinite NL elastic solid material with voids has been examined by Singh *et al.* [195]. Kaur *et al.* [95] considered Rayleigh type wave propagation in an isotropic homogeneous NL elastic solid half-space with voids. Furthermore, Kaur *et al.* [96] extended their investigation in analyzing the propagation of Love waves in a NL elastic layer with voids resting over a NL solid half-space. NL and nonlinear contributions to the thermal and elastic high-frequency wave propagations at the nanoscale are explored by Sellitto and Domenico [174]. For solving dynamic problems, Martowicz *et al.* [130] used NL elasticity in shape memory alloys, modeled using peridynamics. Ebrahimi *et al.* [50] investigated wave propagation characteristics in magneto-electro-elastic (MEE) nanotube considering shell model in the framework of the NL theory. Using Hamilton's principle, NL governing equations of MEE nanotube have been derived. Later Ebrahimi and Seyfi [51] analyzed wave propagation in smart inhomogeneous PE nanosize beams rested on an elastic medium using NL theory. Sarkar and Tomar [172] examined plane waves in NL thermoelastic solid with voids. Rayleigh-type surface waves in a NL thermoelastic solid half-space with voids are investigated by Singh [197]. Constitutive relations and field equations are developed by Kumar and Tomar [107], for an isotropic linear MP thermoelastic material with voids within the context of Eringen's theory of NL elasticity. It is found that six plane waves may propagate in this medium consisting of four sets of coupled dilatational waves and two sets of coupled transverse waves. All the waves are found to be affected by the nonlocality of the medium. Biswas [21] studied the propagation of Rayleigh waves in a NL thermoelastic layer lying over a NL thermoelastic half-space. Gholami *et al.* [70] developed a size-dependent Euler-Bernoulli beam model to analyze the nonlinear free vibration of a bidirectional functionally graded nanobeam with immovable ends, based on the NL theory.

Chapter 2

Modelling of Love-type waves in an elastic layer sandwiched between viscous liquid half-space and size-dependent couple stress substrate[1]

2.1 Introduction

A surface acoustic wave (SAW) is an acoustic wave that propagates along the surface of a material with an amplitude that decays exponentially with depth into the substrate. Acoustic wave based sensors are extensively used for a range of sensor fields including physical sensing, chemical sensing, and biosensing employing in both gas and liquid environments ([163], [164]). To explore more applications of the sensors, occasionally they are laden with viscous liquid (VL) layer ([43], [104]). These types of hydro-structural problems while dealing with viscous incompressible fluid arise frequently in several important industrial applications, such as melting and solidification, crystal growth, glass and metal forming processes, etc [47]. For liquid sensing applications those acoustic waves are preferred which have the particle displacement parallel to the device surface and normal to the direction of wave propagation [91]. The energy of these acoustic waves is concentrated in the proximity of the surface being in contact with the measured liquid. Although Rayleigh waves can be utilized in sensors working in liquid environment ([106], [179]) but Love-type wave based devices are preferred due to high sensitivities. Due to the shear horizontal particle displacements, Love-type wave based devices can operate effectively both in liquid and gas environments [19]. So these devices are being used as viscosity sensors, biosensors, and chemical sensors ([220], [225], [237]). To enhance the performance of conventional SAW devices based on such periodic wave guiding layers, several structure models were reviewed ([17], [228]). These Love-type wave based devices consist of an elastic layer bonded to an elastic substrate. Due to the difference in mechanical properties of the substrate, the

[1]Contents of this chapter are published in SCIE indexed journal, Journal of Theoretical and Applied Mechanics, 57(4), 1009-1019, 2019. DOI:10.15632/jtam-pl/112457 with I.F. = 0.927

layer acoustic energy gets entrapped near the surface causing penetration of the wave in the substrate. A larger part of the wave is confined in the guiding layer only because of its in-plane behavior, thus enhancing the sensitivity of the device [94]. Many researchers have studied the influence of VL on acoustic waves propagating in layered structures. Propagation of Bleustein-Gulyaev (BG) wave in 6 mm piezoelectric (PE) materials loaded with VL is studied by Guo and Sun [85]. Du *et al.* ([45], [46]) analyzed VL loading effect on surface waves propagating in layered structures comprising of PE material layers. Kielczynski *et al.* [101] studied the effect of VL loading on Love wave propagation. Vikstrom and Voinova [221] investigated surface acoustic waves with horizontal polarization (SH-SAWs) propagating in a three-layer system consisting of an elastic substrate and two viscoelastic overlayers. Baroi *et al.* [15] studied the propagation of polarized shear horizontal waves in the VL layer resting over a porous PE half-space.

For designing Love-type wave based devices, the dispersion relation so obtained is very important. This relation provides the phase velocity of a wave in terms of guiding layer thickness and physical properties of substrate and layer. As discussed in Chapter 1, different researchers have provided the dispersion curves for one or more layers on a substrate. However, ignoring the size dependency of the substrate may lead to less valid results. Therefore, for designing more efficient Love-type wave based devices, a general dispersion relation is needed by considering the size-dependent properties of the substrate. Considering the merits of size-dependent model over the classical model, in this chapter we intend to study the impact of VL (Newtonian) loading on Love-type wave propagation in an elastic layer overlying half-space substrate exhibiting microstructural properties by employing the consistent couple stress (CS) theory given by Hadjesfandiari and Dargush [87]. This model considers one length scale parameter η^c called a couple stress coefficient and two Lam*é* parameters λ^c and μ^c. Further, η^c is associated with characteristic length parameter l^c as $\eta^c = \mu^c (l^c)^2$.

2.1.1 Formulation of the problem

To model the present problem, we have considered a hybrid structure consisting of an elastic layer loaded with a VL (Newtonian) lying over a CS half-space substrate. The thickness of the elastic layer is h. The wave fields are functions of x and y, so the problem considered here is two dimensional. The Cartesian coordinate system is considered in such a way that a Love-type wave is propagating along y-axis and x-axis is considered positive in the vertically downward direction as shown in Fig. 2.1.

Let $\overrightarrow{U^o} = (u_1^o, u_2^o, u_3^o)$ and $\overrightarrow{U^c} = (u_1^c, u_2^c, u_3^c)$ be the mechanical displacement components in the middle elastic layer and the lower CS half-space substrate, respectively. The Love-type wave is transmutating along the direction of y-axis, inducing displacement in z-direction

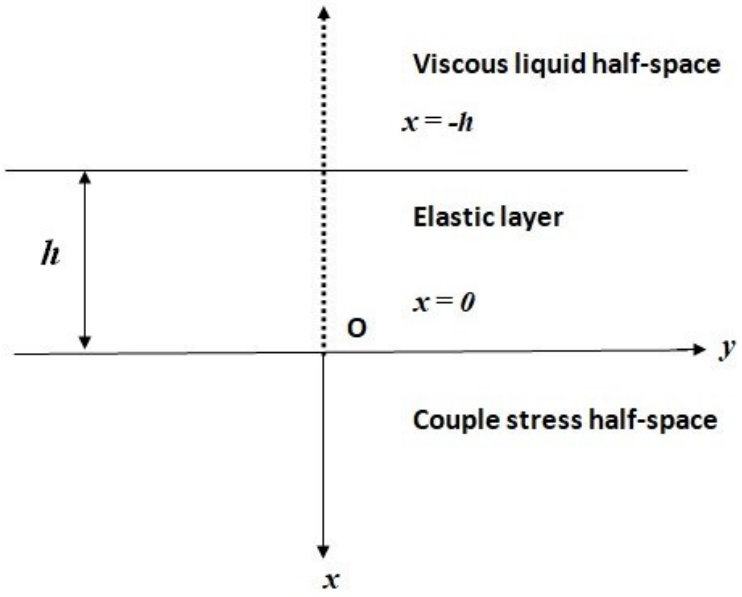

Figure 2.1: Schematic illustration

only. We shall assume that

$$\begin{aligned} u_1^o = u_2^o = 0, \quad u_3^o = u_3^o(x, y, t), \\ u_1^c = u_2^c = 0, \quad u_3^c = u_3^c(x, y, t), \text{ and } \frac{\partial}{\partial z} \equiv 0. \end{aligned} \tag{2.1.1}$$

2.1.2 Viscous liquid (VL) region

A nonconductive VL layer is considered. The liquid motion is evoked by the propagation of Love-type waves traveling in harmonic wave-form. The embroil inertial term is deserted in the Navier-Stokes equation. Also, for the wave propagation, only shear deformation is deliberated and the pressure gradient is ignored. The Navier-Stokes equation for a VL (Newtonian) half-space with velocity field v^l in the z-direction is given by [85]

$$\frac{\partial v^l}{\partial t} - \frac{\eta^l}{\rho^l}\left(\frac{\partial^2 v^l}{\partial x^2} + \frac{\partial^2 v^l}{\partial y^2}\right) = 0, \tag{2.1.2}$$

where superscript 'l' indicates the entities in VL. η^l is the coefficient of viscosity and ρ^l is the density of the VL (Newtonian).
We assume the solution of Eq. (2.1.2) of the velocity field v^l in the VL be

$$v^l(x, y, t) = V(x)e^{ik(y-ct)}, \tag{2.1.3}$$

where k is a wave number and c is a phase velocity of wave.
Invoking Eq. (2.1.3) into Eq. (2.1.2) gives

$$V''(x) - (\gamma^l)^2 V(x) = 0, \tag{2.1.4}$$

where $\gamma^l = \sqrt{k^2 - \frac{ikc\rho^l}{\eta^l}}$ and $Re(\gamma^l) > 0$.
Solving (2.1.4) we get

$$V(x) = A_1 e^{\gamma^l x} + \hat{A}_1 e^{-\gamma^l x}, \tag{2.1.5}$$

where A_1 and $\hat{A}_1$ are arbitrary constants.
By invoking Eq. (2.1.5) into Eq. (2.1.3), we get the velocity component in VL as

$$v^l(x, y, t) = (A_1 e^{\gamma^l x} + \hat{A}_1 e^{-\gamma^l x}) e^{ik(y-ct)}. \tag{2.1.6}$$

With the help of Eq. (2.1.6), the only non-vanishing shear stress component is given by

$$\sigma^l_{zx} = \eta^l \frac{\partial v^l}{\partial x} \quad = \eta^l \gamma^l (A_1 e^{\gamma^l x} - \hat{A}_1 e^{-\gamma^l x}) e^{ik(y-ct)}. \tag{2.1.7}$$

With increasing distance from the wave guide surface, $x \to -\infty$, the amplitude of the Love-type wave decays to zero. The condition $Re(\gamma^l) > 0$ assures this phenomenon.
From Eqs. (2.1.6) and (2.1.7), the final solution for the velocity and shear stress components in VL is

$$\begin{aligned} v^l(x, y, t) &= A_1 e^{\gamma^l x} e^{ik(y-ct)}, \\ \sigma^l_{zx} = \eta^l \frac{\partial v^l}{\partial x} &= A_1 \eta^l \gamma^l e^{\gamma^l x} e^{ik(y-ct)}. \end{aligned} \tag{2.1.8}$$

2.1.3 Elastic surface layer

The basic governing equation of motion in the absence of body forces for the elastic surface layer is given by [203]

$$\frac{1}{a_1^2} \frac{\partial^2 u_3^o}{\partial t^2} = \frac{\partial^2 u_3^o}{\partial x^2} + \frac{\partial^2 u_3^o}{\partial y^2}, \tag{2.1.9}$$

where superscript 'o' indicates the entities in elastic layer. $a_1 = \sqrt{\frac{\mu^o}{\rho^o}}$ is bulk shear wave velocity, μ^o is the shear modulus of elasticity, and ρ^o is the density of the elastic layer.
Assuming the solution of Eq. (2.1.9) of the mechanical displacement component in the elastic layer as

$$u_3^o(x, y, t) = \overline{U^o}(x) e^{ik(y-ct)}. \tag{2.1.10}$$

Implementing Eq. (2.1.10) into Eq. (2.1.9) results in a differential equation

$$\overline{U^o}''(x) + a_2^2\overline{U^o}(x) = 0, \tag{2.1.11}$$

where $a_2 = \sqrt{\frac{k^2c^2}{a_1^2} - k^2}$.
Solution to this differential equation (2.1.11) under the assumption that $c > a_1$, is substituted in Eq. (2.1.10), we get the displacement component as

$$u_3^o(x, y, t) = (A_2\cos(a_2x) + A_3\sin(a_2x))e^{ik(y-ct)}, \tag{2.1.12}$$

where A_2 and A_3 are arbitrary constants.
The shear stress component will be given by

$$\sigma_{zx}^o = \mu^o\frac{\partial u_3^o}{\partial x} = \mu^o a_2(-A_2\sin(a_2x) + A_3\cos(a_2x))e^{ik(y-ct)}. \tag{2.1.13}$$

2.1.4 Couple stress (CS) theory

The basic governing equation of motion of CS theory for isotropic material in vector form, in the absence of body forces [87] is given by

$$(\lambda^c + \mu^c + \eta^c\nabla^2)\nabla(\nabla.\overrightarrow{U^c}) + (\mu^c - \eta^c\nabla^2)\nabla^2\overrightarrow{U^c} = \rho^c\frac{\partial^2\overrightarrow{U^c}}{\partial t^2}. \tag{2.1.14}$$

Here superscript 'c' indicates the entities in CS substrate. λ^c and μ^c are Lam*é* constants, $\eta^c = \mu^c(l^c)^2$ is CS coefficient, l^c is characteristic length, ρ^c is density of the material, and $\nabla^2 = \frac{\partial^2}{\partial x^2} + \frac{\partial^2}{\partial y^2} + \frac{\partial^2}{\partial z^2}$.
The constitutive relations of CS theory are given by

$$\sigma_{ji}^c = \lambda^c u_{k,k}^c\delta_{ij} + \mu^c(u_{i,j}^c + u_{j,i}^c) - \eta^c\nabla^2(u_{i,j}^c - u_{j,i}^c), \tag{2.1.15}$$

$$\mu_{ji}^c = 4\eta^c(\omega_{i,j}^c - \omega_{j,i}^c), \quad \omega_i^c = \frac{1}{2}\epsilon_{ijk}u_{k,j}^c, \tag{2.1.16}$$

where σ_{ji}^c is the non-symmetric stress tensor, δ_{ij} is Kronecker's delta, ω_i^c is a rotation vector, ϵ_{ijk} is a permutation tensor, and μ_{ji}^c is skew-symmetric CS tensor.
Imposing conditions from Eq. (2.1.1), into equation of motion (2.1.14), we obtain

$$\frac{\partial^2 u_3^c}{\partial x^2} + \frac{\partial^2 u_3^c}{\partial y^2} - (l^c)^2\left(\frac{\partial^4 u_3^c}{\partial x^4} + 2\frac{\partial^4 u_3^c}{\partial x^2\partial y^2} + \frac{\partial^4 u_3^c}{\partial y^4}\right) = \frac{1}{a_3^2}\frac{\partial^2 u_3^c}{\partial t^2}, \tag{2.1.17}$$

where $a_3 = \sqrt{\frac{\mu^c}{\rho^c}}$, μ^c is the shear modulus of elasticity, and ρ^c is the material density of the CS substrate.
The shear stress component and CS component are given by

$$\sigma_{zx}^c = \mu^c \frac{\partial u_3^c}{\partial x} + \eta^c \left(\frac{\partial^3 u_3^c}{\partial y^2 \partial x} + \frac{\partial^3 u_3^c}{\partial x^3} \right), \tag{2.1.18}$$

$$\mu_{xy}^c = -2\eta^c \left(\frac{\partial^2 u_3^c}{\partial x^2} + \frac{\partial^2 u_3^c}{\partial y^2} \right). \tag{2.1.19}$$

Presuming the solution of differential equation (2.1.17) as

$$u_3^c(x, y, t) = F(x) e^{ik(y-ct)}, \tag{2.1.20}$$

where k is the wave number and c is the phase velocity.
Thus, differential equation (2.1.17) reduces to

$$\frac{d^4 F(x)}{dx^4} - \Re_1 \frac{d^2 F(x)}{dx^2} + \Re_2 F(x) = 0, \tag{2.1.21}$$

where

$$\Re_1 = \tfrac{1}{(l^c)^2} + 2k^2, \qquad \Re_2 = k^4 + \left(\tfrac{k}{l^c}\right)^2 - \left(\tfrac{kc}{l^c a_3}\right)^2.$$

Solution of the above differential equation becomes

$$F(x) = A_4 e^{-a_4 x} + A_5 e^{-a_5 x} + \hat{A}_4 e^{a_4 x} + \hat{A}_5 e^{a_5 x} \tag{2.1.22}$$

where A_4, A_5, $\hat{A}_4$, and $\hat{A}_5$ are arbitrary constants. Here
$a_4 = \sqrt{\frac{\Re_1 + \sqrt{\Re_1^2 - 4\Re_2}}{2}}$,
$a_5 = \sqrt{\frac{\Re_1 - \sqrt{\Re_1^2 - 4\Re_2}}{2}}$.
Using the radiation condition, as $x \to \infty$, the amplitude of the Love-type wave decays to zero. Then the displacement component under the assumption $c < a_3$ may be expressed as

$$u_3^c(x, y, t) = \left(A_4 e^{-a_4 x} + A_5 e^{-a_5 x} \right) e^{ik(y-ct)}. \tag{2.1.23}$$

Using Eq. (2.1.23) in above Eqs. (2.1.18) and (2.1.19), we get

$$\sigma_{zx}^c = \left(A_4 a_4 a_6 e^{-a_4 x} + A_5 a_5 a_7 e^{-a_5 x} \right) e^{ik(y-ct)}, \tag{2.1.24}$$

$$\mu_{xy}^c = -2\eta^c \left(A_4 (a_4^2 - k^2) e^{-a_4 x} + A_5 (a_5^2 - k^2) e^{-a_5 x} \right) e^{ik(y-ct)}, \tag{2.1.25}$$

where
$a_6 = -\mu^c + k^2\eta^c - a_4^2\eta^c$,
$a_7 = -\mu^c + k^2\eta^c - a_5^2\eta^c$.

2.2 Boundary conditions

Following are the boundary conditions for the considered model.

- Velocity components should be continuous at the interfacial surface.

$$\frac{\partial u_3^o}{\partial t} = v^l \quad \text{at } x = -h. \tag{2.2.1}$$

- Displacement components must be continuous at the interface.

$$u_3^o = u_3^c \quad \text{at } x = 0. \tag{2.2.2}$$

- The magnitude of shear component of the stress tensors should be equal at the interface.

$$\sigma_{zx}^l = \sigma_{zx}^o \quad \text{at } x = -h. \tag{2.2.3}$$

$$\sigma_{zx}^c = \sigma_{zx}^o \quad \text{at } x = 0. \tag{2.2.4}$$

- CS component of substrate should vanish at the interface.

$$\mu_{xy}^c = 0 \quad \text{at } x = 0. \tag{2.2.5}$$

2.3 Derivation of dispersion relation

Using above mentioned boundary conditions from Eqs. (2.2.1) to (2.2.5), the following equations in terms of five unknown coefficients $A_1,\ A_2,\ A_3,\ A_4$, and A_5 are procured

$$e^{-\gamma^l h}A_1 + ikc\cos(a_2 h)A_2 - ikc\sin(a_2 h)A_3 = 0 \tag{2.3.1}$$

$$A_2 - A_4 - A_5 = 0 \tag{2.3.2}$$

$$\eta^l\gamma^l e^{-\gamma^l h}A_1 - \mu^o a_2\sin(a_2 h)A_2 - \mu^o a_2\cos(a_2 h)A_3 = 0 \tag{2.3.3}$$

$$\mu^o a_2 A_3 - a_4 a_6 A_4 - a_5 a_7 A_5 = 0 \tag{2.3.4}$$

$$(a_4^2 - k^2)A_4 + (a_5^2 - k^2)A_5 = 0 \tag{2.3.5}$$

2.3.1 Dispersion relation

To get the non-trivial solution and hence the dispersion relation, we equate the determinant of these coefficients to zero. By solving the determinant, we get the following dispersion equation for Love-type wave in a sandwiched elastic layer loaded with VL lying over CS substrate.

$$\begin{aligned}&\mu^o a_2 \cos(a_2 h)[a_5 a_7(a_4^2 - k^2) - a_4 a_6(a_5^2 - k^2)] - \mu^{o2} a_2^2 \sin(a_2 h)(a_5^2 - a_4^2) \\ &+ ikc\eta^l \gamma^l \left\{\sin(a_2 h)[a_4 a_6(a_5^2 - k^2) - a_5 a_7(a_4^2 - k^2)] - \mu^o a_2 \cos(a_2 h)(a_5^2 - a_4^2)\right\} = 0.\end{aligned} \tag{2.3.6}$$

The real part of Eq. (2.3.6) gives the dispersion equation and the imaginary part gives the damping equation associated with Love-type surface wave propagation. After separating real and imaginary parts of (2.3.6), we get the dispersion equation and damping equation as (2.3.7) and (2.3.8), respectively.

$$(P_3 + \gamma_2 P_5)P_1 - (P_4 - \gamma_2 P_6)P_2 = 0, \tag{2.3.7}$$

$$P_5 P_1 + P_6 P_2 = 0, \tag{2.3.8}$$

where
$P_1 = a_5 a_7(a_4^2 - k^2) - a_4 a_6(a_5^2 - k^2)$,
$P_2 = \mu^o a_2(a_5^2 - a_4^2)$,
$P_3 = \mu^o a_2 \cos(a_2 h)$,
$P_4 = \mu^o a_2 \sin(a_2 h)$,
$P_5 = \eta^l kc \sin(a_2 h)$,
$P_6 = \eta^l kc \cos(a_2 h)$,
$T = \frac{kc\rho^l}{\eta^l}$,
$\gamma^l = \gamma_1 + i\gamma_2$,
$\gamma_1 = \sqrt{\frac{T}{2}} + \frac{k^2}{2\sqrt{2T}}$,
$\gamma_2 = -\sqrt{\frac{T}{2}} + \frac{k^2}{2\sqrt{2T}}$.

2.3.2 Particular cases and validation of result

Case-I

In the absence of VL layer i.e. $\eta^l \to 0$, $\rho^l \to 0$ will lead to $P_5 = 0$ and $P_6 = 0$, then the dispersion equation (2.3.7) will reduce to

$$\frac{P_1}{P_2} = \tan(a_2 h). \tag{2.3.9}$$

Eq. (2.3.9) represents the dispersion equation of Love-type wave in an elastic layer of finite thickness h overlying semi-infinite CS substrate.

Case-II

Furthermore in Case-I, if $l^c \to 0$ then semi-infinite CS substrate reduces to isotropic elastic half-space substrate and the dispersion equation reduces to

$$\mu^o \sqrt{\frac{c^2}{{a_1}^2} - 1} \tan\left(kh\sqrt{\frac{c^2}{a_1^2} - 1}\right) = \mu^1 \sqrt{1 - \frac{c^2}{\overline{a_3}^2}}, \tag{2.3.10}$$

where c is the phase velocity of Love-type wave, $a_1 = \sqrt{\frac{\mu^o}{\rho^o}}$, and $\overline{a_3} = \sqrt{\frac{\mu^1}{\rho^1}}$. μ^1 is the shear modulus of elasticity and ρ^1 is the density of isotropic elastic half-space. This Eq. (2.3.10) is the well-known dispersion relation for Love-type waves in the classical structure [128] under the assumption $a_1 < c < \overline{a_3}$ which validates the outcomes of the present problem.

2.4 Numerical results and discussion

Numerical computations have been performed to analyze the theoretical result obtained as dispersion relation in the previous section. To demonstrate the numerical computations, an isotropic, homogeneous, Copper (Cu) surface layer is considered as middle elastic layer and Dionysos marble is considered as CS half-space substrate. Following data has been taken into account for the graphical illustrations.

Table 2.1: Material constants for VL layer [101]

$\eta^l = 50\ Pas, \qquad \rho^l = 10^3\ kg/m^3$

Table 2.2: Material constants for elastic layer (Cu surface layer) [101]

$\mu^o = 3.91 \times 10^{10}\ N/m^2,\ \ \rho^o = 8.9 \times 10^3 kg/m^3,\ \ a_1 = (\mu^o/\rho^o)^{1/2} = 2096 m/s$

Table 2.3: For semi-infinite CS substrate [218]

$\mu^c = 3.05 \times 10^{10}\ N/m^2,$	$\rho^c = 2.717 \times 10^3\ kg/m^3,$	$a_3 = (\mu^c/\rho^c)^{1/2} = 3350\ m/s$

The graphs depicting the microstructural effects of substrate, viscosity, and density effects of VL loadings, and thickness effect of sandwiched elastic layer are shown in Figs. 2.2-2.6, for dimensionless phase velocity (c/a_1) versus dimensionless wave number (kh). The Love-type wave exhibits a multimode character. In various practical applications (e.g., in sensors and non-destructive testing techniques (NDTs)), the most important is the fundamental (the lowest) mode of Love-type waves. Therefore, our attention is confined to the fundamental mode of propagating Love-type wave. One common feature observed among all profiles is that phase velocity is decreasing as wave number is increasing.

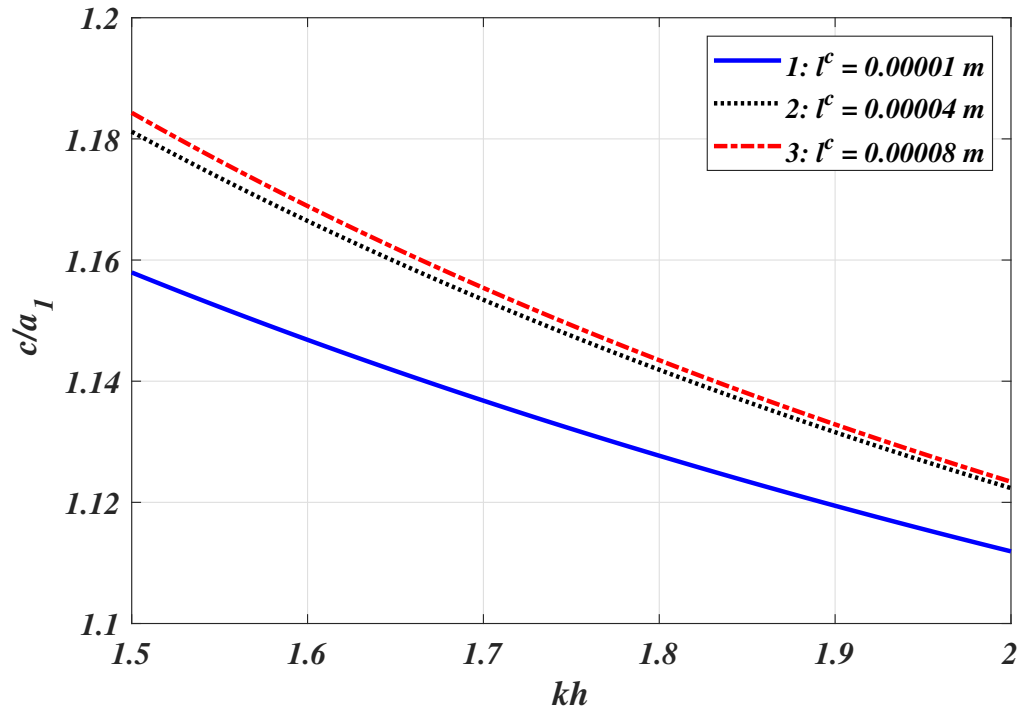

Figure 2.2: Dispersion curves (c/a_1 versus kh) for varying values of characteristic length parameter (l^c)

2.4.1 Effect of microstructure

To better observe the dependence of Love-type wave propagation on material length scale parameter, the dispersion curves are compared for distinct values of characteristic lengths as shown in Fig. 2.2. It is pointed out by the researchers that it is not possible to find the exact value of the characteristic length. It is of the order of cell size of the considered

material. The profile has been plotted by taking the characteristic length to be of the order of 10^{-5}. The thickness of the sandwiched elastic layer is fixed as $h = 0.0004$ m. It is concluded that the characteristic length of the material significantly affects the phase velocity profiles. The increase in values of characteristic length parameter (l^c) results in the increase in the phase velocity of the Love-type wave.

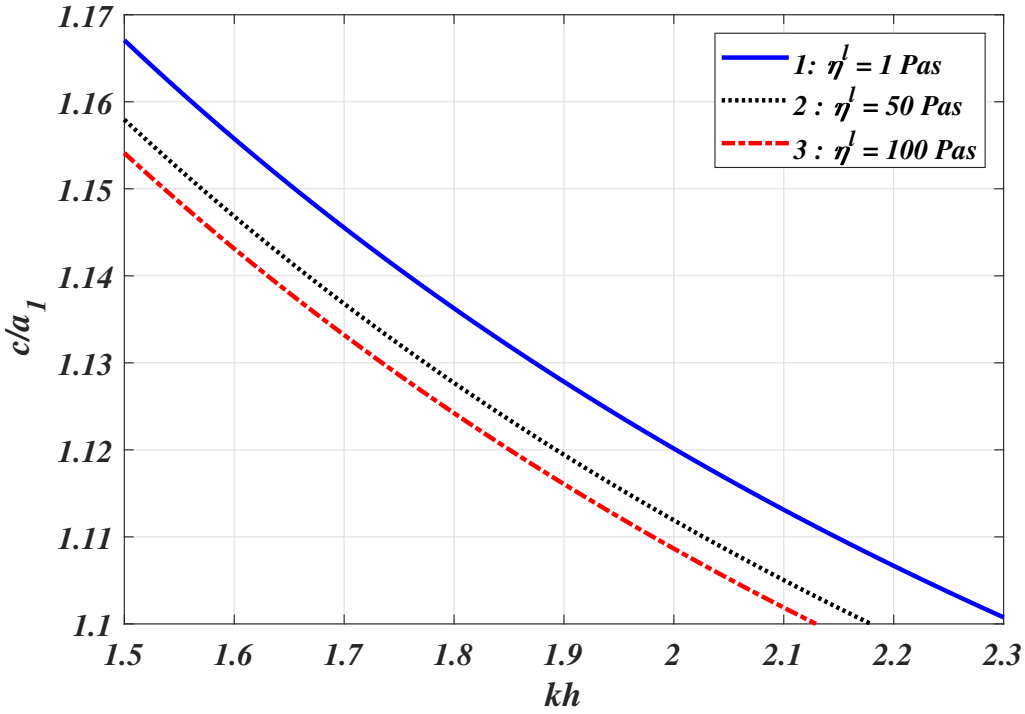

Figure 2.3: Dispersion curves (c/a_1 versus kh) for varying values of coefficient of viscosity parameter (η^l)

2.4.2 Effect of VL loading

The effect of the coefficient of viscosity is depicted in Fig. 2.3. The dispersion curves are computed for varying values of coefficient of viscosity parameter (η^l). Here characteristic length of the material is assumed as $l^c = 0.00001\ m$. The thickness of elastic layer is employed as $h = 0.0004\ m$. The density of the VL is also fixed i.e., $\rho^l = 1000\ kg/m^3$. It is observed that the viscosity parameter disfavors the phase velocity. As the viscosity of the liquid is increasing, the phase velocity of the Love-type wave is decreasing.

To study the effect of liquid mass density of VL (Newtonian) layer on the velocity profile we considered different VLs of different densities and nearly equal viscosities. For graphical illustration, following data has been taken into account:

1. Gasoline: $\eta^l = 0.006$ Pas, $\rho^l = 719.7\ kg/m^3$.
2. Kerosene: $\eta^l = 0.00164$ Pas, $\rho^l = 820\ kg/m^3$.

3. Water: $\eta^l = 0.001$ Pas, $\rho^l = 1000\ kg/m^3$.

It can be spotted from Fig. 2.4 that as the density of the liquid is increasing, it leads to an increase in the phase velocity of the propagating wave. As an illustration, to confer the entire effect of VL loading on the hybrid structure, Fig. 2.5 is plotted under the presence and absence of VL loading and it can be concluded that VL loading has a suppressing effect on the transmittance of Love-type wave.

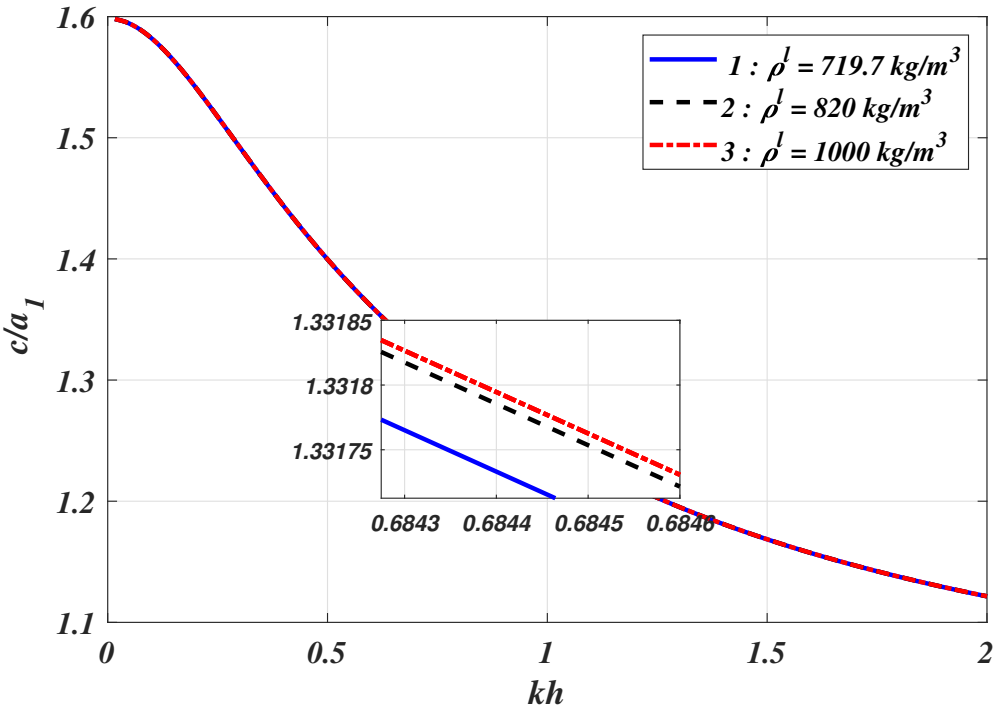

Figure 2.4: Dispersion curves (c/a_1 versus kh) for varying values of density parameter (ρ^l) of VL loading

2.4.3 Effect of thickness of sandwiched elastic layer

The impact of thickness of the sandwiched elastic layer on Love-type wave propagation in the considered structure is shown in Fig. 2.6. To capture this effect we have considered different values of thickness $h = 0.0006\ m, 0.0008\ m, 0.001\ m$ of sandwiched elastic layer. Also, the characteristic length of the material is laid out as $l^c = 0.00001\ m$. It is observed that with the increase in thickness of the sandwiched elastic layer, the phase velocity of the propagating wave decreases.

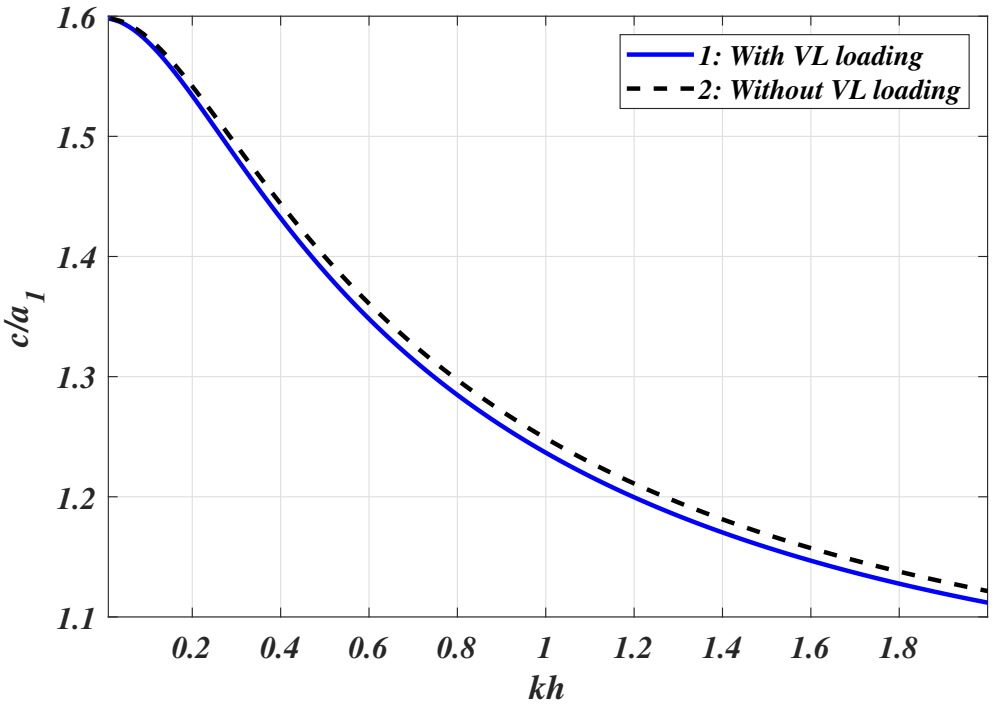

Figure 2.5: Dispersion curves (c/a_1 versus kh) for the entire effect of VL loading

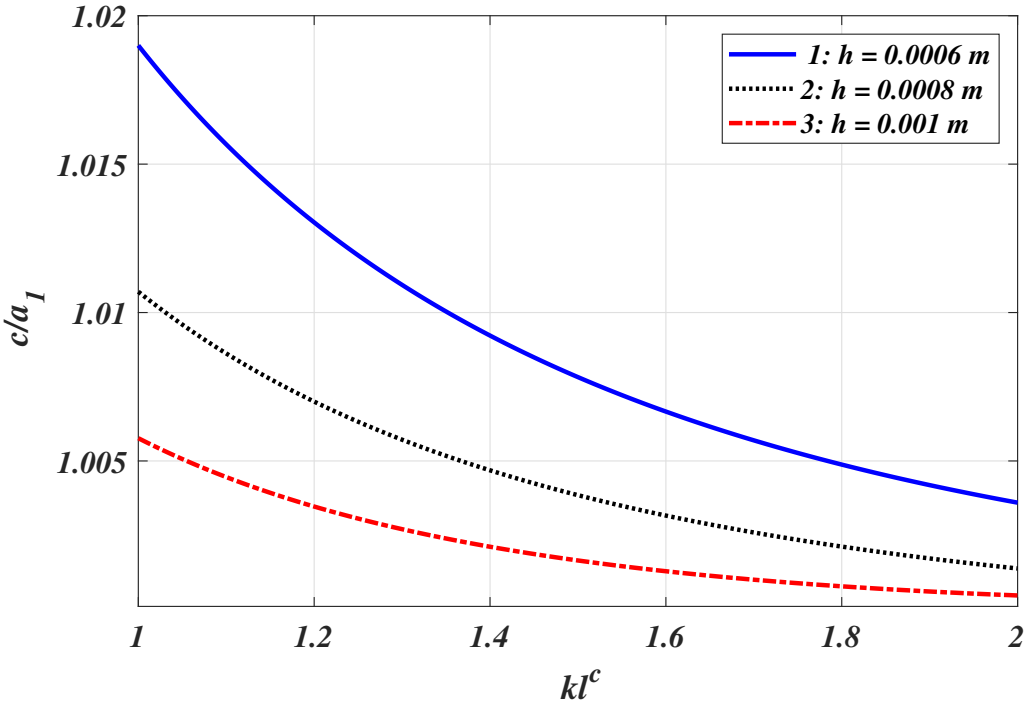

Figure 2.6: Dispersion curves (c/a_1 versus kl^c) for varying values of thickness (h) of elastic layer

2.5 Conclusions

Following conclusions are observed in the present study.

- The graphical representations reveal that the phase velocity increases with the increase in characteristic length parameter.
- The viscosity parameter has a reverse effect on the phase velocity. As the viscosity parameter of the VL (Newtonian) increases, the phase velocity of the wave decreases.
- The density of the VL (Newtonian) is favorable to the velocity profile of the Love wave. The increase in density of the VL (Newtonian), increases the phase velocity profile of Love-type wave propagation.
- The entire effect of VL loading on the phase velocity profile of the propagating Love-type wave is suppressing.
- The thickness of sandwiched elastic layer disfavors the velocity profile of the wave. The increase in the thickness of the elastic layer leads to a decrease in phase velocity of the wave.

Chapter 3

Microstructural and viscous liquid loading effects on the propagation of Love waves in a piezomagnetic layered structure [2]

3.1 Introduction

Piezomagnetic (PM) materials can couple mechanical and magnetic energies via linking material stress and strain to magnetic signals and vice versa. In other words, when the PM materials are subjected to an external magnetic field, they get deformed whereas mechanical stress induces a change in the magnetic state (reverse effect) of the material. This can be explained by the dependence of the stress tensor σ^p and the magnetic field H^p toward the magnetic induction B^p and the strain tensor S^p. Embracing unique and eminent properties, this smart material has enormous possible benefits in smart devices and even nanoscale devices and structures owing to representing outstanding magnetic and mechanical coupling performances. Compared with piezoelectric (PE) sensors, the PM sensor has a simple structure, large output power, convenient manufacture, low cost, strong signal, and good anti-interference performance. In PM sensor signal, amplifier circuit is simple without charge amplifier and is suitable for static and dynamic force measurement. Experimental data is stable and can be directly measured with general wire [188]. Research on the PM properties of force-sensitive films of sensors has become a subject undergoing intense study ([156], [243]). Due to the promising applications of PM materials as multifunctional devices ([35], [102]) viz. magnetomechanical sensors, actuators, acoustic and ultrasonic transducers, wave propagation phenomena in these materials captured mass attention ([66], [67]). Sometimes SAW devices are immersed in viscous fluid or loaded with viscous liquid (VL) layer to explore more utilizations like the measurement of viscosity, mass density and the acoustic-electric phenomenon of liquids ([1], [152]). To extend the study of Love-type waves carried in Chapter 2 propagating in the smart material layer, the elastic layer is replaced with PM material layer. PM materials are smart materials.

[2]Contents of this chapter are published in SCIE indexed journal, Mechanics of Advanced Materials and Structures, 28(16), 1703-1713, 2021. DOI: 10.1080/15376494.2019.1702235 with I.F. = 4.030

From physical consideration, the magnetostriction phenomenon is associated with a strong coupling between the magnetic and mechanical properties of materials. Some common examples of piezomagnetic materials are uranium dioxide, terfenol-D, ferromagnetic materials, etc. Among magnetostrictive phases, $CoFe_2O_4$ stands out because of its very high magnetostriction which is due to high magneto-crystalline anisotropy and coercive field. Immense applications in the configuration of SAW devices, transducers, Love wave sensors, and other similar types of devices are perceived by the surface wave propagation in a stratified structure comprising of PM layer followed by a semi-infinite substrate. To confer the VL loading effect and microstructural effect on the propagation of Love-type waves in a smart material, a mathematical model comprising of PM material embedded on a CS half-space substrate [87] exhibiting microstructural properties laden with VL (Newtonian) is discussed in this chapter. Dispersion relations for magnetically open (MO) and magnetically short (MS) conditions are obtained. Graphical illustrations reveal that the phase velocity of the propagating wave is remarkably affected by VL loading, microstructural parameter, and PM parameters. The obtained findings may significantly contribute to enhance the performance of Love-type wave based SAW devices comprising of smart material layer functioning in a liquid environment.

3.1.1 Formulation of the problem

Consider semi-infinite couple stress (CS) substrate covered with a piezomagnetic (PM) layer of thickness h_p. The PM layer is considered as transversely isotropic in nature, loaded with VL (Newtonian) layer of thickness h_l shown in Fig. 3.1. The Cartesian coordinate system is considered in such a way that a Love-type wave is propagating along y-axis and x-axis is considered positive in the vertically downward direction. The displacement components along with stress components in VL layer can be procured from Eqs. (2.1.6), and (2.1.7) in Chapter 2.

The basic governing equation of motion and constitutive relations of CS theory for isotropic material in the absence of body forces are discussed in Chapter 2 and the displacement components along with stress components can be acquired from Eqs. (2.1.23), (2.1.24), and (2.1.25).

3.1.2 Piezomagnetic (PM) layer

Let $\overrightarrow{U^p} = (u_1^p, u_2^p, u_3^p)$ be the mechanical displacement components in the middle PM layer obtained due to the propagation of Love-type wave. Love-type wave is propagating along the direction of y-axis causing displacement in z-direction only. We shall assume that

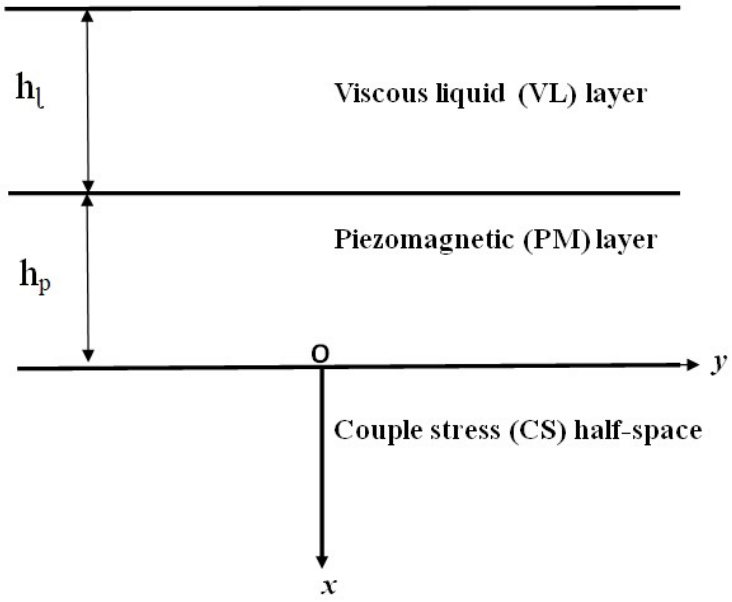

Figure 3.1: Schematic illustration

$$u_1^p = u_2^p = 0, \quad u_3^p = u_3^p(x, y, t). \tag{3.1.1}$$

The basic governing equation and constitutive relations of the PM layer in the absence of body forces are given by [143]

$$\begin{aligned} \sigma_{ij,j}^p &= \rho^p \frac{\partial^2 u_i^p}{\partial t^2}, \\ B_{i,i}^p &= 0, \quad (i, j = 1, 2, 3), \end{aligned} \tag{3.1.2}$$

$$\begin{aligned} \sigma_{ij}^p &= c_{ijkl}^p S_{kl}^p - h_{kij}^p H_k^p, \\ B_j^p &= h_{jkl}^p S_{kl}^p + m_{jk}^p H_k^p, \qquad (i, j, k, l = 1, 2, 3) \end{aligned} \tag{3.1.3}$$

respectively. Here superscript 'p' indicates the entities in PM layer. ρ^p denotes the mass density. σ_{ij}^p and S_{kl}^p are the stress and strain tensors, respectively. c_{ijkl}^p, h_{kij}^p, m_{ij}^p, H_i^p, and B_i^p are the stiffness, PM constants, magnetic permeability, magnetic field, and magnetic inductions, respectively.

The constitutive relations can be written as [80]

$$
\begin{aligned}
\sigma_x^p &= c_{11}^p S_x^p + c_{12}^p S_y^p + c_{13}^p S_z^p - h_{31}^p H_z^p, \\
\sigma_y^p &= c_{12}^p S_x^p + c_{11}^p S_y^p + c_{13}^p S_z^p - h_{31}^p H_z^p, \\
\sigma_z^p &= c_{13}^p S_x^p + c_{13}^p S_y^p + c_{33}^p S_z^p - h_{33}^p H_z^p, \\
\sigma_{zx}^p &= c_{44}^p S_{zx}^p - h_{15}^p H_x^p, \\
\sigma_{yz}^p &= c_{44}^p S_{yz}^p - h_{15}^p H_y^p, \\
\sigma_{xy}^p &= \frac{1}{2}(c_{11}^p - c_{12}^p) S_{xy}^p, \\
B_x^p &= h_{15}^p S_{zx}^p + m_{11}^p H_x^p, \\
B_y^p &= h_{15}^p S_{yz}^p + m_{11}^p H_y^p, \\
B_z^p &= h_{31}^p S_x^p + h_{31}^p S_y^p + h_{33}^p S_z^p + m_{33}^p H_z^p.
\end{aligned}
\tag{3.1.4}
$$

The strain components are defined as

$$
\begin{aligned}
S_x^p = u^p{}_{1,x}, \quad S_y^p = u^p{}_{2,y}, \quad S_z^p = u^p{}_{3,z}, \\
S_{yz}^p = u^p{}_{3,y} + u^p{}_{2,z}, \quad S_{zx}^p = u^p{}_{1,z} + u^p{}_{3,x}, \quad S_{xy}^p = u^p{}_{1,y} + u^p{}_{2,x}.
\end{aligned}
\tag{3.1.5}
$$

The relation between magnetic field and the magnetic potential function can be calculated through following formula:

$$
H_x^p = -\phi_{,x}^p, \quad H_y^p = -\phi_{,y}^p, \quad H_z^p = -\phi_{,z}^p, \tag{3.1.6}
$$

where ϕ^p represents the magnetic potential.
Substituting Eq. (3.1.1) in Eqs. (3.1.5) and (3.1.6), we get

$$
\begin{aligned}
S_x^p = S_y^p = S_z^p = 0, \\
S_{yz}^p = u^p{}_{3,y}, \quad S_{zx}^p = u^p{}_{3,x}, \quad S_{xy}^p = 0, \\
H_x^p = -\phi_{,x}^p, \quad H_y^p = -\phi_{,y}^p, \quad H_z^p = 0.
\end{aligned}
\tag{3.1.7}
$$

Putting Eqs. (3.1.7) in Eqs. (3.1.3) and then substituting in Eqs. (3.1.2), we obtain the governing equations for the PM layer as

$$
\begin{aligned}
\nabla^2 u_3^p &= \frac{1}{b_1^2} \frac{\partial^2 u_3^p}{\partial t^2}, \\
\nabla^2 \phi^p &= \frac{1}{b_1^2} \left(\frac{h_{15}^p}{m_{11}^p} \right) \frac{\partial^2 u_3^p}{\partial t^2},
\end{aligned}
\tag{3.1.8}
$$

where $c_{44}^{*} = c_{44}^{p} + \frac{{h_{15}^{p}}^{2}}{m_{11}^{p}}$ and $b_1 = \sqrt{\frac{c_{44}^{*}}{\rho^p}}$ is the shear wave velocity in the PM layer.
We assume the following solutions of the mechanical displacement component and magnetic potential function of the Love-type wave in the PM layer

$$\begin{aligned} u_3^p(x,y,t) &= \hat{U}_p(x)e^{ik(y-ct)}, \\ \phi^p(x,y,t) &= \Phi_p(x)e^{ik(y-ct)}, \end{aligned} \tag{3.1.9}$$

where k is the wave number and c is the phase velocity of the wave. Invoking Eqs. (3.1.9) in Eqs. (3.1.8), we obtain

$$\begin{aligned} \hat{U_p}''(x) + b_2^2 k^2 \hat{U}_p(x) &= 0, \\ \Phi_p''(x) - k^2\Phi_p(x) + \left(\frac{k^2c^2h_{15}^p}{b_1^2 m_{11}^p}\right)(B_1\sin(kb_2x) + B_2\cos(kb_2x)) &= 0, \end{aligned} \tag{3.1.10}$$

where $b_2 = \sqrt{\frac{c^2}{b_1^2} - 1}$.
On solving differential equations (3.1.10), the displacement component and magnetic potential function under the assumption $c > b_1$ can be expressed as

$$u_3^p(x,y,t) = (\sin(kb_2x)B_1 + \cos(kb_2x)B_2)e^{ik(y-ct)}, \tag{3.1.11}$$

$$\phi^p(x,y,t) = \left(\frac{h_{15}^p}{m_{11}^p}\sin(kb_2x)B_1 + \frac{h_{15}^p}{m_{11}^p}\cos(kb_2x)B_2 + e^{-kx}B_3 + e^{kx}B_4\right)e^{ik(y-ct)}, \tag{3.1.12}$$

where B_1, B_2, B_3, and B_4 are arbitrary constants.

3.2 Boundary conditions

Following are the boundary conditions for the considered model.

(i) The mechanical traction free condition at $x = -(h_l + h_p)$ is

$$\sigma_{zx}^l = 0. \tag{3.2.1}$$

(ii) The velocity and stress components are continuous at the interfacial surface $x = -h_p$

$$\begin{aligned} \frac{\partial u_3^p}{\partial t} &= v^l, \\ \sigma_{zx}^p &= \sigma_{zx}^l. \end{aligned} \tag{3.2.2}$$

(iii) The magnetic circuit conditions at $x = -h_p$ are given as

$$\begin{aligned} B_x^p &= 0, \quad \{\text{magnetically open (MO) condition}\}, \\ \phi^p &= 0, \quad \{\text{magnetically short (MS) condition}\}. \end{aligned} \tag{3.2.3}$$

(iv) At the interface $x = 0$, the displacement and stress components are continuous

$$\begin{aligned} u_3^p &= u_3^c, \\ \sigma_{zx}^p &= \sigma_{zx}^c, \\ \mu_{xy}^c &= 0, \\ \phi^p &= 0. \end{aligned} \tag{3.2.4}$$

3.3 Derivation of dispersion relations

From above mentioned boundary conditions (3.2.1) to (3.2.4), the following equations in terms of eight unknown coefficients $A_1,\ \hat{A}_1\ B_1,\ B_2,\ B_3,\ B_4,\ A_4,$ and A_5 are obtained.

$$e^{-\gamma^l(h_l+h_p)}A_1 - e^{\gamma^l(h_l+h_p)}\hat{A}_1 = 0, \tag{3.3.1}$$

$$e^{-\gamma^l h_p}A_1 + e^{\gamma^l h_p}\hat{A}_1 - ikc\sin(b_2 k h_p)B_1 + ikc\cos(b_2 k h_p)B_2 = 0, \tag{3.3.2}$$

$$\begin{aligned} &\eta^l\gamma^l e^{-\gamma^l h_p}A_1 - \eta^l\gamma^l e^{\gamma^l h_p}\hat{A}_1 - c_{44}^* k b_2\cos(b_2 k h_p)B_1 - c_{44}^* k b_2\sin(b_2 k h_p)B_2 \\ &+ k h_{15}^p e^{k h_p}B_3 - k h_{15}^p e^{-k h_p}B_4 = 0, \end{aligned} \tag{3.3.3}$$

$$e^{k h_p}B_3 - e^{-k h_p}B_4 = 0, \tag{3.3.4}$$

$$-\frac{h_{15}^p}{m_{11}^p}\sin(b_2 k h_p)B_1 + \frac{h_{15}^p}{m_{11}^p}\cos(b_2 k h_p)B_2 + e^{k h_p}B_3 + e^{-k h_p}B_4 = 0, \tag{3.3.5}$$

$$B_2 - A_4 - A_5 = 0, \tag{3.3.6}$$

$$c_{44}^* k b_2 B_1 - k h_{15}^p B_3 + k h_{15}^p B_4 - a_6 A_4 - a_7 A_5 = 0, \tag{3.3.7}$$

$$(k^2 - a_4^2)A_4 + (k^2 - a_5^2)A_5 = 0, \tag{3.3.8}$$

$$\frac{h_{15}^p}{m_{11}^p}B_2 + B_3 + B_4 = 0. \tag{3.3.9}$$

3.3.1 Dispersion relations

To get the non-trivial solution and hence the dispersion relation, we equate the determinant of these coefficients to zero. The dispersion equation will be given by the real part of the dispersion relation and the damping equation will be given by the imaginary part of the dispersion relation. After separating real and imaginary parts, we get the dispersion equations for magnetically open and short condition, respectively.

3.3.1.1 Dispersion relation for MO condition

After eliminating the unknown constants from Eqs. (3.3.1)-(3.3.4) and (3.3.6)-(3.3.9), we get the following dispersion equation for Love-type wave propagation in PM layer loaded with VL, overlying semi-infinite CS substrate, for MO condition.

$$c_{44}^{*}b_2\left[\wp_1-\wp_6 tan(b_2kh_p)\right]-\left[tan(b_2kh_p)\wp_1+\wp_6\right]\wp_4=0. \tag{3.3.10}$$

3.3.1.2 Dispersion relation for MS condition

After eliminating the unknown constants from Eqs. (3.3.1)-(3.3.3) and (3.3.5)-(3.3.10), we get the following dispersion equation for Love-type wave propagation in PM layer loaded with VL, overlying semi-infinite CS substrate, for MS condition.

$$\left(\frac{2{h_{15}^{p}}^2}{m_{11}^{p}}\right)\left[1-\frac{\sec(b_2kh_p)}{\cosh(kh_p)}\right]\wp_6+k(a_4^2-a_5^2)\wp_3\wp_7-\wp_2\wp_5+\left[k(a_4^2-a_5^2)\wp_2-\wp_5\wp_7\right]\wp_4=0. \tag{3.3.11}$$

$T=\frac{kc\rho^l}{\eta^l}$,
$\gamma^l=\gamma_1+i\gamma_2$,
$\gamma_1=\sqrt{\frac{T}{2}}+\frac{k^2}{2\sqrt{2T}}$,
$\gamma_2=-\sqrt{\frac{T}{2}}+\frac{k^2}{2\sqrt{2T}}$,
$\wp_1=\wp_5-\left(\frac{k{h_{15}^{p}}^2}{m_{11}^{p}}\right)\tanh(kh_p)(a_4^2-a_5^2)$,
$\wp_2=c_{44}^{*}b_2\tanh(kh_p)-\tan(b_2kh_p)\left(\frac{{h_{15}^{p}}^2}{m_{11}^{p}}\right)$,
$\wp_3={c_{44}^{*}}^2b_2^2-\frac{{h_{15}^{p}}^4}{{m_{11}^{p}}^2}$,
$\wp_4=\eta^l c(\gamma_1\tan(\gamma_2h_l)+\gamma_2\tanh(\gamma_1h_l))$,
$\wp_5=a_6(a_5^2-k^2)-a_7(a_4^2-k^2)$,
$\wp_6=c_{44}^{*}b_2k(a_4^2-a_5^2)$,
$\wp_7=\tan(b_2kh_p)\tanh(kh_p)$.

3.3.2 Particular cases and validation of results

Case-I

In the absence of VL layer i.e. $\eta^l \to 0$ and $\rho^l = 0$ will lead to $\wp_4 = 0$, then the dispersion equations (3.3.10) and (3.3.11) will reduce to

$$\tan(b_2 k h_p)\wp_6 - \wp_1 = 0, \tag{3.3.12}$$

$$\left(\frac{2h_{15}^{p\ 2}}{m_{11}^p}\right)\left[1 - \frac{\sec(b_2 k h_p)}{\cosh(k h_p)}\right]\wp_6 + k(a_4^2 - a_5^2)\wp_3\wp_7 - \wp_2\wp_5 = 0, \tag{3.3.13}$$

respectively. Eqs. (3.3.12) and (3.3.13) represent the dispersion equations of Love-type wave in PM layer overlying semi-infinite CS substrate, for MO and MS conditions, respectively.

Case-II

Pondering the previous case, if the PM constant h_{15}^p is removed by taking $h_{15}^p = 0$. Then $c_{44}^* = c_{44} = \mu^o$ (say), $\wp_1 \to \wp_5$, and Eqs. (3.3.12) and (3.3.13) can be diminished to

$$\tan(\overline{b_2} k h_p)\overline{\wp_6} = \wp_5, \tag{3.3.14}$$

$$k(a_4^2 - a_5^2)\overline{\wp_3}\ \overline{\wp_7} = \overline{\wp_2}\wp_5, \tag{3.3.15}$$

respectively. Eqs. (3.3.14) and (3.3.15) describes the dispersion equations of Love-type wave in an isotropic elastic layer of thickness h_p overlying semi-infinite CS substrate for MO and MS conditions, respectively.

Here $\overline{b_2} = \sqrt{\frac{c^2}{a_1{}^2} - 1}$, $a_1 = \sqrt{\frac{\mu^o}{\rho^o}}$, where μ^o is the shear modulus of elasticity, and ρ^o is the density of isotropic elastic layer.

Values of newly introduced $\overline{\wp_2}$, $\overline{\wp_3}$, $\overline{\wp_6}$, and $\overline{\wp_7}$ are as follows

$\overline{\wp_2} = \mu^o \overline{b_2} \tanh(k h_p)$,

$\overline{\wp_3} = \mu^{o2} \overline{b_2}^2$,

$\overline{\wp_6} = \mu^o \overline{b_2} k(a_4^2 - a_5^2)$,

$\overline{\wp_7} = \tan(\overline{b_2} k h_p) \tanh(k h_p)$.

Case-III

Furthermore in Case-II, if $l^c \to 0$ then semi-infinite CS substrate reduces to isotropic elastic half-space substrate and the dispersion equations for both open and short conditions reduce

to

$$\tan\left(kh_p\sqrt{\frac{c^2}{a_1^2}-1}\right)=\frac{\mu^1\sqrt{1-\frac{c^2}{\overline{a_3}^2}}}{\mu^o\sqrt{\frac{c^2}{a_1^2}-1}}, \tag{3.3.16}$$

where c is the phase velocity of Love wave.
Here $\overline{a_3}=\sqrt{\frac{\mu^1}{\rho^1}}$, μ^1 is the shear modulus of elasticity, and ρ^1 is the density of isotropic elastic half-space.
This Eq. (3.3.16) is the well-known dispersion relation for Love waves in the classical structure [128] under the assumption $a_1 < c < \overline{a_3}$ that validates the outcomes of the present problem.

3.4 Numerical results and discussion

The objective of this section is to unravel the influence of various affecting parameters, viz., coefficient of viscosity, liquid mass density, microstructural parameter, the thickness of VL layer, and thickness of PM layer on the phase velocity of Love-type wave by employing the dispersion curves plotted under the variation of dimensionless phase velocity (c/b_1) against dimensionless wave number (kh_p). To exhibit the analytical outcomes numerically, PM layer of $CoFe_2O_4$, CS substrate which is made of Dionysos marble bearing microstructural properties are considered. The values of material constants for VL layer and CS half-space are provided in Chapter 2 in Section 2.4. as Tables 2.1 and 2.3, respectively. For PM layer the values for material constants are as follows:

Table 3.1: Material constants for PM layer [147]

Material	Elastic constant c_{44}^p $(10^9 Nm^{-2})$	Mass density ρ^p (kgm^{-3})	PM constant h_{15}^p $(NA^{-1}m^{-1})$	Magnetic permeability m_{11}^p $(10^{-6}\ Ns^2C^{-2})$
$CoFe_2O_4$	45.3	5300	550	157

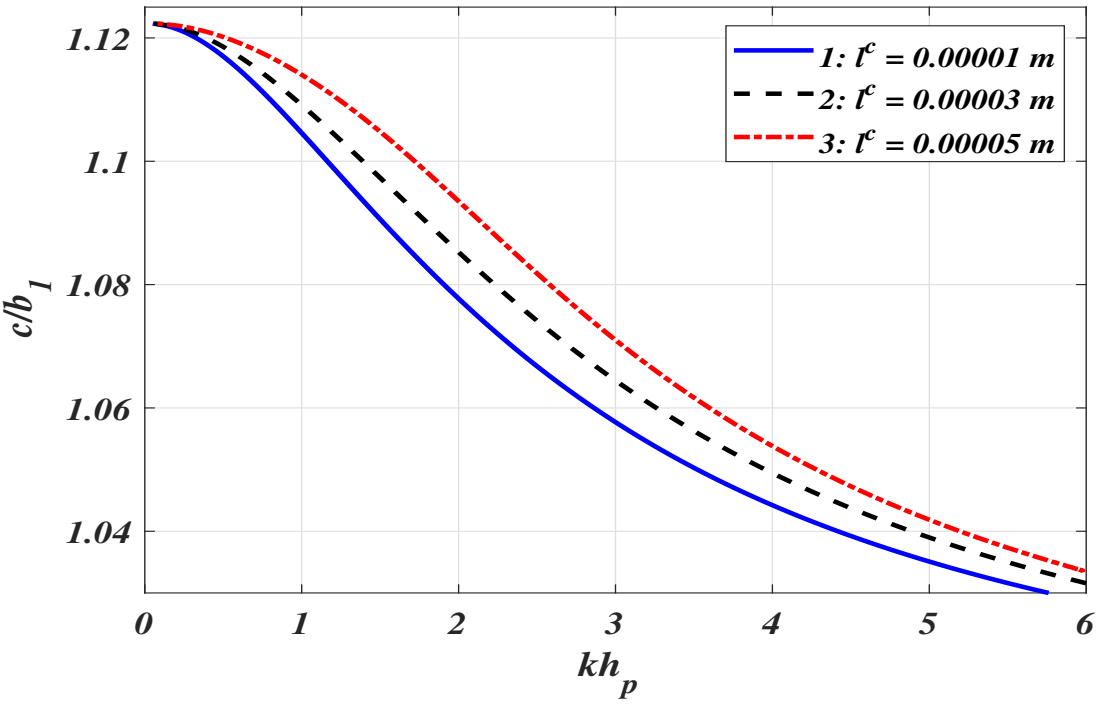

(a) MO condition

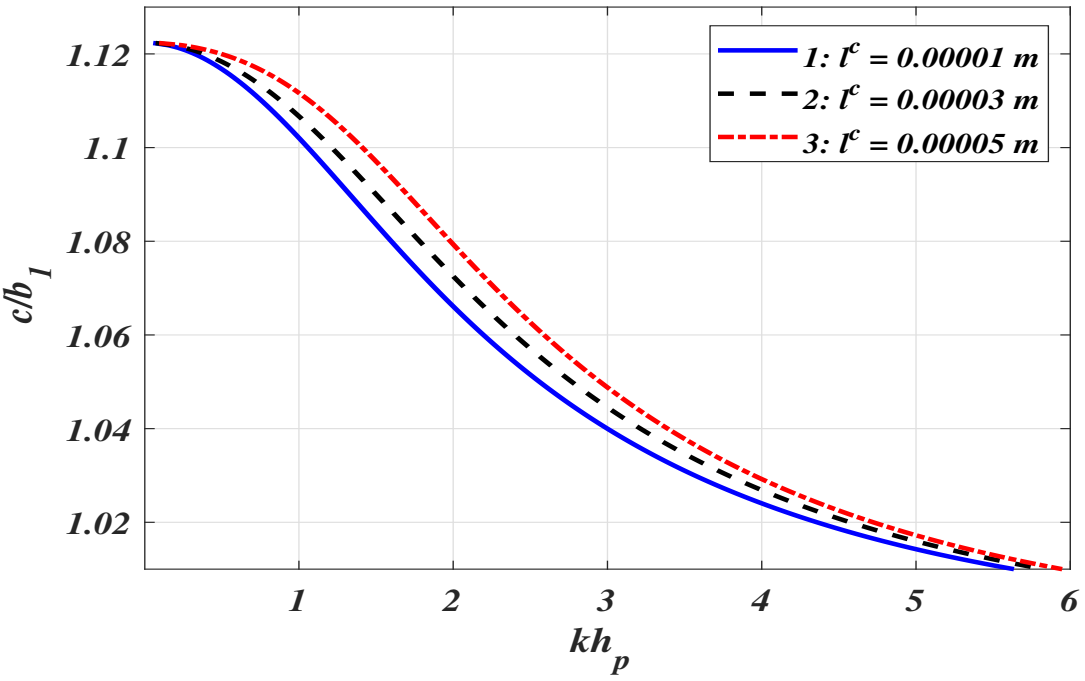

(b) MS condition

Figure 3.2: Dispersion curves (c/b_1 versus kh_p) for varying values of characteristic length parameter (l^c).

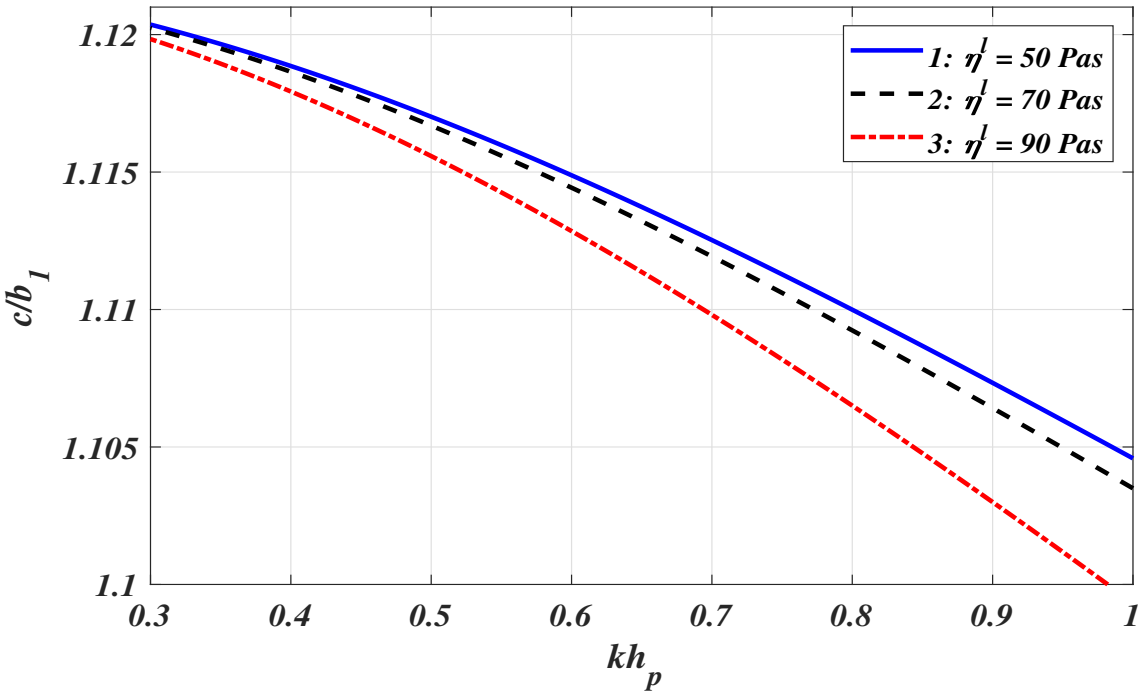

(a) MO condition

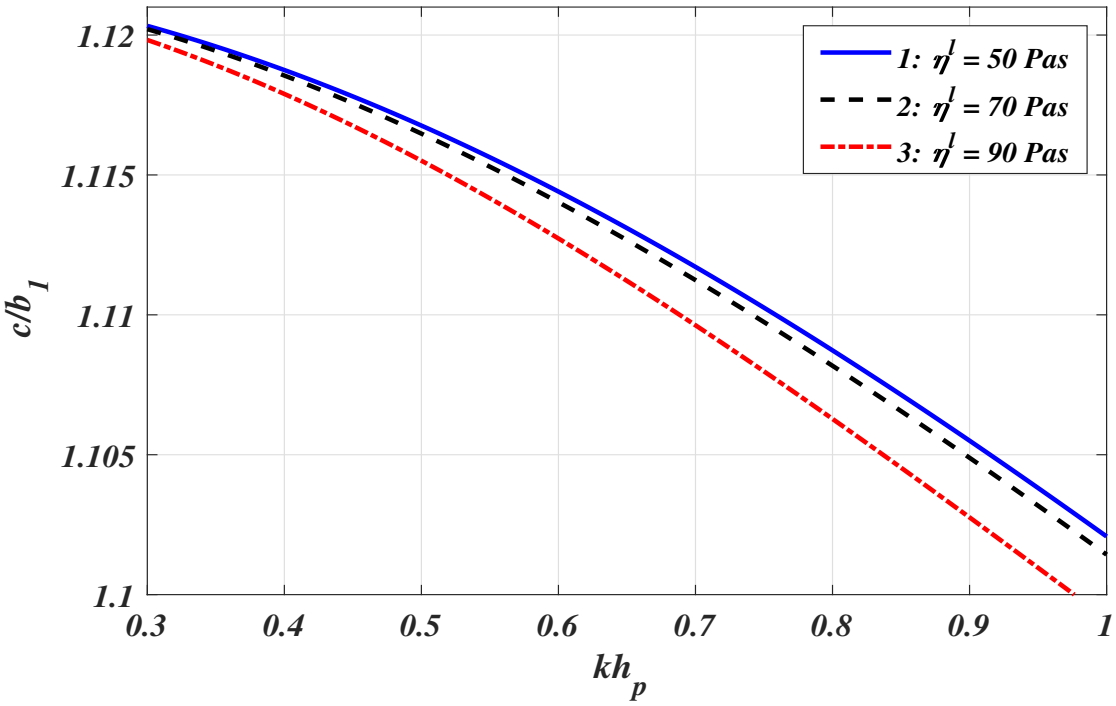

(b) MS condition

Figure 3.3: Dispersion curves (c/b_1 versus kh_p) for varying values of coefficient of viscosity (η^l) of VL layer

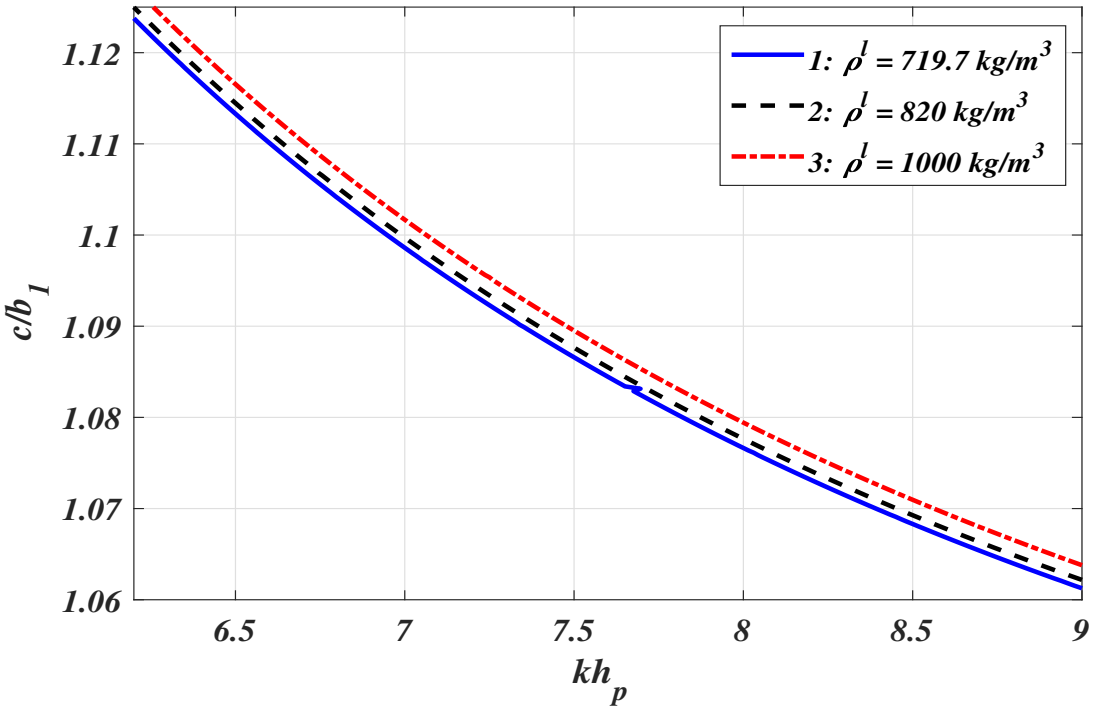

(a) MO condition

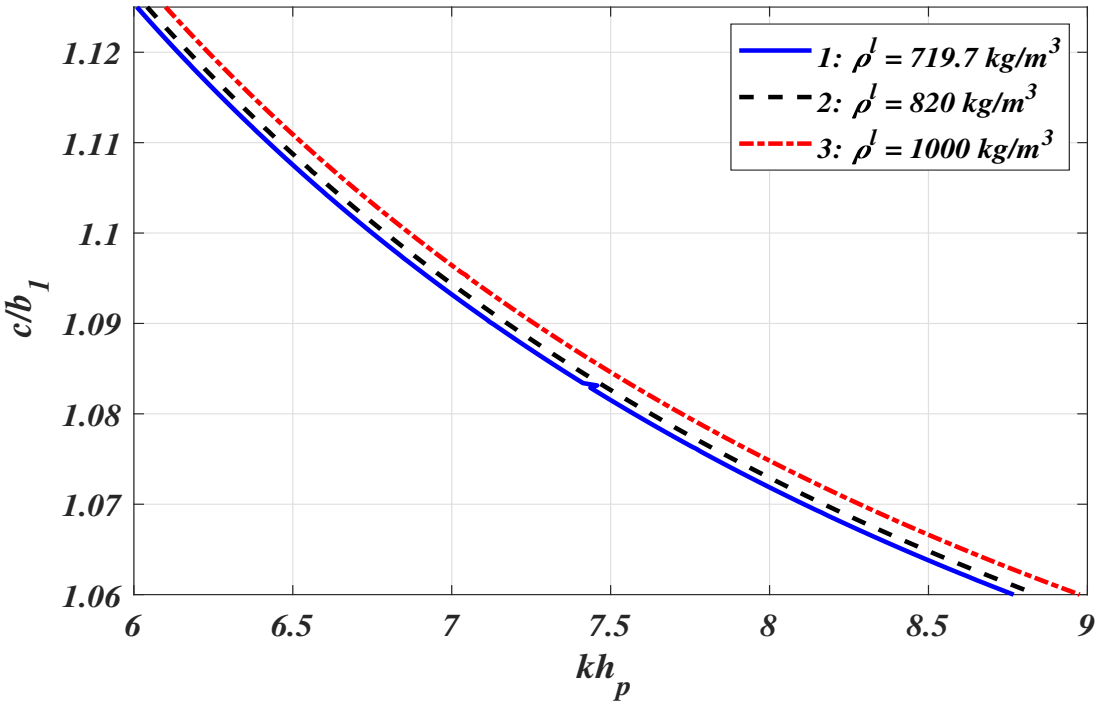

(b) MS condition

Figure 3.4: Dispersion curves (c/b_1 versus kh_p) for varying values of liquid mass density (ρ^l) of VL layer

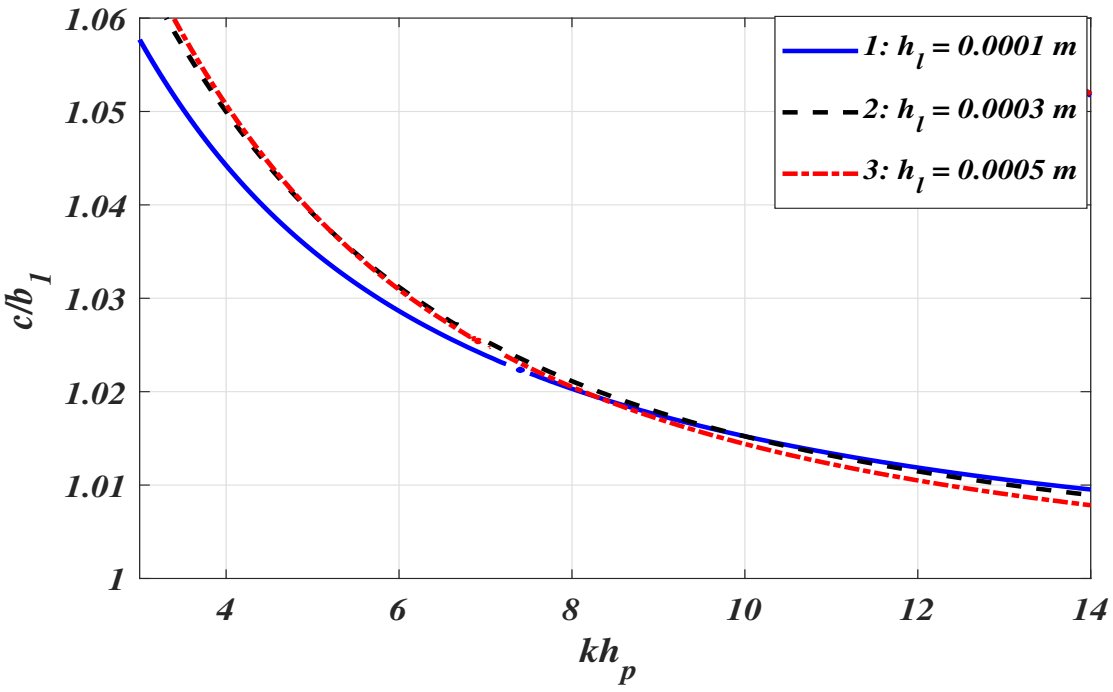

(a) MO condition

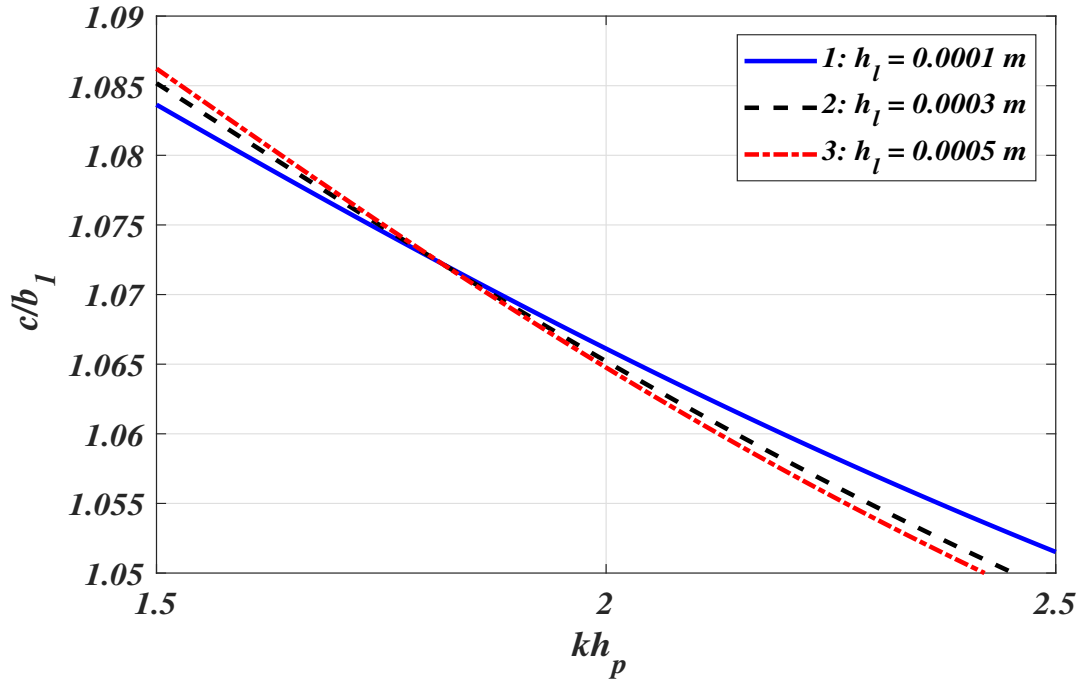

(b) MS condition

Figure 3.5: Dispersion curves (c/b_1 versus kh_p) for varying values of thickness (h_l) of VL layer.

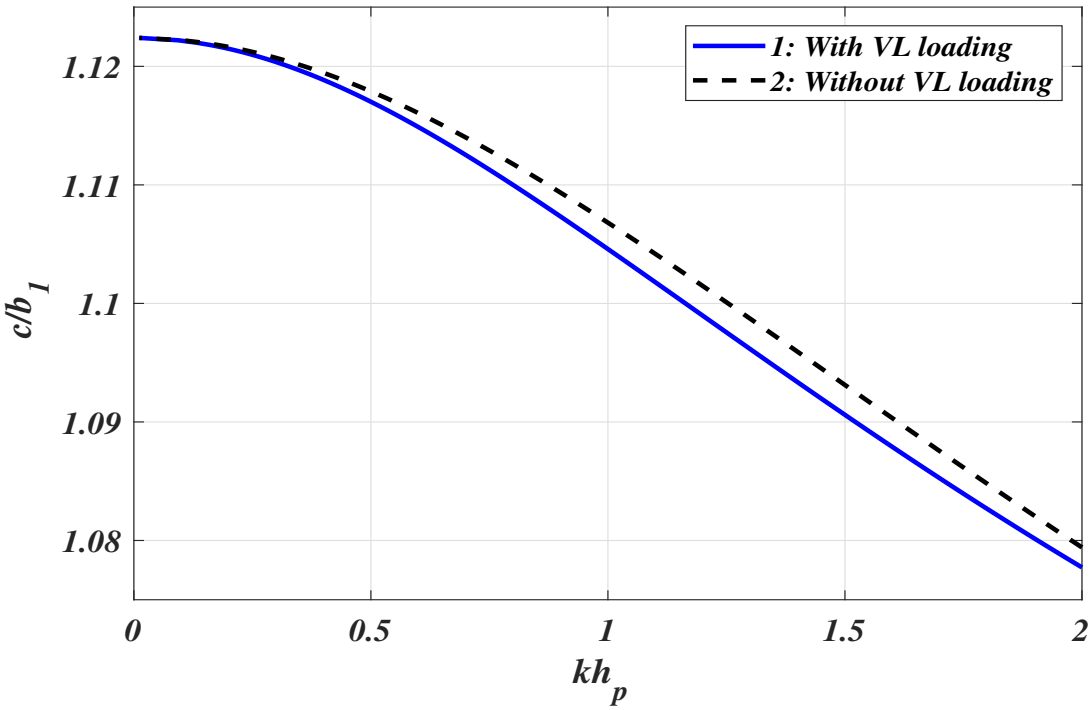

(a) MO condition

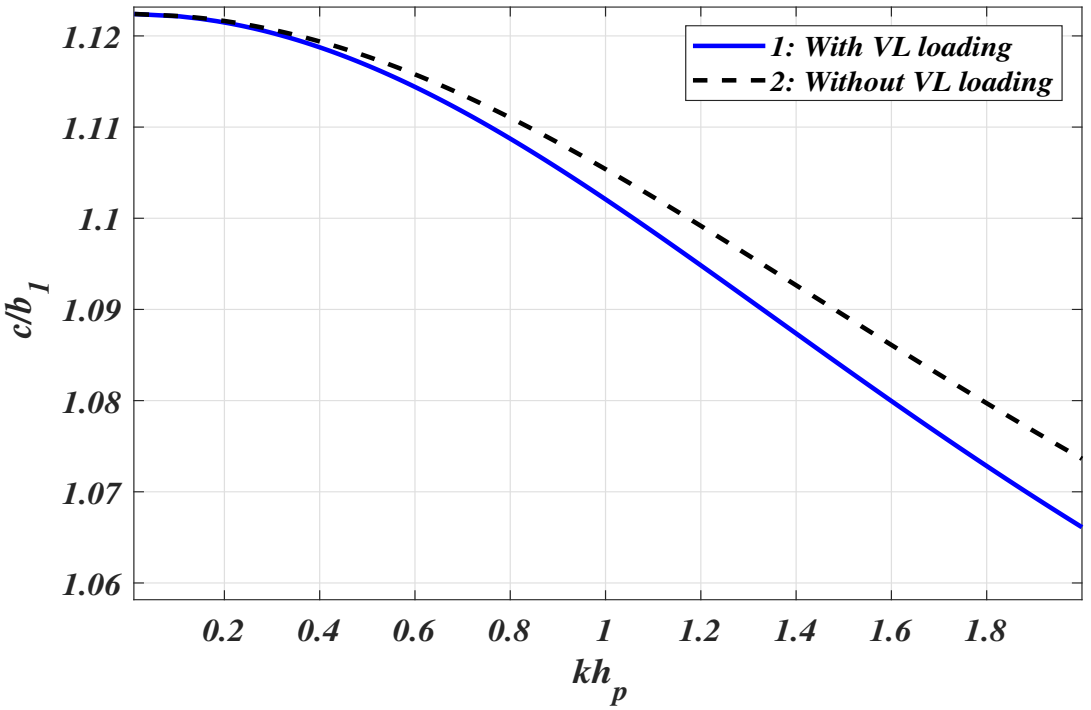

(b) MS condition

Figure 3.6: Dispersion curves (c/b_1 versus kh_p) for the analysis of VL loading effect

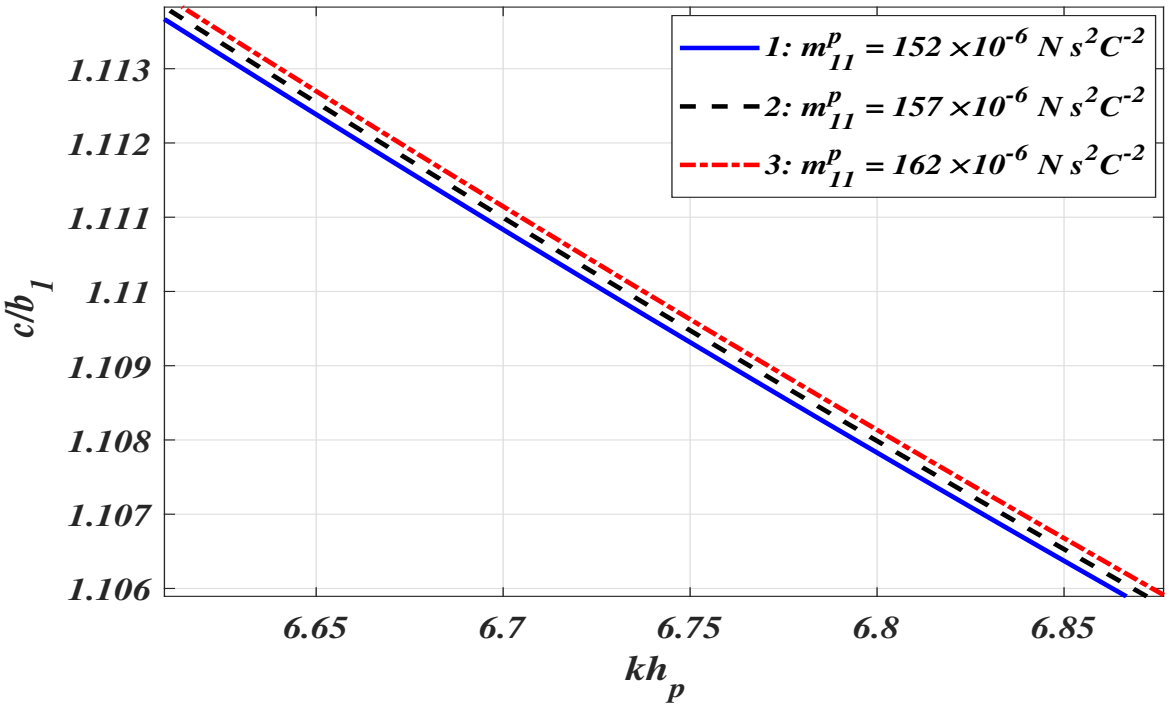

(a) MO condition

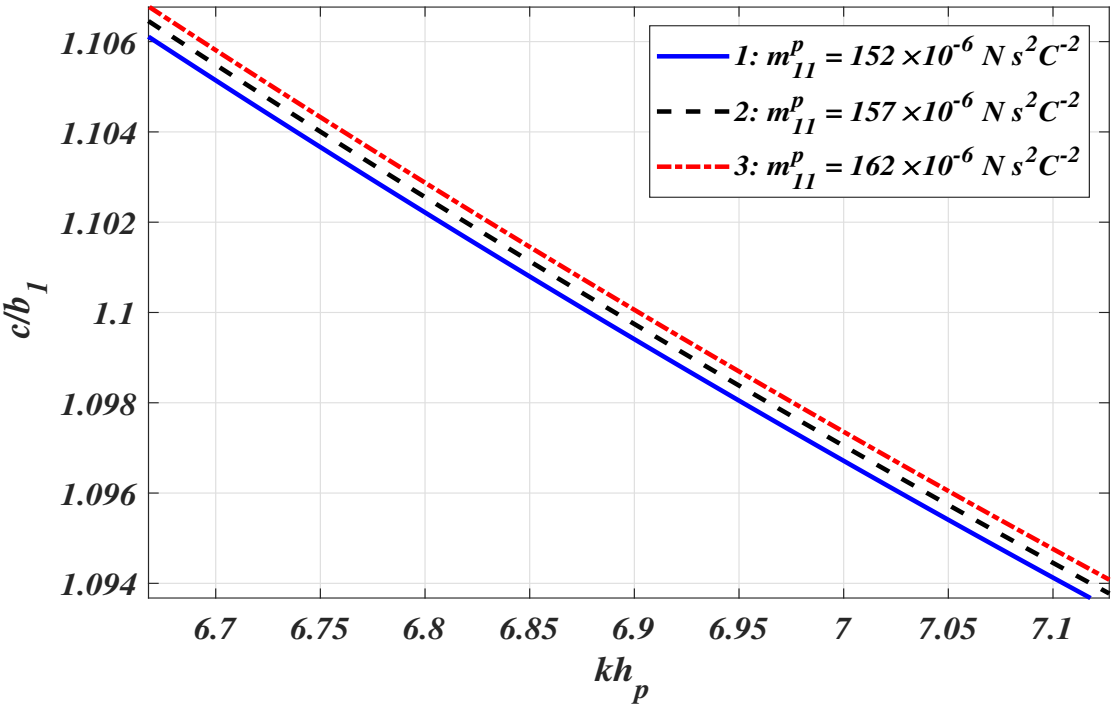

(b) MS condition

Figure 3.7: Dispersion curves (c/b_1 versus kh_p) for varying values of magnetic permeability (m_{11}^p) of PM layer

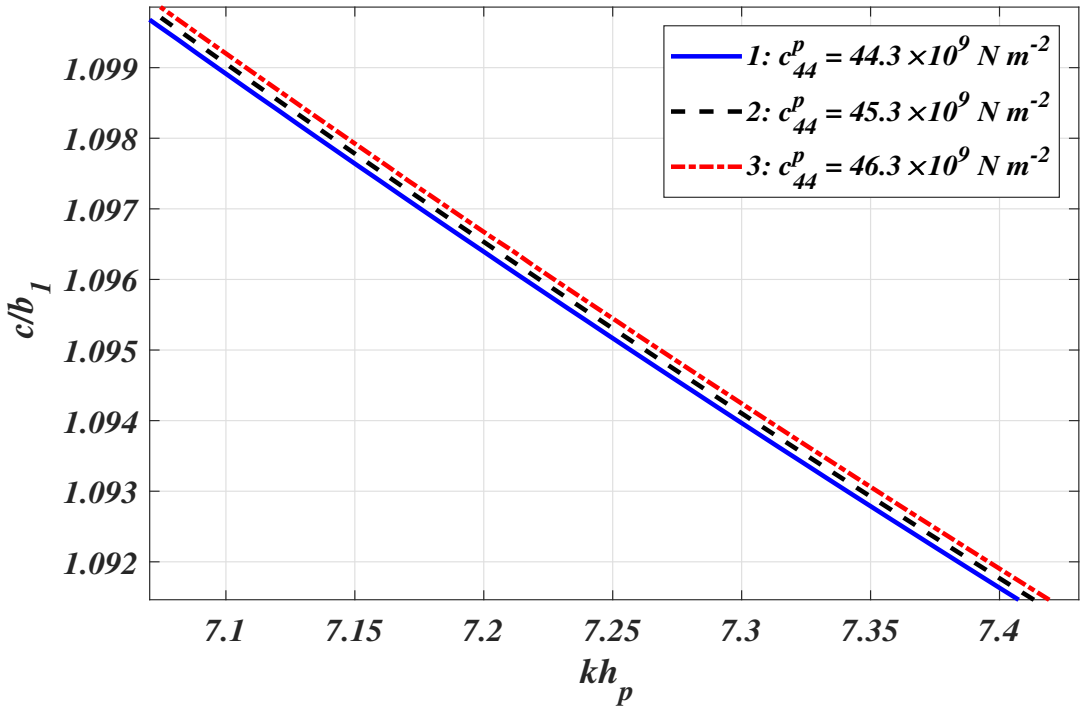

(a) MO condition

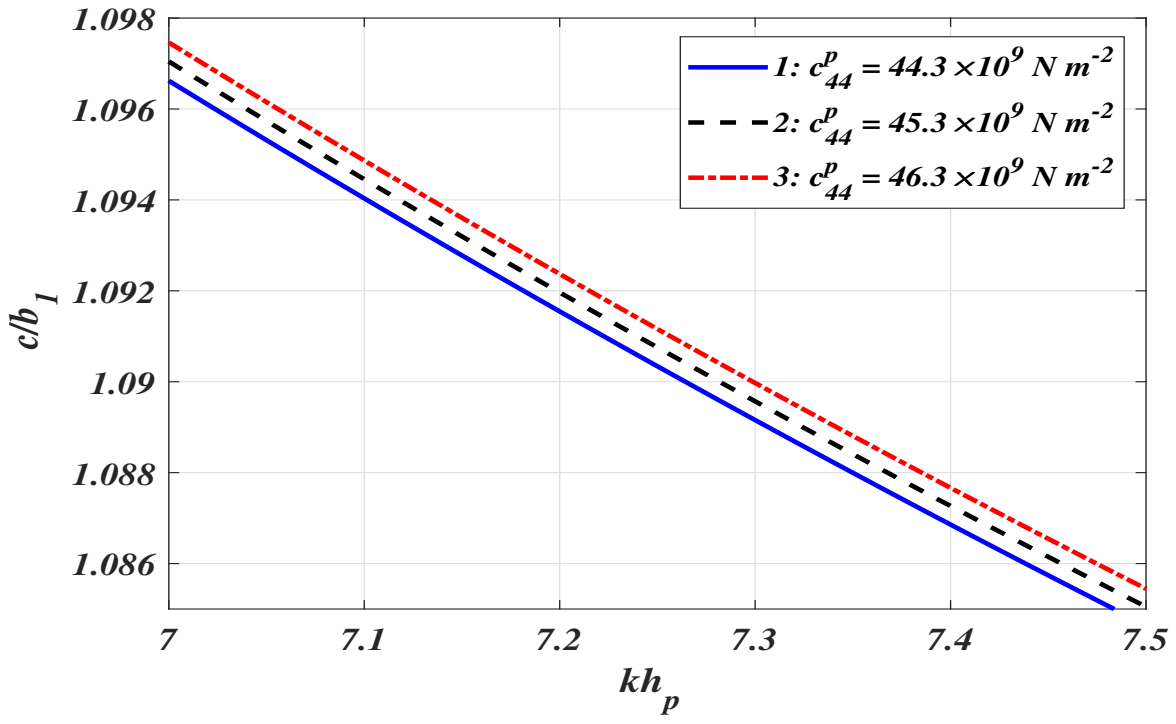

(b) MS condition

Figure 3.8: Dispersion curves (c/b_1 versus kh_p) for varying values of elastic constant (c_{44}^p) of PM layer

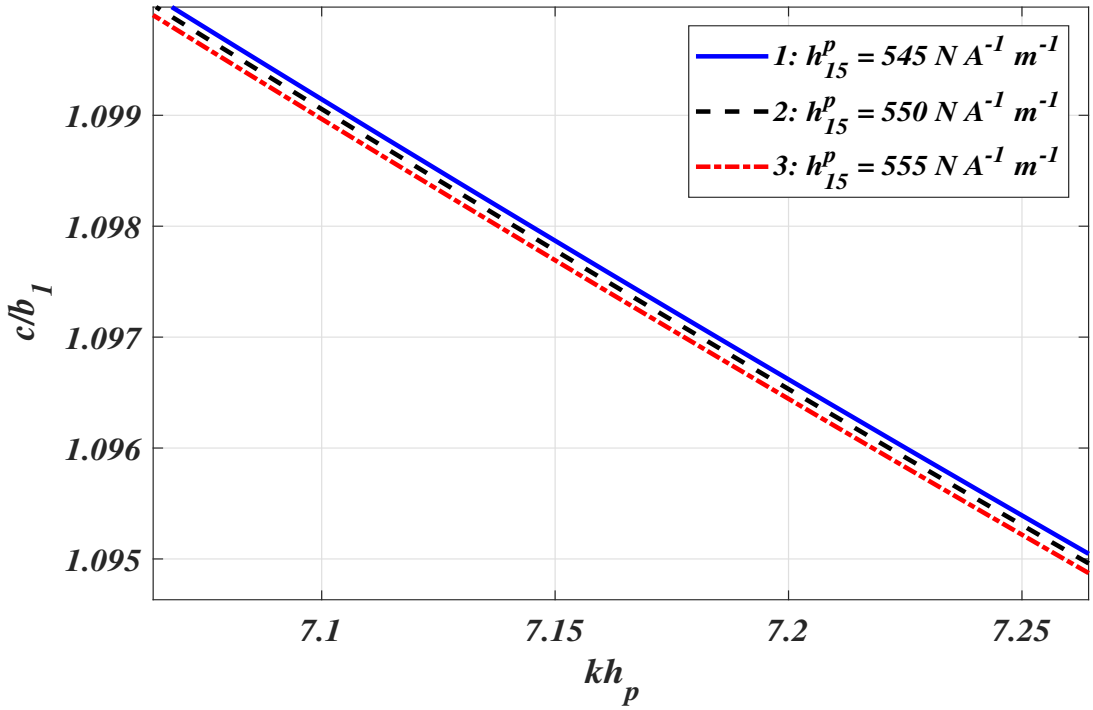

(a) MO condition

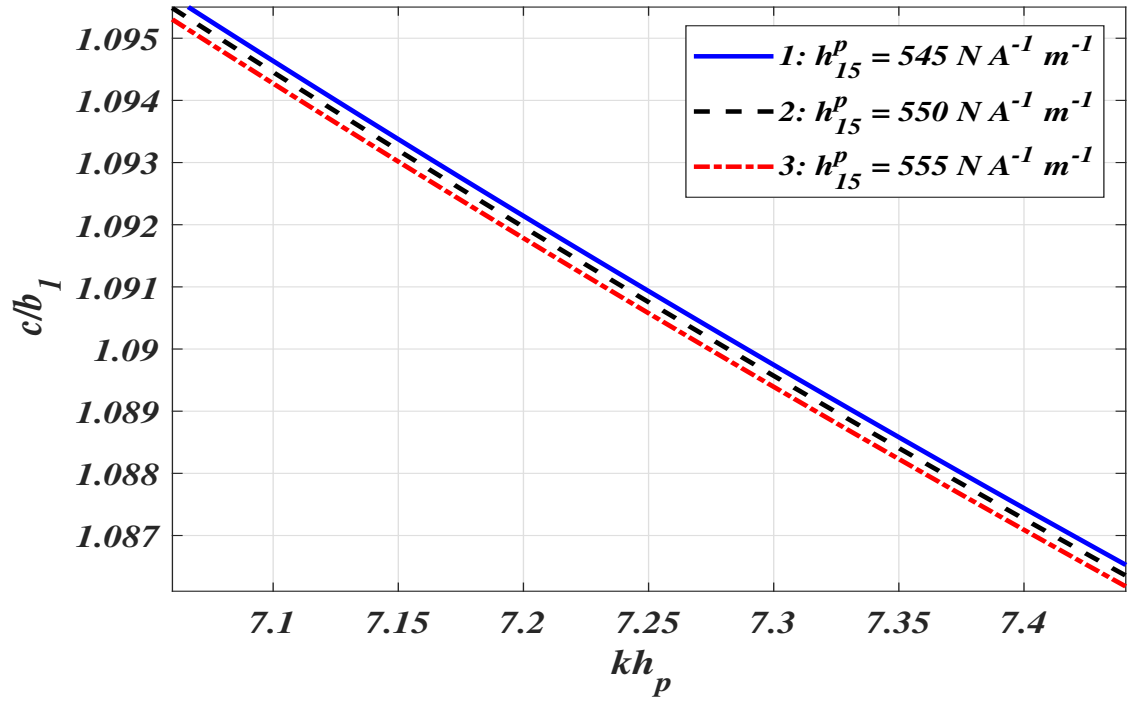

(b) MS condition

Figure 3.9: Dispersion curves (c/b_1 versus kh_p) for varying values of PM constant (h^p_{15}) of PM layer

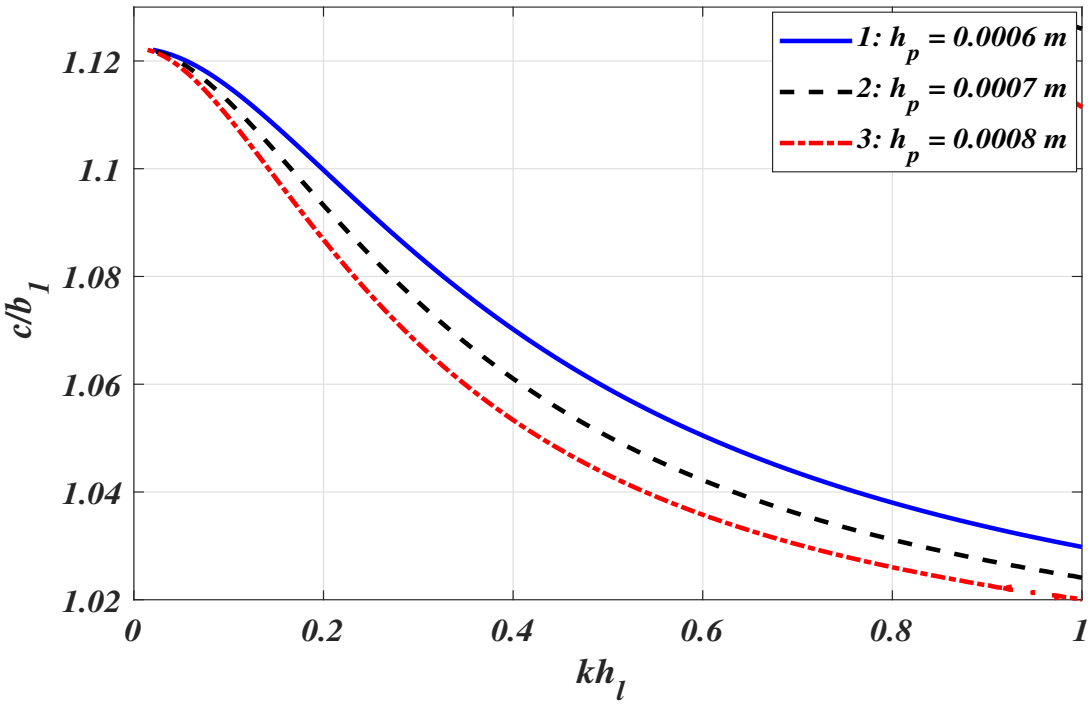

(a) MO condition

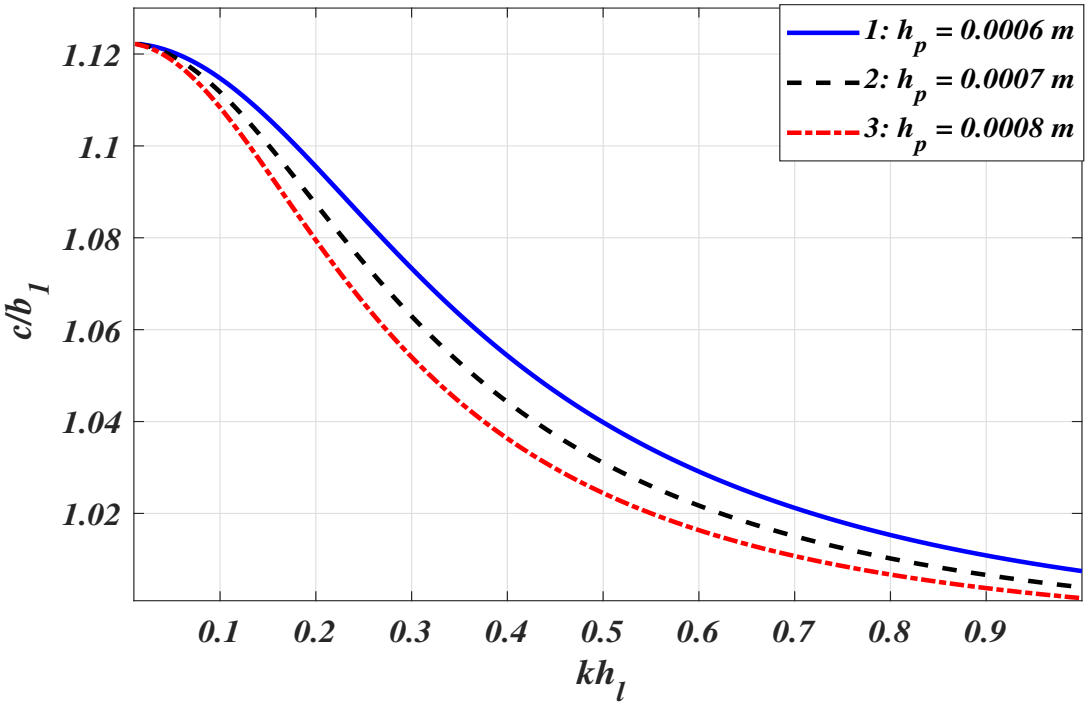

(b) MS condition

Figure 3.10: Dispersion curves (c/b_1 versus kh_l) for varying values of thickness (h_p) of PM layer

3.4.1 Effect of microstructures

The dependence of the material length scale parameter on the propagation of a Love-type wave can be observed by comparing dispersion curves for different values of characteristic length (l^c). It is of the order of internal cell size of microstructure. So the characteristic length is varied as 0.00001 m, 0.00003 m, and 0.00005 m. Fig. 3.2 establishes that an increase in values of length scale parameter, increases the phase velocity of Love-type waves for both MO and MS conditions, respectively. This is ascribed due to the additional couple stress and rotation of the particles at the microscale level.

3.4.2 Effect of VL loading

Due to the fluctuations in the environmental conditions such as rising or dropping of the temperature, scrutinizing the effects of the liquid mass density and the coefficient of viscosity on the wave propagation is essential. Figs. 3.3 a) and b) reveal the effect of the coefficient of viscosity and Figs. 3.4 a) and b) reveal the effect of the liquid mass density, on the velocity of the propagating wave in the considered structure for MO and MS conditions, respectively. These figures advocate that the coefficient of viscosity has a suppressing effect on the phase velocity of the wave. The increment in the values of the coefficient of viscosity leads to a decrease in the phase velocity of the wave while the liquid mass density has a favoring effect on the phase velocity of the wave. With the rising value of the liquid mass density, the phase velocity of the wave increases. For MO and MS conditions, Figs. 3.5 a) and b), respectively delineate that the phase velocity of a Love-type wave increases with the increasing value of the thickness of VL layer but decreases after some particular value of kh_p. To compare the entire effect of VL loading on the phase velocity of the wave, Figs. 3.6 a) and b) are plotted for two dispersion curves. One is plotted under the presence of VL layer and the other in the absence of VL loading for MO and MS conditions, respectively. It can be visualized that VL loading has a suppressing effect on the phase velocity of the propagating wave for both MO and MS conditions.

3.4.3 Effect of PM parameters

To check the impact of the material parameters related to PM material layer ($CoFe_2O_4$) on the dispersion equations, Figs. 3.7-3.9 are plotted. It can be observed from Figs. 3.7 a) and 3.7 b) that magnetic permeability has an encouraging effect on the phase velocity of the

wave under MO and MS conditions, respectively. With the increasing values of magnetic permeability, the phase velocity of the wave also increases. This may be explained by the fact that as the magnitude of the said parameter is increased, it decreases the intensity of magnetic field. Then possibility may arise that weak magnetic field may offer less resistance to the transmutation of wave thereby, increasing the phase velocity of the transferring wave. On examining Figs. 3.8 a) and 3.8 b), it is reported that the elastic constant has a favorable effect on the phase velocity of the wave. An increase in the values of the elastic constant leads to an increase in the phase velocity of the propagating wave. The effect of the PM constant on the phase velocity of the wave is depicted by Figs. 3.9 a) and 3.9 b) for MO and MS conditions, respectively. PM constant has a discouraging effect on the phase velocity of the wave. This may be evident that with the increase in the values of the specified parameter, the magnetic field gets remarkably intensified, thus contributing to more resistance and will cause loss of energy of the wave particles, resulting in reducing the velocity of the wave. Figs 3.10 a) and 3.10 b) depict the effect of the thickness of the PM layer on the phase velocity of the wave for MO and MS conditions, respectively. The thickness of the PM layer has an unfavorable effect on the phase velocity of the wave. As the thickness of the PM layer increases, the phase velocity of the wave decreases.

Conclusions

Following are the pertinent outcomes of the present work.

- Phase velocity of the considered wave decreases with the increase in the value of a wave number.
- Material length scale parameter has a prominent effect on the phase velocity. As the value of the parameter increases, the phase velocity of the wave also increases.
- The coefficient of viscosity of the VL layer disfavors the phase velocity of the wave. As the value of the coefficient of viscosity increases, the phase velocity of the wave decreases.
- The liquid mass density of the VL layer favors the phase velocity of the Love-type waves. With the increase in values of liquid mass density, the phase velocity of the considered wave also increases.
- As the magnitude of thickness of the VL layer is increased, the phase velocity of the Love-type wave increases upto a particular value of wave number and then decreases afterward.
- The entire effect of VL loading on the phase velocity curve of the Love-type wave in the considered structure for both the MO and MS conditions is suppressing.

- The phase velocity increases with an increase in values of magnetic permeability.
- With the increment in the value of elastic constant, the phase velocity of the wave increases.
- With the increase in the magnitude of PM constant, the phase velocity of the wave decreases.
- Broader the width of the PM layer, lower is the phase velocity of the Love-type wave in the considered structure.

Chapter 4

Analysis of size dependency on Love-type wave propagation in a functionally graded PE smart material[3]

4.1 Introduction

Functionally graded materials (FGMs) are leading compounds with graded properties. FGMs are unique concepts in the structural design of materials and have numerous applications in the aircraft, aerospace engineering, and automotive industry. FGM's may be characterized by the variation in configuration and structure moderately over volume resulting in equivalent changes in the properties of the material. The unique concept of FGMs is to make a composite material by changing the microstructure from one material to another material. This empowers the material to have the best of both materials. The strengths of both materials are used in case of thermal, or corrosion resistivity or malleability and toughness to avoid fatigue, fracture, cracking due to stress. Piezoelectric (PE) materials under mechanical stress, are capable of producing electric fields and are considered as smart materials. Although PE materials embedded in such structures have numerous applications but these materials have many shortcomings. PE materials are very fragile and are brittle in nature. Under electrical and mechanical loading these materials may cause failure. To address the requirement of aggressive environmental conditions like thermal shock, vibration, stress, etc., the FGMs are preferred over conventional laminated materials. These materials have numerous applications in various engineering fields like electronics, aerospace engineering, optics, chemical engineering, biomedical implants etc. The structures including functionally graded materials bonded with PE actuators respond smartly to environmental changes. Various researchers have investigated wave propagation phenomenon in functionally graded material in layered structures but literature still lacks to analyze the effect of microstructural size dependency on the phase velocity of the waves in these composites. In this chapter our focus is to analyze the emphatic influence

[3]Contents of this chapter are published in SCIE indexed journal, Mathematics and Mechanics of Solids, 25(8), 1517-1533, 2020. DOI: 10.1080/15376494.2019.1702235 with I.F. = 2.341

of functional gradedness on the Love-type wave propagation in functionally graded piezoelectric material (FGPEM) layer followed by semi-infinite couple stress (CS) substrate. Here we have considered a functionally graded material with exponential variation when the electrical and mechanical constants vary distinctively in the FGPEM layer. Dispersion equations for two different conditions (i.e. electrically open (EO) and electrically short (ES) conditions) are obtained. The obtained results may be useful for attaining better performance in Love-type wave based SAW devices.

4.1.1 Formulation of the problem

Consider a FGPEM layer of finite thickness (h_e) overlying a semi-infinite couple stress (CS) substrate as shown in Fig. 4.1. The Cartesian coordinate system is considered in such a way that Love-type wave is propagating along y-axis and x-axis is considered positive in the vertically downward direction. The electrical and mechanical properties of the FGPEM vary continuously along the x-axis direction. The considered substrate is a semi-infinite CS substrate bearing microstructural properties, given by $x > 0$.

The basic governing equation of motion and constitutive relations of CS theory for

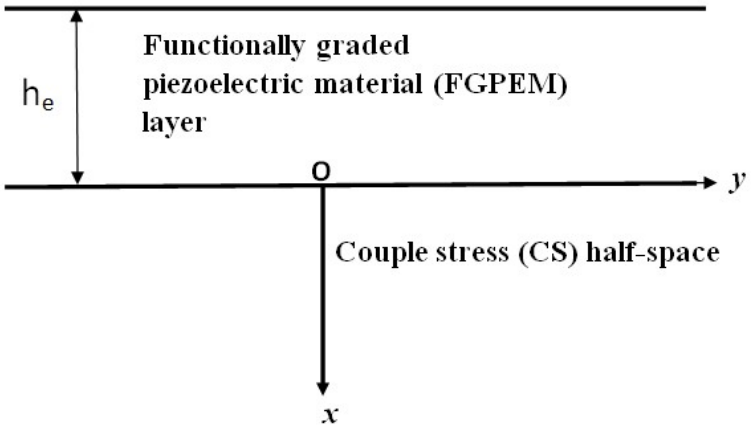

Figure 4.1: Schematic illustration

isotropic material in the absence of body forces are discussed in Chapter 2 and the displacement components along with stress components are given in Eqs. (2.1.23), (2.1.24), and (2.1.25).

4.1.2 Dynamics of the functionally graded piezoelectric material (FGPEM) layer

Let $\overrightarrow{U^e} = (u_1^e, u_2^e, u_3^e)$ be the mechanical displacement components in the FGPEM layer obtained due to the propagation of Love-type wave. Love-type wave is propagating along the direction of y-axis causing displacement in z-direction only. We shall assume that

$$u_1^e = u_2^e = 0, \quad u_3^e = u_3^e(x, y, t), \text{ and } \frac{\partial}{\partial z} \equiv 0. \tag{4.1.1}$$

The basic governing equations of FGPEM in the absence of body forces are given by [28]

$$\begin{aligned} \sigma_{ij,j}^e &= \rho^e \frac{\partial^2 u_i^e}{\partial t^2}, \\ D_{i,i}^e &= 0, \qquad\qquad (i, j = 1, 2, 3) \end{aligned} \tag{4.1.2}$$

Here superscript 'e' indicates the entities in FGPEM layer. ρ^e denotes the mass density and also a function of x. u_i^e and D_i^e denote the mechanical and electric displacements in the i^{th} direction of FGPEM layer, respectively. The comma $(,)$ followed by the subscript i indicates space coordinate differentiation and the repeated subscript index implies summation with respect to that index.

The constitutive equations for a transversely isotropic FGPEM layer with z-axis being the symmetric axis can be expressed as [28]

$$\begin{cases} \sigma_x^e = c_{11}^e(x) S_x^e + c_{12}^e(x) S_y^e + c_{13}^e(x) S_z^e - d_{31}^e(x) E_z^e, \\ \sigma_y^e = c_{12}^e(x) S_x^e + c_{11}^e(x) S_y^e + c_{13}^e(x) S_z^e - d_{31}^e(x) E_z^e, \\ \sigma_z^e = c_{13}^e(x) S_x^e + c_{13}^e(x) S_y^e + c_{33}^e(x) S_z^e - d_{33}^e(x) E_z^e, \\ \sigma_{zx}^e = c_{44}^e(x) S_{zx}^e - d_{15}^e(x) E_x^e, \\ \sigma_{yz}^e = c_{44}^e(x) S_{yz}^e - d_{15}^e(x) E_y^e, \\ \sigma_{xy}^e = \dfrac{1}{2}(c_{11}^e(x) - c_{12}^e(x)) S_{xy}^e, \\ D_x^e = d_{15}^e(x) S_{zx}^e + \epsilon_{11}^e(x) E_x^e, \\ D_y^e = d_{15}^e(x) S_{yz}^e + \epsilon_{11}^e(x) E_y^e, \\ D_z^e = d_{31}^e(x) S_x^e + d_{31}^e(x) S_y^e + d_{33}^e(x) S_z^e + \epsilon_{33}^e(x) E_z^e, \end{cases} \tag{4.1.3}$$

where σ_{ij}^e and S_{kl}^e are the stress and strain tensors, respectively. c_{ijkl}^e, d_{kij}^e, ϵ_{ij}^e, and E_i^e are the elastic constants, PE constants, dielectric constants, and electric field respectively.

The strain components are defined as

$$\begin{aligned} S_x^e = u_{1,x}^e, \quad S_y^e = u_{2,y}^e, \quad S_z^e = u_{3,z}^e, \\ S_{yz}^e = u_{3,y}^e + u_{2,z}^e, \quad S_{zx}^e = u_{1,z}^e + u_{3,x}^e, \quad S_{xy}^e = u_{1,y}^e + u_{2,x}^e. \end{aligned} \tag{4.1.4}$$

The relation between electric field and the electric potential function can be defined as

$$E_x^e = -\phi_{,x}^e, \quad E_y^e = -\phi_{,y}^e, \quad E_z^e = -\phi_{,z}^e, \tag{4.1.5}$$

where ϕ^e represents the electric potential function.
Substituting Eq. (4.1.1) in Eqs. (4.1.4) and (4.1.5) we get

$$\begin{aligned} S_x^e = S_y^e = S_z^e = 0, \\ S_{yz}^e = u_{3,y}^e, \quad S_{zx}^e = u_{3,x}^e, \quad S_{xy}^e = 0, \\ E_x^e = -\phi_{,x}^e, \quad E_y^e = -\phi_{,y}^e, \quad E_z^e = 0. \end{aligned} \tag{4.1.6}$$

Substituting values from Eq. (4.1.6) in Eq. (4.1.3) and then substituting in Eq. (4.1.2), we obtain the governing equations for the FGPEM layer as

$$\begin{aligned} c_{44}^e(x)\nabla^2 u_3^e + d_{15}^e(x)\nabla^2\phi^e + \frac{\partial c_{44}^e(x)}{\partial x}\frac{\partial u_3^e}{\partial x} + \frac{\partial d_{15}^e(x)}{\partial x}\frac{\partial \phi^e}{\partial x} = \rho^e \frac{\partial^2 u_3^e}{\partial t^2}, \\ d_{15}^e(x)\nabla^2 u_3^e - \epsilon_{11}^e(x)\nabla^2\phi^e + \frac{\partial d_{15}^e(x)}{\partial x}\frac{\partial u_3^e}{\partial x} - \frac{\partial \epsilon_{11}^e(x)}{\partial x}\frac{\partial \phi^e}{\partial x} = 0. \end{aligned} \tag{4.1.7}$$

The exponential inhomogeneity has been considered in the elastic, PE, dielectric constants and density of the FGPEM layer. Thus, the material properties of the FGPEM layer are considered as

$$c_{44}^e(x) = c_{44}^{(0)} e^{gx}, \quad d_{15}^e(x) = d_{15}^{(0)} e^{gx}, \quad \epsilon_{11}^e(x) = \epsilon_{11}^{(0)} e^{gx}, \quad \text{and} \quad \rho^e(x) = \rho^{(0)} e^{gx}, \tag{4.1.8}$$

where g is the material gradient factor resonsible for functional gradedness in the FGPEM layer and $c_{44}^{(0)}$, $d_{15}^{(0)}$, $\epsilon_{11}^{(0)}$, and $\rho^{(0)}$, are the values of c_{44}^e, d_{15}^e, ϵ_{11}^e, and ρ^e, respectively at $x = 0$. Employing Eqs. (4.1.8) into Eq. (4.1.7), we instate

$$\begin{cases} c_{44}^{(0)}\left(\nabla^2 u_3^e + g\dfrac{\partial u_3^e}{\partial x}\right) + d_{15}^{(0)}\left(\nabla^2\phi^e + g\dfrac{\partial \phi^e}{\partial x}\right) = \rho^{(0)}\dfrac{\partial^2 u_3^e}{\partial t^2}, \\ d_{15}^{(0)}\left(\nabla^2 u_3^e + g\dfrac{\partial u_3^e}{\partial x}\right) = \epsilon_{11}^{(0)}\left(\nabla^2\phi^e + g\dfrac{\partial \phi^e}{\partial x}\right). \end{cases} \tag{4.1.9}$$

Eqs. (4.1.9) can be rewritten as

$$\begin{cases} \nabla^2 u_3^e + g\dfrac{\partial u_3^e}{\partial x} = \dfrac{1}{c_1^2}\dfrac{\partial^2 u_3^e}{\partial t^2}, \\ \nabla^2 \phi^e + g\dfrac{\partial \phi^e}{\partial x} = \dfrac{1}{c_1^2}\left(\dfrac{d_{15}^{(0)}}{\epsilon_{11}^{(0)}}\right)\dfrac{\partial^2 u_3^e}{\partial t^2}, \end{cases} \tag{4.1.10}$$

where $c_1 = \sqrt{\frac{\overline{c_{44}^{(0)}}}{\rho^{(0)}}}$, $\quad \overline{c_{44}^{(0)}} = c_{44}^{(0)} + \frac{(d_{15}^{(0)})^2}{\epsilon_{11}^{(0)}}$, and c_1 is the shear wave velocity in the FGPEM layer.

We assume the following solutions of the mechanical displacement component and electric potential function of the Love-type wave in the FGPEM layer

$$\begin{aligned} u_3^e(x,y,t) &= \hat{U}(x)e^{ik(y-ct)}, \\ \phi^e(x,y,t) &= \hat{\Phi}(x)e^{ik(y-ct)}, \end{aligned} \tag{4.1.11}$$

where k is the wave number and c is the phase velocity of the wave.

Invoking Eq. (4.1.11) in Eq. (4.1.10) we get,

$$\begin{aligned} \hat{U}''(x) + g\hat{U}'(x) + k^2 c_2^2 \hat{U}(x) &= 0, \\ \hat{\Phi}''(x) + g\hat{\Phi}'(x) - k^2\hat{\Phi}(x) &= \left(\frac{-k^2c^2 d_{15}^{(0)}}{c_1^2 \epsilon_{11}^{(0)}}\right)\hat{U}(x), \end{aligned} \tag{4.1.12}$$

where $c_2 = \sqrt{\frac{c^2}{c_1^2} - 1}$.

On solving differential equations in Eq. (4.1.12) under the assumption $c > c_1$, the displacement component and electric potential function can be expressed as

$$\begin{aligned} u_3^e(x,y,t) &= [\cos(c_3 x)C_1 + \sin(c_3 x)C_2]e^{-gx/2}e^{ik(y-ct)}, \\ \phi^e(x,y,t) &= \left[\frac{d_{15}^{(0)}}{\epsilon_{11}^{(0)}}\left(\cos(c_3 x)C_1 + \sin(c_3 x)C_2\right)e^{-gx/2} + e^{c_4 x}C_3 + e^{c_5 x}C_4\right]e^{ik(y-ct)}, \end{aligned} \tag{4.1.13}$$

Here C_1, C_2, C_3, and C_4 are arbitrary constants.

$c_3 = \frac{\sqrt{4k^2c_2^2 - g^2}}{2}$,

$c_4 = -\frac{g}{2} - \frac{\sqrt{g^2+4k^2}}{2}$,

$c_5 = -\frac{g}{2} + \frac{\sqrt{g^2+4k^2}}{2}$.

4.2 Boundary conditions

Following are the boundary conditions for the considered model.

(i) The electrical boundary conditions at the free surface i.e., at $x = -h_e$ are

$$D_x^e(x, y) = 0, \quad \{\text{electrically open (EO) condition}\} \tag{4.2.1}$$

$$\phi^e(x, y) = 0. \quad \{\text{electrically short (ES) condition}\} \tag{4.2.2}$$

(ii) The mechanical traction free condition at $x = -h_e$ is

$$\sigma_{zx}^e(x, y) = 0. \tag{4.2.3}$$

(iii) The continuity conditions at the interfacial surface i.e., at $x = 0$

$$\begin{aligned} u_3^e(x, y) &= u_3^c(x, y), \\ \sigma_{zx}^e(x, y) &= \sigma_{zx}^c(x, y), \\ \mu_{xy}^c(x, y) &= 0, \\ \phi^e(x, y) &= 0. \end{aligned} \tag{4.2.4}$$

4.3 Derivation of dispersion relations

From above mentioned boundary conditions (4.2.1) to (4.2.4), the following system of equations in terms of six unknown coefficients $C_1,\ C_2,\ C_3,\ C_4,\ A_4,$ and A_5 are obtained.

$$c_4 e^{-c_4 h_e} C_3 + c_5 e^{-c_5 h_e} C_4 = 0, \tag{4.3.1}$$

$$\left(\frac{d_{15}^{(0)}}{\epsilon_{11}^{(0)}}\right) e^{gh_e/2} \cos(c_3 h_e) C_1 - \left(\frac{d_{15}^{(0)}}{\epsilon_{11}^{(0)}}\right) e^{gh_e/2} \sin(c_3 h_e) C_2 + e^{-c_4 h_e} C_3 + e^{-c_5 h_e} C_4 = 0, \tag{4.3.2}$$

$$\begin{aligned} \overline{c_{44}^{(0)}} e^{gh_e/2} \left[\left(c_3 \sin(c_3 h_e) - \left(\frac{g}{2}\right) \cos(c_3 h_e)\right) C_1 + \left(c_3 \cos(c_3 h_e) + \left(\frac{g}{2}\right) \sin(c_3 h_e)\right) C_2\right] \\ + d_{15}^{(0)} \left(c_4 e^{-c_4 h_e} C_3 + c_5 e^{-c_5 h_e} C_4\right) = 0 \end{aligned} \tag{4.3.3}$$

$$C_1 - A_4 - A_5 = 0, \tag{4.3.4}$$

$$-\overline{c_{44}^{(0)}}\left(\frac{g}{2}\right)C_1 + \overline{c_{44}^{(0)}}c_3C_2 + d_{15}^{(0)}c_4C_3 + d_{15}^{(0)}c_5C_4 - a_4a_6A_4 - a_5a_7A_5 = 0, \tag{4.3.5}$$

$$\left(\frac{d_{15}^{(0)}}{\epsilon_{11}^{(0)}}\right)C_1 + C_3 + C_4 = 0, \tag{4.3.6}$$

$$(a_4^2 - k^2)A_4 + (a_5^2 - k^2)A_5 = 0. \tag{4.3.7}$$

To get the non-trivial solution and hence the dispersion relation, we equate the determinant of these coefficients to zero.

4.3.1 Dispersion relation for EO condition

After eliminating the unknown constants C_1, C_2, C_3, C_4, A_4, and A_5 from Eqs. (4.3.1) and (4.3.3)-(4.3.7), we get the following dispersion relation for Love-type wave propagating in FGPEM layer overlying CS half-space substrate, for EO condition.

$$\left[\overline{c_{44}^{(0)}}c_6\left(\frac{g}{2}c_8 + c_3c_7\right) - \left(\frac{(d_{15}^{(0)})^2}{\epsilon_{11}^{(0)}}\right)c_4c_5c_8c_{11}\right]c_{10} - c_6c_8c_9 = 0, \tag{4.3.8}$$

where
$c_6 = c_5e^{-c_5h_e} - c_4e^{-c_4h_e}$,
$c_7 = c_3\sin(c_3h_e) - \frac{g}{2}\cos(c_3h_e)$,
$c_8 = c_3\cos(c_3h_e) + \frac{g}{2}\sin(c_3h_e)$,
$c_9 = (a_5^2 - k^2)a_4a_6 - (a_4^2 - k^2)a_5a_7$,
$c_{10} = a_4^2 - a_5^2$,
$c_{11} = e^{-c_4h_e} - e^{-c_5h_e}$.

4.3.2 Dispersion relation for ES condition

After eliminating the unknown constants C_1, C_2, C_3, C_4, A_4, and A_5 from equations (4.3.2)-(4.3.7), we get the following dispersion relation for Love-type wave propagating in FGPEM layer overlying CS half-space substrate, for ES condition.

$$\left[\overline{c_{44}^{(0)}}\left(\frac{g}{2}\right)c_{14} + \left(\frac{(d_{15}^{(0)})^2}{\epsilon_{11}^{(0)}}\right)c_{15} + \overline{c_{44}^{(0)}}c_7c_{16} + \overline{c_{44}^{(0)}}\left(\frac{(d_{15}^{(0)})^2}{\epsilon_{11}^{(0)}}\right)\cos(c_3h_e)c_{17}\right]c_{10} - c_9c_{14} = 0, \tag{4.3.9}$$

where
$c_{12} = \overline{c_{44}^{(0)}} c_8 + c_5 \left(\frac{(d_{15}^{(0)})^2}{\epsilon_{11}^{(0)}} \right) \sin(c_3 h_e),$
$c_{13} = \overline{c_{44}^{(0)}} c_8 + c_4 \left(\frac{(d_{15}^{(0)})^2}{\epsilon_{11}^{(0)}} \right) \sin(c_3 h_e),$
$c_{14} = \overline{c_{44}^{(0)}} c_8 c_{11} - \left(\frac{(d_{15}^{(0)})^2}{\epsilon_{11}^{(0)}} \right) \sin(c_3 h_e) c_6,$
$c_{15} = \overline{c_{44}^{(0)}} c_3 e^{-(c_4+c_5+g/2)h_e}(c_4 - c_5) - c_4 c_{12} e^{-c_5 h_e} + c_5 c_{13} e^{-c_4 h_e},$
$c_{16} = \overline{c_{44}^{(0)}} c_3 c_{11} + \left(\frac{(d_{15}^{(0)})^2}{\epsilon_{11}^{(0)}} \right) e^{g h_e/2} \sin(c_3 h_e)(c_4 - c_5),$
$c_{17} = c_3 c_6 + e^{g h_e/2} c_8 (c_4 - c_5).$

4.4 Particular cases and validation of results

Case-I

If we consider $l^c \to 0$ then CS half-space substrate reduces to isotropic elastic half-space substrate and the dispersion relations for both EO and ES conditions reduce to

$$\left[\overline{c_{44}^{(0)}} c_6 \left(\frac{g}{2} c_8 + c_3 c_7 \right) - \left(\frac{(d_{15}^{(0)})^2}{\epsilon_{11}^{(0)}} \right) c_4 c_5 c_8 c_{11} \right] = c_6 c_8 k \mu^1 \sqrt{1 - \frac{c^2}{\overline{a_3}^2}}, \tag{4.4.1}$$

$$\left[\overline{c_{44}^{(0)}} \left(\frac{g}{2} \right) c_{14} + \left(\frac{(d_{15}^{(0)})^2}{\epsilon_{11}^{(0)}} \right) c_{15} + \overline{c_{44}^{(0)}} c_7 c_{16} + \overline{c_{44}^{(0)}} \left(\frac{(d_{15}^{(0)})^2}{\epsilon_{11}^{(0)}} \right) \cos(c_3 h_e) c_{17} \right] = c_{14} k \mu^1 \sqrt{1 - \frac{c^2}{\overline{a_3}^2}}, \tag{4.4.2}$$

respectively. Here $\overline{a_3} = \sqrt{\frac{\mu^1}{\rho^1}}$, μ^1 is shear modulus of elasticity and ρ^1 is density of isotropic elastic half-space. Eqs. (4.4.1) and (4.4.2) represent the dispersion relations in FGPEM layer overlying isotropic elastic half-space for EO and ES conditions, respectively.

Case-II

In the absence of functional gradedness from FGPEM layer (i.e. $g = 0$), the dispersion relations for EO and ES conditions from Eqs. (4.3.8) and (4.3.9), respectively take the following form

$$k c_{10} c_{18} - c_9 = 0, \tag{4.4.3}$$

$$k c_{10} c_{20} - c_9 c_{19} = 0, \tag{4.4.4}$$

where
$c_{18} = \overline{c_{44}^{(0)}} c_2 \tan(k c_2 h_e) + \left(\frac{(d_{15}^{(0)})^2}{\epsilon_{11}^{(0)}} \right) \tanh(k h_e),$

$c_{19} = \overline{c_{44}^{(0)}} c_2 \tanh(kh_e) - \left(\frac{(d_{15}^{(0)})^2}{\epsilon_{11}^{(0)}}\right) \tan(kc_2h_e),$

$c_{20} = \left(\frac{2(d_{15}^{(0)})^2 \overline{c_{44}^{(0)}} c_2}{\epsilon_{11}^{(0)}}\right) \left[1 - \frac{\sec(kc_2h_e)}{\cosh(kh_e)}\right] + \left((\overline{c_{44}^{(0)}})^2 c_2^2 - \frac{(d_{15}^{(0)})^4}{(\epsilon_{11}^{(0)})^2}\right) \tan(kc_2h_e) \tanh(kh_e).$

Eqs. (4.4.3) and (4.4.4) represent the dispersion relations of Love-type wave in a PE layer overlying semi-infinite CS substrate, for EO and ES conditions, respectively.

Subcase-I

Pondering the case-II, if the PE constant $(d_{15}^{(0)})$ is removed by taking $d_{15}^{(0)} = 0$. Then $\overline{c_{44}^{(0)}} = c_{44}^{(0)} = \mu^o$ (say) and Eqs. (4.4.3) and (4.4.4) can be reduced to

$$\mu^o c_2 \tan(kc_2h_e) kc_{10} = c_9. \tag{4.4.5}$$

Eq. (4.4.5) describes the dispersion relation of a Love-type wave in an isotropic elastic layer of thickness h_e overlying semi-infinite CS substrate.

Case-III

If we consider $l^c \to 0$ in case-II, then semi-infinite CS substrate reduces to isotropic half-space elastic substrate and the dispersion relations for both open (4.4.3) and short (4.4.4) conditions reduce to

$$c_{18} = \mu^1 \sqrt{1 - \frac{c^2}{\overline{a_3}^2}}, \tag{4.4.6}$$

$$c_{20} = c_{19} \mu^1 \sqrt{1 - \frac{c^2}{\overline{a_3}^2}}, \tag{4.4.7}$$

respectively. Eqs. (4.4.6) and (4.4.7) represent the dispersion relations of Love-type waves in a PE layer of thickness h_e overlying isotropic elastic half-space substrate.

Subcase-I

Furthermore in case-III, if PE constant is removed i.e. $d_{15}^{(0)} = 0$, then dispersion relation for both the cases reduce to

$$\tan\left(kh_e \sqrt{\frac{c^2}{{a_1}^2} - 1}\right) = \frac{\mu^1 \sqrt{1 - \frac{c^2}{\overline{a_3}^2}}}{\mu^o \sqrt{\frac{c^2}{{a_1}^2} - 1}}, \tag{4.4.8}$$

where c is the phase velocity of Love-type wave and $a_1 = \sqrt{\frac{\mu^o}{\rho^o}}$. This equation (4.4.8) is the well-known dispersion relation for Love waves in the classical structure [128] with the condition $a_1 < c < \overline{a_3}$, that validates the outcomes of the present problem.

4.5 Numerical results and discussion

To unfold the influence of various affecting parameters, viz., length scale parameter present in the size-dependent substrate, PE material parameters, viz., PE constant, dielectric constant, elastic constant, thickness, and material gradient parameter associated with the functional gradedness of the FGPEM layer on the phase velocity of the Love-type waves, the dispersion curves elucidating the variation of c/c_1 against kh_e are plotted. $PZT-5H$ ceramic material as FGPEM layer and Dionysos marble as CS substrate exhibiting microstructural properties are considered. The thickness of the FGPEM layer is fixed as $h_e = 0.0007$ m. The values of material constants for CS half-space are provided in Chapter 2 in Section 2.4. as Table 2.3. The value of the material gradient parameter responsible for functional gradedness in FGPEM layer is fixed as $g = 500$. Graphical illustrations have been carried out for FGPEM layer by taking the data provided in Table 4.1.

Table 4.1: Material constants for FGPEM layer (a- [171], b- [2])

Materials	Elastic constant $c_{44}^{(0)}$ $(10^{10}Nm^{-2})$	Mass density $\rho^{(0)}$ $(10^{3}kg/m^{3})$	PE constant $d_{15}^{(0)}$ (Cm^{-2})	Dielectric constant $\epsilon_{11}^{(0)}$ $(10^{-10}Fm^{-1})$
PZT-5H^{a}	2.30	7.50	17.0	277.0
PZT-4^{b}	2.56	7.5	12.7	64.99
$BaTiO_3^{a}$	4.40	7.28	11.4	128.0

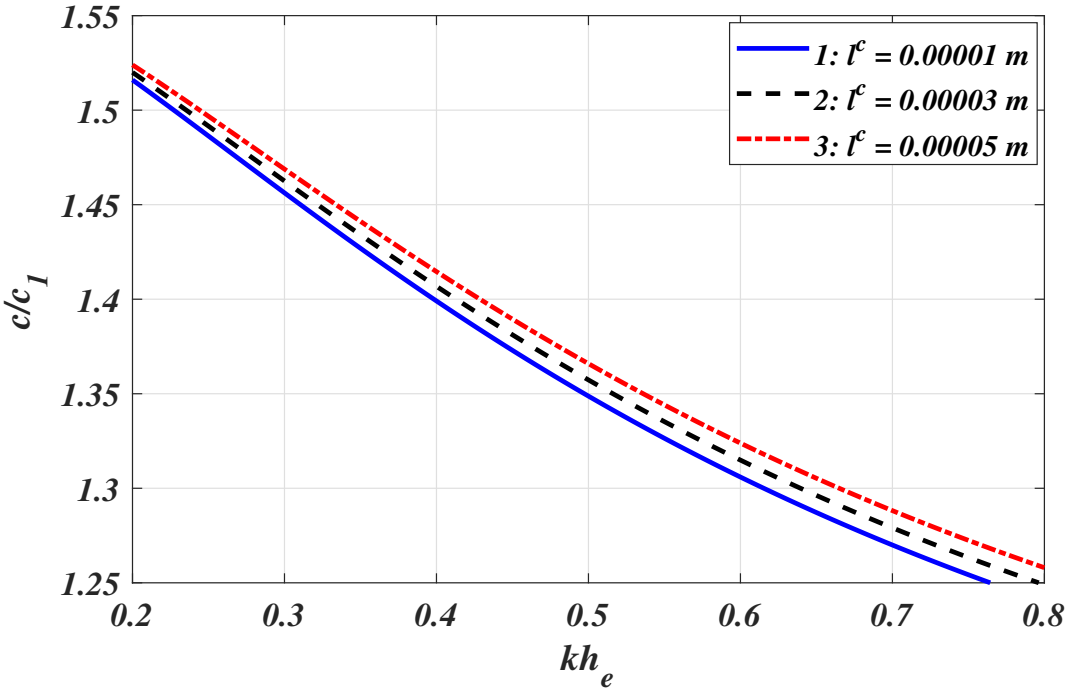

(a) Open circuit condition

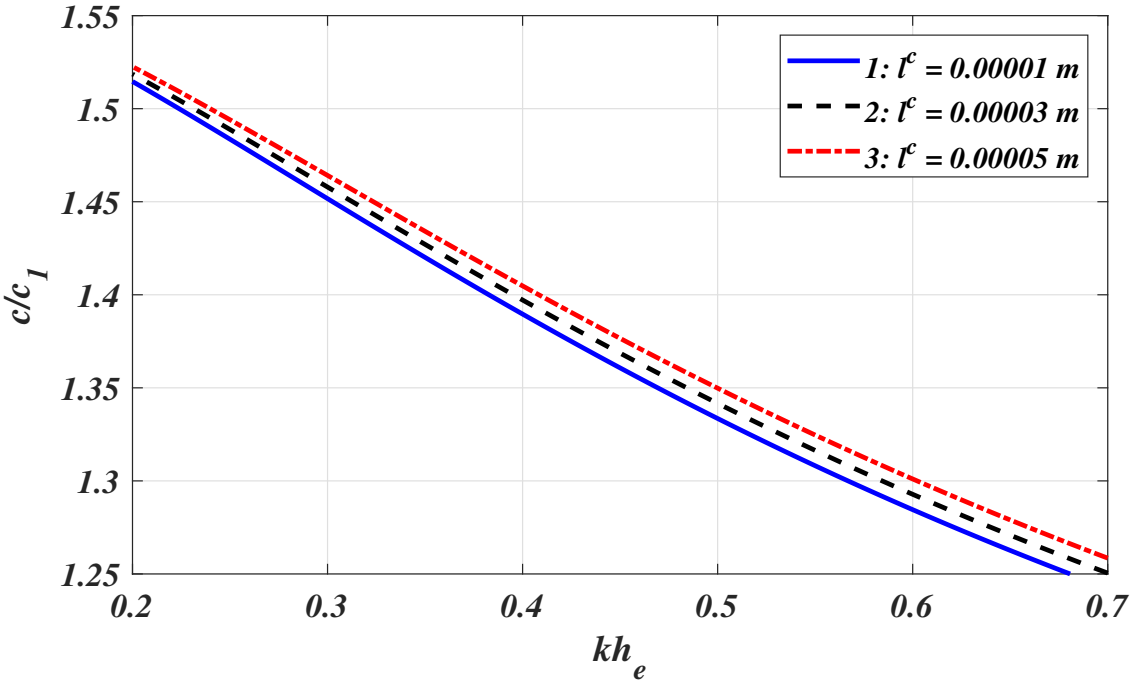

(b) Short circuit condition

Figure 4.2: Dispersion curves (c/c_1 *vs* kh_e) of Love-type waves for different values of characteristic length parameter (l^c).

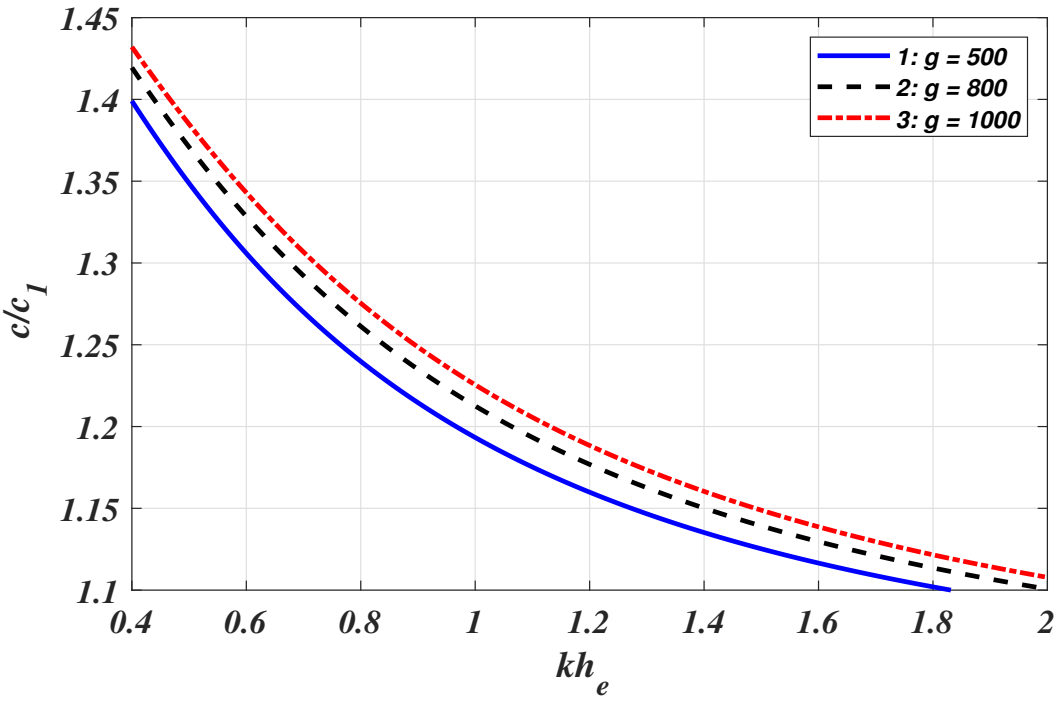

(a) Open circuit condition

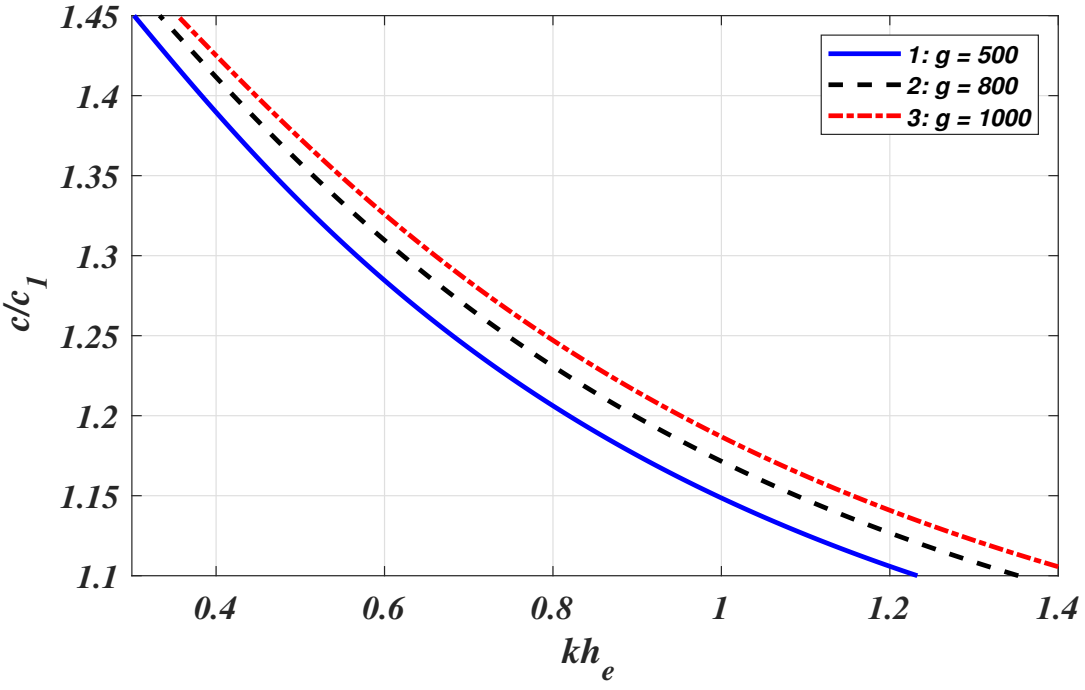

(b) Short circuit condition

Figure 4.3: Dispersion curves (c/c_1 *vs* kh_e) of Love-type waves for different values of material gradient parameter (g).

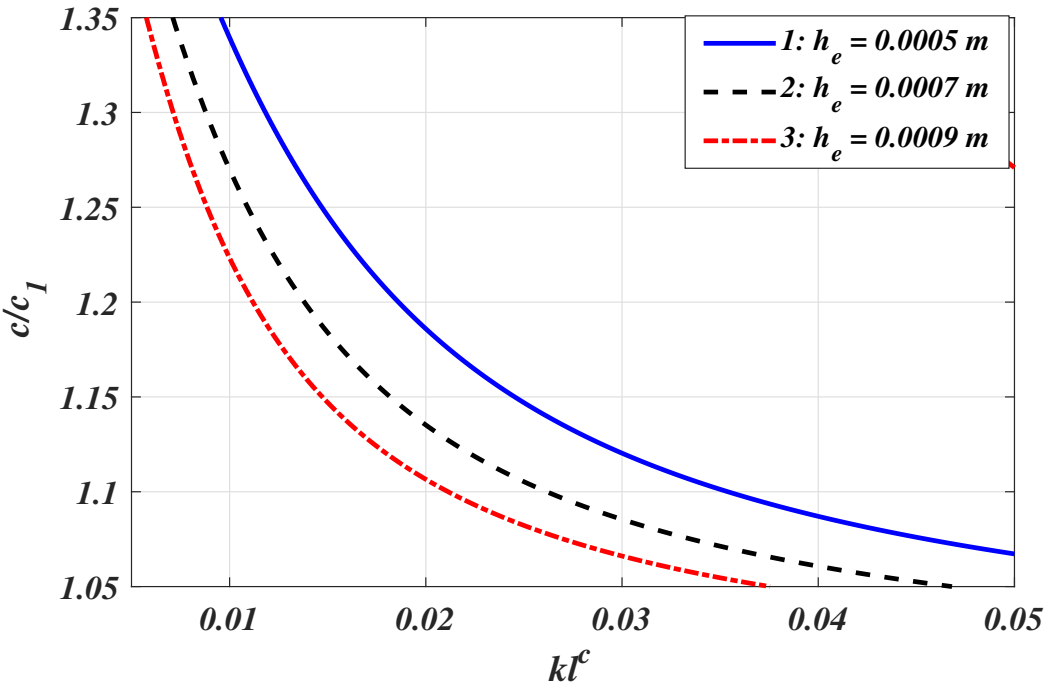

(a) Open circuit condition

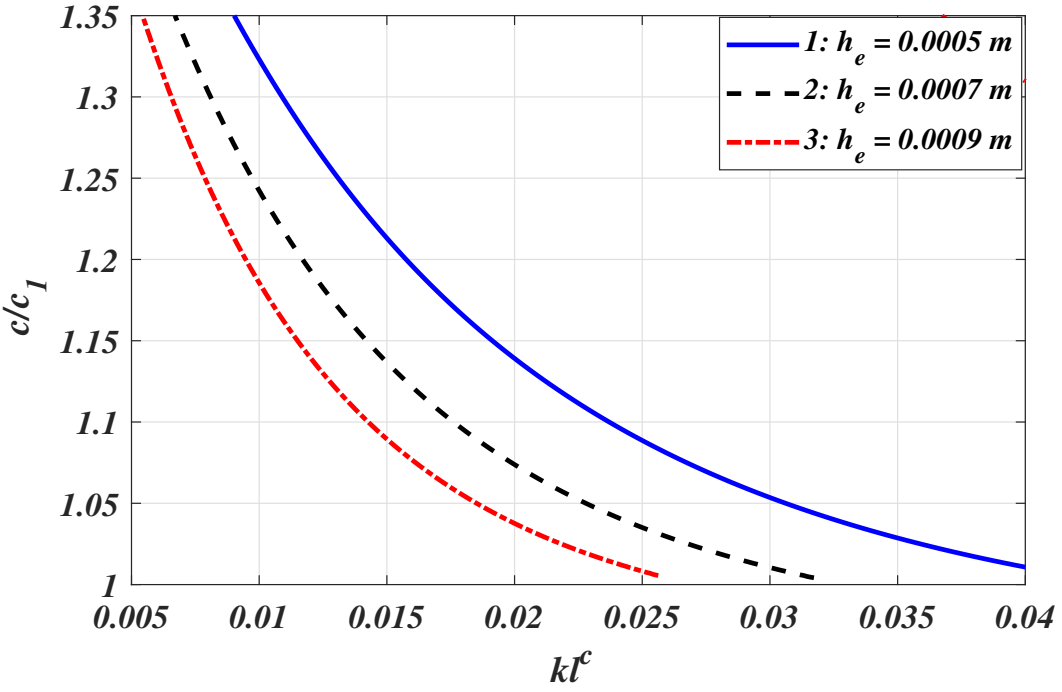

(b) Short circuit condition

Figure 4.4: Dispersion curves (c/c_1 *vs* kl^c) of Love-type waves for different values of thickness (h_e) of FGPEM layer.

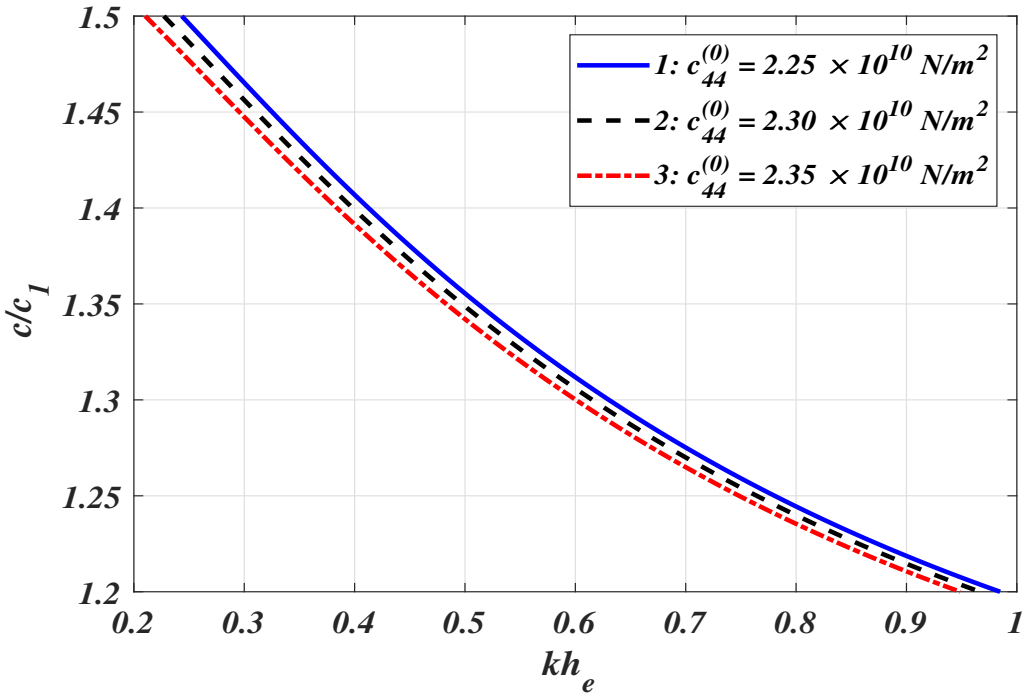

(a) Open circuit condition

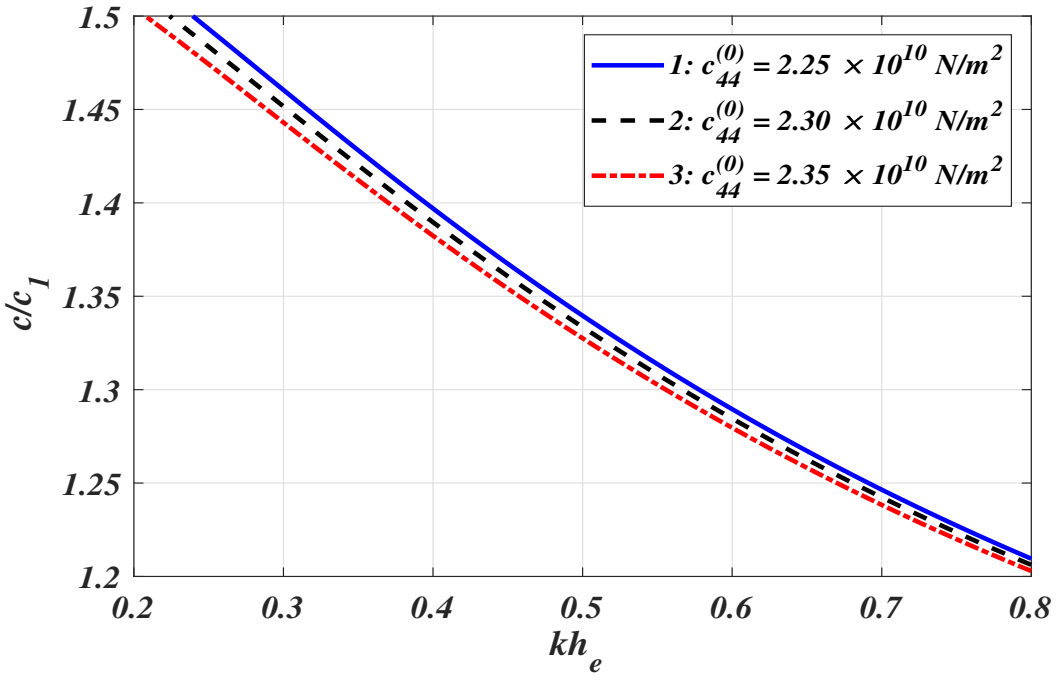

(b) Short circuit condition

Figure 4.5: Dispersion curves (c/c_1 *vs* kh_e) of Love-type waves for different values of elastic constant ($c_{44}^{(0)}$).

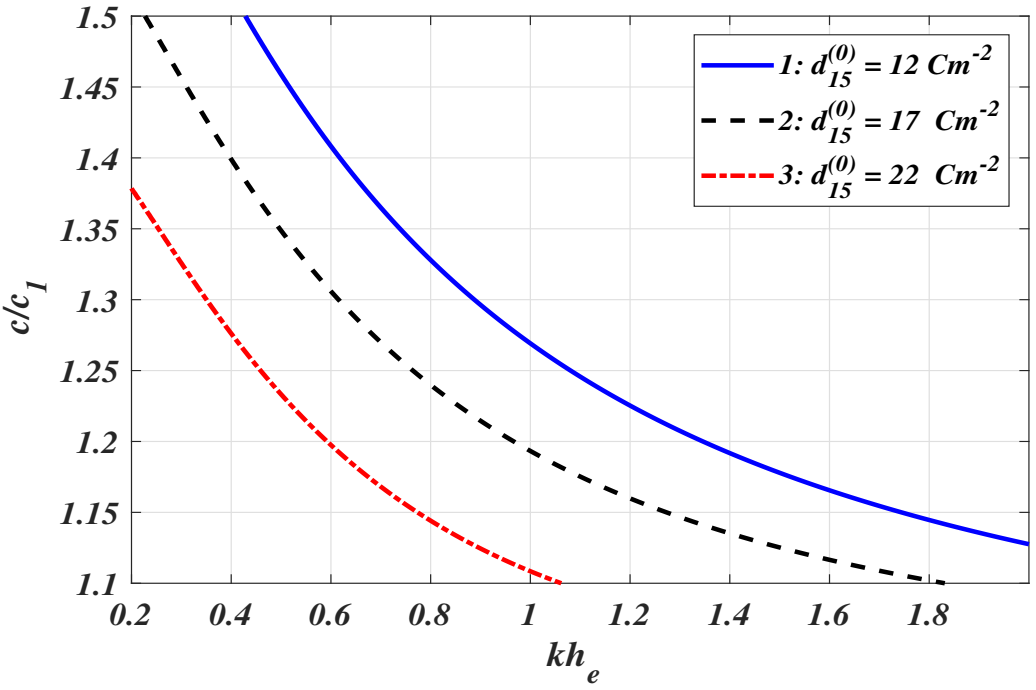

(a) Open circuit condition

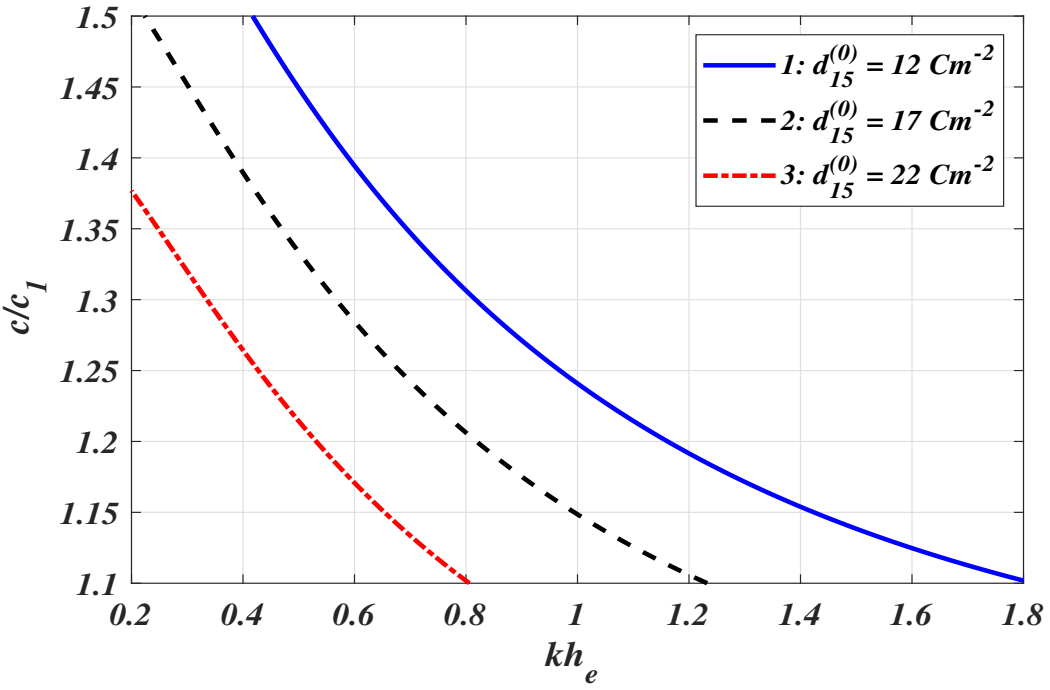

(b) Short circuit condition

Figure 4.6: Dispersion curves (c/c_1 *vs* kh_e) of Love-type waves for different values of PE constant ($d_{15}^{(0)}$).

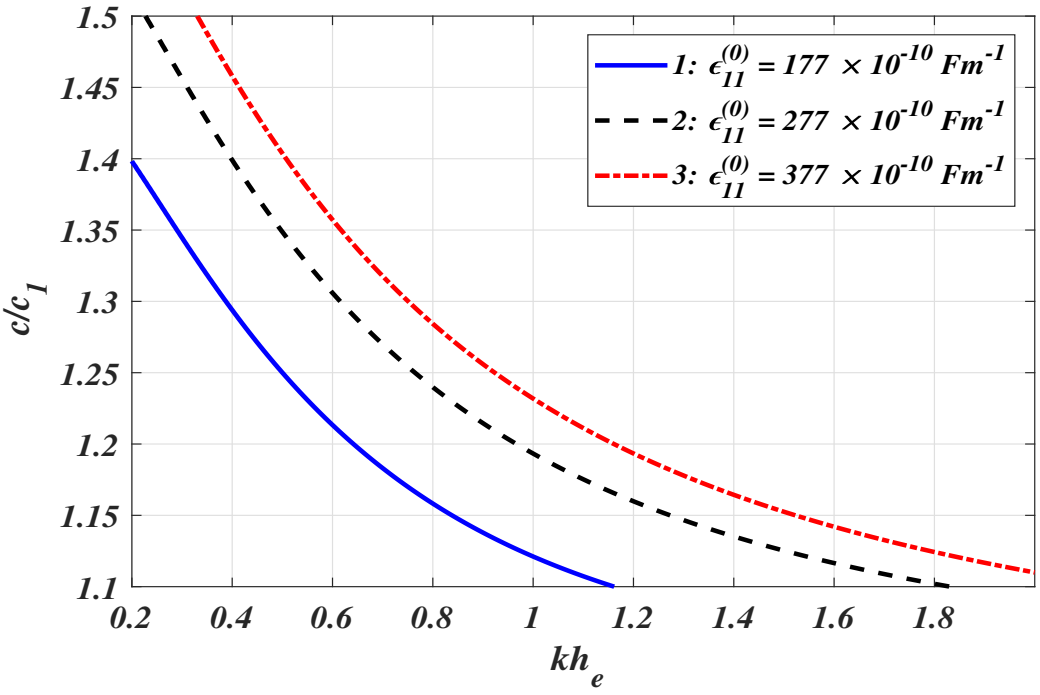

(a) Open circuit condition

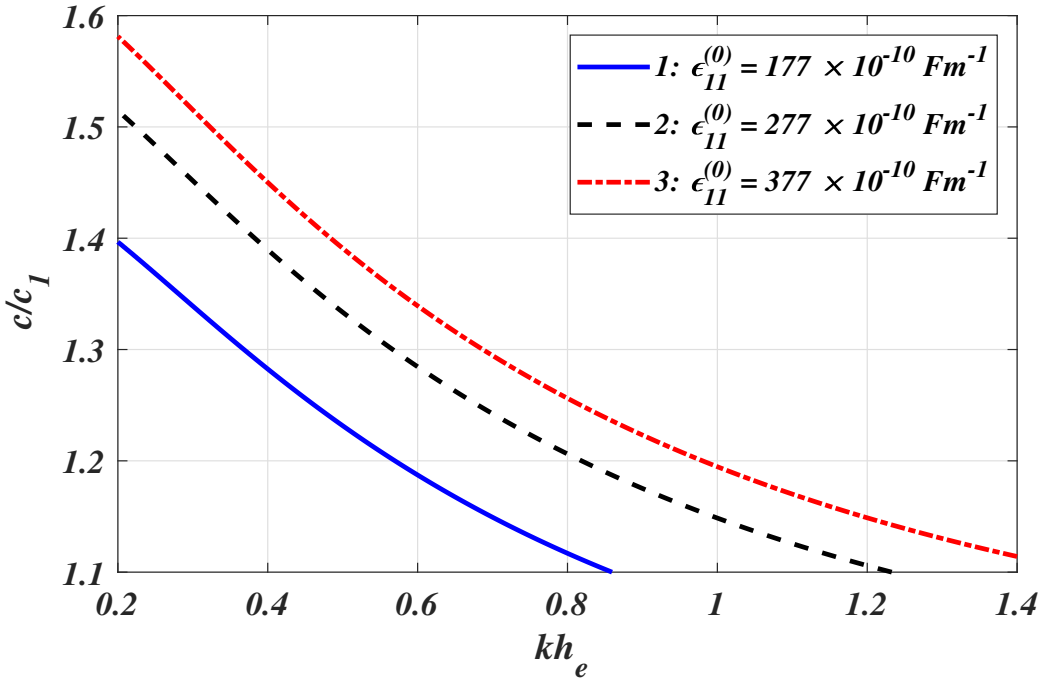

(b) Short circuit condition

Figure 4.7: Dispersion curves (c/c_1 *vs* kh_e) of Love-type waves for different values of dielectric constant ($\epsilon_{11}^{(0)}$).

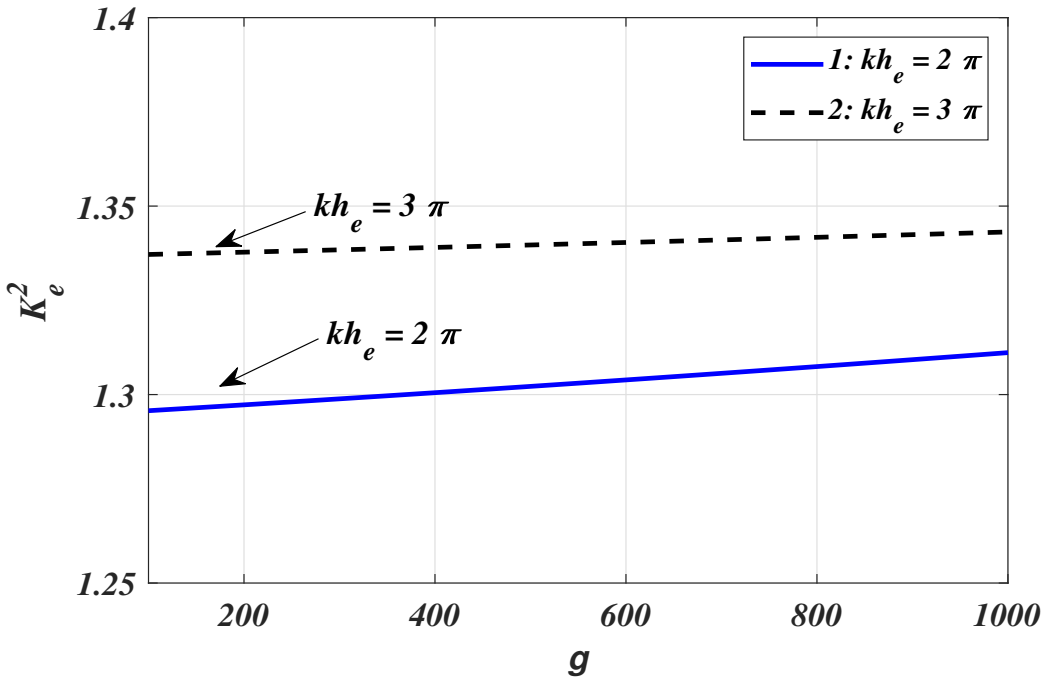

(a)

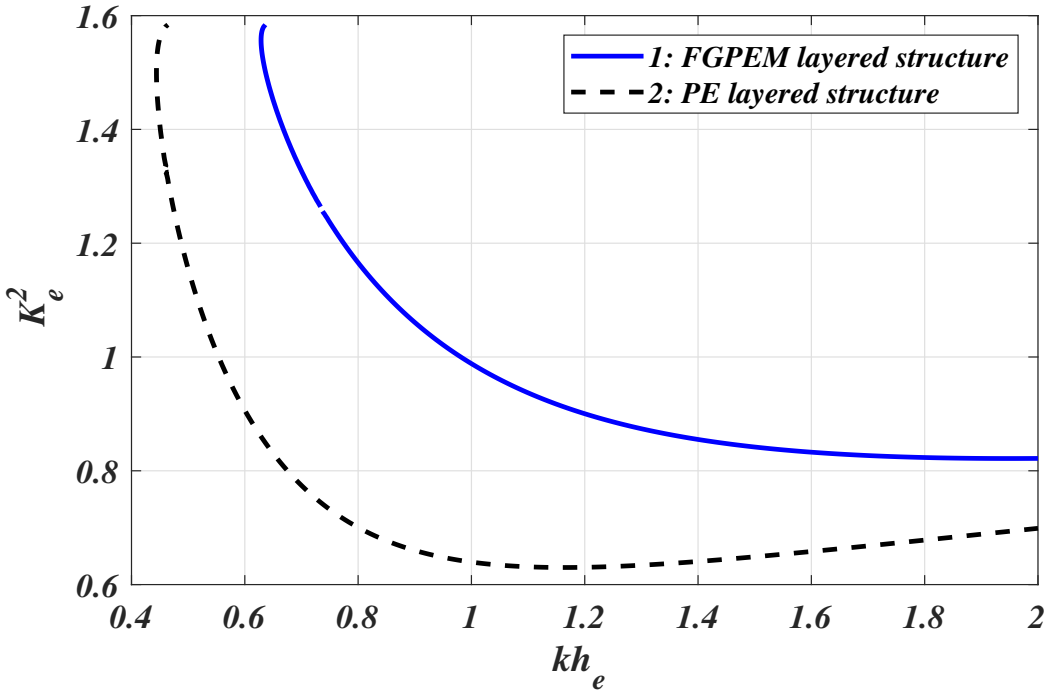

(b)

Figure 4.8: (a) Relation between K_e^2 and g. (b) Comparison of K_e^2 between FGPEM layered structure and PE layered structure.

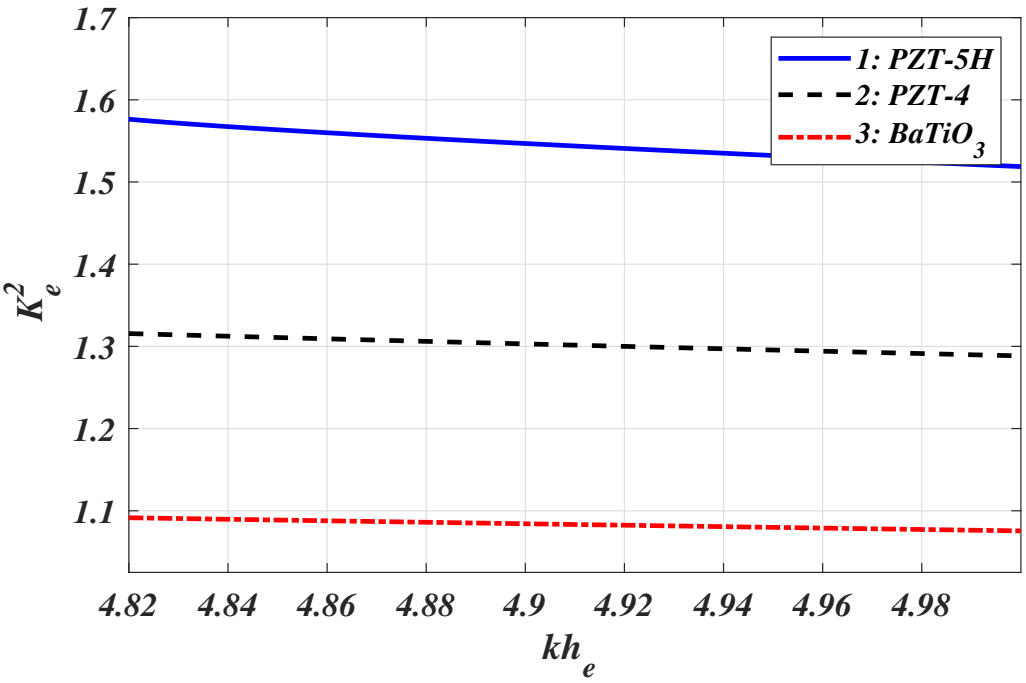

(a)

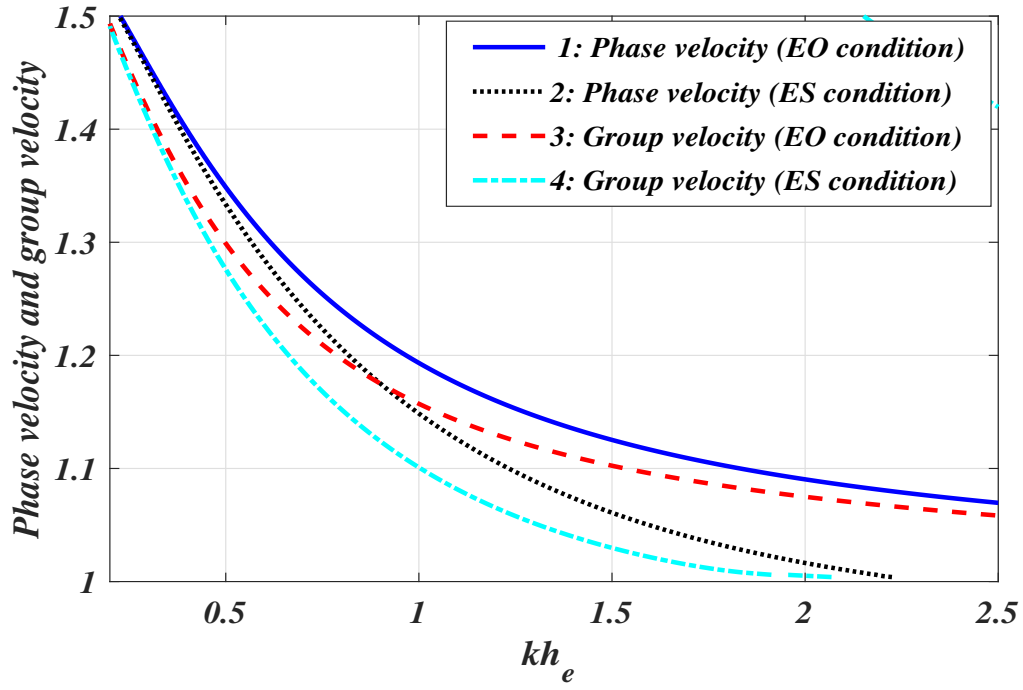

(b)

Figure 4.9: (a) K_e^2 versus non-dimensional wave number (kh_e) for PZT-5H, PZT-4 and $BaTiO_3$. (b) Variation of phase velocity and group velocity in the FGPEM structure for EO and ES conditions.

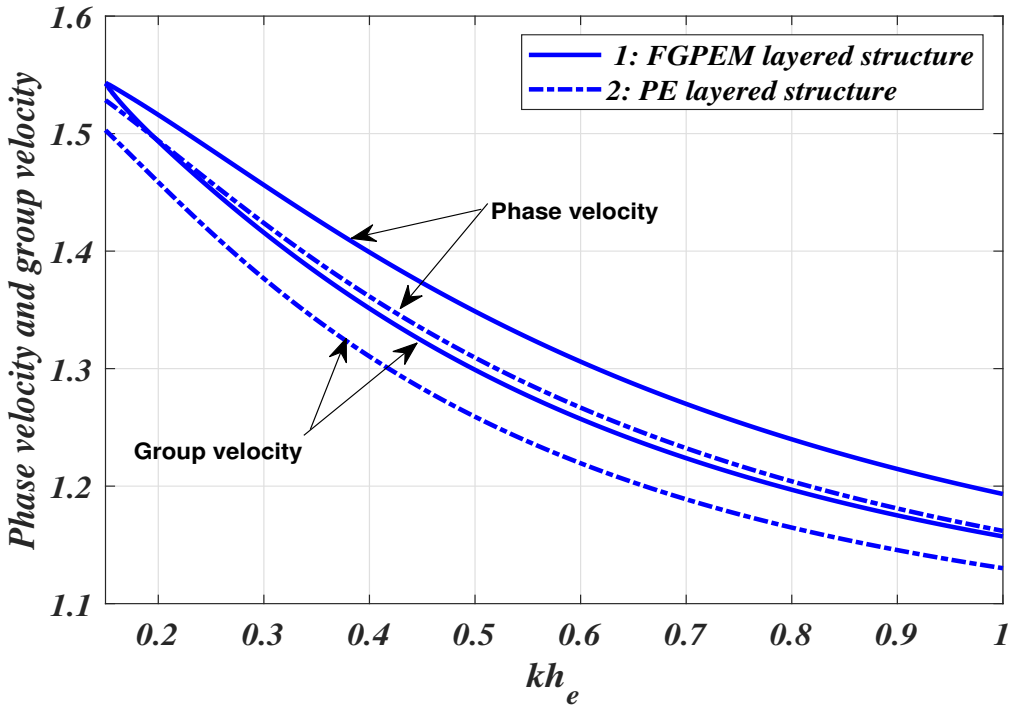

(a) Open circuit condition

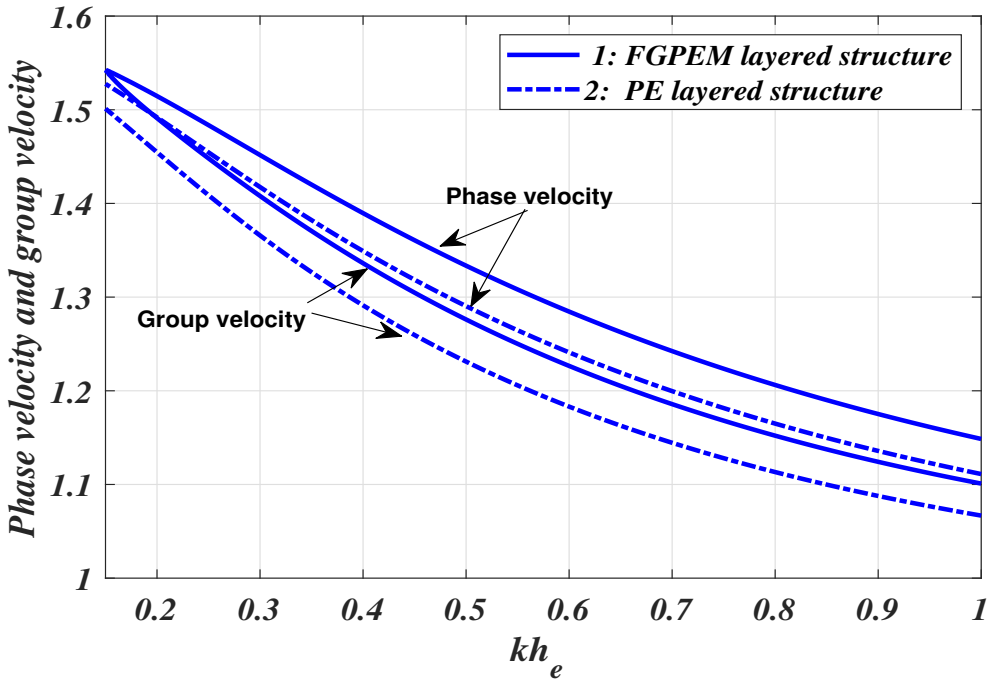

(b) Short circuit condition

Figure 4.10: Comparison of the phase velocity and group velocity between the FGPEM layered structure and PE layered structure.

4.5.1 Effect of microstructures

To grab the microstructural effects exhibited by the size-dependent substrate on the phase velocity of the propagating wave Figs. 4.2 a) and b) are plotted for open and short electrical circuit conditions, respectively. These effects are revealed through a parameter called characteristic length (l^c), which is associated with the substrate. Here values of l^c are varied as 0.00001 m, 0.00003 m and 0.00005 m. It can be depicted from the graphical representations that the characteristic length parameter (l^c) favors the phase velocity of the propagating wave in the considered structure for both open and short circuit conditions.

4.5.2 Effect of functional gradedness

As functionally graded materials are considered superior to conventional laminated materials so it is important to analyze the effect of functional gradedness exhibited by the material on the wave transference in the considered structure. Figs. 4.3 a) and b) display the effect of material gradient parameter (g) responsible for functional gradedness in FGPEM layer. The graphs are plotted for different values of g i.e., 500, 800, 1000. The impact of functional gradedness on the phase velocity of the transferring wave is significantly effective. This parameter favors the phase velocity of the wave transferring in the considered structure for both electrical circuit conditions.

4.5.3 Effect of thickness of FGPEM layer

The thickness of FGPEM layer has a substantial impact on the wave propagation. To capture the effect of thickness, its values are varied as h_e = 0.0005 m, 0.0007 m, and 0.0009 m. Figs. 4.4 a) and b) depict the dependence of phase velocity of propagating wave on the thickness of FGPEM layer. As the thickness of the layer is increasing, the phase velocity of the wave is decreasing.

4.5.4 Effect of material parameters of FGPEM layer

An attempt has been made to capture the effect of the material parameters of the FGPEM layer i.e., elastic constant ($c_{44}^{(0)}$), PE constant ($d_{15}^{(0)}$) and dielectric constant ($\epsilon_{11}^{(0)}$) on the Love-type wave propagation. The elastic constant and PE constant disfavor the phase velocity of the propagating wave. As the values of these parameters ($c_{44}^{(0)} = 2.25 \times 10^{10},\ 2.30 \times 10^{10},\ 2.35 \times 10^{10}\ \ Nm^{-2}$ and $d_{15}^{(0)} = 12,\ 17,\ 22\ Cm^{-2}$) increases, the phase velocity of the transferring wave decreases. Figs. 4.5 a) and b) for elastic constant and

Figs. 4.6 a) and b) for PE constant, elucidate this phenomenon. The effect of dielectric constant ($\epsilon_{11}^{(0)} = 177 \times 10^{-10}$, 277×10^{-10}, 377×10^{-10} Fm^{-1}) on the phase velocity is manifested in Figs. 4.7 a) and b), for both electrical circuit condition. It is reported that dielectric constant has an encouraging effect on the phase velocity of the propagating wave. The increase in the magnitude of dielectric constant leads to an increase in phase velocity of the propagating wave.

4.5.5 Electromechanical coupling factor (K_e^2)

The electromechanical coupling factor (K_e^2) corresponding to the surface waves can be calculated from the following formula [28]

$$K_e^2 = 2\frac{(c_o - c_s)}{c_o}, \tag{4.5.1}$$

where c_o and c_s are the phase velocities for EO and ES circuit conditions, respectively. For conventional engineering applications, greater electromechanical coupling factor is expected in SAW devices. This factor is an essential parameter in designing acoustic sensors. It has a relation with the efficiency of sensors. The relation of electromechanical coupling factor (K_e^2) with the material gradient factor (g) is manifested in Fig. 4.8 a) for two values of $kh_e = 2\pi$ and 3π. The value of electromechanical coupling factor (K_e^2) increases moderately as the material gradient factor (g) increases. It is interesting to observe that the relation between K_e^2 and g is almost constant. Fig. 4.8 b) shows the variation of electromechanical coupling factor (K_e^2) in two different layered structures i.e., FGPEM layered structure and PE layered structure. It can be concluded from this figure that electromechanical coupling factor (K_e^2) drops sharply as kh_e is increasing upto a particular value of wave number then it varies moderately afterward. In FGPEM layered structures electromechanical coupling factor (K_e^2) is more as compared to PE layered structures which interprets that functional gradedness in a smart material enhances electromechanical coupling factor (K_e^2) thus making FGPEM embedded structures more desirable over conventional layered PE structure. Fig. 4.9 a) shows the comparison of electromechanical coupling factor (K_e^2) versus kh_e for different materials namely, PZT-5H, PZT-4 and $BaTiO_3$. It can be observed that K_e^2 is more for PZT-5H ceramic material than the other two materials but as wave number is further increased, K_e^2 varies fairly constant .

4.5.6 Group velocity

As a further exploration, the group velocity (c_g) of the propagating wave is also investigated. It expresses the rate at which transportation of energy is carried out. The group

velocity can be evaluated with the help of following formula [28]

$$c_g = c + k\frac{dc}{dk}, \tag{4.5.2}$$

where k is the wave number and c is the phase velocity. Usually, the association between group velocity and phase velocity is examined by the dispersion property and the relation is termed 'anomalous', if group velocity is found to be greater than the phase velocity otherwise it is called 'normal'. Fig. 4.9 b) exemplifies this phenomenon. It can be concluded that dispersion relation turn out to be 'normal' as phase velocity is found to be more than the group velocity for both the EO and ES conditions. Phase velocity for the EO condition is more than that of ES condition. Phase velocity and group velocity graphs are plotted against non-dimensional wave number (kh_e) for two different structures i.e., FGPEM layered structure and PE layered structure. From Fig. 4.10 a), it can be remarked that for EO condition, the dispersion relation is normal for both the mentioned structures. Similar is the behavior for the ES condition as observed from Fig. 4.10 b). From both the graphs, it is also interpreted that phase velocity and group velocity for FGPEM layered structure are more as compared to the PE layered structure.

Conclusions

The pertinent outcomes of the present work are as follows.

- The phase velocity of the considered propagating wave decrease with the increase in wave number for both electrical circuit condition.
- Characteristic length parameter has a prominent influence on the phase velocity. The increasing values of the parameter results in the increase of the phase velocity of the propagating wave.
- The material gradient parameter has a favorable impact on the phase velocity of the propagating wave.
- The increase in the width of the FGPEM layer results in lowering the phase velocity of the propagating wave.
- The elastic constant and the PE constant associated with the FGPEM layer disfavors the phase velocity of the wave while the dielectric constant has favorable impact for both the electrical circuit conditions.
- Phase velocity of the propagating wave for the EO circuit condition is always more than that of the ES circuit condition.
- As phase velocity is appeared to be greater than the group velocity so the dispersion relation is referred as 'normal' in the considered structure.

Chapter 5

Comparative study of micro-scale size effects on mechanical coupling factors and SH-wave propagation in functionally graded piezoelectric/piezomagnetic structures[4]

5.1 Introduction

Conventional laminated piezo materials are fragile and under extreme environmental conditions these exhibits cracks. The structures involving functionally graded materials (FGMs) bonded with piezo material sensors and actuators behave smartly in response to environmental changes. One of the eminent application areas for FGMs is semiconductor microelectronics. Many FGMs comprise traditional materials such as aluminium, zirconium, etc. These materials are coated with appropriate oxides of technological or natural origin and are further used to manufacture semiconductor products for microelectronics. Elastic moduli of oxides, nitrides, etc. significantly differ from those of the base material, and sometimes the thickness of the coating comprises a substantial part of the total thickness of the product material. For accurate analysis of the mechanical, electrical, and magnetostatic state of such products, it is essential to consider the changes in elastic moduli, electrical, and magnetic resistance along the length or depth of the product material. For this purpose, an exponential law of variation is most often considered due to the simplicity of analysis and also due to its wide occurrence in materials as a result of natural and technological processes [238]. Torsion of an exponentially graded half-space is explored by Selvadurai *et al.* [175]. The action of a point force on a half-space with power law and exponential law inhomogeneity and indentation of the half-space by an axisymmetric indenter is investigated by Giannakopoulos and Suresh ([71], [72]). Selvadurai and Katebi [176] considered Mindlin's problem for an incompressible elastic half-space with an exponential variation in the linear elastic shear modulus. The elastic equilibrium of an ex-

[4]Contents of this chapter are published in SCIE indexed journal, Waves in Random and Complex Media, 2020. DOI: 10.1080/17455030.2020.1851068 with I.F. = 4.853

ponentially inhomogeneous layer is examined by Tokovyy and Ma [206]. They constructed a numerical procedure for the calculation of stresses in the layer in the case of an arbitrarily specified loading on the surface. For the designing of acoustic sensors, the mechanical coupling factors (electromechanical coupling factor, K_e^2 and magnetomechanical coupling factor, K_p^2) are important parameters. These parameters are directly related to the efficiency of a transducer in converting electrical/magnetic energy to mechanical energy, or vice versa [28]. A high value of mechanical coupling factors is desired. The identification of these parameters helps us in the selection of suitable piezo material in designing SAW devices. Abd-alla and Asker [2] carried out numerical simulations for the phase velocities and the electromechanical coupling factor of the BG waves in some piezoelectric smart materials. The graphical illustrations for these factors are procured in this chapter. Since micro-scale size effects are studied in minute dimensions, the classical theory is unable to predict the mechanical properties and dynamic behavior of such structures accurately at micro-scales. Hence, continuum theories which analyze the behavior of materials at micro-scales as well as at macro-scale were proposed by various researchers. Hence, in this chapter micropolar (MP) theory of elasticity proposed by Eringen [60] is considered as a size-dependent mathematical model. This theory grabbing the size effects have numerous applications in investigating anisotropic fluids, bones, cellular solids, platelet composites, polymers, clouds with dust and many other complex microstructures. This is favored for interpreting the behavior of media due to its competence to depict the size effects on a small length scale by considering the additional degrees of freedom ([40], [137]).

In this chapter the propagation of SH-waves in the layered structure in two distinct models is examined. Model I is comprising of functionally graded piezomagnetic material (FGPMM) layer overlying MP half-space substrate and Model II is comprising of functionally graded piezoelectric material (FGPEM) layer overlying MP half-space substrate. All material parameters are assumed to vary along the layer thickness direction with the same exponential function distribution. The focus of the study is to reveal how the inhomogeneity of the functionally graded layer and the micro-scale size effects exhibited by the half-space substrate effect the dispersion behavior of the SH waves. Dispersion equations for two different circuit conditions associated with Model I (i.e. magnetically open (MO) and magnetically short (MS) cases) and Model II (i.e. electrically open (EO) and electrically short (ES) cases) are obtained. The mechanical coupling factors viz. magnetomechanical coupling factor associated with Model I and electromechanical coupling factor associated with Model II alongwith the group velocity of the propagating wave in the considered structures are also investigated and the results are demonstrated graphically.

5.2 Problem formulation

Considering two distinct models, viz. Model I which is constituted by a functionally graded piezomagnetic material (FGPMM) layer of finite thickness h_p overlying MP half-space substrate and Model II which is comprised of functionally graded piezoelectric material (FGPEM) layer of finite thickness h_e overlying MP half-space substrate. Schematic illustrations are shown in Fig. 5.1.

Considering a Cartesian co-ordinate system for both models in such a way that SH-wave is propagating along y-axis and x-axis is considered positive in the vertically downward direction in both the models. The considered substrate is a MP half-space substrate bearing microstructural properties, given by $x > 0$. The considered problem is two dimensional having no variation along the z-axis.

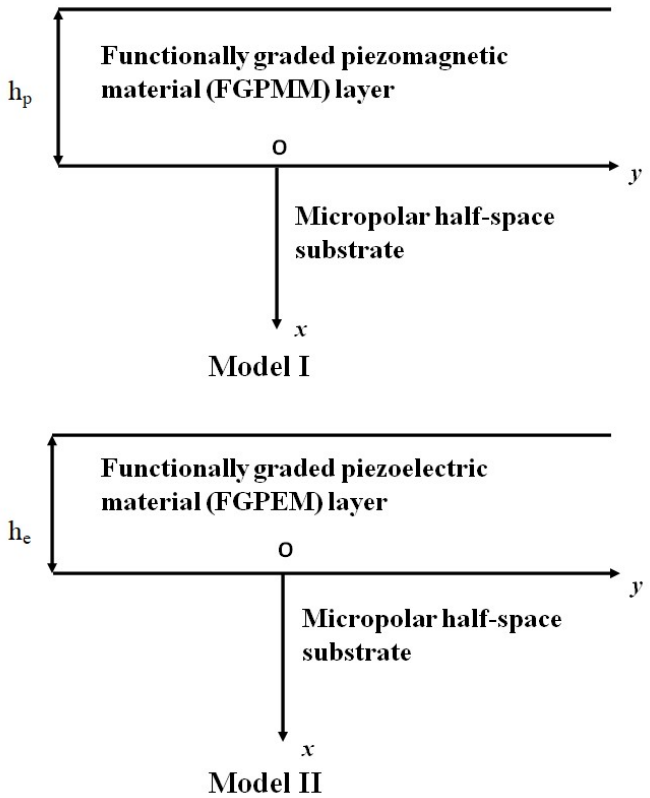

Figure 5.1: Schematic illustration

5.2.1 Dynamics of the functionally graded piezomagnetic material (FGPMM) layer in Model I

The mechanical displacement components for the FGPMM layer (associated with Model I) are assumed as $\overrightarrow{U}^p = (u_1^p, u_2^p, u_3^p)$. As SH-wave is propagating in y-direction and inducing displacement in z-direction, it may be assumed that

$$u_1^p = u_2^p = 0, \quad u_3^p = u_3^p(x, y, t). \tag{5.2.1}$$

The governing equation of motion for FGPMM layer in the absence of body forces are given by [143]

$$\begin{aligned} \sigma_{ij,j}^p &= \rho^p \frac{\partial^2 \overrightarrow{U}^p}{\partial t^2}, \\ B_{i,i}^p &= 0, \qquad (i, j = 1, 2, 3). \end{aligned} \tag{5.2.2}$$

Here superscript 'p' indicates the quantities in FGPMM layer. ρ^p is the mass density and also a function of x. σ_{ij}^p are the stress tensors. B_i^p are the magnetic inductions.
The constitutive equations for a transversely isotropic FGPMM layer with z-axis being the symmetric axis can be expressed as

$$\begin{cases} \sigma_x^p = c_{11}^p(x) S_x^p + c_{12}^p(x) S_y^p + c_{13}^p(x) S_z^p - h_{31}^p(x) H_z^p, \\ \sigma_y^p = c_{12}^p(x) S_x^p + c_{11}^p(x) S_y^p + c_{13}^p(x) S_z^p - h_{31}^p(x) H_z^p, \\ \sigma_z^p = c_{13}^p(x) S_x^p + c_{13}^p(x) S_y^p + c_{33}^p(x) S_z^p - h_{33}^p(x) H_z^p, \\ \sigma_{zx}^p = c_{44}^p(x) S_{zx}^p - h_{15}^p(x) H_x^p, \\ \sigma_{yz}^p = c_{44}^p(x) S_{yz}^p - h_{15}^p(x) H_y^p, \\ \sigma_{xy}^p = \dfrac{1}{2}(c_{11}^p(x) - c_{12}^p(x)) S_{xy}^p, \\ B_x^p = h_{15}^p(x) S_{zx}^p + m_{11}^p(x) H_x^p, \\ B_y^p = h_{15}^p(x) S_{yz}^p + m_{11}^p(x) H_y^p, \\ B_z^p = h_{31}^p(x) S_x^p + h_{31}^p(x) S_y^p + h_{33}^p(x) S_z^p + m_{33}^p(x) H_z^p, \end{cases} \tag{5.2.3}$$

where S_{kl}^p are the strain tensors. $c_{ijkl}^p(x)$, $h_{kij}^p(x)$, $m_{ij}^p(x)$, and H_i^p are the stiffness coefficients, PM coefficients, and magnetic permeability respectively.
Magnetic field intensity H^p is related to magnetic potential function ϕ^p as

$$H^p = -\nabla \phi^p \tag{5.2.4}$$

where ∇ represents gradient of a function.
The strain components are defined as

$$\begin{aligned} S_x^p = u_{1,x}^p, \quad S_y^p = u_{2,y}^p, \quad S_z^p = u_{3,z}^p, \\ S_{yz}^p = u_{3,y}^p + u_{2,z}^p, \quad S_{zx}^p = u_{1,z}^p + u_{3,x}^p, \quad S_{xy}^p = u_{1,y}^p + u_{2,x}^p. \end{aligned} \tag{5.2.5}$$

Invoking (5.2.1) in (5.2.4) and (5.2.5), we get the strain and magnetic potential components as

$$\begin{aligned} S_x^p = S_y^p = S_z^p = 0, \quad S_{yz}^p = u_{3,y}^p, \quad S_{zx}^p = u_{3,x}^p, \quad S_{xy}^p = 0, \\ H_x^p = -\phi_{,x}^p, \quad H_y^p = -\phi_{,y}^p, \quad H_z^p = 0. \end{aligned} \tag{5.2.6}$$

Enforcing Eq. (5.2.6) in Eq. (5.2.3) and then in Eq. (5.2.2), the governing equations for the FGPMM layer are procured as

$$\left.\begin{aligned} c_{44}^p(x)\nabla^2 u_3^p + h_{15}^p(x)\nabla^2\phi^p + \frac{\partial c_{44}^p(x)}{\partial x}\frac{\partial u_3^p}{\partial x} + \frac{\partial h_{15}^p(x)}{\partial x}\frac{\partial \phi^p}{\partial x} = \rho^p(x)\frac{\partial^2 u_3^p}{\partial t^2}, \\ h_{15}^p(x)\nabla^2 u_3^p - m_{11}^p(x)\nabla^2\phi^p + \frac{\partial h_{15}^p(x)}{\partial x}\frac{\partial u_3^p}{\partial x} - \frac{\partial m_{11}^p(x)}{\partial x}\frac{\partial \phi^p}{\partial x} = 0. \end{aligned}\right\} \tag{5.2.7}$$

Presuming the material properties of the FGPMM layer to have positive exponential inhomogeneity along the x-axis as

$$c_{44}^p(x) = c_{44}^{(1)}e^{g_1 x}, \quad h_{15}^p(x) = h_{15}^{(1)}e^{g_1 x}, \quad m_{11}^p(x) = m_{11}^{(1)}e^{g_1 x}, \text{ and } \rho^p(x) = \rho^{(1)}e^{g_1 x}, \tag{5.2.8}$$

where g_1 is the material gradient factor which characterizes the degree of the functional gradedness of the FGPMM layer and superscript '(1)' indicates the values of c_{44}^p, h_{15}^p, m_{11}^p, and ρ^p at $x = 0$. Implementing Eq. (5.2.8) into Eq. (5.2.7), it can be instated that

$$\begin{cases} c_{44}^{(1)}\left(\nabla^2 u_3^p + g_1\dfrac{\partial u_3^p}{\partial x}\right) + h_{15}^{(1)}\left(\nabla^2\phi^p + g_1\dfrac{\partial \phi^p}{\partial x}\right) = \rho^{(1)}\dfrac{\partial^2 u_3^p}{\partial t^2}, \\ h_{15}^{(1)}\left(\nabla^2 u_3^p + g_1\dfrac{\partial u_3^p}{\partial x}\right) = m_{11}^{(1)}\left(\nabla^2\phi^p + g_1\dfrac{\partial \phi^p}{\partial x}\right) \end{cases} \tag{5.2.9}$$

Rewriting Eqs. (5.2.9) as

$$\begin{cases} \nabla^2 u_3^p + g_1\dfrac{\partial u_3^p}{\partial x} = \dfrac{1}{d_1^2}\dfrac{\partial^2 u_3^p}{\partial t^2}, \\ \nabla^2\phi^p + g_1\dfrac{\partial \phi^p}{\partial x} = \dfrac{1}{d_1^2}\left(\dfrac{h_{15}^{(1)}}{m_{11}^{(1)}}\right)\dfrac{\partial^2 u_3^p}{\partial t^2}, \end{cases} \tag{5.2.10}$$

where $\overline{c_{44}^{(1)}} = c_{44}^{(1)} + \frac{(h_{15}^{(1)})^2}{m_{11}^{(1)}}$, and $d_1 = \sqrt{\frac{\overline{c_{44}^{(1)}}}{\rho^{(1)}}}$, is the shear wave velocity in the FGPMM layer. Following solutions of the mechanical displacement component and magnetic potential

function of the SH-wave in the FGPMM layer are assumed.

$$\begin{aligned} u_3^p(x,y,t) &= \breve{P}(x)e^{ik(y-ct)}, \\ \phi^p(x,y,t) &= \breve{Q}(x)e^{ik(y-ct)} \end{aligned} \tag{5.2.11}$$

Invoking Eq. (5.2.11) in Eq. (5.2.10) we attained

$$\begin{aligned} \breve{P}''(x) + g_1\breve{P}'(x) + k^2 d_2^2 \breve{P}(x) &= 0, \\ \breve{Q}''(x) + g_1\breve{Q}'(x) - k^2\breve{Q}(x) &= \left(\frac{-k^2c^2h_{15}^{(1)}}{d_1^2 m_{11}^{(1)}}\right)\breve{P}(x), \end{aligned} \tag{5.2.12}$$

where $d_2 = \sqrt{\frac{c^2}{d_1^2} - 1}$.
Differential equations (5.2.12) are solved and their solutions are implemented in Eq. (5.2.11). Then, the displacement component and magnetic potential function can be asserted as

$$\begin{aligned} u_3^p(x,y,t) &= [\cos(d_3x)D_1 + \sin(d_3x)D_2]e^{-g_1x/2}e^{ik(y-ct)}, \\ \phi^p(x,y,t) &= \left[\frac{h_{15}^{(1)}}{m_{11}^{(1)}}\left(\cos(d_3x)D_1 + \sin(d_3x)D_2\right)e^{-g_1x/2} + e^{d_4x}D_3 + e^{d_5x}D_4\right]e^{ik(y-ct)}, \end{aligned} \tag{5.2.13}$$

where D_1, D_2, D_3, and D_4 are arbitrary constants. Here
$d_3 = \frac{\sqrt{4k^2d_2^2 - g_1^2}}{2}$,
$d_4 = -\frac{g_1}{2} - \frac{\sqrt{g_1^2+4k^2}}{2}$,
$d_5 = -\frac{g_1}{2} + \frac{\sqrt{g_1^2+4k^2}}{2}$.

5.2.2 Dynamics of the functionally graded piezoelectric material (FGPEM) layer in Model II

The governing equations and constitutive relations for the FGPEM layer in the absence of body forces are discussed in Chapter 4 and can be accessed from Eqs. (4.1.2) and (4.1.3). The displacement component and electric potential function for the FGPEM layer can be obtained from Eq. (4.1.13).

5.2.3 Dynamics of semi-infinite micropolar (MP) elastic substrate

In a homogeneous MP isotropic elastic media ($x > 0$), the propagation of SH-wave in y-direction induces displacement $\overrightarrow{U^m}$ and microrotation $\overrightarrow{M^m}$ as

$$\begin{aligned} u_1^m = u_2^m = 0, \quad u_3^m = u_3^m(x,y,t), \\ M_1^m = M_1^m(x,y,t), \quad M_2^m = M_2^m(x,y,t), \quad M_3^m = 0, \end{aligned} \tag{5.2.14}$$

respectively.

Following are the equation of motion and constitutive relations as suggested by Eringen [60] for semi-infinite MP elastic substrate in the absence of body forces in vector form

$$\left.\begin{aligned} (\lambda^m + \mu^m)\nabla(\nabla.\overrightarrow{U^m}) + (\mu^m + \kappa^m)\nabla^2\overrightarrow{U^m} + \kappa^m(\nabla \times \overrightarrow{M^m}) = \rho^m \frac{\partial^2 \overrightarrow{U^m}}{\partial t^2}, \\ (\alpha^m + \beta^m + \gamma^m)\nabla(\nabla.\overrightarrow{M^m}) - \gamma^m \nabla \times (\nabla \times \overrightarrow{M^m}) + \kappa^m(\nabla \times \overrightarrow{U^m}) - 2\kappa^m \overrightarrow{M^m} = \jmath^m \rho^m \frac{\partial^2 \overrightarrow{M^m}}{\partial t^2}. \end{aligned}\right\} \tag{5.2.15}$$

$$\left.\begin{aligned} \sigma_{ij}^m = \lambda^m u_{k,k}^m \delta_{ij} + \mu^m(u_{i,j}^m + u_{j,i}^m) + \kappa^m(u_{j,i}^m - \epsilon_{ijk} M_k^m), \\ \mu_{ij}^m = \alpha^m M_{k,k}^m \delta_{ij} + \beta^m M_{i,j}^m + \gamma^m M_{j,i}^m, \qquad (i,j,k = 1,2,3) \end{aligned}\right\} \tag{5.2.16}$$

where λ^m and μ^m are Lamé constants. ρ^m is density of MP elastic material, σ_{ij}^m and μ_{ij}^m are the force stress tensors and the CS tensors, respectively of the semi-infinite MP elastic substrate. α^m, β^m, γ^m, κ^m are the additional MP elastic constants. $\jmath^m$ is the micro inertia. δ_{ij} is kronecker delta. ϵ_{ijk} is a permutation tensor.

In the MP model the parametric relations [68] are characterized as

$$\gamma^m = 4(l^m)^2\left(\mu^m + \frac{\kappa^m}{2}\right), \qquad \kappa^m = \frac{2(N^m)^2\mu^m}{1 - 2(N^m)^2}, \tag{5.2.17}$$

where N^m $(0 < N^m < 1)$ is a coupling constant. It regulates the degree of micropolarity produced by the materials.

Moreover, the length scale parameter is estimated by the characteristic length (l^m).

Employing the Helmholtz decomposition of vectors, we can write

$$\overrightarrow{M^m} = \nabla\Im + \nabla \times \vec{\xi}, \qquad \nabla.\vec{\xi} = 0, \tag{5.2.18}$$

where $\vec{\xi} = (0, 0, -\xi)$. $\Im$ is a scalar potential and $\vec{\xi}$ is a vector potential function.
The microrotation vector components can be written as

$$M_1^m = \frac{\partial \Im}{\partial x} - \frac{\partial \xi}{\partial y}, \quad M_2^m = \frac{\partial \Im}{\partial y} + \frac{\partial \xi}{\partial x}, \quad \text{and} \quad M_3^m = 0. \tag{5.2.19}$$

Substituting Eqs. (5.2.14) and (5.2.19), in Eq. (5.2.16) and then in Eq. (5.2.15), we get

$$\left.\begin{aligned} \nabla^2 u_3^m + T_1 \nabla^2 \xi &= \frac{1}{T_2^2} \frac{\partial^2 u_3^m}{\partial t^2}, \\ \nabla^2 \Im - \left(\frac{2T_5^2}{T_3^2 + T_4^2}\right) \Im &= \left(\frac{1}{T_3^2 + T_4^2}\right) \frac{\partial^2 \Im}{\partial t^2}, \\ \nabla^2 \xi - \frac{2T_5^2}{T_3^2} \xi - \frac{T_5^2}{T_3^2} u_3^m &= \frac{1}{T_3^2} \frac{\partial^2 \xi}{\partial t^2}, \end{aligned}\right\} \tag{5.2.20}$$

where
$T_1 = \frac{\kappa^m}{\mu^m + \kappa^m}$, $T_2 = \sqrt{\frac{\mu^m + \kappa^m}{\rho^m}}$, $T_3 = \sqrt{\frac{\gamma^m}{\jmath^m \rho^m}}$, $T_4 = \sqrt{\frac{\alpha^m + \beta^m}{\jmath^m \rho^m}}$, $T_5 = \sqrt{\frac{\kappa^m}{\jmath^m \rho^m}}$.
Let us assume the solutions of Eqs. (5.2.20) as

$$\begin{aligned} u_3^m(x, y, t) &= \tilde{P}(x) e^{ik(y - ct)}, \\ \Im(x, y, t) &= \tilde{Q}(x) e^{ik(y - ct)}, \\ \xi(x, y, t) &= \Xi(x) e^{ik(y - ct)}, \end{aligned} \tag{5.2.21}$$

where k is the wave number and c is the phase velocity.
Solving Eqs. (5.2.20) with the help of Eqs. (5.2.21) and using the radiation conditions $\tilde{P}(x)$, $\tilde{Q}(x)$ and $\Xi(x) \to 0$ as $x \to \infty$ on the general solutions of Eqs. (5.2.21), we get the following solutions of potential functions and displacement component in semi-infinite MP elastic substrate

$$\begin{aligned} \Im(x, y, t) &= e^{-e_1 x} D_5 e^{ik(y - ct)}, \\ \xi(x, y, t) &= [e^{-e_2 x} D_6 + e^{-e_3 x} D_7] e^{ik(y - ct)}, \\ u_3^m(x, y, t) &= [\chi_1 e^{-e_2 x} D_6 + \chi_2 e^{-e_3 x} D_7] e^{ik(y - ct)}, \end{aligned} \tag{5.2.22}$$

where D_5, D_6, and D_7 are arbitrary constants. Here
$e_1^2 = k^2 + \frac{2T_5^2}{T_3^2 + T_4^2} - \frac{k^2 c^2}{T_3^2 + T_4^2}$,
$e_2^2, e_3^2 = \frac{S_1 \pm \sqrt{S_1^2 - 4S_2}}{2}$,
$S_1 = -k^2 c^2 (\frac{1}{T_2^2} + \frac{1}{T_3^2}) - \frac{T_5^2}{T_3^2}(T_1 - 2) + 2k^2$,
$S_2 = (\frac{k^2 c^2}{T_3^2} - \frac{2T_5^2}{T_3^2} - k^2)(\frac{k^2 c^2}{T_2^2} - k^2) - \frac{T_5^2 T_1 k^2}{T_3^2}$,
$\chi_1 = \frac{T_3^2}{T_5^2}\left(e_2^2 + \frac{k^2 c^2}{T_3^2} - \frac{2T_5^2}{T_3^2} - k^2\right)$,
$\chi_2 = \frac{T_3^2}{T_5^2}\left(e_3^2 + \frac{k^2 c^2}{T_3^2} - \frac{2T_5^2}{T_3^2} - k^2\right)$.

5.3 Boundary conditions

Following are the boundary conditions for the above-mentioned models (Model I and II).

5.3.1 For Model I

(i) The magnetic boundary conditions at the free surface above the layer i.e., at $x = -h_p$ is

$$\begin{aligned} B_x^p(x,y) &= 0, \quad \{\text{magnetically open (MO) condition}\}, \\ \phi^p(x,y) &= 0, \quad \{\text{magnetically short (MS) condition}\}. \end{aligned} \tag{5.3.1}$$

(ii) The mechanical traction free condition at $x = -h_p$ is

$$\sigma_{zx}^p(x,y) = 0. \tag{5.3.2}$$

(iii) The continuity conditions at the interfacial surface between FGPMM layer and semi-infinite MP substrate i.e., at $x = 0$

$$\begin{aligned} u_3^p(x,y) &= u_3^m(x,y), \\ \sigma_{zx}^p(x,y) &= \sigma_{zx}^m(x,y), \\ \mu_{xy}^m(x,y) &= 0, \\ \mu_{xx}^m(x,y) &= 0, \\ \phi^p(x,y) &= 0. \end{aligned} \tag{5.3.3}$$

5.3.2 For Model II

(i) The electric boundary conditions at the free surface above the layer i.e., at $x = -h_e$ is

$$\begin{aligned} D_x^e(x,y) &= 0, \quad \{\text{electrically open (EO) condition }\}, \\ \phi^e(x,y) &= 0, \quad \{\text{electrically short (ES) condition }\}. \end{aligned} \tag{5.3.4}$$

(ii) The mechanical traction free condition at $x = -h_e$ is

$$\sigma_{zx}^e(x,y) = 0. \tag{5.3.5}$$

(iii) The continuity conditions at the interfacial surface between FGPEM layer and semi-infinite MP substrate i.e., at $x = 0$

$$\begin{aligned} u_3^e(x,y) &= u_3^m(x,y), \\ \sigma_{zx}^e(x,y) &= \sigma_{zx}^m(x,y), \\ \mu_{xy}^m(x,y) &= 0, \\ \mu_{xx}^m(x,y) &= 0, \\ \phi^e(x,y) &= 0. \end{aligned} \tag{5.3.6}$$

5.4 Derivation of dispersion relations associated with Model I

Considering MO condition from Eq. (5.3.1) together with Eqs. (5.3.2) and (5.3.3) incorporate the requisite boundary conditions for MO case and considering MS condition from Eq. (5.3.1) together with Eqs. (5.3.2) and (5.3.3) incorporate the requisite boundary conditions for MS case of Model I. Hence, we obtain the homogeneous system of equations in terms of seven unknown coefficients $D_1,\ D_2,\ D_3,\ D_4,\ D_5,\ D_6$, and D_7.

$$\chi_3\overline{c_{44}^{(1)}}e^{g_1h_p/2}D_1 + \chi_4\overline{c_{44}^{(1)}}e^{g_1h_p/2}D_2 + d_4h_{15}^{(1)}e^{-d_4h_p}D_3 + d_5h_{15}^{(1)}e^{-d_5h_p}D_4 = 0, \tag{5.4.1}$$

$$D_1 - \chi_1D_6 - \chi_2D_7 = 0, \tag{5.4.2}$$

$$-\overline{c_{44}^{(1)}}\left(\frac{g_1}{2}\right)D_1 + \overline{c_{44}^{(1)}}d_3D_2 + d_4h_{15}^{(1)}D_3 + d_5h_{15}^{(1)}D_4 + ik\kappa^mD_5 + \chi_5D_6 + \chi_6D_7 = 0, \tag{5.4.3}$$

$$\left(\frac{h_{15}^{(1)}}{m_{11}^{(1)}}\right)D_1 + D_3 + D_4 = 0, \tag{5.4.4}$$

$$-ike_1\chi_7D_5 + \chi_8D_6 + \chi_9D_7 = 0, \tag{5.4.5}$$

$$\chi_{10}D_5 + ike_2\chi_7D_6 + ike_3\chi_7D_7 = 0, \tag{5.4.6}$$

$$d_4e^{-d_4h_p}D_3 + d_5e^{-d_5h_p}D_4 = 0. \tag{5.4.7}$$

Here
$\chi_3 = d_3 \sin(d_3 h_p) - \left(\frac{g_1}{2}\right) \cos(d_3 h_p)$,
$\chi_4 = d_3 \cos(d_3 h_p) + \left(\frac{g_1}{2}\right) \sin(d_3 h_p)$,
$\chi_5 = (\mu^m \chi_1 - \kappa^m) e_2$,
$\chi_6 = (\mu^m \chi_2 - \kappa^m) e_3$,
$\chi_7 = \beta^m + \gamma^m$,
$\chi_8 = \beta^m k^2 + \gamma^m e_2^2$,
$\chi_9 = \beta^m k^2 + \gamma^m e_3^2$,
$\chi_{10} = (\alpha^m + \beta^m + \gamma^m) e_1^2 - \alpha^m k^2$.

To get the non-trivial solution and hence the dispersion relation, we equate the determinant of these coefficients to zero.

5.4.1 Dispersion relation for MO case

We get the following dispersion relation for SH-wave propagation in FGPMM layer overlying semi-infinite MP substrate, for MO case.

$$\left[\overline{c_{44}^{(1)}} \left(d_3 \chi_3 + \left(\frac{g_1}{2}\right) \chi_4\right) \chi_{11} + \chi_4 d_4 d_5 \left(\frac{(h_{15}^{(1)})^2}{m_{11}^{(1)}}\right) (e^{-d_4 h_p} - e^{-d_5 h_p})\right] [\chi_1 \Theta_2 - \chi_2 \Theta_1] + \Theta_4 \chi_4 \chi_{11} = 0. \tag{5.4.8}$$

5.4.2 Dispersion relation for MS case

We get the following dispersion relation for SH-wave propagation in FGPMM layer overlying semi-infinite MP substrate, for MS case.

$$\left[\overline{c_{44}^{(1)}} \left(\chi_3 \chi_{16} + \left(\frac{g_1}{2}\right) \chi_{14} + \left(\frac{(h_{15}^{(1)})^2}{m_{11}^{(1)}}\right) \cos(d_3 h_p) \chi_{17}\right) + \left(\frac{(h_{15}^{(1)})^2}{m_{11}^{(1)}}\right) \chi_{15}\right] [\chi_1 \Theta_2 - \chi_2 \Theta_1] + \chi_{14} \Theta_4 = 0, \tag{5.4.9}$$

where
$\Theta_1 = k^2 e_1 e_2 \chi_7^2 - \chi_8 \chi_{10}$,
$\Theta_2 = k^2 e_1 e_3 \chi_7^2 - \chi_9 \chi_{10}$,
$\Theta_3 = e_3 \chi_8 - e_2 \chi_9$,
$\Theta_4 = -k^2 \kappa^m \chi_7 \Theta_3 - \chi_5 \Theta_2 + \chi_6 \Theta_1$,
$\Theta_5 = \chi_1 \Theta_2 - \chi_2 \Theta_1$,
$\chi_{11} = d_4 e^{-d_4 h_p} - d_5 e^{-d_5 h_p}$,
$\chi_{12} = \overline{c_{44}^{(1)}} \chi_4 + d_5 \frac{(h_{15}^{(1)})^2}{m_{11}^{(1)}} \sin(d_3 h_p)$,
$\chi_{13} = \overline{c_{44}^{(1)}} \chi_4 + d_4 \frac{(h_{15}^{(1)})^2}{m_{11}^{(1)}} \sin(d_3 h_p)$,

$\chi_{14} = \overline{c_{44}^{(1)}}\chi_4(e^{-d_4 h_p} - e^{-d_5 h_p}) - \frac{(h_{15}^{(1)})^2}{m_{11}^{(1)}}\sin(d_3 h_p)\chi_{11},$
$\chi_{15} = \overline{c_{44}^{(1)}}d_3 e^{-(d_4+d_5+g_1/2)h_p}(d_4 - d_5) - d_4\chi_{12}e^{-d_5 h_p} + d_5\chi_{13}e^{-d_4 h_p},$
$\chi_{16} = \overline{c_{44}^{(1)}}d_3(e^{-d_4 h_p} - e^{-d_5 h_p}) + \frac{(h_{15}^{(1)})^2}{m_{11}^{(1)}}e^{g_1 h_p/2}\sin(d_3 h_p)(d_4 - d_5),$
$\chi_{17} = d_3\chi_{11} + e^{g_1 h_p/2}\chi_4(d_4 - d_5).$

5.4.3 Some special cases and validation of Model I

Some special cases of proposed Model I are discussed in this section.

1. Considering α^m, β^m, γ^m, $\jmath^m$, and $\kappa^m \to 0$ then semi-infinite MP substrate reduces to isotropic elastic half-space substrate and the dispersion relations for both MO and MS cases reduce to

$$\overline{c_{44}^{(1)}}\chi_{11}\left(\frac{g_1}{2}\chi_4 + d_3\chi_3\right) - \left(\frac{(h_{15}^{(1)})^2}{m_{11}^{(1)}}\right)d_4 d_5\chi_4\chi_{11} = \chi_4\chi_{11}k\mu^1\sqrt{1 - \frac{c^2}{\overline{a_3}^2}}, \tag{5.4.10}$$

$$\left[\overline{c_{44}^{(1)}}\left(\frac{g_1}{2}\right)\chi_{14} + \left(\frac{(h_{15}^{(1)})^2}{m_{11}^{(1)}}\right)\chi_{15} + \overline{c_{44}^{(1)}}\chi_3\chi_{16} + \overline{c_{44}^{(1)}}\left(\frac{(h_{15}^{(1)})^2}{m_{11}^{(1)}}\right)\cos(d_3 h_p)\chi_{17}\right] = \chi_{14}k\mu^1\sqrt{1 - \frac{c^2}{\overline{a_3}^2}}, \tag{5.4.11}$$

respectively. Here $\overline{a_3} = \sqrt{\frac{\mu^1}{\rho^1}}$, μ^1 is shear modulus of elasticity and ρ^1 is density of isotropic elastic half-space. Eqs. (5.4.10) and (5.4.11) represent the dispersion relations in FGPMM layer overlying isotropic elastic half-space for MO and MS cases, respectively.

2. In the absence of functional gradedness in the FGPMM layer (i.e., $g_1 = 0$), the dispersion relations for MO (5.4.8) and MS (5.4.9) cases, respectively take the following form

$$k\Theta_5\chi_{18} - \Theta_4 = 0, \tag{5.4.12}$$

$$k\Theta_5\chi_{20} - \Theta_4\chi_{19} = 0. \tag{5.4.13}$$

Eqs. (5.4.12) and (5.4.13) represent the dispersion relations of SH-wave in PM layer overlying semi-infinite MP substrate, for MO and MS cases, respectively. Here
$\chi_{18} = \overline{c_{44}^{(1)}}d_2\tan(kd_2 h_p) + \frac{(h_{15}^{(1)})^2}{m_{11}^{(1)}}\tanh(kh_p),$
$\chi_{19} = \overline{c_{44}^{(1)}}d_2\tanh(kh_p) - \frac{(h_{15}^{(1)})^2}{m_{11}^{(1)}}\tan(kd_2 h_p),$
$\chi_{20} = \left(\frac{2(h_{15}^{(1)})^2\overline{c_{44}^{(1)}}d_2}{m_{11}^{(1)}}\right)\left[1 - \frac{\sec(kd_2 h_p)}{\cosh(kh_p)}\right] + \left((\overline{c_{44}^{(1)}})^2 d_2^2 - \frac{(h_{15}^{(1)})^4}{(m_{11}^{(1)})^2}\right)\tan(kd_2 h_p)\tanh(kh_p).$

Subcase

(a) Pondering the above case, if the PM constant (i.e., $h_{15}^{(1)}$) is removed by taking $h_{15}^{(1)} = 0$. Then $\overline{c_{44}^{(1)}} = c_{44}^{(1)} = \mu^o$ (say) and Eqs. (5.4.12) and (5.4.13) can be reduced to

$$\mu^o d_2 \tan(k d_2 h_p) k\Theta_5 = \Theta_4. \tag{5.4.14}$$

Eq. (5.4.14) describes the dispersion relation of SH-wave in an isotropic elastic layer of thickness h_p overlying semi-infinite MP substrate.

(b) If we consider α^m, β^m, γ^m, $\jmath^m$, and $\kappa^m \to 0$ in case (2), then semi-infinite MP substrate reduces to isotropic elastic half-space substrate and the dispersion relations for both open and short cases reduce to

$$\chi_{18} = \mu^1 \sqrt{1 - \frac{c^2}{\overline{a_3}^2}}, \tag{5.4.15}$$

$$\chi_{20} = \chi_{19} \mu^1 \sqrt{1 - \frac{c^2}{\overline{a_3}^2}}, \tag{5.4.16}$$

respectively. Eqs. (5.4.15) and (5.4.16) represent the dispersion relations of SH-wave in PM layer of thickness h_p overlying isotropic elastic half-space substrate.

(c) Furthermore in above subcase (b), if the PM constant is removed i.e., $h_{15}^{(1)} = 0$, then dispersion relation for both the cases reduce to

$$\tan\left(k h_p \sqrt{\frac{c^2}{a_1^2} - 1}\right) = \frac{\mu^1 \sqrt{1 - \frac{c^2}{\overline{a_3}^2}}}{\mu^o \sqrt{\frac{c^2}{a_1^2} - 1}}, \tag{5.4.17}$$

where $a_1 = \sqrt{\frac{\mu^o}{\rho^o}}$, μ^o is shear modulus of elasticity and ρ^o is density of isotropic elastic layer.

This Eq. (5.4.17) is the well-known dispersion relation for Love waves in the classical structure [128] with the condition $a_1 < c < \overline{a_3}$ that validates the outcomes of the Model I.

5.5 Derivation of dispersion relations associated with Model II

Considering EO condition from Eq. (5.3.4) together with Eqs. (5.3.5) and (5.3.6) incorporate the requisite boundary conditions for EO case and considering ES condition from Eq. (5.3.4) together with Eqs. (5.3.5) and (5.3.6) incorporate the requisite boundary conditions for ES case of Model II. Hence, we obtain the equations in terms of seven unknown coefficients $C_1,\ C_2,\ C_3,\ C_4,\ D_5,\ D_6$, and D_7.

$$\chi_3'\overline{c_{44}^{(0)}}e^{gh_e/2}C_1+\chi_4'\overline{c_{44}^{(0)}}e^{gh_e/2}C_2+c_4d_{15}^{(0)}e^{-c_4h_e}C_3+c_5d_{15}^{(0)}e^{-c_5h_e}C_4=0, \tag{5.5.1}$$

$$C_1-\chi_1D_6-\chi_2D_7=0, \tag{5.5.2}$$

$$-\overline{c_{44}^{(0)}}\left(\frac{g}{2}\right)C_1+\overline{c_{44}^{(0)}}c_3C_2+c_4d_{15}^{(0)}C_3+c_5d_{15}^{(0)}C_4+ik\kappa^mD_5+\chi_5D_6+\chi_6D_7=0, \tag{5.5.3}$$

$$\left(\frac{d_{15}^{(0)}}{\epsilon_{11}^{(0)}}\right)C_1+C_3+C_4=0, \tag{5.5.4}$$

$$-ike_1\chi_7D_5+\chi_8D_6+\chi_9D_7=0, \tag{5.5.5}$$

$$\chi_{10}D_5+ike_2\chi_7D_6+ike_3\chi_7D_7=0, \tag{5.5.6}$$

$$c_4e^{-c_4h_e}C_3+c_5e^{-c_5h_e}C_4=0. \tag{5.5.7}$$

To get the non-trivial solution and hence the dispersion relation, we equate the determinant of these coefficients to zero. Here
$\chi_3'=c_3\sin(c_3h_e)-\left(\frac{g}{2}\right)\cos(c_3h_e)$,
$\chi_4'=c_3\cos(c_3h_e)+\left(\frac{g}{2}\right)\sin(c_3h_e)$,
$\chi_{11}'=c_4e^{-c_4h_e}-c_5e^{-c_5h_e}$.

5.5.1 Dispersion relation for EO case

We get the following dispersion relation for SH-wave propagation in FGPEM layer overlying semi-infinite MP substrate, for EO case.

$$\left[\overline{c_{44}^{(0)}}\left(c_3\chi_3' + \left(\frac{g}{2}\right)\chi_4'\right)\chi_{11}' + \chi_4' c_4 c_5 \left(\frac{(d_{15}^{(0)})^2}{\epsilon_{11}^{(0)}}\right)(e^{-c_4 h_e} - e^{-c_5 h_e})\right][\chi_1\Theta_2 - \chi_2\Theta_1] + \Theta_4\chi_4'\chi_{11}' = 0. \tag{5.5.8}$$

5.5.2 Dispersion relation for ES case

We get the following dispersion relation for SH-wave propagation in FGPEM layer overlying semi-infinite MP substrate, for ES case.

$$\left[\overline{c_{44}^{(0)}}\left(\chi_3'\chi_{16}' + \left(\frac{g}{2}\right)\chi_{14}' + \left(\frac{(d_{15}^{(0)})^2}{\epsilon_{11}^{(0)}}\right)\cos(c_3 h_e)\chi_{17}'\right) + \left(\frac{(d_{15}^{(0)})^2}{\epsilon_{11}^{(0)}}\right)\chi_{15}'\right][\chi_1\Theta_2 - \chi_2\Theta_1] + \chi_{14}'\Theta_4 = 0, \tag{5.5.9}$$

where

$\chi_{12}' = \overline{c_{44}^{(0)}}\chi_4' + c_5\frac{(d_{15}^{(0)})^2}{\epsilon_{11}^{(0)}}\sin(c_3 h_e)$,

$\chi_{13}' = \overline{c_{44}^{(0)}}\chi_4' + c_4\frac{(d_{15}^{(0)})^2}{\epsilon_{11}^{(0)}}\sin(c_3 h_e)$,

$\chi_{14}' = \overline{c_{44}^{(0)}}\chi_4'(e^{-c_4 h_e} - e^{-c_5 h_e}) - \frac{(d_{15}^{(0)})^2}{\epsilon_{11}^{(0)}}\sin(c_3 h_e)\chi_{11}'$,

$\chi_{15}' = \overline{c_{44}^{(0)}}c_3 e^{-(c_4+c_5+g/2)h_e}(c_4 - c_5) - c_4\chi_{12}' e^{-c_5 h_e} + c_5\chi_{13}' e^{-c_4 h_e}$,

$\chi_{16}' = \overline{c_{44}^{(0)}}c_3(e^{-c_4 h_e} - e^{-c_5 h_e}) + \frac{(c_{15}^{(0)})^2}{\epsilon_{11}^{(0)}}e^{g h_e/2}\sin(c_3 h_e)(c_4 - c_5)$,

$\chi_{17}' = c_3\chi_{11}' + e^{g h_e/2}\chi_4'(c_4 - c_5)$.

5.5.3 Some special cases and validation of Model II

Some special cases of proposed Model II are discussed in this section.

1. Considering α^m, β^m, γ^m, $\jmath^m$, and $\kappa^m \to 0$ then semi-infinite MP substrate reduces to isotropic elastic half-space substrate and the dispersion relations for both EO and ES cases reduce to

$$\overline{c_{44}^{(0)}}\chi_{11}'\left(\frac{g}{2}\chi_4' + c_3\chi_3'\right) - \left(\frac{(d_{15}^{(0)})^2}{\epsilon_{11}^{(0)}}\right)c_4 c_5\chi_4'\chi_{11}' = \chi_4'\chi_{11}' k\mu^1\sqrt{1 - \frac{c^2}{\overline{a_3}^2}}, \tag{5.5.10}$$

$$\left[\overline{c_{44}^{(0)}}\left(\frac{g}{2}\right)\chi_{14}' + \left(\frac{(d_{15}^{(0)})^2}{\epsilon_{11}^{(0)}}\right)\chi_{15}' + \overline{c_{44}^{(0)}}\chi_3'\chi_{16}' + \overline{c_{44}^{(0)}}\left(\frac{(d_{15}^{(0)})^2}{\epsilon_{11}^{(0)}}\right)\cos(c_3 h_e)\chi_{17}'\right] = \chi_{14}' k\mu^1\sqrt{1 - \frac{c^2}{\overline{a_3}^2}}, \tag{5.5.11}$$

respectively. Here $\overline{a_3} = \sqrt{\frac{\mu^1}{\rho^1}}$. Eqs. (5.5.10) and (5.5.11) represent the dispersion relations in FGPEM layer overlying isotropic elastic half-space for EO and ES cases, respectively.

2. In the absence of functional gradedness in the FGPEM layer (i.e., $g = 0$), the dispersion relations for EO (5.5.8) and ES (5.5.9) cases, respectively take the following form

$$k\Theta_5\chi'_{18} - \Theta_4 = 0, \tag{5.5.12}$$

$$k\Theta_5\chi'_{20} - \Theta_4\chi'_{19} = 0. \tag{5.5.13}$$

Eqs. (5.5.12) and (5.5.13) represent the dispersion relations of SH-wave in PE layer overlying semi-infinite MP substrate, for EO and ES case, respectively. Here
$\chi'_{18} = \overline{c_{44}^{(0)}} c_2 \tan(kc_2h_e) + \frac{(d_{15}^{(0)})^2}{\epsilon_{11}^{(0)}} \tanh(kh_e)$,
$\chi'_{19} = \overline{c_{44}^{(0)}} c_2 \tanh(kh_e) - \frac{(d_{15}^{(0)})^2}{\epsilon_{11}^{(0)}} \tan(kc_2h_e)$,
$\chi'_{20} = \left(\frac{2(d_{15}^{(0)})^2\overline{c_{44}^{(0)}}c_2}{\epsilon_{11}^{(0)}}\right)\left[1 - \frac{\sec(kc_2h_e)}{\cosh(kh_e)}\right] + \left((\overline{c_{44}^{(0)}})^2c_2^2 - \frac{(d_{15}^{(0)})^4}{(\epsilon_{11}^{(0)})^2}\right)\tan(kc_2h_e)\tanh(kh_e)$.

Subcase

(a) Pondering the above case, if the PE constant (i.e., $d_{15}^{(0)}$) is removed by taking $d_{15}^{(0)} = 0$. Then $\overline{c_{44}^{(0)}} = \mu^o$ (say) and Eqs. (5.5.12) and (5.5.13) can be reduced to

$$\mu^o c_2 \tan(kc_2h_e)k\Theta_5 = \Theta_4. \tag{5.5.14}$$

Eq. (5.5.14) describes the dispersion relation of SH-wave in an isotropic elastic layer of thickness h_e overlying semi-infinite MP substrate.

(b) If we consider α^m, β^m, γ^m, $\jmath^m$, and $\kappa^m \to 0$ in case (2), then semi-infinite MP substrate reduces to isotropic elastic half-space substrate and the dispersion relations for both open and short cases reduce to

$$\chi'_{18} = \mu^1\sqrt{1 - \frac{c^2}{\overline{a_3}^2}}, \tag{5.5.15}$$

$$\chi'_{20} = \chi'_{19}\mu^1\sqrt{1 - \frac{c^2}{\overline{a_3}^2}}, \tag{5.5.16}$$

respectively. Eqs. (5.5.15) and (5.5.16) represent the dispersion relations of

SH-wave in PE layer of thickness h_e overlying an isotropic elastic half-space substrate.

(c) Furthermore in above subcase (b), if the PE constant is removed i.e., $d_{15}^{(0)} = 0$, then dispersion relation for both the cases reduce to

$$\tan\left(kh_e\sqrt{\frac{c^2}{a_1^2}-1}\right) = \frac{\mu^1\sqrt{1-\frac{c^2}{\overline{a_3}^2}}}{\mu^o\sqrt{\frac{c^2}{a_1^2}-1}}, \tag{5.5.17}$$

where $a_1 = \sqrt{\frac{\mu^o}{\rho^o}}$.

This Eq. (5.5.17) is the well-known dispersion relation for Love waves in the classical structure [128] with the condition $a_1 < c < \overline{a_3}$ that validates the outcomes of the Model II.

5.6 Numerical results and discussion

Numerical computations are executed and graphical illustrations are shown in order to unravel the impact of various affecting parameters on the phase velocity of the SH-wave. The focus of the investigation is on the key parameters confronted during the analysis viz., MP constant, characteristic length parameter present in the substrate exhibiting size effects, thickness, and material gradient factors related with functionally graded layers as considered in the two Models I and II, respectively for both open and short circuit cases. The dispersion curves for the open circuit case as thick solid lines and short circuit case as thin dashed lines are shown within the same graphs. For both the considered models (i.e., Model I and Model II), the behavior of dispersion curves (for the fundamental mode) in response to the varied values of affecting parameters are demonstrated through Figs. 5.2 a)- 5.12 a) which are related with Model I and Figs. 5.2 b)- 5.12 b) portray the variations (for the fundamental mode) for Model II. To demonstrate the analytical outcomes graphically $Terfenol-D$ as FGPMM layer and $Aluminium-Epoxy$ as MP half-space substrate bearing microstructural properties are considered. The values for the material constants are reported in Table 5.1 and Table 5.2, respectively. The material constant values for $PZT-5H$ ceramic which is considered as the FGPEM layer can be obtained from Table 4.1. The thicknesses of the FGPMM and FGPEM layers, are fixed as $h_p = h_e = 0.02$ m. The value of the material gradient factors linked with Model I and Model II are fixed as $g_1 = 50$ and $g = 20$. The formula for electromechanical coupling coefficient (k_e^2) and magnetomechanical coupling coefficient (k_m^2) are defined as [148] $k_e^2 = \frac{{d_{15}^{(0)}}^2}{\epsilon_{11}^{(0)} c_{44}^{(0)}}$ and

$k_p^2 = \frac{{h(1)_{15}}^2}{m_{11}^{(1)} c_{44}^{(1)}}$. Theoretically, for $PZT-5H$ ceramic material, the value of k_e^2 is 0.31206 and for $Terfenol-D$, the value of k_p^2 is 0.5417.

Table 5.1: Material constants for PM layer [147]

Material	Elastic constant c_{44}^p $(10^9 Nm^{-2})$	Mass density ρ^p (kgm^{-3})	PM constant h_{15}^p $(NA^{-1}m^{-1})$	Magnetic permeability m_{11}^p $(10^{-6}Ns^2C^{-2})$
Terfenol-D	5.99	9.23	167.66	3.97

Table 5.2: Material constants for MP elastic half-space substrate [69]

Material	ρ^m $(10^3\ kgm^{-3})$	μ^m $(10^{10}\ Nm^{-2})$	λ^m $(10^{10}\ Nm^{-2})$	$\jmath^m$ $(10^{-4}\ m^2)$	α^m $(10^6\ N)$	β^m $(10^6\ N)$
Aluminium-Epoxy	2.19	1.89	7.59	0.196	0.01	0.015

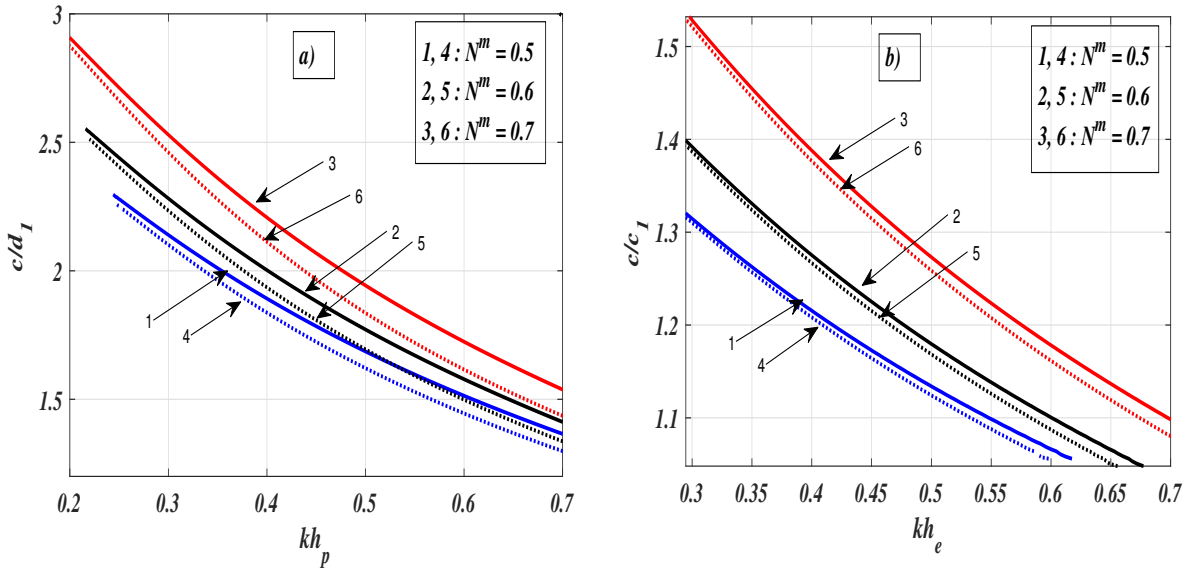

Figure 5.2: Dispersion curves for different values of MP constant for open (thick solid lines) and short circuit condition (thin dashed lines) in, (a) Model I and (b) Model II.

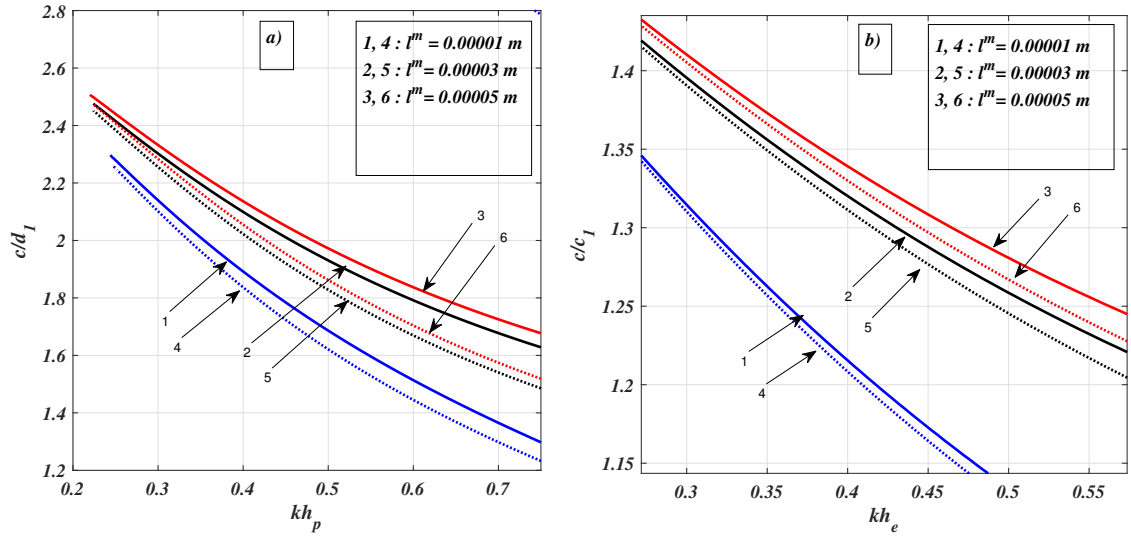

Figure 5.3: Dispersion curves for different values of characteristic length parameter (l^m) for open (thick solid lines) and short circuit condition (thin dashed lines) in, (a) Model I and (b) Model II.

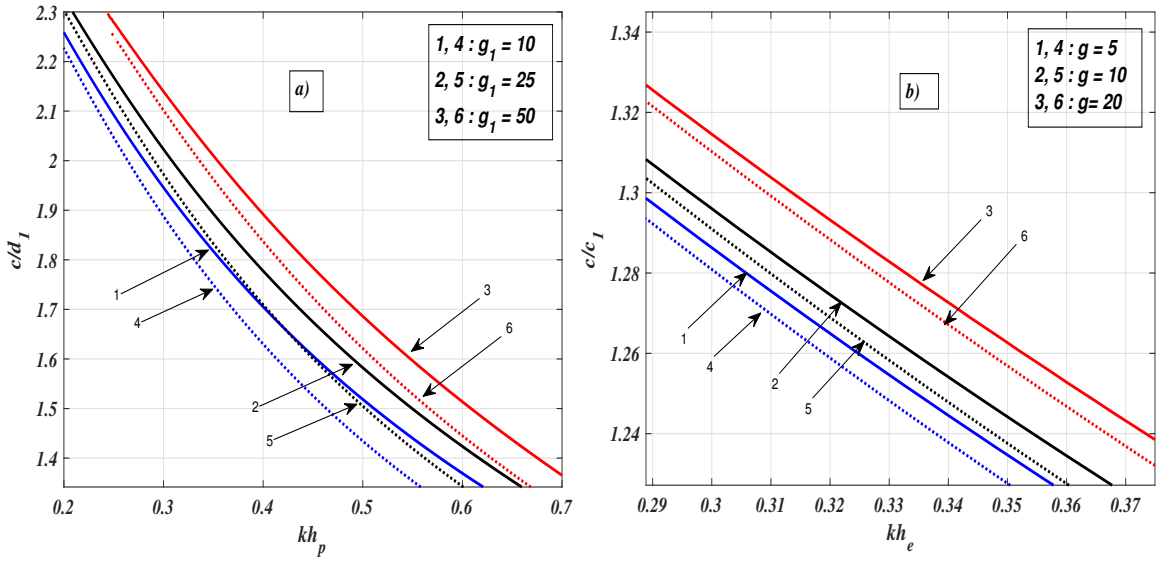

Figure 5.4: Dispersion curves for different values of material gradient factors for open (thick solid lines) and short circuit condition (thin dashed lines) in, (a) Model I and (b) Model II.

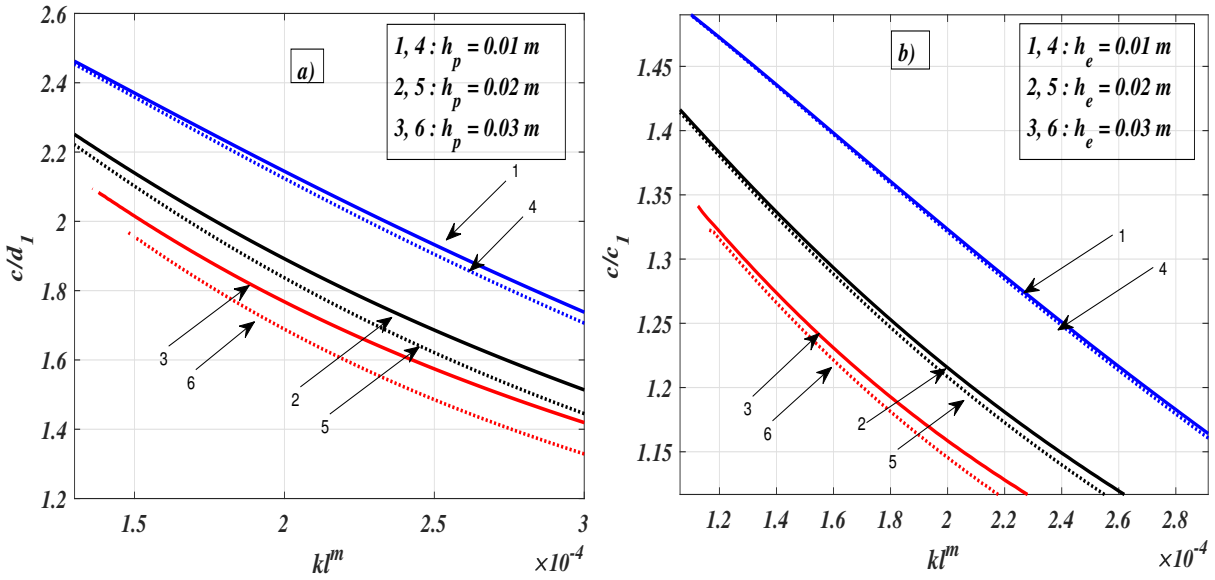

Figure 5.5: Dispersion curves for different values of thickness of piezo material layers for open (thick solid lines) and short circuit condition (thin dashed lines) in, (a) Model I and (b) Model II.

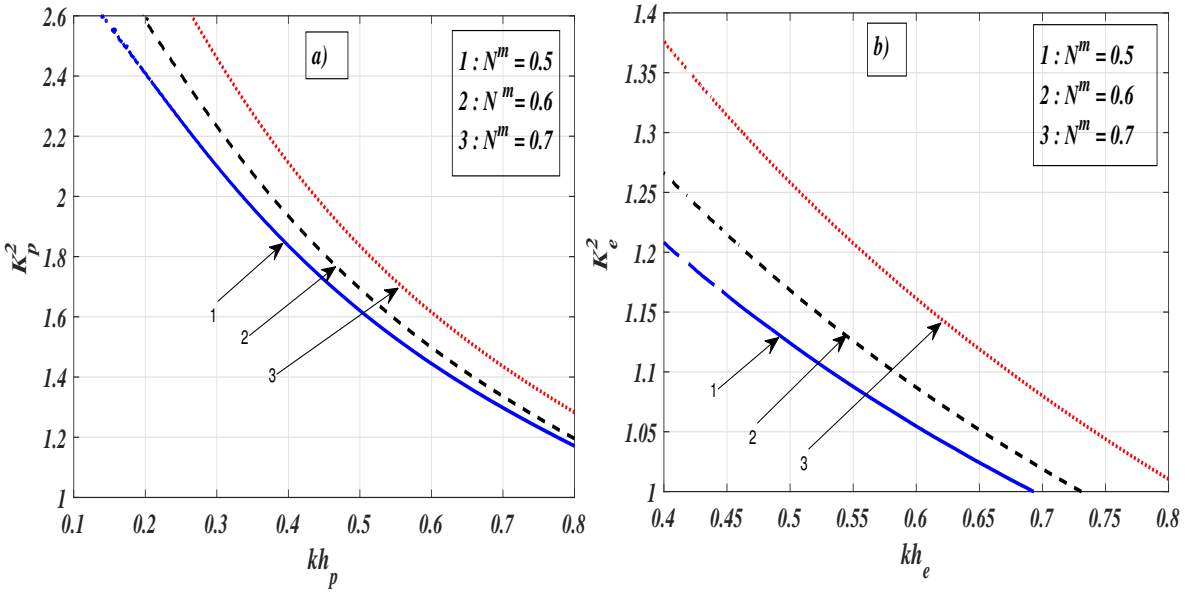

Figure 5.6: (a) K_p^2 versus kh_p for different values of MP constant (N^m), (b) K_e^2 versus kh_e for different values of MP constant (N^m).

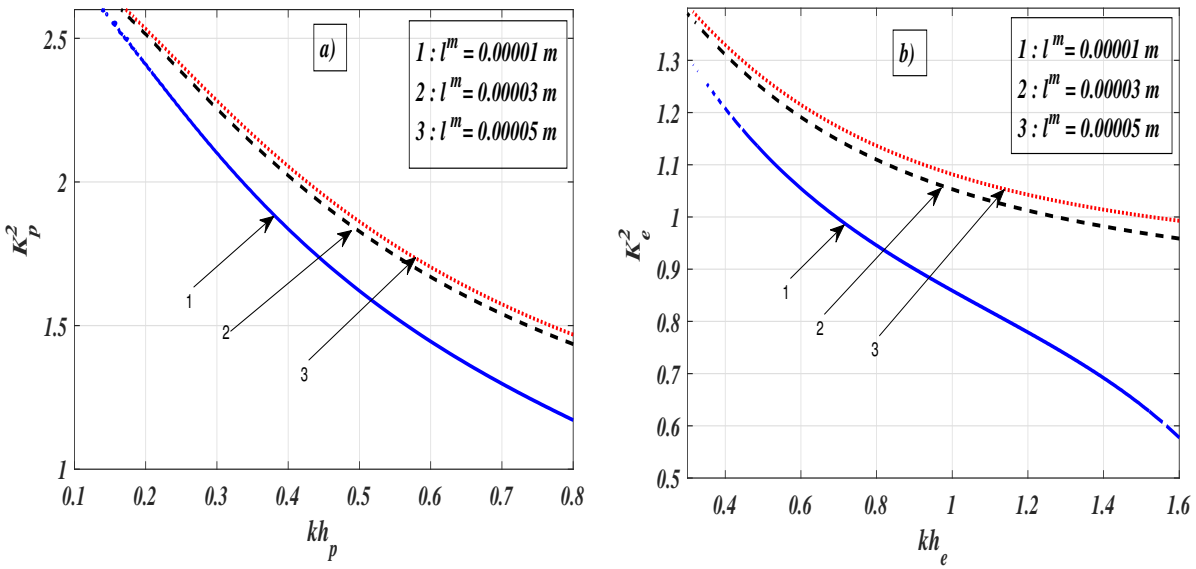

Figure 5.7: (a) K_p^2 versus kh_p for different values of characteristic length (l^m) parameter, (b) K_e^2 versus kh_e for different values of characteristic length parameter (l^m).

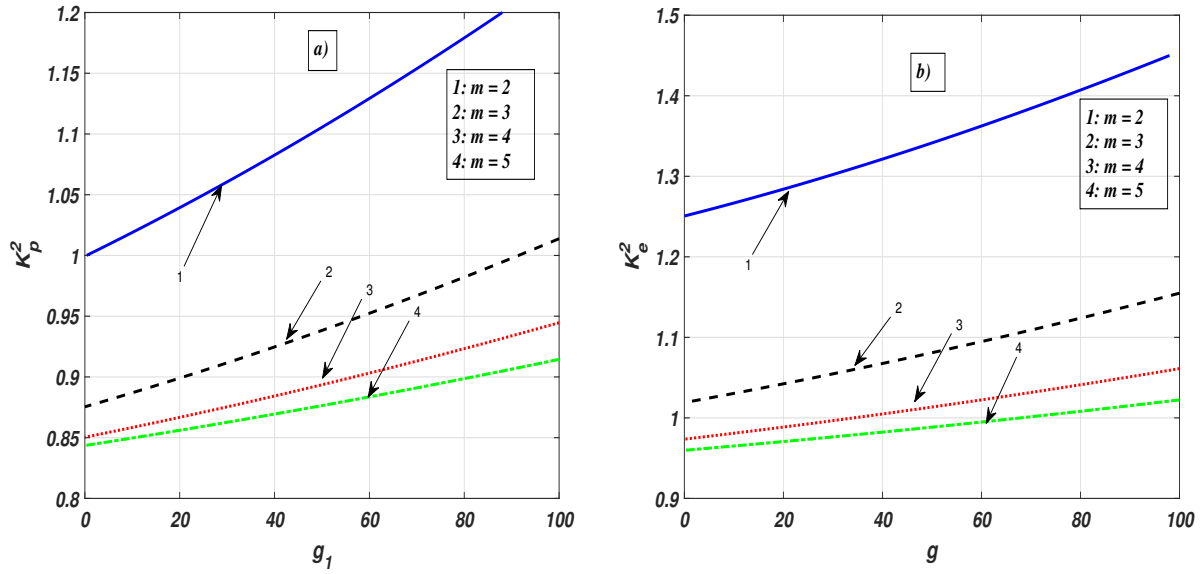

Figure 5.8: (a) K_p^2 factor versus material gradient factor for different values of $m(= h/\lambda)$, (b) K_e^2 factor versus material gradient factor for different values of $m(= h/\lambda)$

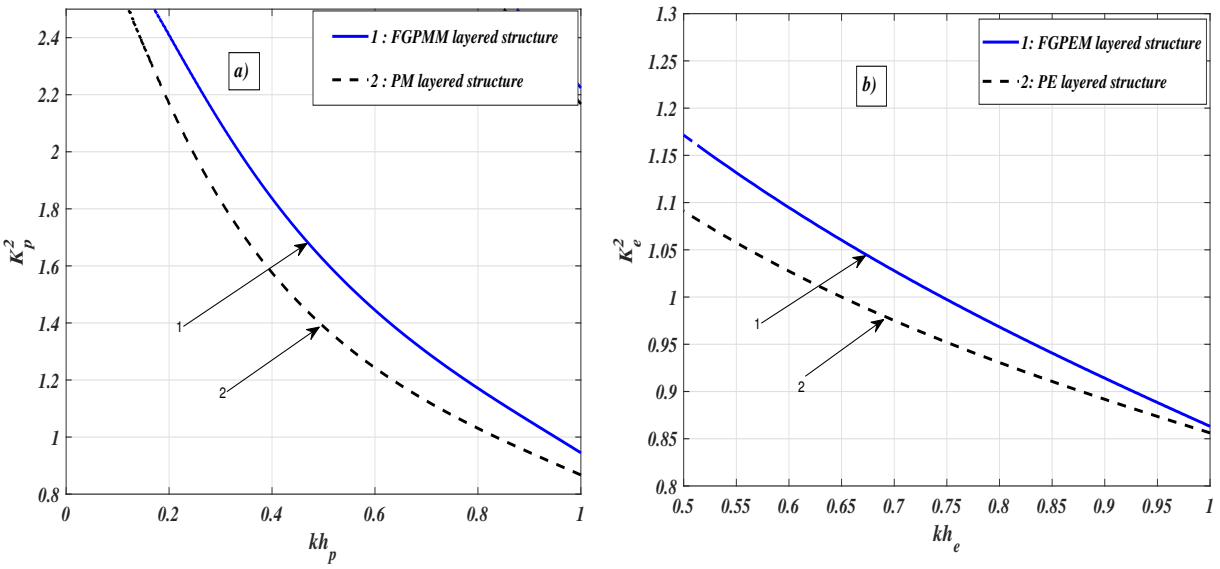

Figure 5.9: (a) Comparison of K_p^2 versus kh_p for FGPMM layered structure and PM layered structure, (b) Comparison of K_e^2 versus kh_e for FGPEM layered structure and PE layered structure.

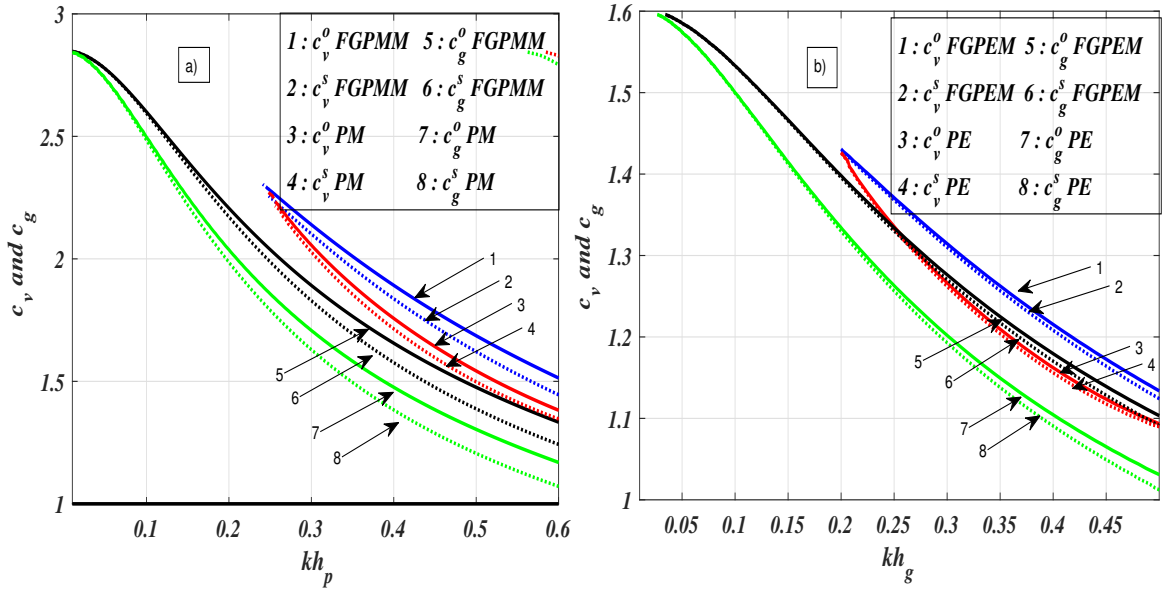

Figure 5.10: (a) Comparison of phase velocity (c_v) and group velocity (c_g) in FGPMM and PM layered structure for MO and MS circuit conditions, (b) Comparison of phase velocity (c_v) and group velocity (c_g) in FGPEM and PE layered structure for EO and ES circuit conditions.

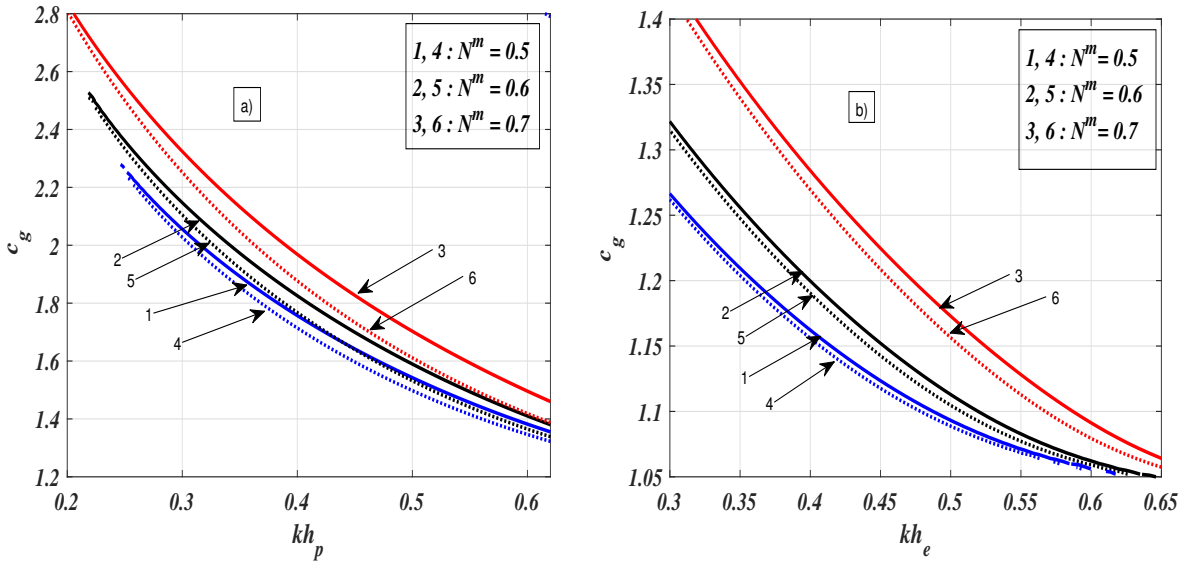

Figure 5.11: (a) Dispersion curve of group velocity (c_g) in FGPMM layered structure for different values of MP constant (N^m), for MO (thick solid lines) and MS circuit condition (thin dashed lines), (b) Dispersion curve of group velocity (c_g) in FGPEM layered structure for different values of MP constant (N^m), for EO (thick solid lines) and ES circuit condition (thin dashed lines).

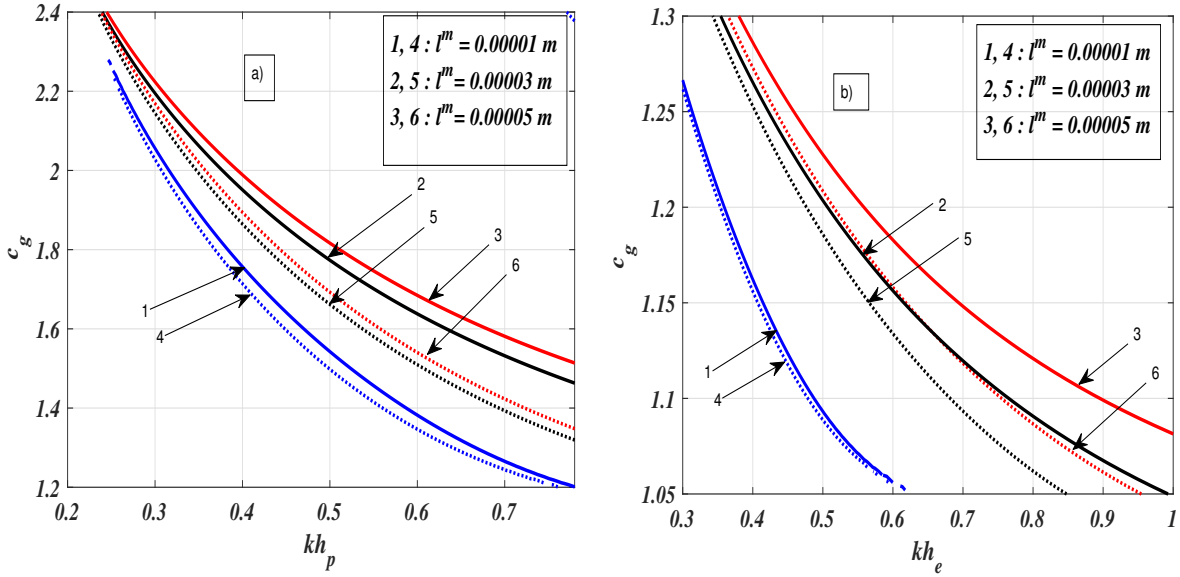

Figure 5.12: (a) Dispersion curve of group velocity (c_g) in FGPMM layered structure for different values of characteristic length parameter (l^m), for MO (thick solid lines) and MS circuit condition (thin dashed lines), (b) Dispersion curve of group velocity (c_g) in FGPEM layered structure for different values of characteristic length parameter (l^m), for EO (thick solid lines) and ES circuit condition (thin dashed lines).

5.6.1 Influence of size effects exhibited by microscale structures on the phase velocity of SH-waves

The effect of microscale structures on the phase velocity of the propagating wave is captured through MP constant (N^m) and characteristic length parameter (l^m). The phase velocity variations in response to varying values of MP constant and characteristic length parameter as associated with MP half-space substrate are manifested through Figs. 5.2 a)- 5.2 b) and 5.3 a)- 5.3 b) for Model I and II, respectively. It is noted that as the values of both the parameters i.e., MP and characteristic length are increasing, the dispersion curves shift upward. Therefore, it can be remarked that both the parameters favor the phase velocity of SH-wave for both open and short circuit cases in the considered models (i.e., Model I and Model II).

5.6.2 Influence of material gradient factors on the phase velocity of SH-waves

As material gradient factors (g_1 and g) that are responsible for functional gradedness in the material layers in Model I and II, respectively have a significant impact on the phase velocity of the propagating wave so it is very important to scrutinize these factors. Figs. 5.4 a)- 5.4 b) reveal the effect of the material gradient factors (g_1 and g), linked with functionally graded layers considered in Model I and II, respectively. These factors have an enhancing effect on the phase velocity of SH-wave for both open and short circuit cases in both the models. Therefore, we can conclude that as the inhomogeneity in the smart material layers is increased then the phase velocity of the propagating wave also increases.

5.6.3 Influence of thickness of the functionally graded piezo material layer on the phase velocity of SH-waves

The thickness (h_p) of the FGPMM layer associated with Model-I and the thickness (h_e) of the FGPEM layer associated with Model-II, have a substantial effect on the propagation of SH-waves. Variation of phase velocity in response to varied values of thicknesses of functionally graded layers associated with the considered models is graphically irradiated in Figs. 5.5 a)- 5.5 b). It can be observed that the thickness of the piezo layers (for both open and short circuit cases) has a decreasing effect on the phase velocity of the SH-wave.

5.6.4 Mechanical coupling factors (K_p^2 and K_e^2)

The mechanical coupling factors (K_p^2 and K_e^2) are key parameters in acoustic devices that manifest the piezo effect on the phase velocity of the elastic waves. The higher the value of these factors, the stronger is the dependence of the attributes of wave propagation on the system parameters. For differentiating various active materials the mechanical coupling factors are widely used as figures of merit. The electromechanical coupling factor (K_e^2) is an indicator of the effectiveness with which a PE material converts electrical energy into mechanical energy or vice versa. K_e^2 values quoted in piezoelectric supplier's specifications are typically the maximum theoretical values. For low input frequencies, a typical PE ceramic can covert 30-75 % of the energy delivered to it from one form into the other form, depending on the formulation of the ceramic. A high K_e^2 usually is desirable for efficient energy conversion, but K_e^2 does not account for dielectric losses or mechanical losses, nor recovery of unconverted energy. The magnetomechanical coupling factor (K_p^2), is a measure of the transduction efficiency of the material and the energy density gives a measure of the energy that can be obtained from the material. The electromechanical coupling factor (K_e^2) [26] and the magnetomechanical coupling factor (K_p^2) [66], corresponding to the surface waves can be evaluated from the following formulae

$$K_e^2 = 2\frac{(c_o^e - c_s^e)}{c_o^e}, \qquad K_p^2 = 2\frac{(c_o^p - c_s^p)}{c_o^p}, \tag{5.6.1}$$

where c_o^e, c_s^e, c_o^p, and c_s^p are the phase velocities for EO, ES, MO, and MS cases, respectively. To unravel the influence of size effects on the mechanical coupling factors, graphical illustrations for variation of mechanical coupling factors against dimensionless wave number in response to varying values of MP constant and characteristic length parameter are manifested through Figs. 5.6 a)- 5.6 b) and 5.7 a)- 5.7 b), respectively. Fig 5.6 a) reveals the influence of MP constant on the K_p^2 associated with FGPMM layer in Model I and Fig 5.6 b) reveals the influence of MP constant on the K_e^2 associated with FGPEM layer in Model II. Similarly, the effect of characteristic length parameter on the mechanical coupling factors viz., K_p^2 and K_e^2 is traced out in Figs. 5.7 a)- 5.7 b), respectively. It is examined from the figures that both the parameters have enhancing effect on the mechanical coupling factors. Therefore, it is noted that size effects exhibited by the microscale structures favor the mechanical coupling factors and high mechanical coupling factors are desired in SAW devices for numerous engineering applications. These factors are associated with the efficiency of sensors and hence, play a vital role in designing acoustic sensors.

The relations of mechanical coupling factors viz., K_p^2 and K_e^2 with the material gradient factors (g_1 and g) respectively, are manifested in Figs. 5.8 a) and 5.8 b) for different values of m =2, 3, 4, 5 where, $m = h/\lambda$, ($h = h_p = h_e$) is the ratio of the layer thickness h to the

wavelength λ. It is seen from Fig. 5.8 a) that the value of K_p^2 increases with the increase in magnitude of material gradient factor g_1. K_p^2 takes its maximum value as $m = 2$. Similarly, from Fig. 5.8 b) it can be observed that the value of K_e^2 also increases as material gradient factor (g) increases. Fig. 5.9 a) portrays the plot of K_p^2 against dimensionless wave number (kh_p) to depict the comparative result for FGPMM and PM layered structures. It can be concluded that K_p^2 drops sharply as wave number is increasing and is more in FGPMM layered structure as compared to PM layered structure. From Fig. 5.9 b) the plot of K_e^2 against dimensionless wave number (kh_e) for the comparative result for FGPEM and PE layered structure is obtained. K_e^2 is more in FGPEM layered structure as compared to PE layered structure which interprets that functional gradedness in a smart material enhances mechanical coupling factors as desired for acoustic devices.

5.6.5 Group velocity

To determine the rate at which the energy of the wave is propagated it is required to find the group velocity. For further investigation, the group velocity of the propagating wave is also explored. Theoretically, the group velocity c_g can be evaluated by the formula given in Chapter 4 as Eq. (4.5.2). Figs. 5.10 a) and 5.10 b) exemplify this phenomenon. Phase velocity and group velocity graphs are plotted against non-dimensional wave number (kh_p) for FGPMM layered structure and PM layered structure in Fig 5.10 a) and for FGPEM layered structure and PE layered structure in Fig. 5.10 b). Here c_v^o, c_v^s, c_g^o, and c_g^s represent the phase velocity for open case, phase velocity for short case, group velocity for open case and group velocity for short case, respectively. By observing the SH-wave dispersion curves in both the figures, it is seen that the dispersion relation is 'normal' as phase velocity is found to be greater than the group velocity for both the open and short circuit cases. In addition to this, the phase velocity for an open circuit case is more than that of the short circuit case. Further, it is also concluded that the phase velocity and group velocity curves observed from these illustrations for functionally graded layered structures are more as compared to the conventional piezo layered structures. This is because functional gradedness in the piezo layer enhances the phase velocity (as observed from Figs. 5.4 a)-5.4 b)) and hence the group velocity. To delineate the influence of size effects exhibited by microscale structures associated with MP half-space substrate on the group velocity, the graphical illustrations are shown as Figs. 5.11 a)-5.11 b) and 5.12 a)-5.12 b). The impact of the micropolar constant (N^m) on the group velocity is illustrated in Figs. 5.11 a)-5.11 b) and of characteristic length parameter (l^m), in Figs. 5.12 a)-5.12 b) for Model I and Model II, respectively. It can be depicted from the figures that both the parameters favor the group velocity curves for both open and short circuit cases associated with both the models.

5.7 Conclusions

Following are the outcomes for open and short circuit cases in both considered models (Model I and Model II).

- The phase velocity of the SH-waves monotonously decreases with the increase in wave number.
- MP constant and characteristic length parameter pertinent with the MP half-space substrate bearing micro-scale structures favor the phase velocity of the SH-wave.
- The material gradient factors associated with the functionally graded piezo material layers also have an enhancing effect on the phase velocity of the SH-wave.
- Broader the width of the functionally graded piezo layer, lower is the phase velocity of the SH-wave in the considered structures.
- MP constant and characteristic length parameter encourage the mechanical coupling factors.
- The layer thickness ratio to the wavelength has an eminent impact on the mechanical coupling factors. Both K_p^2 and K_e^2 take their maximum values as $m = 2$ for increasing values of material gradient factors.
- In the absence of functional gradedness, the mechanical coupling factors reduce.
- Phase velocity for open circuit case is always greater than that of short circuit case.
- The dispersion relation appears 'normal' as the phase velocity of the SH-wave is greater than the group velocity in the considered structures.

Chapter 6

Nonlocal aspect of piezoelectric composite on the transmission of mechanical Bleustein-Gulyaev wave[5]

6.1 Introduction

In nanoelectromechanical systems (NEMS), the nanoscale size effect plays an important role. Experimental analysis indicates that the NEMS at nanoscale shows a size-dependent manner and do not obey the continuum theory. Overlooking the size effect in designing of NEMS may lead to completely incorrect predictions and hence inaccurate designs and irreparable damages. The classical continuum theories suffer from inaccurate predictions done for the mechanical behavior of nanostructures, which can be justified by the presence of small-scale effects at the nanoscale. In this regard, the nonlocal (NL) elasticity theory initiated by Eringen ([61]- [64]) has provided a powerful tool in the mathematical modeling and investigation of engineering problems corresponding to the applications involving nanoscale structures. In the preceding chapters, the microstructural effects were captured through length scale parameter present in the substrate material only, that were in welded contact with smart material layers. But in this chapter we have utilized Eringen's NL theory to grab the microstructural effect from the piezoelectric (PE) smart material and the length scale parameter is present in the layer as well as in the substrate also.

One type of shear horizontal (SH) electro-acoustic surface wave in which the direction of material particle motion is perpendicular to the propagating direction and parallel to the surface of half-space which can propagate in a class of transversely isotropic PE media, is commonly known as Bleustein-Gulyaev (BG) wave or electro-acoustic wave. These waves were simultaneously observed by Bleustein and Gulyaev ([22], [83]). These waves can propagate in highly symmetric PE materials because they have no elastic counterparts in purely elastic homogeneous materials ([234], [235], [239]). Studies indicate that BG wave can propagate in the structure comprising of thin film/substrate layered structures

[5]Contents of this chapter are published in SCIE indexed journal, Mechanics of Advanced Materials and Structures, 2020. DOI:10.1080/15376494.2020.1854907 with I.F. = 4.030

made of the same PE material but opposite poling directions and its penetration depth is in the same order as the wavelength [92]. In the absence of the PE effect, the BG wave degenerates to the shear bulk wave. Thorough investigations of propagation characteristics of BG wave have been done by many researchers to successfully apply it to SAW devices ([112], [113], [233]). BG wave is an another promising candidate in the category of surface waves to be employed for sensors and acoustic devices ([2], [7]). Due to the high sensitivity, BG waves are widely used for liquid sensing applications ([18], [85], [100], [155]). Recently this study has gained momentum because of its enormous applications in nanoscale structures. Despite much popularity, the propagation characteristics of BG wave based on NL theory is yet to be explored. The main intent of this chapter is to analyze the effect of nonlocality on the propagation of BG waves in PE layered structures. Appropriate boundary conditions are employed at the free surface and at the interface between the layer and the half-space to obtain the dispersion relations for both open and short circuit conditions. It is found that BG waves are dispersive in nature and are affected by nonlocality. The nonlocality parameter is present in both open and short circuit conditions. Furthermore, it has been observed that for both cases the wave cease to propagate beyond the critical frequencies. The variation of phase velocities with frequency has been graphically illustrated. The effects of PE material parameters and nonlocality parameter on the phase velocity of BG wave have been shown graphically.

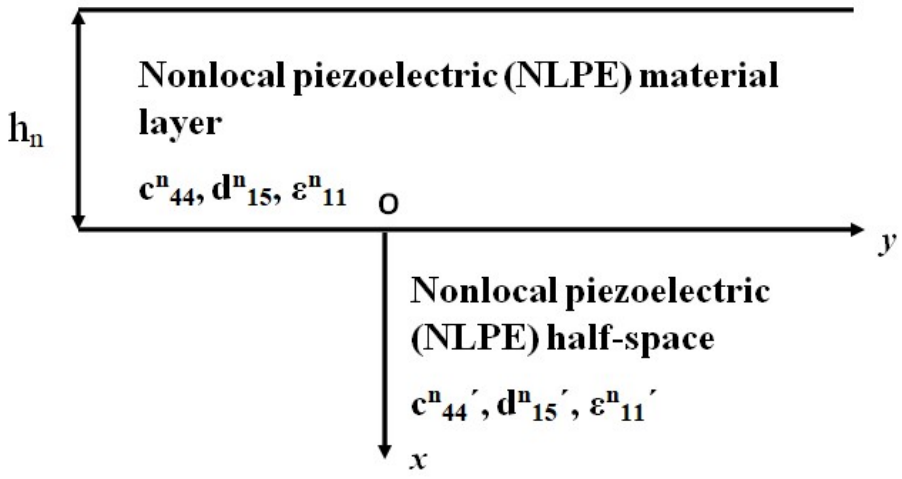

Figure 6.1: Schematic illustration

6.2 Nonlocal (NL) theory of elasticity in PE media

The equations of wave motion and constitutive relations in PE medium based on NL elastic theory can be expressed as [34]

$$\begin{aligned} \sigma^n_{ij,j} &= \rho^n \ddot{u}^n_i, \\ D^n_{i,i} &= 0, \qquad\qquad (i,j=1,2,3), \end{aligned} \tag{6.2.1}$$

$$\begin{aligned} (1-\Upsilon^2\nabla^2)\sigma^n_{ij} &= c^n_{ijkl}S^n_{kl} - d^n_{kij}E^n_k, \\ (1-\Upsilon^2\nabla^2)D^n_j &= d^n_{jkl}S^n_{kl} + \epsilon^n_{jk}E^n_k, \quad (i,j,k,l=1,2,3), \end{aligned} \tag{6.2.2}$$

where ρ^n is the density of the PE material. σ^n_{ij} are the stress tensors. D^n_i and E^n_i are the components of electric displacement vector and electric field vector, respectively. c^n_{ijkl}, d^n_{kij}, and ϵ^n_{jk} are the elastic stiffness constants, PE constants, and dielectric constants, respectively. ∇^2 denotes the Laplace operator. $\Upsilon = e_0 l^n$ is the NL parameter which denotes the small scale effect. Here e_0 is the material constant and l^n is the internal characteristic length. A comma $(,)$ in the subscript denotes the differentiation with respect to some spatial coordinates while a superposed dot notation signifies time (t) derivative. $S^n_{i,j}$ is the strain tensor derived from the displacement field u^n_i as

$$S^n_{ij} = \frac{1}{2}(u^n_{i,j} + u^n_{j,i}), \quad (i,j=1,2,3). \tag{6.2.3}$$

At a glance it can be seen that in the absence of nonlocality, the constitutive Eqs. (6.2.2) reduce to those for local PE medium [147].
E^n_i is electric field components along (x,y,z) which can be derived as

$$E^n_i = -\varphi_{,i} \quad (i=1,2,3). \tag{6.2.4}$$

in which φ indicates the planar distribution of electric potential.

6.3 Mathematical model and solution of the problem

Consider a transversely isotropic nonlocal piezoelectric (NLPE) layer having hexagonal symmetry (6 mm class) of uniform thickness h_n lying over a NLPE half-space. The upper surface of the layer is assumed to be mechanically stress free and the lower surface is assumed to be in welded contact with the half-space. Considering a rectangular Cartesian coordinate system in such a way that BG wave is propagating along y-axis and x-axis

is considered positive in the vertically downward direction as shown in Fig. 6.1. We shall consider a two dimensional problem for the propagation of BG surface waves in the considered structure. For this purpose, the displacement components and the electric potentials in the layer and half-space may be assumed as

$$\begin{aligned} u_1^n = u_2^n = 0, \quad u_3^n = u_3^n(x,y,t), \quad \varphi_1 = \varphi_1(x,y,t), \\ v_1^n = v_2^n = 0, \quad v_3^n = v_3^n(x,y,t), \quad \varphi_2 = \varphi_2(x,y,t), \quad \text{and} \quad \frac{\partial}{\partial z} \equiv 0, \end{aligned} \tag{6.3.1}$$

where x, y, z are the spatial variable. t is the time variable. u_i^n are displacement components and φ_1 is electric potential component in NLPE layer. v_i^n are the displacement components and φ_2 is electric potential component in NLPE half-space. It is assumed that the layer and the substrate are in identical transversely isotropic PE media but with opposite polarization. This implies that the $x-y$ coordinate plane is an isotropic plane. The polarization direction of the layer is the same as the positive direction of the z-axis, whereas the polarization direction of the substrate is opposite to the former. Thus, we assume that

$$c_{44}^{n\,\prime} = c_{44}^n \quad d_{15}^{n\,\prime} = -d_{15}^n, \quad \epsilon_{11}^{n\,\prime} = \epsilon_{11}^n, \tag{6.3.2}$$

where c_{44}^n, d_{15}^n, and ϵ_{11}^n are elastic stiffness coefficient, PE constant, and dielectric constant for NLPE layer and $c_{44}^{n\,\prime}$, $d_{15}^{n\,\prime}$, and $\epsilon_{11}^{n\,\prime}$ are elastic stiffness coefficient, PE constant, and dielectric constant for NLPE half-space, respectively. With these considerations and using Eqs. (6.2.2), (6.2.3), (6.2.4), (6.3.1), and (6.3.2), the equations of motion (6.2.1), for the BG wave propagation, in the absence of body forces yield

$$\left.\begin{aligned} c_{44}^{n\,*}\nabla^2 u_3^n + d_{15}^n \nabla^2 \varphi_1 = \rho^n \ddot{u_3^n}, \\ d_{15}^n \nabla^2 u_3^n - \epsilon_{11}^n \nabla^2 \varphi_1 = 0, \quad x \in [-h_n, 0] \end{aligned}\right\} \tag{6.3.3}$$

$$\left.\begin{aligned} c_{44}^{n\,*}\nabla^2 v_3^n - d_{15}^n \nabla^2 \varphi_2 = \rho^n \ddot{v_3^n}, \\ d_{15}^n \nabla^2 v_3^n + \epsilon_{11}^n \nabla^2 \varphi_2 = 0, \quad x \in [0, \infty) \end{aligned}\right\} \tag{6.3.4}$$

Here $c_{44}^{n\,*} = c_{44}^n + \Upsilon^2 \rho^n \frac{\partial^2}{\partial t^2}$ and $\nabla^2 \equiv \frac{\partial^2}{\partial x^2} + \frac{\partial^2}{\partial y^2}$. For the solution of differential equations (6.3.3), we have two uncoupled equations to deal with. For BG waves propagating in the positive direction of y-axis with phase velocity c, we take the solution of these differential equations as

$$\begin{aligned} u_3^n(x,y,t) = \overline{u_3^n}(x) e^{ik(y-ct)}, \\ \varphi_1(x,y,t) = \overline{\varphi_1}(x) e^{ik(y-ct)}, \end{aligned} \tag{6.3.5}$$

where k is the wave number and c is the phase velocity of the wave. On substituting Eq. (6.3.5) in Eq. (6.3.3) we obtain

$$\begin{aligned} \overline{u_3^n}''(x) - k^2 f_3^2 \overline{u_3^n}(x) = 0, \\ \overline{\varphi_1}''(x) - k^2 \overline{\varphi_1}(x) = \frac{d_{15}^n}{\epsilon_{11}^n} \left(\overline{u_3^n}''(x) - k^2 \overline{u_3^n}(x) \right), \end{aligned} \tag{6.3.6}$$

where $f_3 = \sqrt{1 - \frac{c^2}{f_2^2}}$, $\quad f_2 = \sqrt{f_1^2 - \Upsilon^2 \omega^2}$, $\quad f_1 = \sqrt{\frac{\overline{c_{44}^n}}{\rho^n}}$, $\overline{c_{44}^n} = c_{44}^n + \frac{{d_{15}^n}^2}{\epsilon_{11}^n}$. f_2 is the velocity of the shear wave in NLPE layer and f_1 is the velocity of classical wave. ω is the angular frequency related to phase velocity c by $\omega = kc$.
On solving (6.3.6), the displacement component and the electric potential component in the NLPE layer can be obtained as

$$\begin{aligned} u_3^n(x,y,t) &= (e^{kf_3 x} F_1 + e^{-kf_3 x} F_2) e^{ik(y-ct)}, \\ \varphi_1(x,y,t) &= \left(\frac{d_{15}^n}{\epsilon_{11}^n} e^{kf_3 x} F_1 + \frac{d_{15}^n}{\epsilon_{11}^n} e^{-kf_3 x} F_2 + e^{kx} F_3 + e^{-kx} F_4 \right) e^{ik(y-ct)}, \end{aligned} \tag{6.3.7}$$

where F_1, F_2, F_3, and F_4 are arbitrary constants. Eq. (6.3.4) can be solved by a similar procedure. Taking into consideration the conditions $\overline{v_3^n}$ and $\overline{\varphi_2} \to 0$ as $x \to \infty$ on the general solutions of Eqs. (6.3.4) for the NLPE half-space, we get the following displacement and electric potential components

$$\begin{aligned} v_3^n(x,y,t) &= e^{-kf_3 x} F_5 e^{ik(y-ct)}, \\ \varphi_2(x,y,t) &= \left(- \left(\frac{d_{15}^n}{\epsilon_{11}^n} \right) e^{-kf_3 x} F_5 + e^{-kx} F_6 \right) e^{ik(y-ct)}, \end{aligned} \tag{6.3.8}$$

where F_5 and F_6 are arbitrary constants.

6.4 Boundary conditions

The upper surface of the layer is assumed to be traction free and the interface between the layer and the half-space is in welded contact. Therefore, the appropriate boundary conditions are as follows.

(i) Considering vacuum above the free surface of the NLPE layer, the electric boundary conditions at free surface i.e., at $x = -h_n$ are as follows.

$$\begin{aligned} (D_x^n)_L &= 0 \quad \{\text{electrically open (EO) condition}\}, \\ (\varphi_1)_L &= 0 \quad \{\text{electrically short (ES) condition}\}. \end{aligned} \tag{6.4.1}$$

(ii) The mechanical traction free condition at $x = -h_n$ is

$$(\sigma_{zx}^n)_L = 0. \tag{6.4.2}$$

(iii) The continuity conditions at the interfacial surface i.e., at $x = 0$

$$\begin{aligned} (u_3^n)_L &= (v_3^n)_H, \\ (\sigma_{zx}^n)_L &= (\sigma_{zx}^n)_H, \\ (\varphi_1)_L &= (\varphi_2)_H, \\ (D_x^n)_L &= (D_x^n)_H. \end{aligned} \tag{6.4.3}$$

Here subscript 'L' is used for the entities corresponding to NLPE layer and subscript 'H' is used for the entities corresponding to NLPE half-space. Using (6.2.1), (6.3.7), and (6.3.8) in these boundary conditions we get a system of six homogeneous equations in six unknowns $F_1,\ F_2,\ F_3,\ F_4,\ F_5$, and F_6.

$$-e^{-kh_n}F_3 + e^{kh_n}F_4 = 0, \tag{6.4.4}$$

$$\frac{d_{15}^n}{\epsilon_{11}^n}e^{-kf_3h_n}F_1 + \frac{d_{15}^n}{\epsilon_{11}^n}e^{kf_3h_n}F_2 + e^{-kh_n}F_3 + e^{kh_n}F_4 = 0, \tag{6.4.5}$$

$$f_3\overline{c_{44}^n}e^{-kf_3h_n}F_1 - f_3\overline{c_{44}^n}e^{kf_3h_n}F_2 + d_{15}^n e^{-kh_n}F_3 - d_{15}^n e^{kh_n}F_4 = 0, \tag{6.4.6}$$

$$F_1 + F_2 - F_5 = 0, \tag{6.4.7}$$

$$f_3\overline{c_{44}^n}F_1 - f_3\overline{c_{44}^n}F_2 + d_{15}^n F_3 - d_{15}^n F_4 + f_3\overline{c_{44}^n}F_5 - d_{15}^n F_6 = 0, \tag{6.4.8}$$

$$\frac{d_{15}^n}{\epsilon_{11}^n}F_1 + \frac{d_{15}^n}{\epsilon_{11}^n}F_2 + F_3 + F_4 + \frac{d_{15}^n}{\epsilon_{11}^n}F_5 - F_6 = 0, \tag{6.4.9}$$

$$-F_3 + F_4 - F_6 = 0. \tag{6.4.10}$$

6.5 Derivation of dispersion relations

To get the non-trivial solution and hence, the dispersion relations for the EO and ES circuit conditions, the determinant of the corresponding coefficient matrices must vanish.

6.5.1 Dispersion relation for EO condition

Considering Eq. (6.4.4) alongwith Eqs. (6.4.6)-(6.4.10), we get the dispersion relation as

$$f_3\epsilon_{11}^n\overline{c_{44}^n} - {d_{15}^n}^2\tanh(kh_n)(1+e^{-2kf_3h_n})(1+e^{-2kh_n}) = 0. \tag{6.5.1}$$

6.5.2 Dispersion relation for ES condition

Considering Eqs. (6.4.5)-(6.4.10), we get the dispersion relation as

$$\left(\frac{{d_{15}^n}^2}{\epsilon_{11}^n}\right)\left\{\overline{c_{44}^n}f_3[(1+e^{-2kf_3h_n})(1+e^{-2kh_n}) - 4e^{-kh_n}e^{-kf_3h_n}+1] - \frac{{d_{15}^n}^2}{\epsilon_{11}^n}(1-e^{-2kf_3h_n})(1-e^{-2kh_n})\right\} - \overline{c_{44}^n}^2 f_3^2 = 0. \tag{6.5.2}$$

We note that these dispersion relations depend on the NL parameter of the layered media. The condition for existence of BG waves is $c < f_2$ provided, $\omega < \frac{f_1}{\Upsilon}$.

6.5.3 Limiting cases

Here we shall investigate the behavior of BG wave propagation in the limiting cases of frequency and thickness of the PE layer.

6.5.3.1 Limiting frequency

1. For the case of low limiting frequency, i.e., when $\omega \to 0$ then $c \to f_1$. Thus, it can be concluded that for limiting low frequency case, the phase velocity of the BG waves tends to the phase velocity of the classical shear wave in the PE half-space.

2. For the limiting high frequency case, i.e., when $\omega \to \infty$, then the existence of BG wave cannot be ensured theoretically at once. This is due to the fact that the shear wave and the wave corresponding to the NLPE medium encounter the critical frequency. The critical frequency is given by $\omega_c = \frac{f_1}{\Upsilon}$. Beyond this critical frequency, the respective wave ceases to propagate. Thus, limiting high frequency case reduces to the case when $\omega \to \omega_c$. With this limiting value of frequency, we get, $c \to 0$. Thus, it can be concluded that for limiting high frequency case, the phase velocity of the BG waves tends to 0.

6.5.3.2 Limiting thickness

If the thickness of the layer in the model is very thin, i.e. when $h_n \to 0$, then $c \to f_2$. This delineates that when the thickness of the layer approaches zero, then the phase velocity of the BG wave becomes equal to the phase velocity of the shear wave in the NLPE half-space.

6.6 Particular cases

a) Local PE medium

In the absence of nonlocality (i.e., $\Upsilon = 0$) from the layered media, the dispersion relation and the condition of propagation of the BG wave exactly reduce to classical case of PE medium for the corresponding problem. As $\Upsilon = 0$ then $f_2 \to f_1$ and $f_3 \to \sqrt{1 - \frac{c^2}{f_1^2}} = f_4$ (say). With these considerations, the dispersion relations (6.5.1) and (6.5.2) would correspond to the dispersion relations of BG waves for EO and ES conditions in the local PE layered structure.

Dispersion relation for EO condition

$$f_4 \epsilon_{11}^n \overline{c_{44}^n} - {d_{15}^n}^2 \tanh(kh_n)(1 + e^{-2kf_4h_n})(1 + e^{-2kh_n}) = 0. \tag{6.6.1}$$

Dispersion relation for ES condition

$$\left(\frac{{d_{15}^n}^2}{\epsilon_{11}^n}\right)\left\{\overline{c_{44}^n} f_4[(1 + e^{-2kf_3h_n})(1 + e^{-2kh_n}) - 4e^{-kh_n}e^{-kf_4h_n} + 1] - \left(\frac{{d_{15}^n}^2}{\epsilon_{11}^n}\right)(1 - e^{-2kf_4h_n})(1 - e^{-2kh_n})\right\} - \overline{c_{44}^n}^2 f_4^2 = 0. \tag{6.6.2}$$

b) Local PE half-space

Pondering the case a), if $h_n \to 0$ i.e., when there is only a local PE half-space the dispersion relations reduce to

$$c = f_2\sqrt{1 - k_e^4} \qquad \text{where} \quad k_e^2 = \frac{{d_{15}^n}^2}{\epsilon_{11}^n \overline{c_{44}^n}} \tag{6.6.3}$$

which is the classical BG wave velocity of a transversely isotropic local PE half-space obtained by Bleustein [22].

6.7 Numerical results and discussions

In this section, the numerical results of BG surface waves in the considered model comprising of NLPE layer resting over NLPE half-space are presented. The material properties of the PE layer and half-space comprising of $PZT - 5H$ ceramic material having hexagonal symmetry (6 mm class) are assumed in Table 6.1. For convenience, the NL parameter associated with the layer and the half-space is assumed to be the same (i.e. $\Upsilon = 1\ nm$) and

thickness of the layer is taken to be $h_n = 10\ nm$ [9]. The formula for electromechanical coupling coefficient is defined as [147] $k_e^2 = \frac{{d_{15}^n}^2}{\epsilon_{11}^n c_{44}^n}$. Theoretically, for $PZT-5H$ ceramic material, the value of k_e^2 is 0.31206. The following data has been taken into account for numerical computation and graphical representations.

Table 6.1: Material constants for PE layer [2].

Materials	Elastic constant c_{44}^n $(10^{10}Nm^{-2})$	Mass density ρ^n $(10^3 kgm^{-3})$	PE constant d_{15}^n (Cm^{-2})	Dielectric constant ϵ_{11}^n $(10^{-10}C^2N^{-1}m^{-2})$
$PZT-5H$	2.30	7.50	17.0	277.0
$PZT-4$	2.56	7.50	12.7	65.0
$BaTiO_3$	5.43	6.0	21.3	174.42
$LaTiO_3$	9.4	7.45	2.6	3.630
$LiNbO_3$	6.0	4.7	3.7	3.895

Fig. 6.2 a) illustrates the shear velocity (f_2) graph versus the linear frequency in the range $0 < f < 3.5 \times 10^{11}$ Hz. It indicates that shear velocity initiates at 2111.34 m/s which is the velocity of classical shear wave and decreases rapidly with further increase in frequency. For $f > 3.2 \times 10^{11}$ Hz the shear wave in the NLPE elastic solid ceases to propagate further. This shows that shear velocity faces a critical frequency above which it cease to propagate. Fig. 6.2 b) exemplifies the effect of the nonlocality parameter on the shear velocity of the BG wave. Four different values of nonlocality parameter are considered namely [9], $\Upsilon = 0$, 1 nm, 1.5 nm, 2 nm. The effect of the nonlocality parameter on the critical frequency of the shear wave can be interpreted from this figure. As the value of the nonlocality parameter is increasing, the critical frequency of the wave is decreasing. The case of classical PE structure without the NL effect is also included by considering $\Upsilon = 0$. To obtain the critical frequency of BG wave in EO and ES conditions the graphical representations of phase velocity against linear frequency are manifested in Fig. 6.3 a). It shows that at limiting low frequency (i.e., $f \to 0$), the phase velocity c_{BG} for EO condition (represented with thick solid line) initiates at f_1 (= 2111.34 m/s) which is the velocity of the classical shear wave in the PE half-space, as observed analytically in Section 6.5.3.1. while for the ES condition the phase velocity is $c_{BG} = 2010$ m/s which is again less than f_1. Similar interpretations can be made through Fig. 6.3 b) where phase velocity of BG wave is plotted against penetration depth (h_n/λ) which may be defined as the ratio between the layer thickness (h_n) and the wavelength (λ) for EO and ES conditions, respectively. It is again observed from this figure that BG wave initiates at 2111.34 m/s for EO condition (with thick solid line) and at 2010 m/s for ES condition (with thick dashed line). With the further increase in penetration depth (h_n/λ), the phase

velocity is decreasing. The prominent result that is found from both the Figs. 6.3 a) and 6.3 b) is that the phase velocity of BG wave in NLPE layered structure is always less than the shear velocity of BG wave in the fundamental vibrational mode which is the required condition for the existence of BG wave. This proves the existence condition of BG wave [22] ($i.e., c_{BG} < (c_{shear})_{layer} < (c_{shear})_{half-space}$) in the considered structure and hence, validate the results. Another prominent observation that can be obtained from Fig. 6.3 a) is the range of the critical frequencies of the wave in the considered structure for both circuit conditions. For EO condition, the critical frequency lies in 3×10^{11} Hz $< f < 3.5 \times 10^{11}$ Hz while for ES condition, it lies in 2.5×10^{11} Hz $< f < 3 \times 10^{11}$ Hz. As the critical frequency of propagating wave is sensitive to nonlocality, consequently it is worthwhile to study the influence of this parameter on the characteristics of propagating wave in the considered structure. Thus, to explore the effect of nonlocality on the critical frequency the graphical representations are made between phase velocity and frequency for open and short conditions as Figs. 6.4 a) and 6.4 b), respectively. It is concluded that with the increase in the NL parameter the critical frequency decreases. This can be explained by the fact that the presence of the nonlocality leads to the tendency towards a smaller stiffness of the PE material, and hence, decreases the linear frequencies. As a prominent exploration, it can be observed from Figs. 6.5 a) and 6.5 b) that in the absence of nonlocality from the media there do not exist critical frequencies and their phase velocity remain constant with frequency as can be seen from the dispersion curve plotted for local case (i.e. $\Upsilon = 0$). For EO and ES conditions the constant phase velocity is approximately equal to 2000 m/s.

To explore the effect of PE material parameters on the wave propagation Figs. 6.6, 6.7, and 6.8 are plotted. These figures present decreasing/enhancing impact of material parameters on the phase velocity of BG wave plotted against penetration depth. Figs. 6.6 a) and 6.6 b) indicate the effect of elastic stiffness constant (c_{44}^n) on the phase velocity considering different values of c_{44}^n . From the figures, it is deduced that c_{44}^n has an enhancing effect on the phase velocity of the wave. Similarly, from Figs. 6.7 a) and 6.7 b), it can be noted that PE constant (d_{15}^n) also favors the phase velocity of the propagating wave while observing the Figs. 6.8 a) and 6.8 b), it can be remarked that the increase in dielectric constant (ϵ_{11}^n) leads to a decrease in phase velocity of the wave.

6.7.1 Electromechanical coupling factor (K_e^2)

The electromechanical coupling factor (K_e^2) can be calculated from (4.5.1). From Fig. 6.9 a) it is found that $K_e^2 = 0.95\%$ (approx) in the beginning and then it decreases with the further increase of penetration depth for both the values of $k\lambda = 2\pi$ and $k\lambda = 3\pi$. For

$k\lambda = 2\pi$, the value of K_e^2 is more as compared to $k\lambda = 3\pi$. To capture the effect of nonlocality parameter on K_e^2, Fig. 6.9 b) is plotted and it can be seen that as the values of nonlocality parameter is increasing, K_e^2 is decreasing. Thus, nonlocality has suppressing effect on the K_e^2.

6.7.2 Group velocity

The group velocity curve of the wave can be calculated from the formula (4.5.2). It is reported from Figs. 6.10 a) and 6.10 b) that the phase velocity of the BG wave is more than the group velocity of the wave, for both open and short circuit conditions. Thus, the dispersion relation is normal for both circuit conditions. Further to explore the effect of nonlocality on the group velocity, Figs. 6.11 a) and 6.11 b) are plotted and it is seen that the presence of nonlocality decreases the group velocity of BG wave for both open and short circuit conditions.

6.7.3 Result validation

For validation of results, the dispersion relations obtained for EO (6.5.1) and ES conditions (6.5.2) in the absence of nonlocality, are plotted as Figs. 6.11 a) and 6.11 b). Various PE materials are considered viz., $LiNbO_3$, $LaTiO_3$, $BaTiO_3$, $PZT-4$ and $PZT-5H$ (material constant values are provided in Table 6.1). The graphical illustrations obtained for phase velocity against penetration depth for different PE materials are similar to the graphs obtained by Abd-alla and Asker [2], for EO and ES conditions, thereby exemplifying the validation of obtained results.

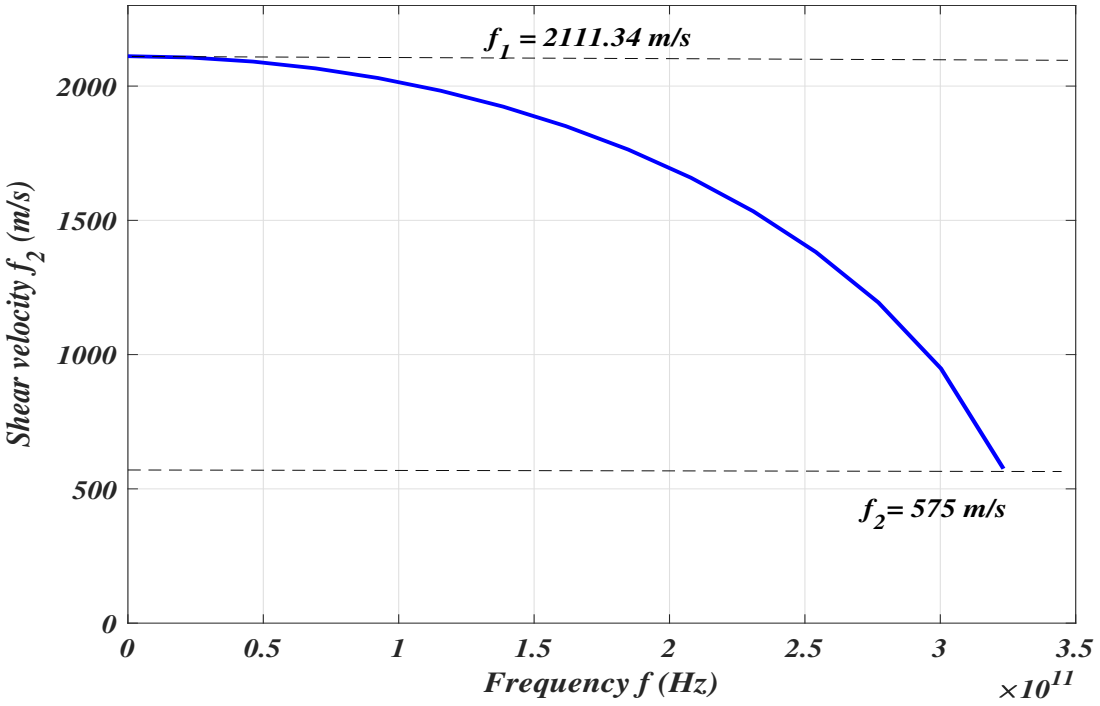

(a) Open circuit condition

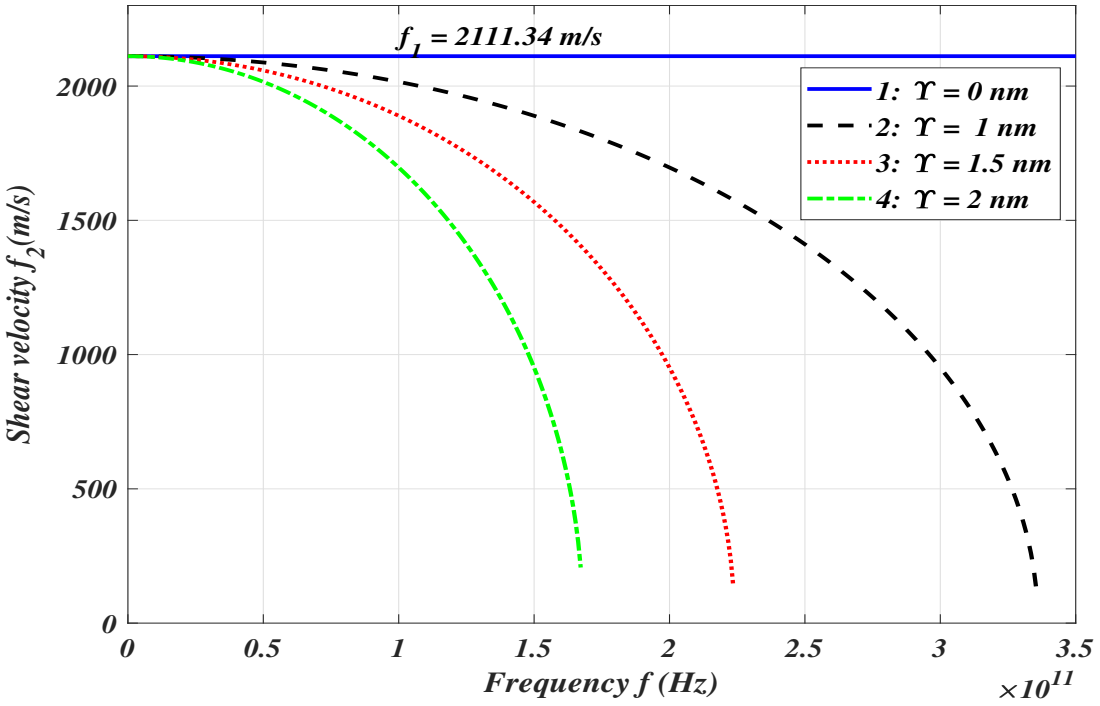

(b) Short circuit condition

Figure 6.2: (a) Shear velocity (f_2) versus frequency (f), (b) Shear velocity (f_2) versus frequency (f) for varying values of nonlocality parameter (Υ).

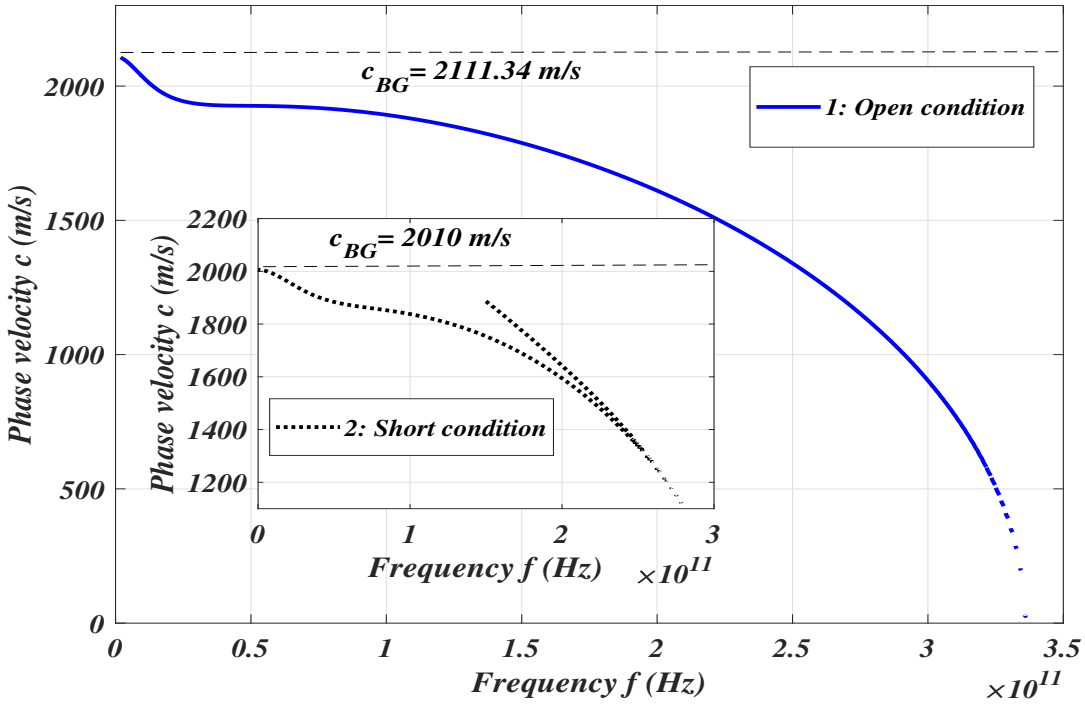

(a) Open circuit condition

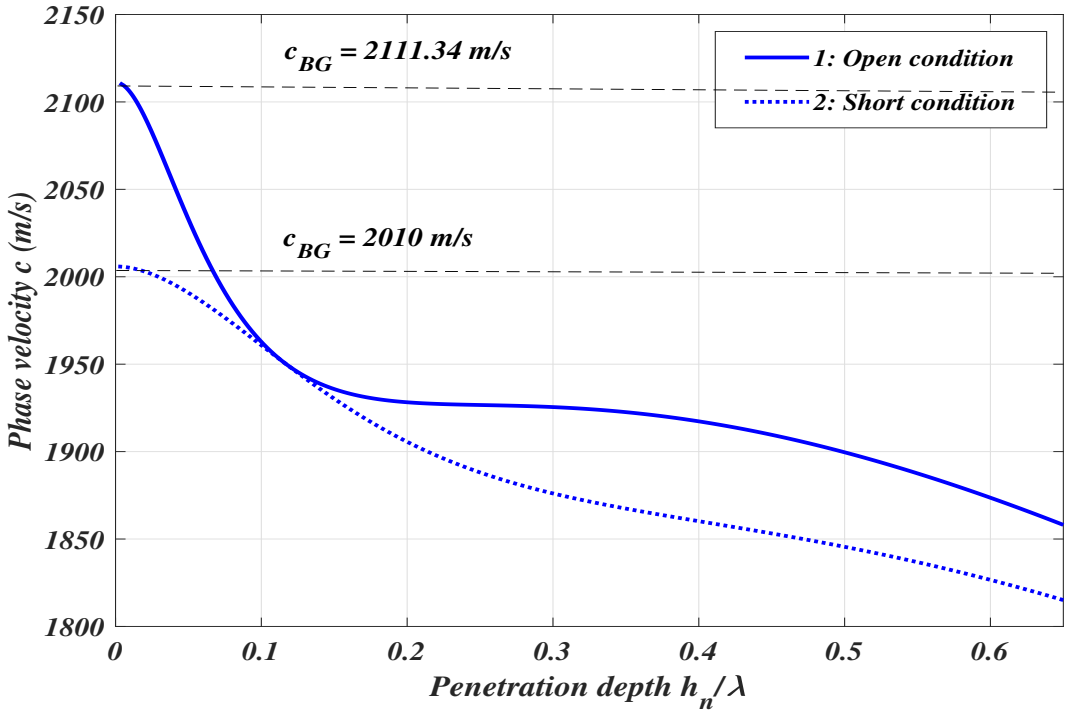

(b) Short circuit condition

Figure 6.3: (a) Dispersion curves of c versus frequency for open circuit condition and short circuit condition (enclosed as subfigure), (b) Dispersion curves of c against penetration depth h_n/λ for open (thick solid line) and short circuit conditions (thick dashed line).

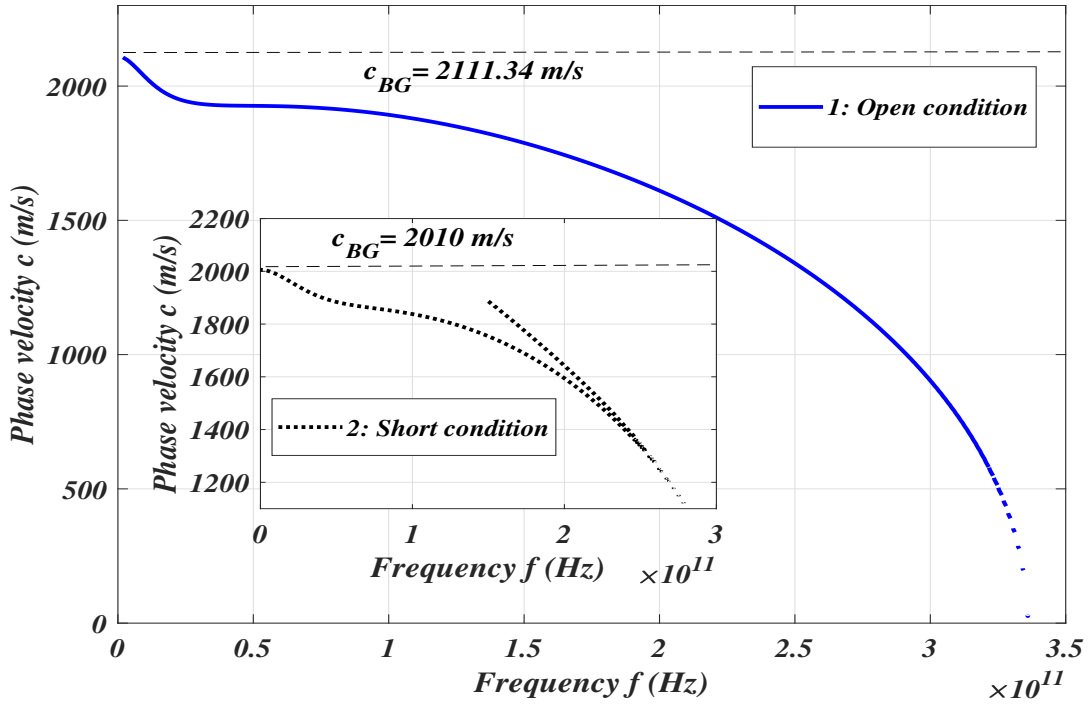

(a) Open circuit condition

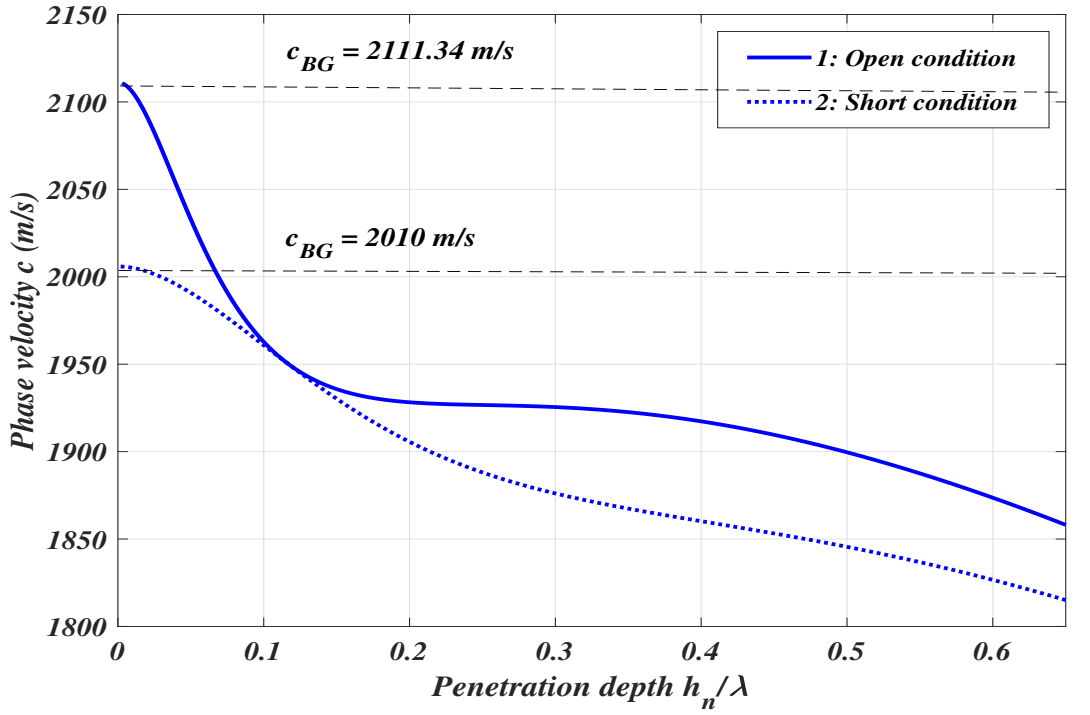

(b) Short circuit condition

Figure 6.4: (a) Dispersion curves of c versus frequency for open circuit condition and short condition (enclosed as subfigure), (b) Dispersion curves of c against h_n/λ for open (thick solid line) and short circuit conditions (thick dashed line).

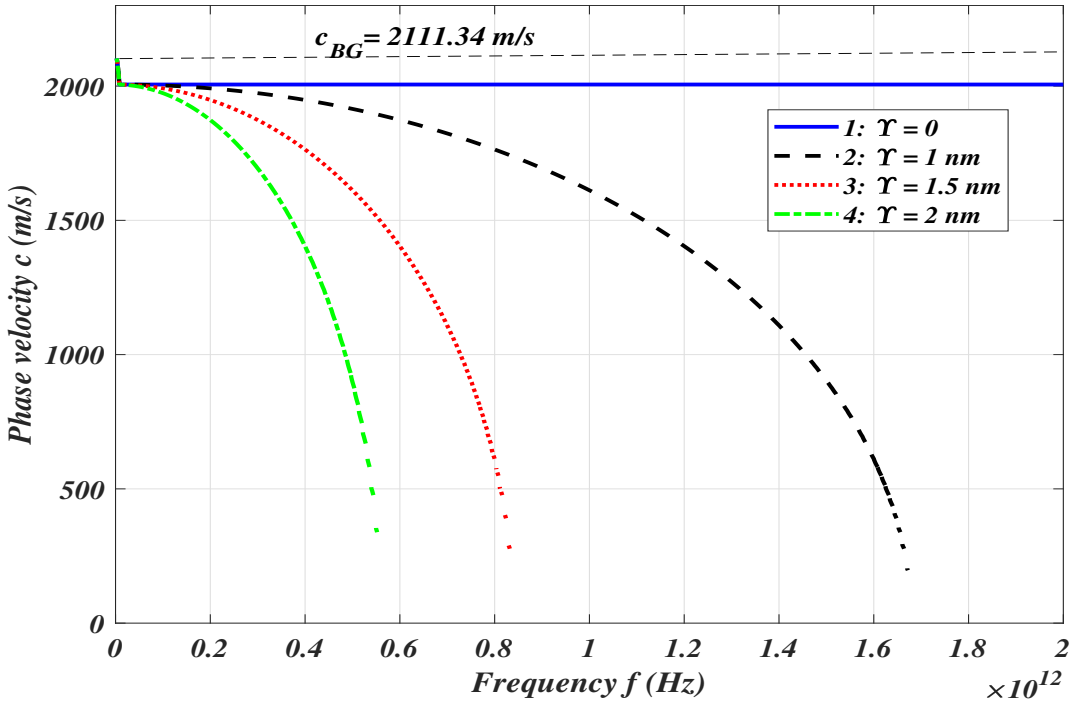

(a) Open circuit condition

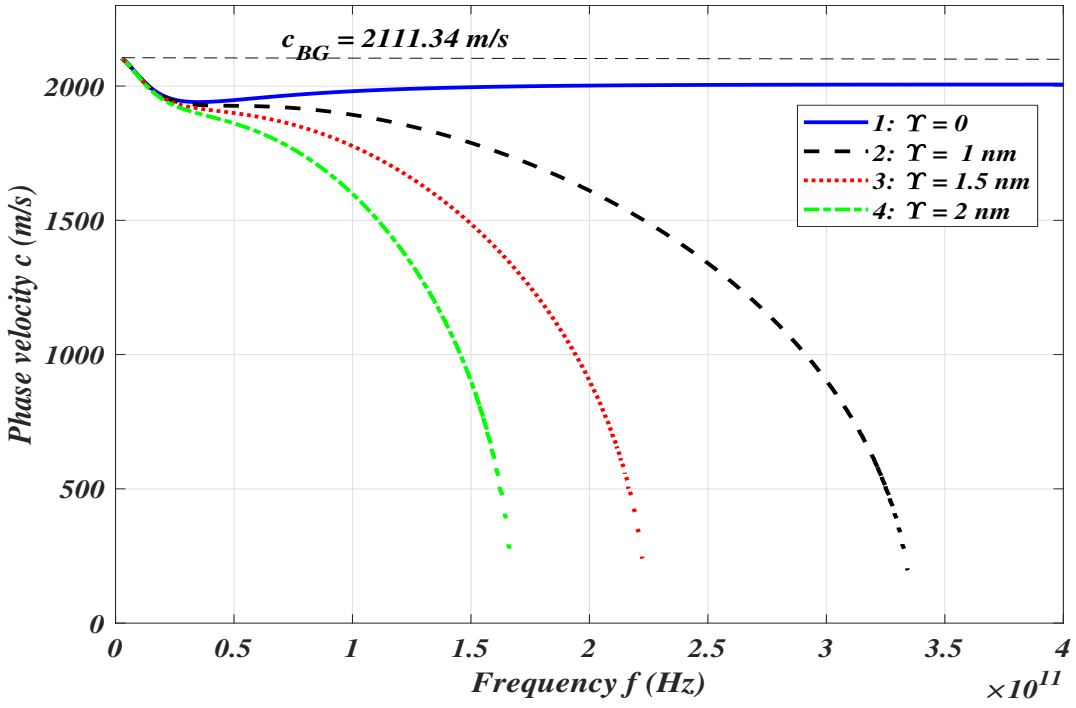

(b) Short circuit condition

Figure 6.5: Dispersion curves of c versus frequency for varying values of nonlocality parameter Υ.

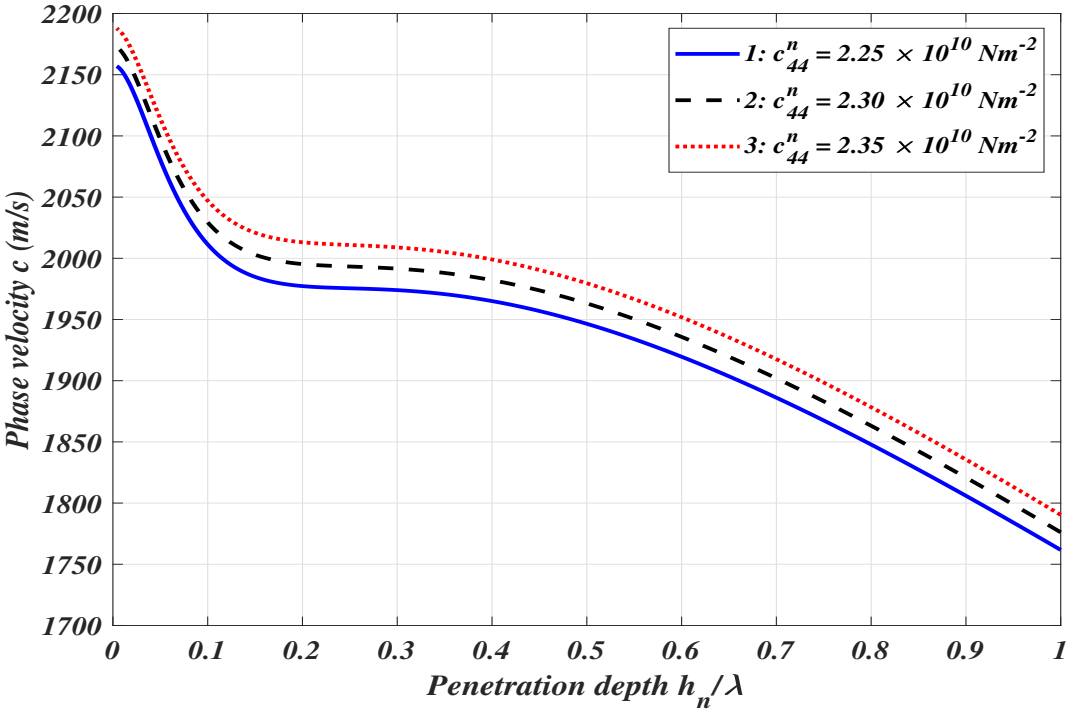

(a) Open circuit condition

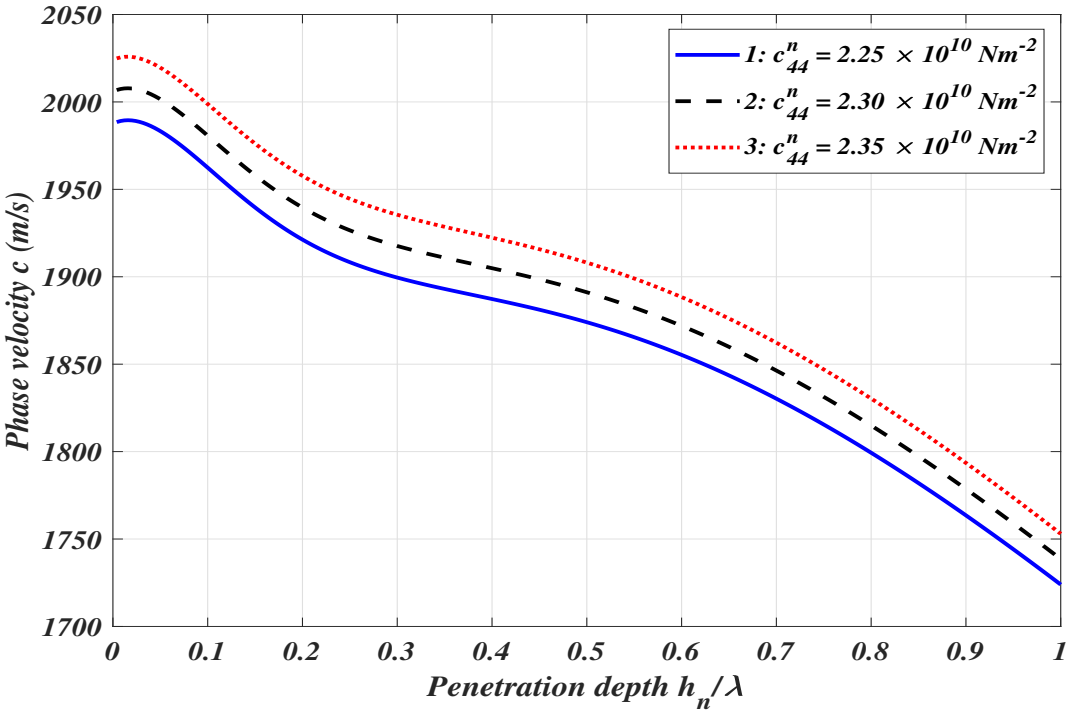

(b) Short circuit condition

Figure 6.6: Dispersion curves of c versus h_n/λ for varying values of elastic stiffness constant (c_{44}^n).

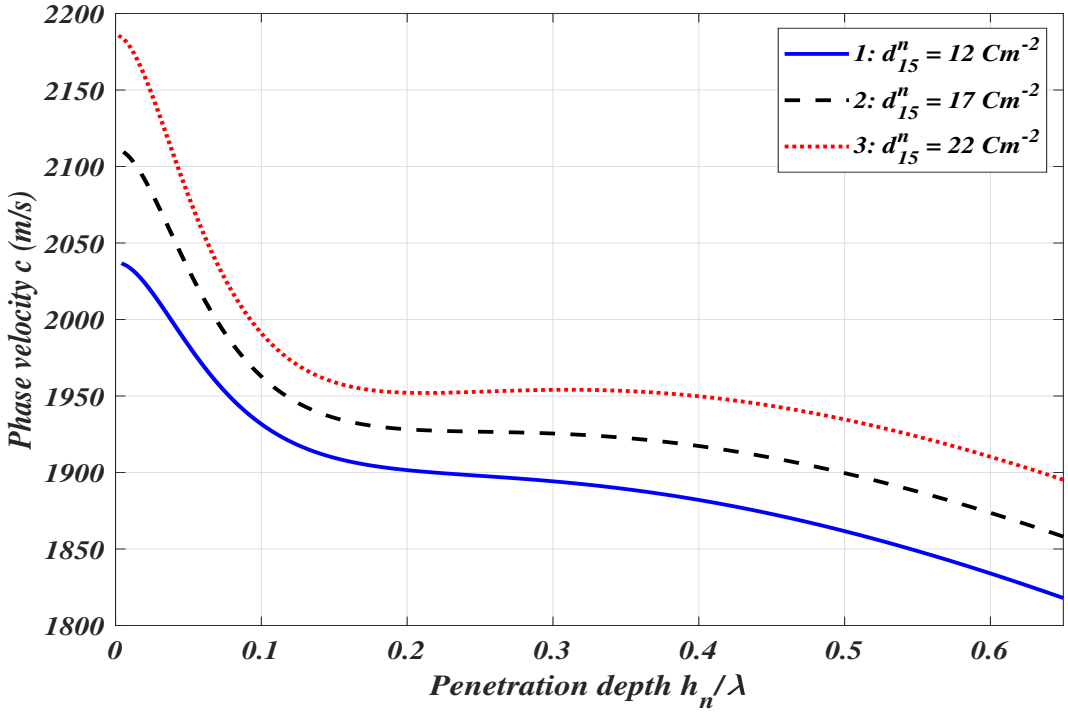

(a) Open circuit condition

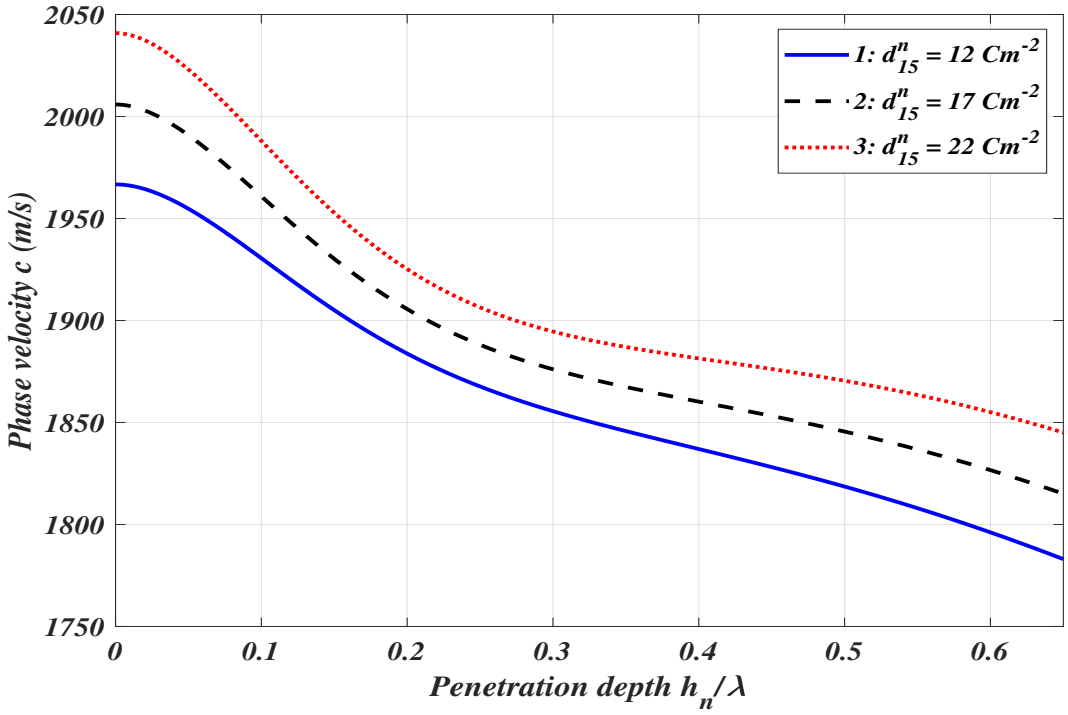

(b) Short circuit condition

Figure 6.7: Dispersion curves of c versus h_n/λ for varying values of PE constant (d^n_{15}).

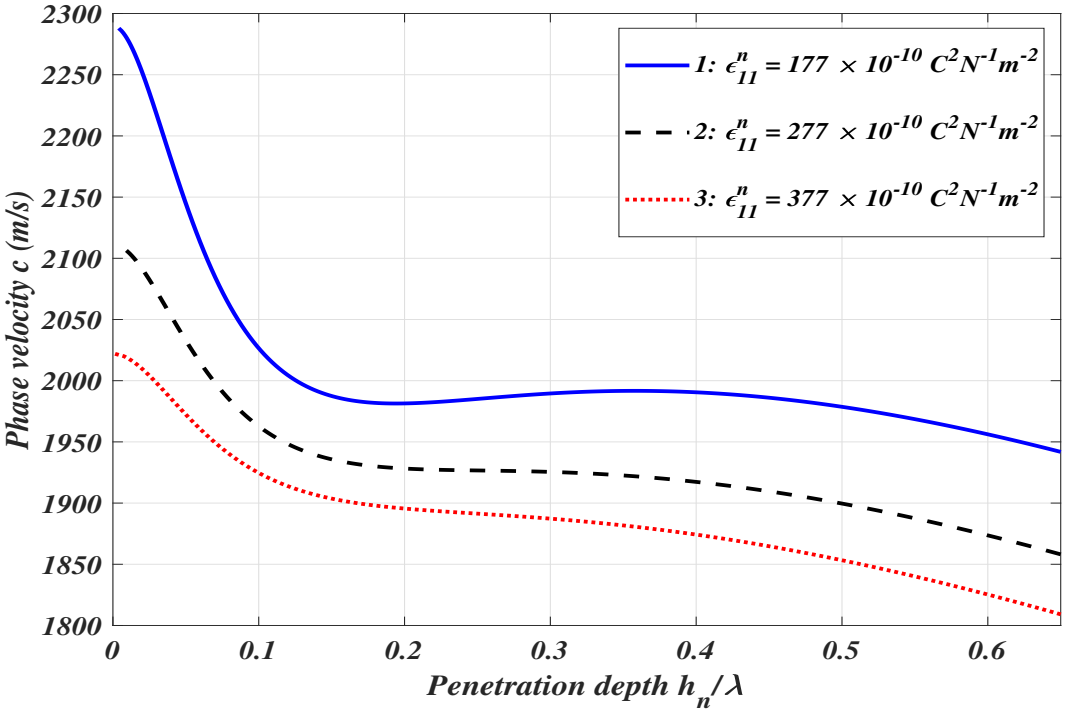

(a) Open circuit condition

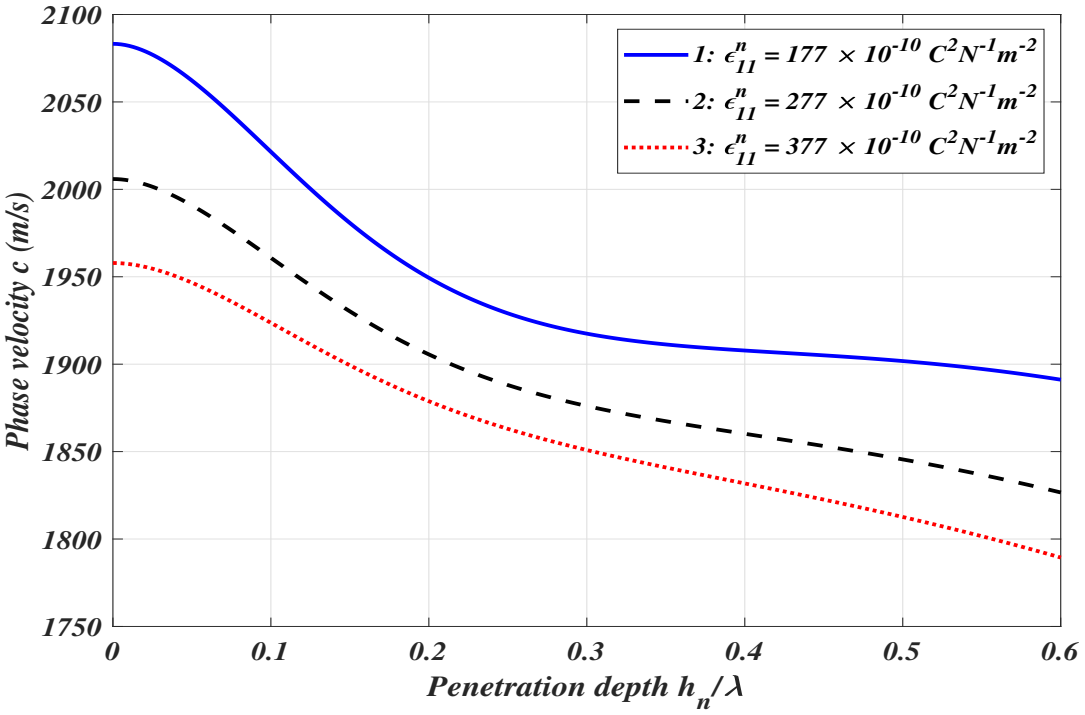

(b) Short circuit condition

Figure 6.8: Dispersion curves of c versus h_n/λ for varying values of dielectric constant (ϵ_{11}^n).

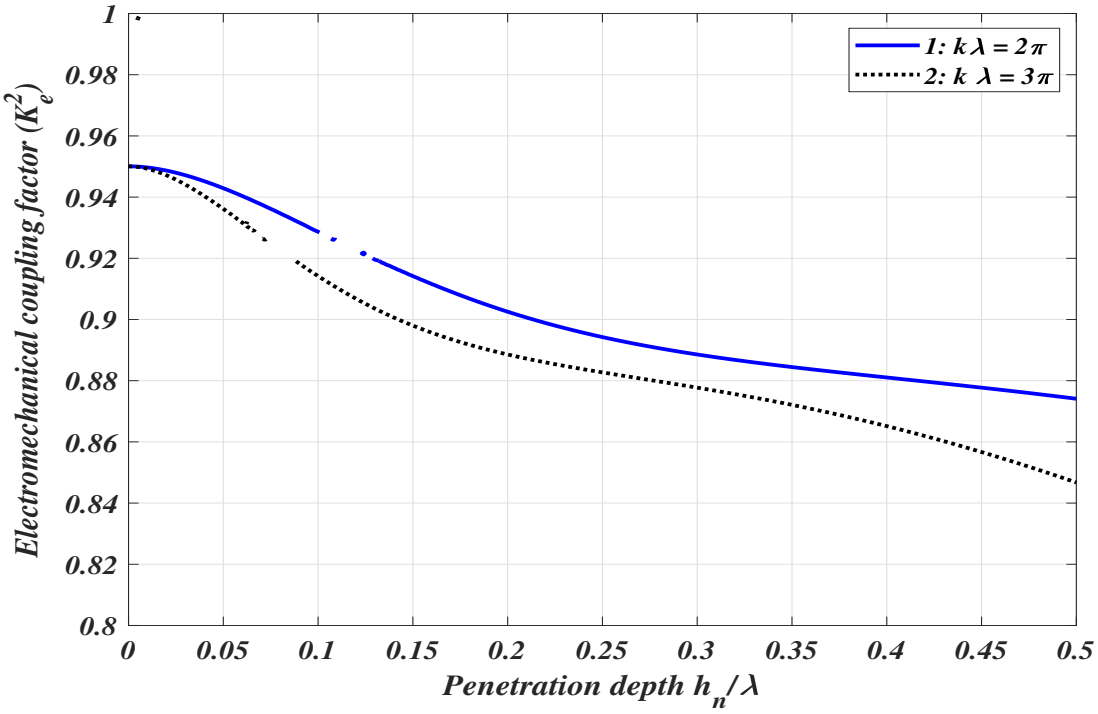

(a) Open circuit condition

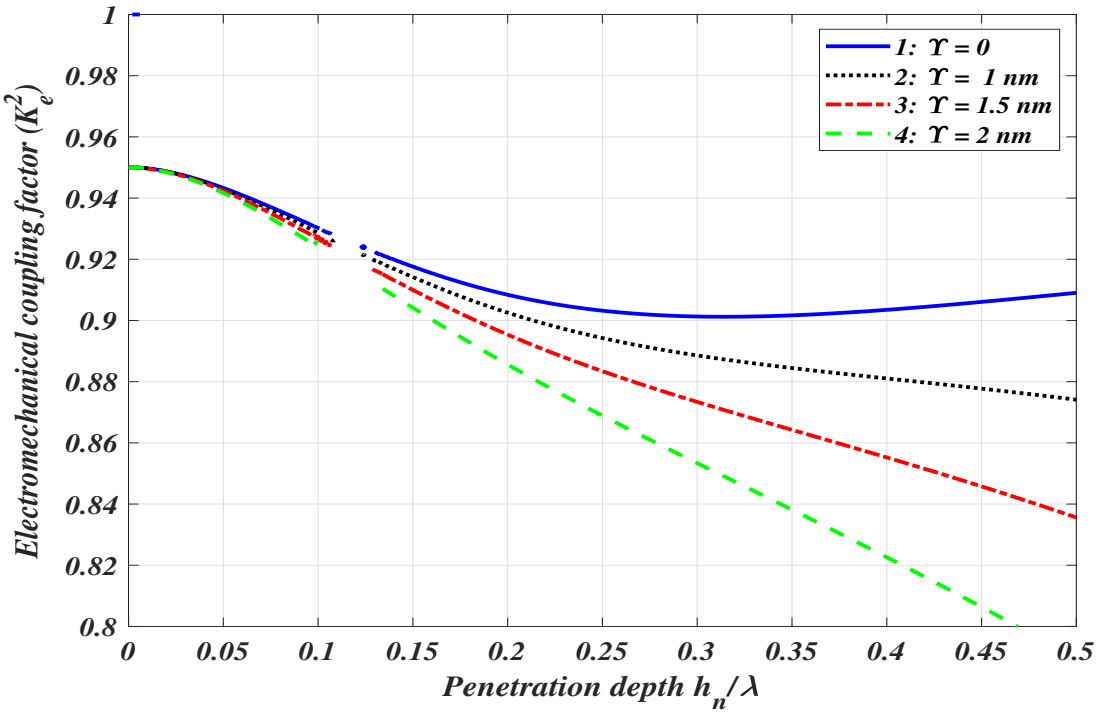

(b) Short circuit condition

Figure 6.9: K_e^2 versus h_n/λ for different values of (a) $k\lambda = 2\pi$ and $k\lambda = 3\pi$, (b) nonlocality parameter (Υ).

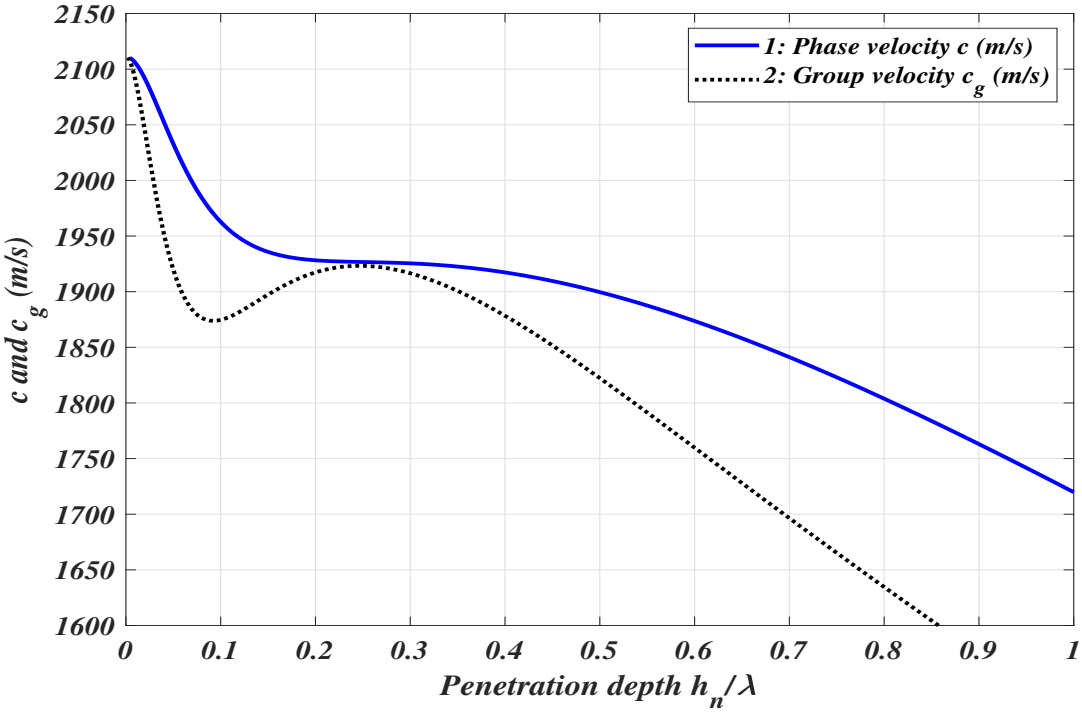

(a) Open circuit condition

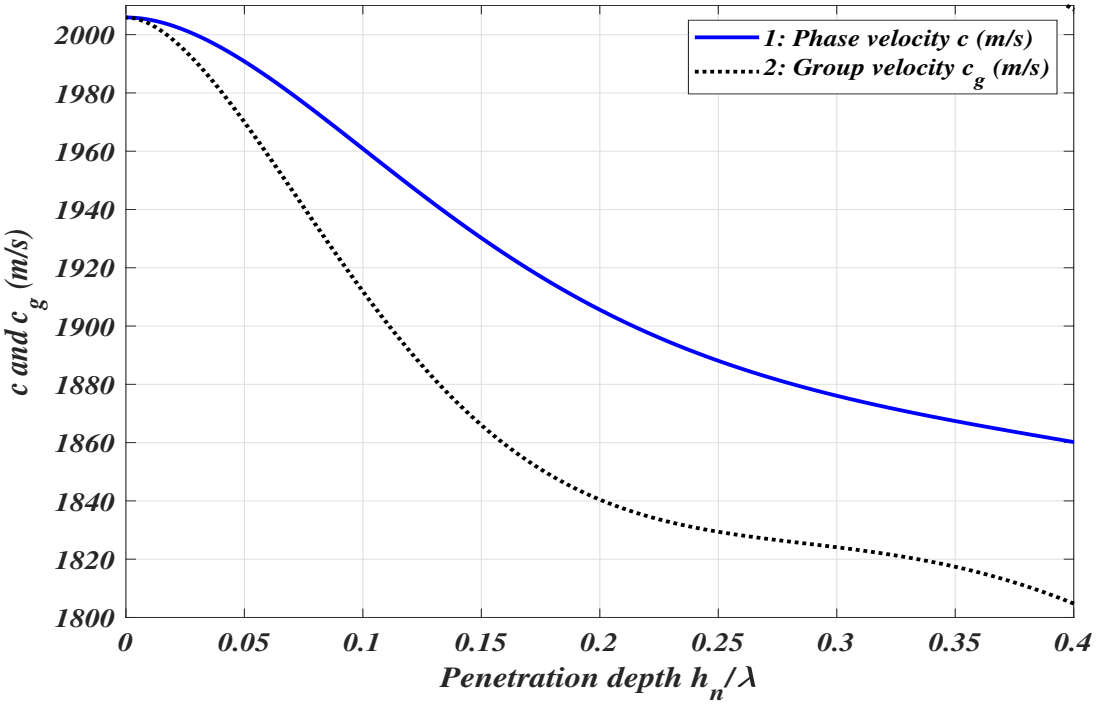

(b) Short circuit condition

Figure 6.10: Variation of c and c_g versus h_n/λ.

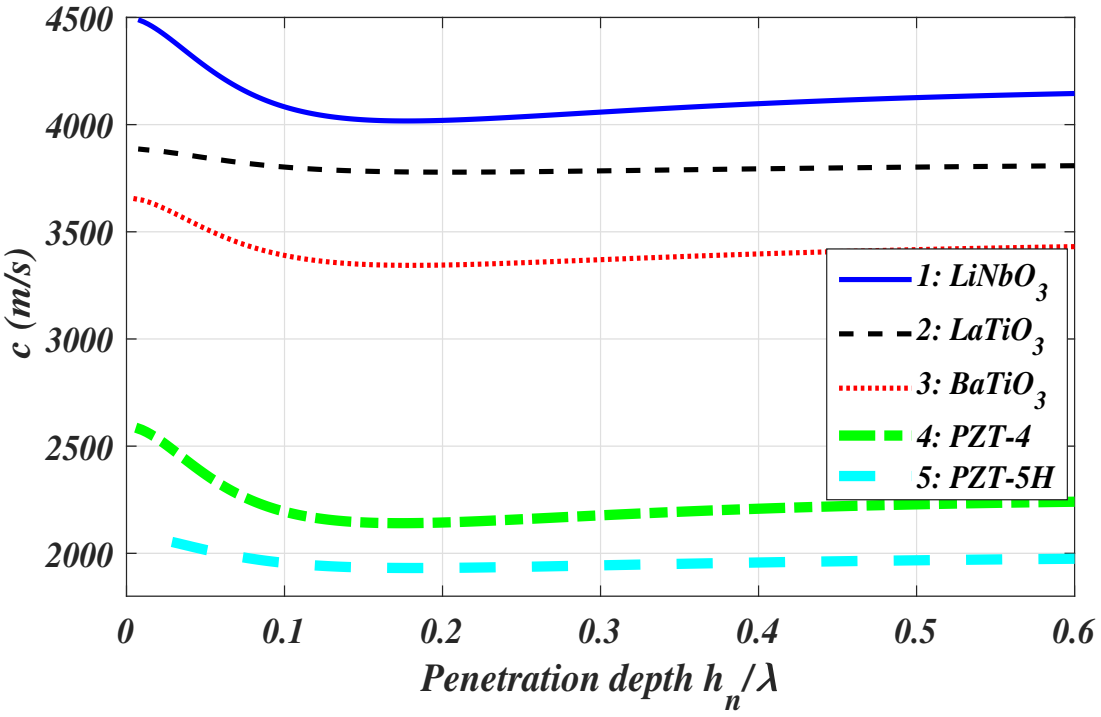

(a) Open circuit condition

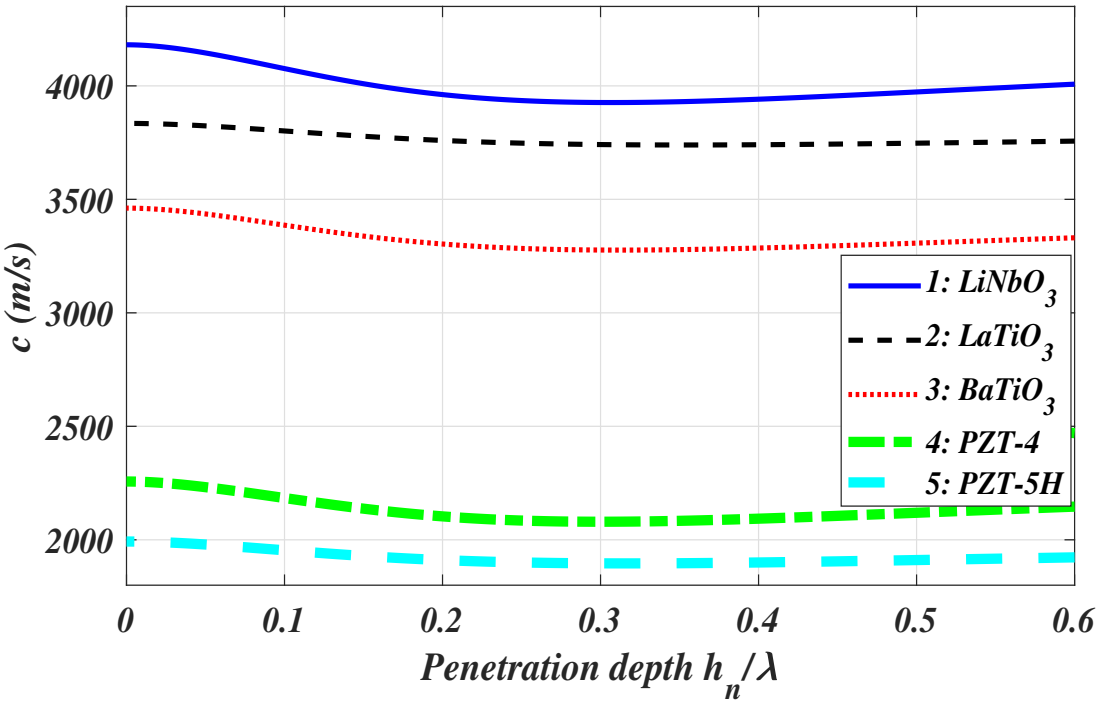

(b) Short circuit condition

Figure 6.11: Dispersion curve of c against (h_n/λ), in the absence of nonlocality.

Conclusions

Following are the pertinent outcomes of this work.

- The dispersion relations are dependent on the nonlocality parameter for both EO and ES conditions thereby exemplifying the significance of NL effects on the phase velocity of propagating BG wave.
- The propagating BG wave faces a critical frequency due to the presence of NL parameter in the media and cease to propagate beyond the corresponding critical frequency.
- Nonlocality has a decaying effect on the critical frequency.
- In the absence of nonlocality in the media there do not exist critical frequency and the phase velocity attains a constant value for the high frequency range.
- Elastic stiffness constant and PE constant has an enhancing effect on the phase velocity and the dielectric constant has a decaying effect on the phase velocity of the BG wave.
- Phase velocity for EO case is greater than that of an ES case.
- The dispersion relation appears 'normal' as the phase velocity is greater than the group velocity of the wave in the considered structure.
- Nonlocality parameter disfavors the group velocity of the BG wave. An increase in NL parameter leads to a decrease in the group velocity of the BG wave.

Physical applications and future scope

Physical applications

- Love wave biosensors can be used to measure a huge number of biological substances (analytes) with significant sensitivity and accuracy. These sensors have numerous applications in biology, chemistry, healthcare, defense, environmental monitoring, and medicine (clinical practice). These surface waves employing in biosensors have a huge potential.
- The basic principle of SAW devices depends on the phase delay. PE/PM materials are able to create an entanglement of the wave, which lowers the phase velocity of the propagating wave and enhances the sensitivity of the Love wave sensors.
- For further optimization high-intensity PE/PM materials can be considered. These features aid in the confinement of waves for a longer period which leads to high sensitivity of the device.
- Extremely thin PE/PM sensors (called thin films) have numerous applications found in medical devices, weapon detection, and data storage.

Future scope

Many crystals and advanced composite materials are capable of offering simultaneous PE, PM, and magnetoelectric (ME) effects and are classified as magnetoelectroelastic material. These materials offer numerous opportunities for the advancement in intelligent or smart structures as these materials are capable of responding to internal or external environmental changes. Till now we have examined the size-dependency effects in structures comprising of either PE material or PM material only. So in the future we are planning to analyze size-dependency effects in structures involving appearance of magnetoelectroelastic media and capture the magnetoelectric effects also.

Bibliography

[1] Abassi, W., Baroudi, A.E. and Razafimahery, F. (2016): Vibration Analysis of Euler-Bernoulli Beams Partially Immersed in a Viscous Fluid. *Physics Research International* **10**(14), 6761372.

[2] Abd-alla, A. and Asker, N. (2016): Numerical simulations for the phase velocities and the electromechanical coupling factor of the Bleustein-Gulyaev waves in some piezoelectric smart materials. *Mathematics and Mechanics of Solids.* **21**(5), 539–551

[3] Acharya, D.P. and Mondal, A. (2002): Propagation of Rayleigh surface waves with small wavelength in nonlocal visco-elastic solids. *Sādhan ā*, **27**(6), 605–612.

[4] Acharya, D.P. and Mondal, A. (2004): Effect of rotation on Rayleigh surface waves under the linear theory of nonlocal elasticity. *Indian Journal of Theoretical Physics* **52**(1), 81–89.

[5] Akgöz, B. and Civalek, O. (2013): Modeling and analysis of micro-sized plates resting on elastic medium using the modified couple stress theory. *Meccanica* **48**(4), 863–873.

[6] Alavi, S.E., Sadighi, M., Danesh Pazhooh, M. and Ganghoffer, J.F. (2020): Development of size-dependent consistent couple stress theory of Timoshenko beams. *Applied Mathematical Modelling* **79**, 685–712.

[7] Alshaikh, F. (2020): Electromechanical coupling of Bleustein-Gulyaev wave propagation in rotating prestressed piezoelectric layered materials. *Continuum Mechanics and Thermodynamics* **32**(7), 749–759.

[8] Alshits, V.I., Darinskii, A.N. and Lothe, J. (1992): On the existence of surface waves in half-infinite anisotropic elastic media with piezoelectric and piezomagnetic properties. *Wave Motion* **16**(3), 265–283.

[9] Amiri, A., Masoumi, A., Talebitooti, R. and Safizadeh, M.S. (2019): Wave propagation analysis of magneto-electro-thermo-elastic nanobeams using sinusoidal shear deformation beam model and nonlocal strain gradient theory. *Journal of Theoretical and Applied Vibration and Acoustics* **5**(2), 153–176.

[10] Ariman, T. (1972): Wave propagation in a micropolar elastic half-space. *Acta Mechanica* **13**(1–2), 11–20.

[11] Atai, A.A., Nikranjbar, A. and Kasiri, R. (2012): Buckling and post-buckling Behaviour of semicircular functionally graded material arches: a theoretical study. Proceedings of the Institution of Mechanical Engineers, Part C: *Journal of Mechanical Engineering Science* **226**(3), 607–614.

[12] Auld, B.A. (1981): Wave propagation and resonance in piezoelectric materials. *The Journal of the Acoustical Society of America* **70**(6), 1577–1585.

[13] Banerjee, M.B., Shandil, R.G., Prakash, J., Bandral, B.S., Lal, P., Kanwar, V. (1997): On Howard's conjecture in heterogeneous shear flows instability of modified s-waves. *Indian Journal of Pure and Applied Mathematics* **28**(6), 825–834.

[14] Bardet, J.P. and Vardoulakis, I. (2001): The asymmetry of stress in granular media. *International Journal of Solids and Structures* **38**(2), 353–367.

[15] Baroi, J., Sahu, S.A. and Singh, M.K. (2018): Dispersion of polarized shear waves in viscous liquid over a porous piezoelectric substrate. *Journal of Intelligent Material Systems and Structures*, **29**(1), 2040–2048.

[16] Baroi, J. and Sahu S.A. (2021): Love-type wave propagation in functionally graded piezomagnetic material resting on piezoelectric half-space. In book: *Advances in Structural Vibration*. DOI: 10.1007/978-981-15-5862-7_{40}

[17] Baroudi, A.E. and Razafimahery F. (2014): Theoretical and numerical investigations of frequency analysis of two circular cylinders ascillating in a incompressible viscous fluid. *International Journal of Applied Mechanics* **6**(5), 20 pages, 1450049.

[18] Baroudi, A.E. and Pommellec, J.Y.L. (2021): Bleustein-Gulyaev waves in a finite piezoelectric material loaded with viscoeleastic fluid. *Wave motion* **101**, 102695.

[19] Billon, F. and Baroudi, A.E. (2021): Mathematical modelling of Love waves propagation in viscoelastic waveguide loaded with complex fluids. *Applied Mathematical Modelling* **96**, 559–569.

[20] Bisheh, H., Wu, N. and Hui, D. (2019): Polarization effects on wave propagation characteristics of piezoelectric coupled laminated fiber-reinforced composite cylindrical shells. *International Journal of Mechanical Sciences* **161-162**(3), 105028.

[21] Biswas, S. (2020): Rayleigh waves in a nonlocal thermoelastic layer lying over a nonlocal thermoelastic half-space. *Acta Mechanica*. DOI:10.1007/s00707-020-02751-2

[22] Bleustein, J.L. (1968): A new surface wave in piezoelectric materials. *Applied Physics Letters* **13**(12), 412–414.

[23] Borodina, I.A., Zaitsev, B.D., Kuznetsova, I.E. and Teplykh, A.A. (2013): Acoustics wave in a structure carrying two piezoelectric plates separated by an air (vaccum) gap. *IEEE Trans Ultrason Ferroelectrics Freq Contr* **60**(12), 2677–2681.

[24] Boxberger, T., Picozzi, M. and Parolai, S. (2011): Shallow Geology characterization using Rayleigh and Love wave dispersion curves derived from seismic noise array measurements. *Journal of Applied Geophysics* **75**, 345–354.

[25] Brandon, D. and Kaplan, W.D. (1999): Microstructural Characterization of Materials, West Sussex: John Wiley and Sons Ltd.

[26] Cao, X., Jin, F. and Wang, Z. (2008a): On dispersion relations of Rayleigh waves in a functionally graded piezoelectric material (FGPM) half-space. *Acta Mechanica* **200**(3), 247–261.

[27] Cao, X., Jin, F. and Wang, Z. (2008b): Theoretical investigation on horizontally shear waves in a functionally gradient piezoelectric material plate. *Advanced Materials Research* **33**, 707–712.

[28] Cao, X., Jin, F., Jeon, I. and Lu, T.J. (2009): Propagation of Love waves in a functionally graded piezoelectric material layer (FGPM) layered composite system. *International Journal of Solids and Structures* **46**, 4123–4132.

[29] Cauchy, A.L. (1823): Recherches sur l' équilibre et le mouvement intérieur des corps solides ou fluides. élastiques ou non élastiques. *Bulletin des sciences par 1 a Societe Philomatique de Paris* 9–13.

[30] Chakraborty, A. (2007): Wave propagation in anisotropic media with nonlocal elasticity. *International Journal of Solids and Structures* **44**(7), 5723–5741.

[31] Chaudhary, S., Sahu, S.A. and Paswan, B. (2019): Transference of SH waves through irregular interface between corrugated piezoelectric layer and pre-stressed viscoelastic layer. *Mechanics of Advanced Materials and Structures* **26**(2), 156–169.

[32] Chaudhary, S., Sahu, S.A. and Singhal, A. (2017): Analytic model for Rayleigh wave propagation in piezoelectric layer overlaid orthotropic substratum. *Acta Mechanica* **228**(2), 495–529.

[33] Chen, P. and Shen, Y. (2007): Propagation of axial shear magneto-electro-elastic waves in piezoelectric–piezomagnetic composites with randomly distributed cylindrical inhomogeneities. *International Journal of Solids and Structures* **44**, 1511–1532.

[34] Chen, A.L., Yan, D.J., Wang, Y.S. and Zhang, C. (2019): In-plane elastic wave propagation in nanoscale periodic piezoelectric/piezomagnetic laminates. *International Journal of Mechanical Sciences* **153–154**, 416–429.

[35] Chu, Z., PourhosseiniAsl, M.J. and Dong, S. (2018): Review of multi-layered magnetoelectric composite materials and devices applications. *Journal of Physics D: Applied Physics* **51**, 243001.

[36] Cordero, A., Franques, A. and Torregrosa, J.R. (2015): Numerical solution of turbulence problems by solving Burger's equation. *Algorithms* **8**, 224–233.

[37] Cordero, A., Gomez, E. and Torregrosa, J.R. (2017): Efficient high-order iterative methods for solving nonlinear systems and their application on heat conduction problems. *Complexity* **4**, 1–11.

[38] Cosserat, E. and Cosserat, F. (1909): Théorie des Corps Déformables, A. Hermann et Fils, Paris.

[39] Curtis, R.G. and Redwood, M. (1973): Transverse surface waves on a piezoelectric material carrying a metal layer of finite thickness. *Journal of Applied Physics* **44**(5), 2002–2007.

[40] Das, P.S. and Sengupta, P.R. (1990): Surface waves in micropolar thermoelasticity under the influence of gravity. *Proceeding of Indian National Science Academy* **56**(5), 459–471.

[41] Deep, S. and Sharma, V. (2021) Love Wave Propagation in Viscoelastic Layer Sandwiched Between Fiber-reinforced Layer and Consistent Couple Stress Substrate. *Iranian Journal of Science and Technology Transactions of Mechanical Engineering*. DOI: 10.1007/s40997-020-00411-3

[42] Dineva, P., Gross, D., Müller, R. and Rangelov, T. (2014): Dynamic Fracture of piezoelectric materials. Springer, Berlin.

[43] Du, J., Harding, G.L., Ogivy, J.A. et al. (1996): A study of Love-wave acoustic sensors" Sensors and Actuators A. *Sensors and Actuators* **56**(3), 211–219.

[44] Du, J., Jin, X., Wang, J. and Xian, K. (2007): Love wave propagation in functionally graded piezoelectric material layer. *Ultrasonics* **46**(1), 13–22.

[45] Du, J., Xian, K., Wang, J. and Yong, Y.K. (2008): Propagation of Love waves in prestressed piezoelectric layered structures loaded with viscous liquid. *Acta Mechanica Solida Sinica* **21**(6), 542–558.

[46] Du, J., Xian, K., Yong, Y.K. and Wang, J. (2010): SH-SAW propagation in layered functionally graded piezoelectric material structures loaded with viscous liquid. *Acta Mechanica Solida Sinica* **212**(3), 271–281.

[47] Duarte, F., Gormaz, R. and Natesan, S. (2004): Arbitrary Lagrangian–Eulerian method for Navier–Stokes equations with moving boundaries. *Computer Methods in Applied Mechanics and Engineering* **193**(45–47), 4819–4836.

[48] Ebrahimi, F. and Salari, E. (2015): Size-dependent thermo-electrical buckling analysis of functionally graded piezoelectric nanobeams. *Smart Materials and Structures*, **24**(12), 125007.

[49] Ebrahimi, F. and Dabbagh, A. (2017): Wave propagation analysis of smart rotating porous heterogeneous piezoelectric nanaobeams. *European Physical Journal Plus* **132**(4), 153. DOI:10.1140/epjp/i2017-11366-3

[50] Ebrahimi, F., Dehghan, M. and Seyfi, A. (2019): Eringen's nonlocal elasticity theory for wave propagation analysis of magneto-electro-elastic nanotubes. *Advances in Nano Research* **7**(1), 1–11.

[51] Ebrahimi, F. and Seyfi, A. (2020): Wave propagation analysis of smart inhomogeneous piezoelectric nanosize beams rested on an elastic medium. *Waves in Random and Complex Media.* DOI:10.1080/17455030.2020.1817625

[52] Edelen, D.G.B. and Laws, N. (1971): On the thermodynamics of systems with nonlocality. *Archive for Rational Mechanics and Analysis* **43**(1), 24–35.

[53] Edelen, D.G.B., Green, A.E. and Laws, N. (1971): Nonlocal continuum mechanics. *Archive for Rational Mechanics and Analysis* **43**(1), 36–44.

[54] Erbay, S., Erbay, H.A. and Dost, S. (1992): Nonlinear wave interactions in a micropolar elastic medium. *WaveMotion* **16**(2), 163–172.

[55] Eremeyev, V.A., Skrzat, A. and Vinakurava, A. (2016): Application of the Micropolar Theory to the Strength Analysis of Bioceramic Materials for Bone Reconstruction. *Strength of Materials* **48**(4), 573–582.

[56] Eringen, A.C. (1962): Nonlinear Theory of Continuous Media, McGraw-Hill, New York.

[57] Eringen, A.C. and Suhubi, E.S. (1964a): Nonlinear theory of simple micro-elastic solids-I. *International Journal of Engineering Science* **2**, 189–203.

[58] Eringen, A.C. and Suhubi, E.S. (1964b): Nonlinear theory of simple micro-elastic solids-II. *International Journal of Engineering Science* **2**, 389–404.

[59] Eringen, A.C. (1966): Mechanics of micromorphic materials. Proceedings of 11th International Congress of Applied Mechanics (Gortler, H., ed.), Springer-Verlag, New York 131–138.

[60] Eringen, A.C. (1966): Linear theory of micropolar elasticity. *Journal of Mathematics and Mechanics* **15**, 909–923.

[61] Eringen, A.C. and Edelen, D.G.B. (1972): On nonlocal elasticity. *International Journal of Engineering Science* **10**, 1–6.

[62] Eringen, A.C. (1978): Line crack subject to shear. *International Journal of Fracture* **14**(4), 367–379.

[63] Eringen, A.C. (1983): On differential equations of nonlocal elasticity and solutions of screw-dislocation and surface waves. *Journal of Applied Physics* **54**(9), 4703–4710.

[64] Eringen, A.C. (1984): Plane waves in nonlocal micropolar elasticity. *International Journal of Engineering Science* **22**, 1113–1121.

[65] Eskandari, M. and Shodja, H. M. (2008): Love waves propagation in functionally graded piezoelectric materials with quadratic variation. *Journal of Sound and Vibration* **313**(1-2), 195–204.

[66] Ezzin, H., Amor, M.B. and Ghozlen, M.H.B. (2016): Love wave propagation in a transversely isotropic piezoelectric layer on a piezomagnetic half-space. *Ultrasonics* **69**, 83–89.

[67] Ezzin, H., Amor, M.B. and Ghozlen, M.H.B. (2017): Propagation behavior of SH waves in layered piezoelectric/piezomagnetic plates. *Acta Mechanica* **228**(3), 1071–1081.

[68] Fatemi, J., Vankeulen, F., Onck, P.R. (2002): Generalized Continuum Theories: Application to Stress Analysis in Bone* *Meccanica* **37**, 385–396.

[69] Gauthier, R.D. (1982): Experimental investigation on micropolar media. Mechanics of Micropolar Media, World Science Singapore, 395–463.

[70] Gholami, M., Zare, E. and Alibazi, A. (2021): Applying Eringen's nonlocal elasticity theory for analyzing the nonlinear free vibration of bidirectional functionally graded Euler–Bernoulli nanobeams. *Archive of Applied Mechanics* **91**(7), 2957–2971.

[71] Giannakopoulos, A.E. and Suresh, S. (1997): Indentation of solids with gradients in elastic properties: Part I. Point force. *International Journal of Solids and Structures* **34**(19), 2357–2392.

[72] Giannakopoulos, A.E. and Suresh, S. (1997): Indentation of solids with gradients in elastic properties: Part II. Axisymmetric indentors. *International Journal of Solids and Structures* **34**(19), 2393–2428.

[73] Goda, I., Assedi, M., Belouettar, S. and Ganghoffer, J.F. (2012): A micropolar anisotropic constitutive model of cancellous bone from discrete homogenization. *Journal of the Mechanical Behavior of Biomedical Materials* **16**, 87–108.

[74] Gopalakrishnan, S. and Narender, S. (2013): Wave Propagation in Nanostructures: Nonlocal Continuum Mechanics, Springer.

[75] Goyal, R., Kumar, S. and Sharma, V. (2018): Microstructural considerations on SH-wave propagation in a piezoelectric layered structure. *Journal of Theoretical and Applied Mechanics* **56**(4), 993–1004.

[76] Goyal, R., Kumar, S. and Sharma V. (2018): A size-dependent micropolar-piezoelectric layered structure for the analysis of wave. *Waves in Random and Complex Media* **30**(3), 1–18.

[77] Goyal, R. and Kumar, S. (2019): Dispersion of Love waves in size-dependent substrate containing finite piezoelectric and viscoelastic layers. *International Journal of Mechanics and Materials in Design* **15**(2), 767–790.

[78] Goyal, R. and Kumar, S. (2019): Quantifying viscoelastic, piezoelectric and couple stress effects on Love-type wave propagation. *Smart Materials and Structures* **28**(10), 105021.

[79] Goyal, R. and Kumar, S. (2021): Estimating the effects of imperfect bonding and size-dependency on Love-type wave propagation in functionally graded orthotropic material under the influence of initial stress. *Mechanics of Materials* **155**(15), 103772.

[80] Goyal, S., Sahu, S.A. and Mondal, S. (2019): Modelling of Love-type wave propagation in piezomagnetic layer over a lossy viscoelastic substrate: Sturm-Liouville problem. *Smart Material and Structures* **28**, 057001.

[81] Goyal, S. and Sahu, S.A. (2021): Love wave transference in piezomagnetic layered structure guided by an imperfect interface. *GEM-International Journal on Geomathematics* **12**, 5. DOI:10.1007/s13137-021-00173-3

[82] Graff, K.F. (1991): Wave motion in elastic solids, Dover Publications, INC., New York.

[83] Gulyaev, Y.V. (1969): Electro-acoustic surface waves in solids. *Soviet Physics-JETP Letters* **9**, 37–38.

[84] Gunther, W. (1958): Zurstatik und kinematik des cosseratschen kontinuums. *Abhandlungen der Braunschweigischen Wissenschaftlichen Gesellschaft* **10**, 195–213.

[85] Guo, F.L. and Sun, R. (2008): Propagation of Bleustein-Gulyaev wave in 6 mm piezoelectric materials loaded with viscous liquid, *International Journal of Solids and Structures,* **45**, 3699–3710.

[86] Gupta, S. and Bhengra, N. (2019): Study of the surface wave vibrations in a functionally graded material layered structure: a WKB method. *Mathematics and Mechanics of Solids* **24**(3), 1204–1220.

[87] Hadjesfandiari, A.R. and Dargush, G.F. (2011): Couple stress theory for solids. *International Journal of Solids and Structures* **48**(18), 2496–2510.

[88] Han, X. and Liu, G.R. (2003): Elastic waves in a functionally graded piezoelectric cylinder. *Smart Materials and Structures* **12**(6), 962-971.

[89] Hashemi, R. (2017): Scattering of shear waves by a two-phase multiferroic sensor embedded in a piezoelectric/piezomagnetic medium. *Smart Materials and Structures* **26**(3), 035016.

[90] Ichinose, N., Miyamoto, N. and Takahashi, S. (2004): Ultrasonic transducers with functionally graded piezoelectric ceramics. *Journal of the European Ceramic Society* **24**(6), 1681–1685.

[91] Jakoby, B. and Vellekoop, M.J. (1997): Properties of Love waves: applications in sensors. *Smart Materials and Structures*, **6**(6), 668–679.

[92] Jin, F., Wang, Z. and Wang, T. (2001): The Bleustein-Gulyaev (BG) wave in a piezoelectric layered half-space. *International Journal of Engineering Science* **39**(11), 1271–1285.

[93] Kaliski, S., Rymarz, C.Z., Sobczyk, K. and Wlodarczyk, E. (1992): Surface Waves in Non-Local Media and in Media with a Microstructure, *S. Kaliski, L. Solarz (Eds.), Studies in Applied Mechanics-B: Waves* **30**, 261–270.

[94] Kanwar, V., Singh, K. and Mamta (2003): An upper bound on the growth rate of a linear instability in an inviscid compressible subsonic parallel shear flow. *Indian Journal of Pure and Applied Mathematics* **34**(11), 1533–1538.

[95] Kaur, G., Singh, D. and Tomar S.K. (2018): Rayleigh type wave in a nonlocal elastic solid with voids. *European Journal of Mechanics and Solids* **71**, 134–150.

[96] Kaur, G., Singh, D. and Tomar, S.K. (2019): Love waves in a nonlocal elastic media with voids. *Journal of Vibration and Control* **25**(8), 1470–1483.

[97] Kaur, T., Sharma, S.K. and Singh, A.K. (2016): Influence of imperfectly bonded micropolar elastic half-space with non-homogeneous viscoelastic layer on propagation behavior of shear wave. *Waves in Random and Complex Media* **26**(4), 650–670.

[98] Khurana, A. and Tomar, S.K. (2013): Reflection of plane longitudinal waves from the stress-free boundary of a nonlocal, micropolar solid halfspace. *Journal of Mechanics of Materials and Structures* **8**, 95–107.

[99] Khurana, A. and Tomar, S.K. (2017): Rayleigh-type waves in nonlocal micropolar solid half-space, *Ultrasonics* **73**, 162–168.

[100] Kielczynski, P., Szalewski, M., Siegoczynski, R.M., Rostocki, A.J. (2008): New ultrasonic Bleustein-Gulyaev method for measuring the viscosity of liquids at high temperature. *Review of Scientific instruments* **79**, 026109.

[101] Kielczynski, P., Szalewski, M. and Balcerzak, A. (2012): Effect of a viscous liquid loading on love wave propagation. *International Journal of Solids and Structures* **49**, 2314–2319.

[102] Kleemann, W. (2017): Multiferroic and magnetoelectric nanocomposites for data processing. *Journal of Physics D: Applied Physics* **50**(22), 223001.

[103] Koiter, W.T. (1964): Couple Stresses in the Theory of Elasticity, I and II. *Proceedings Series B, Koninklijke Nederlandse Akademie van Wetenschappen* **67**, 17–44.

[104] Kovacs, G., Vellekoop, M.J., Haueis, R. et al. (1994): A Love wave sensor for bio chemical sensing in liquids. *Sensors and Actuators* **43**(1), 38–43.

[105] Kumari, R. and Singh, A.K. (2021): Dispersion and attenuation of shear wave in couple stress stratum due to point source. *Journal of Vibration and Control*, DOI: 10.1177/10775463219988801

[106] Kumar, S., Sharma, J.N. and Sharma, Y.D. (2011): Generalized thermoelastic waves in microstrech plates loaded with fluid of varying temperature. *International Journal of Applied Mechanics* **3**(3), 563–586.

[107] Kumar, S. and Tomar, S.K. (2020): Plane waves in nonlocal micropolar thermoelastic material with voids. *Journal of Thermal Stresses* **43**(4), 1–24.

[108] Kundu, S., Kumari, A., Pandit, D.K. and Gupta, S. (2017): Love wave propagation in heterogeneous micropolar media. *Mechanics Research Communications* **83**, 6–11.

[109] Lakes, R.S. (1986): Experimental microelasticity of two porous solids. *International Journal of Solids and Structures* **22**(1), 55–63.

[110] Lakes, R.S. (1991): Experimental Micro Mechanics Methods for Conventional and Negative Poisson's Ratio Cellular Solids as Cosserat Continua. *Journal of Engineering Materials and Technology* **113**(1), 148–155.

[111] Li, X.Y., Wang, Z.K. and Huang, S.H. (2004): Love waves in a functionally graded piezoelectric materials. *International Journal of Solids and Structures* **41**(26), 7309–7328.

[112] Li, P. and Jin, F. (2012): Bleustein-Gulyaev waves in a transversely isotropic piezoelectric layered structure with an imperfectly bonded interface. *Smart Materials and Structures* **21**(4), 045009.

[113] Li, P., Jin, F. and Qian, Z. (2013): Propagation of the Bleustein-Gulyaev waves in a functionally graded transversely isotropic electro-magneto-elastic half-space. *European Journal of Mechanics A/Solids* **37**, 17–23.

[114] Li, L. and Wei, P.J. (2015): Propagation of surface waves in a homogeneous layer of finite thickness over an initially stressed functionally graded magneto-electric-elastic half-space. *Journal of Theoretical and Applied Mechanics* **45**(1), 69–86.

[115] Li, M., Kong, Y., Liu, J. and Nie, G. (2019): Study on the propagation characteristics of SH wave in piezomagnetic-piezoelectric structures. *Materials Research Express* **6**(10), 105707.

[116] Liao, W. (2011): A computational method to estimate the unknown coefficient in a wave equation using boundary measurements. *Inverse Problems in Science and Engineering* **19**(6), 855–877.

[117] Liao, W., Yong, P., Dastour, H. and Huang, J. (2018): Efficient and accurate numerical simulation of acoustic wave propagation in a 2D heterogeneous media. *Applied Mathematics and Computation* **321**, 1339–1351.

[118] Liu, G.R. and Tani, J. (1994): Surface waves in functionally gradient piezoelectric plates. *Journal of Vibration and Acoustics* **116**(4), 440–448.

[119] Liu, G.R., Dai, K.Y., Han, X. and Ohyoshi, T. (2003): Dispersion of waves and charateristic wave surfaces in functionally graded piezoelectric plates. *Journal of Sound and Vibration* **268**(1), 131–147.

[120] Liu, J., Cao, X.S. and Wang, Z.K. (2007): Propagation of Love waves in a smart functionally graded piezoelectric composite structure. *Smart Materials and Structures* **16**(1), 13–24.

[121] Liu, J.X., Fang, D.N., Wei, W.Y. and Zhao, X.F. (2008): Love waves in layered piezoelectric/piezomagnetic structures. *Journal of Sound and Vibration* **315**(1–2), 146–156.

[122] Liu, J., Cao, X.S. and Wang, Z.K. (2009): Love waves in a smart functionally graded piezoelectric composite structure. *Acta Mechanica* **208**(1–2), 63–80.

[123] Liu, J., Wang, L., Lu, Y. and He, S. (2013): Properties of Love waves in a piezoelectric layered structure with a viscoelastic guiding layer. *Smart Materials and Structures* **22**(12), 125034.

[124] Liu, J. (2014): A theoretical study on Love wave sensors in a structure with multiple viscoelastic layers on a piezoelectric substrate. *Smart Materials and Structures* **23**(7), 075015.

[125] Liu, L., Zhao, J., Pan, Y., Bonello, B. and Zhong, Z. (2014): Theoretical study of SH-wave propagation in periodically layered piezomagnetic structure. *International Journal of Mechanical Sciences* **85**, 45–54.

[126] Liu, C., Ke, L.L. and Wang, Y.S. (2015): Nonlinear vibration of nonlocal piezoelectric nanoplates. *International Journal of Structural Stability and Dynamics* **15**(8), 1540013.

[127] Love, A.E.H. (1911): Some Problems in Geodynamics, Cambridge University Press, London.

[128] Love, A.E.H. (1944): A treaties on the mathematical theory of elasticity, Cambridge University Press, London.

[129] Mahanty, M., Kumar, P., Singh, A.K. and Chattopadhyay, A. (2020): On the characteristics of shear acoustic waves propagating in an imperfectly bonded functionally graded piezoelectric layer over a piezoelectric cylinder. *Journal of Engineering Mathematics* **120**(4), 1–22.

[130] Martowicz, A., Bryła, J., Staszewski, W.J., Ruzzene, M. and Uhl, T. (2019): Nonlocal elasticity in shape memory alloys modeled using peridynamics for solving dynamic problems. *Nonlinear Dynamics* **97**(3), 1911–1935.

[131] Mawassy, N., Reda, H., Ganghoffer, J.F., Eremeyev, V.A. and Lakis, H. (2021): Variational approach of homogenization of piezoelectric composites towards piezoelectric and flexoelectric effective media. *International Journal of Engineering Science* **158**(3), 103410.

[132] Midya, G.K. (2004): On Love-type surface waves in homogeneous micropolar elastic media. *International Journal of Engineering and Science* **42**(11–12), 1275–1288.

[133] Mindlin, R.D. and Tiersten, H.F. (1962): Effects of couple-stresses in linear elasticity. *Archive for Rational Mechanics and Analysis* **11**, 415–448.

[134] Mindlin, R.D. (1963): Influence of couple-stresses on stress concentrations. *Experimental Mechanics* **3**(1), 1–7.

[135] Mondal, S., Sahu, S.A. and Pankaj, K.K. (2019): Transference of Love-type waves in a bedded structure containing a functionally graded material and a porous piezoelectric medium. *Applied Mathematics and Mechanics* **40**(8), 1083–1096.

[136] Mseddi, S., Tekeli, F., Njeh, A.,Donner, W. and Ghozlen, M.H.B. (2016): Effect of initial stress on the propagation behavior of SAW in a layered piezoelectric structure of ZnO/Al_2O_3. *Mechanics Resaerch Communications* **76**, 24–31.

[137] Nath, S., Sengupta, P.R. and Debnath, L. (1998): Magneto-thermoelastic surface waves in micropolar elastic media. *Computers & Mathematics with Applications* **35**(3), 47–55.

[138] Nie, G., Liu, J., Fang, X. and An, Z. (2012): Shear horizontal waves propagating in piezoelectric-piezomagnetic bilayer system with an imperfect interface. *Acta Mechanica* **223**, 1999–2009.

[139] Nie, G., Liu, J. and Liu, X. (2017): Propagation behavior of two transverese surface waves in a three-layer piezoelectric/piezomagnetic structure. *Waves in Random and Complex Media* **27**(2): 1–27.

[140] Nowacki, W. and Nowacki, W.K. (1969a) Generation of waves in an infinite micropolar elastic solid body. I. *Bulletin de L' Académie Polonaise des Sciences, Série des Sciences Techniques* **17**(2), 75–82.

[141] Nowacki, W. and Nowacki, W.K. (1969b): Generation of waves in an infinite micropolar elastic solid body . II. *Bulletin de L' Académie Polonaise des Sciences, Série des Sciences Techniques* **17**(2), 83–90.

[142] Nowacki, W. (1974): Micropolar Elasticity, International Center for Mechanical Sciences, Courses and Lectures No. 151, Udine, Springer-Verlag, Wien-New York.

[143] Nowacki, J.P. (2006): Static and dynamic coupled fields in bodies with piezoeffects or polarization gradient, Lecture notes in applied and computational mechanics, **26**, Springer, New York.

[144] Nowinski, J.L. (1993): On the surface waves in an elastic micropolar and microstretch medium with nonlocal cohesion. *Acta Mechanica* **96**(1), 97–108.

[145] Pabst, W. (2005): Micropolar materials, *Ceramics-Silikáty* **49**(3), 170–180.

[146] Palmov, V.A. (1964): Basic equations of the theory of asymmetric elasticity. *Prikladnaya Matematika i Mekhanika* **28**, 401–408.

[147] Pang, Y., Liu, J.X., Wang, Y.S. and Zhao, X.F. (2008): Propagation of Rayleigh type surface waves in a transversely isotropic piezoelectric layer on a piezomagnetic half-space. *Journal of Applied Physics* **103**(7), 074901.

[148] Pang, Y. and Liu, J.X. (2011): Reflection and transmission of plane waves at an imperfectly bonded interface between piezoelectric and piezomagnetic media. *European Journal of Mechanics-A/Solids* **30**(5), 731–740.

[149] Pang, Y., Liu, Y.S., Liu, J.X. and Feng, W.J. (2016): Propagation of SH waves in an infinite/semi-infinite piezoelectric/piezomagnetic periodically layered structure. *Ultrasonics* **67**, 120–128.

[150] Pang, Y., Feng, W., Liu, J. and Zhang, C. (2019): SH wave propagation in a piezoelectric/piezomagnetic plate with an imperfect magnetoelectroelastic interface. *Waves in Random and Complex Media* **29**, 580–594.

[151] Parfitt, V.R. and Eringen, A.C. (1969): Reflection of Plane Waves from the Flat Boundary of a Micropolar Elastic Half-Space. *Journal of the Acoustical Society of America* **45**(5), 1258–1272.

[152] Pommellec, J.Y.L. and Baroudi, A.E. (2021): Correlation between the toroidal modes of an elastic sphere and the viscosity of liquids. *Comptes Rendus Mécanique* **349**(1), 179–188.

[153] Qian, Z., Jin, F., Wang, Z. and Kishimoto, K. (2004): Dispersion relations for SH-wave propagation in periodic piezoelectric composite layered structures. *International Journal of Engineering Science*, **42**(7), 673–689.

[154] Qian, Z., Jin, F., Wang, Z., Kishimoto, K. and Lu, T. (2009): Propagation behavior of Love waves in a functionally graded half-space with initial stress. *International Journal of Solids and Structures* **46**(6), 1354–1361.

[155] Qian, Z., Jin, F., Li, P. and Hirose, S. (2010): Bleustein-Gulyaev waves in 6mm piezoelectric materials loaded with a viscous liquid layer of finite thickness. *International Journal of Solids and Structures* **47**(25-26), 3513–3518.

[156] Qianying, L., Zhenghou, Z., Jie, C., Dengyu, L. and Hui, Z. (2018): A new piezomagnetic film force sensor model for static and dynamic stress measurements. *Journal of Magnetism and Magnetic Materials* **466**, 106-111.

[157] Rabin, B.H. and Shiota, I. (1995): Functionally gradient materials. *MRS Bulletin* **20**(1), 14–18.

[158] Rao, S.S. and Sunar, M. (1994): Piezoelectricity and Its Use in Disturbance Sensing and Control of Flexible Structures: A Survey *Applied Mechanics Reviews* **47**(4), 113–123.

[159] Ray, A., Singh, A.K. and Kumari, R. (2019): Green's function technique to model Love- type wave propagation due to an impulsive point source in a piezomagnetic layered structure. *Mechanics of Advanced Materials and Structures*, **28**(3), 1–12.

[160] Ray, A. and Singh, A.K. (2021): Impact of imperfect corrugated interface in piezoelectric-piezomagnetic composites on reflection and refraction of plane waves. *The Journal of the Acoustical Society of America* **150**(1), 573–591. DOI:10.1121/10.0005544

[161] Rayleigh, J.W.S. (1887): On waves propagating along the plane surface of an elastic solid. *Proceedings of Mathematical Society of London* **17**, 4–11.

[162] Reddy, S.R. and Ramabrahmam, B. (2010): Propagation of Love waves in nonlocal elastic medium with material boundary. *International Journal of Mechanics and Solids* **5**(1), 49–53.

[163] Ristic, V.M. (1983a): Principles of Acoustic Devices. Wiley, New York, 198.

[164] Ristic, V.M. (1983b): Principles of Acoustic Devices. Wiley, New York, 47.

[165] Rymarz, C. (1988): Surface waves in a nonlocal elastic medium D.F. Parker, et al. (Eds.), Recent Developments in Surface Acoustic Waves, Series on Wave Phenomena, Springer-Verlag, **7**, 342-350.

[166] Sadd, M.H. (2004): Elasticity: Theory, Applications, and Numerics, Elsevier Butterworth–Heinemann, U.K.

[167] Sahu, S.A., Singhal, A. and Chaudhary, S. (2017): Surface wave propagation in functionally graded piezoelectric material: An analytical solution. *Journal of Intelligent Material Systems and Structures* **29**(3). DOI:10.1177/1045389X17708047

[168] Sahu, S.A., Mondal, S. and Dewangan, N. (2017): Polarized shear waves in functionally graded piezoelectric material layer sandwiched between corrugated piezomagnetic layer and elastic substrate. *Journal of sandwich structures and materials* **21**(8), 2921–2948.

[169] Sahu, S.A. and Baroi, J. (2018): Analysis of surface wave behavior in corrugated piezomagnetic layer resting on inhomogeneous half-space. *Mechanics of Advanced Materials and Structures* **26**(2), 1–12.

[170] Sahu, S.A. and Nirwal, S. (2021): An asymptotic approximation of Love wave frequency in a piezo-composite structure: WKB approach. *Waves in Random and Complex Media* **31**, 117-145.

[171] Saroj, P.K., Sahu, S.A., Chaudhary, S. and Chattopadhyay, A. (2015): Love-type waves in functionally graded piezoelectric material (FGPM) sandwiched between initially stressed layer and elastic substrate. *Waves in Random and Complex Media* **25**(4), 608–627.

[172] Sarkar, N. and Tomar, S.K. (2019): Plane waves in nonlocal thermoelastic solid with voids. *Journal of Thermal Stresses* **42**(5), 1–27.

[173] Scala, I., Rosi, G., Placidi, L. et al. (2019): Effects of the microstructure and density profiles on wave propagation across an interface with material properties. *Continuum Mechanics and Thermodynamics* **31**(9), 1165–1180.

[174] Sellitto, A. and Di Domenico, M. (2019): Nonlocal and nonlinear contributions to the thermal and elastic high-frequency wave propagations at nanoscale. *Continuum Mechanics and Thermodynamics* **31**(2), 807–821.

[175] Selvadurai, A.P.S, Singh, B.M. and Vrbik, J.A. (1986): A Reissner-Sagoci problem for a non-homogeneous elastic solid. *Journal of Elasticity* **16**(4), 383–391.

[176] Selvadurai, A.P.S and Katebi, A. (2013): Mindlin's problem for an incompressible elastic half-space with an exponential variation in the linear elastic shear modulus. *International Journal of Engineering Science* **65**, 9–21.

[177] Shanmugavel, P., Bhaskar, G.B., Chandrasekaran, M., Mani, P.S. and Srinivasan, S.P. (2012): An overview of fracture analysis in functionally graded materials. *European Journal of Scientific Research* **68**(3), 412–439.

[178] Sharifi, Z., Khordad, R., Gharaati, A. and Forozani, G. (2019): An analytical study of vibration in functionally graded piezoelectric nanoplates: nonlocal strain gradient theory. *Applied Mathematics and Mechanics* **40**(12), 1723–1740.

[179] Sharma, J.N., Kumar, S. and Sharma, Y.D. (2008): Propagation of Rayleigh Surface Waves in Microstretch Thermoelastic Continua Under Inviscid Fluid Loadings. *Journal of Thermal Stresses* **31**(1), 18–39.

[180] Sharma, J.N. and Kumar, S. (2009): Lamb waves in micropolar thermoelastic solid plates immersed in liquid with varying temperature. *Meccanica* **44**(3), 305–319.

[181] Sharma, V. and Kumar, S. (2014): Velocity dispersion in an elastic plate with microstructure: Effects of characteristic length in a couple stress model. *Meccanica* **5**(5), 1083–1090.

[182] Sharma, V. and Kumar, S. (2015): Effects of liquid loadings on Lamb waves in context of size dependent couple stress theory. *Journal of Theoretical and Applied Mechanics* **53**(4), 925–934

[183] Sharma, V. and Kumar, S. (2017): Effects of microstructure and liquid loading on velocity dispersion of leaky Rayleigh waves at liquid-solid interface. *Canadian Journal of Physics* **96**(1), 11–17.

[184] Sharma, V. and Kumar, S. (2018): Dispersion of Rayleigh waves in a microstructural couple stress substrate loaded with liquid layer under the effects of gravity. *Archives of Acoustics* **43**(1), 11–20

[185] Sharma, V. and Kumar, S. (2017): Dispersion of SH waves in a viscoelastic layer imperfectly bonded with a couple stress substrate. *Journal of Theoretical and Applied Mechanics* **55**(2), 535–546.

[186] Sharma, V. and Sharma, S. (2020): Love waves in fiber-reinforced layer imperfectly bonded to microstructural couple stress substrate. *Journal of Theoretical and Applied Mechanics* **58**(1), 221–232.

[187] Sharma, V., Goyal, R. and Kumar, S. (2020): Love waves in a layer with void pores over a microstructural couple stress substrate with corrugated boundary surfaces. *Journal of the Brazilian Society of Mechanical Sciences and Engineering* **42**, 194.

[188] Shi, Y., Li, N., Ye, J. and Ma, J. (2021): Enhanced magnetoelectric response in nanostructures due to flexoelectric and flexomagnetic effects. *Journal of Magnetism and Magnetic Materials* **521**, 167523.

[189] Singh, A.K., Das, A., Mistri, K.C. and Chattopadhyay, A. (2017): Green's function approach to study the propagation of SH-wave in piezoelectric layer influenced by a point source. *Mathematical Methods in the Applied Sciences* **40**(13), 4771–4784.

[190] Singh, A.K., Chaki, M.S. and Chattopadhyay, A. (2018): Remarks on impact of irregularity on SH-type wave propagation in micropolar elastic composite structure. *International Journal of Mechanical Sciences* **135**, 325–341.

[191] Singh, A.K., Kumari, R., Ray, A. and Chattopadhyay, A. (2019): Love-type waves in a piezoelectric-viscoelastic bimaterial composite structure due to an impulsive point source. *International Journal of Mechanical Sciences* **152**, 613–629.

[192] Singh, B. and Tomar, S.K. (2008): Longitudinal waves at a micropolar fluid/solid interface. *International Journal of Solids and Structures* **445**, 225–244.

[193] Singh, B. and Sindhu, R. (2020): Rayleigh wave on transversely isotropic micropolar elastic solid half-space. *International Journal of Basic and Applied Scientific Aspects* **2**(2), 36–42.

[194] Singh, B. (2017): Rayleigh Wave in a Micropolar Elastic Medium with Impedance Boundary Conditions. *Geosciences Research* **2**(1), 6–13.

[195] Singh, D., Kaur, G. and Tomar, S.K. (2017): Waves in nonlocal elastic solid with voids. *Journal of Elasticity* **128**, 85–114.

[196] Singh, B., Sangwan, A. and Singh, J. (2019): Reflection and transmission of elastic waves at an interface between two micropolar piezoelectric half-spaces. *Journal of Ocean Engineering and Science* **4**(3), 227–237.

[197] Singh, B. (2020): Rayleigh-type surface waves in a nonlocal thermoelastic solid half space with voids. *Waves in Random and Complex Media.* DOI: 10.1080/17455030.2020.1721612.

[198] Singh, B. and Kaur, B. (2021): Rayleigh surface wave at an impedance boundary of an incompressible micropolar solid half-space. *Mechanics of Advanced Materials and Structures*. DOI: 10.1080/15376494.2021.1914795

[199] Singh, G. and Natesan, S. (2020): A uniformly convergent numerical scheme for a coupled system of singularly perturbed reaction-diffusion equations. *Numerical Functional Analysis and Optimization* **41**(10), 1–18.

[200] Singhal, A., Sahu, S.A. and Chaudhary, S. (2018): Approximation of surface wave frequency in piezo-composite structure. *Composites Part B: Engineering* **144**, 19–28.

[201] Singhal, A., Sedighi, H.M., Ebrahimi, F. and Kuznetsova, I. (2019): Comparative study of the flexoelectricity effect with a highly/weakly interface in distinct piezoelectric materials (PZT-2, PZT-4, PZT-5H, LiNbO3, BaTiO3). *Waves in Random and Complex Media* DOI: 10.1080/17455030.2019.1699676

[202] Sladeka, J., Sladeka, V., Kasalab, J. and Panc, E. (2017): Nonlocal and gradient theories of piezoelectric nanoplates. *Procedia Engineering* **190**, 178–185.

[203] Sokolnikoff, I.S. (1956): Mathematical theory of elasticity, McGraw-Hill, New York.

[204] Son, M.S. and Kang, Y.J. (2011): The effect of initial stress on the propagation behavior of SH waves in piezoelectric coupled plates. *Ultrasonics* **51**(4), 489–495.

[205] Timoshenko, S. and Goodier, J.N. (1934): Theory of Elasticity, McGraw-Hill, New York.

[206] Tokovyy, Y. and Ma, C.C. (2015): An analytical solution to the three-dimensional problem on elastic equilibrium of an exponentially-inhomogeneous layer. *Journal of Mechanics* **31**, 545–555.

[207] Tomar, S.K. and Gogna, M.L. (1992): Reflection and refraction of a longitudinal micro-rotational wave at an interface between two micropolar elastic solids in welded contact. *International Journal of Engineering Science* **30**(11), 1637–1646.

[208] Tomar, S.K. and Gogna, M.L. (1995a): Reflection and refraction of coupled transverse and micro-rotational waves at an interface between two different micropolar elastic media in welded contact. *International Journal of Engineering Science* **33**(4), 485–496.

[209] Tomar, S.K. and Gogna, M.L. (1995b): Reflection and refraction of longitudinal waves at an interface between two micropolar elastic media in welded contact. *The Journal of the Acoustical Society of America* **97**(2), 822—830.

[210] Tomar, S.K. and Kumar, R. (1995c): Reflection and refraction of longitudinal displacement wave at a liquid-micropolar solid interface. *International Journal of Engineering Science* **33**(10), 1507–1515.

[211] Tomar, S.K. and Kumar, R. (1999): Wave propagation at liquid-micropolar elastic solid interface. *Journal of Sound and Vibration* **222**(5), 858–869.

[212] Tomar, S.K. and Singh, H. (2003): Radial vibrations due to a spherical cavity contained in an unbounded micropolar elastic solid. *Indian Journal of Pure and Applied Mathematics* **34**(12), 1785–1796.

[213] Tomar, S.K. (2005): Wave propagation in a micropolar elastic plate with voids. *Journal of Vibration and Control* **11**(6), 849–863.

[214] Tomar, S.K. (2007): Wave propagation in a micropolar elastic layer sandwiched between liquid half-space and micropolar solid half-space. *International Journal of Applied Mechanics and Engineering* **12**(1), 255–262.

[215] Toupin, R.A. (1962): Elastic materials with couple stresses. *Archive for Rational Mechanics and Analysis* **11**(1), 385–414.

[216] Toupin, R.A. (1964): Theories of elasticity with couple stress. *Archive for Rational Mechanics and Analysis* **17**(2), 85–112.

[217] Uchino, K. (1998): Materials issues in design and performance of piezoelectric actuators: An overview. *Acta Materialia* **46**(11), 3745–3753.

[218] Vardoulakis, I. and Georgiadis, H.G., (1997): SH surface waves in a homogeneous gradient-elastic half-space with surface energy. *Journal of Elasticity* **47**(2), 147-165.

[219] Vasudeva, R.Y. and Bhaskara, R.K. (1978): On wave propagation in a micropolar elastic cylinder. *International Journal of Engineering Science* **16**, 299–302.

[220] Vellekoop, M.J. (1998): Acoustic wave sensors and their technology. *Ultrasonics* **36**, 7–14.

[221] Vikstrom, A. and Voinova, M.V. (2016): Soft film dynamics of SH-SAW sensors in viscous and viscoelastic fluids. *Sensing and Bio-sensing Research* **11**, 78–85.

[222] Voigt, W. (1887): Theoretische studien uberdie elasticitats verhaltnisse der kristalle, *Abhandlungen der Gesellschaft der Wissenschaften zu Göttingen* **34**, 3–51.

[223] Wang, S.S. (1983): Fracture mechanics for delamination problems in composite materials. *Journal of Composite Materials* **17**(3), 210–223.

[224] Wang, Q., Jin, J. and Quek, S.T. (2002): Propagation of a shear direction acoustic wave in piezoelectric coupled cylinders. *Journal of Applied Mechanics* **69**(3), 391–394.

[225] Wang, W., Oh, H., Lee, K., Yang, S. (2008): Enhanced sensitivity of wireless chemical sensor based on Love wave mode. *Japanese Journal of Applied Physics* **47**(9), 7372–7379.

[226] Wei, W., Liu, J. and Fang, D. (2009): Shear horizontal surface waves in a piezoelectric-piezomagnetic coupled layered half-space. *International Journal of Nonlinear Sciences and Numerical Simulation* **10**(6),767–778.

[227] White, R.M. and Voltmer, F.W. (1965): Direct piezoelectric coupling to surface elastic waves. *Applied Physics Letters* **7**(12), 314–316.

[228] Xu, Z. and Yuan, J.Y. (2018): Implementation of guiding layers of surface acoustic wave devices: A Review. *Biosensors and Bioelectronics* **99**, 500–512.

[229] Yan, D.J., Chen, A.L., Wang, Y.S., Zhang, C. and Golub, M. (2018): In-plane elastic wave propagation in nanoscale periodic layered piezoelectric structures. *International Journal of Mechanical Sciences* **142–143**, 276–288.

[230] Yang, J.F.C. and Lakes, R.S. (1982): Experimental study of micropolar and couple stress elasticity in compact bone in bending. *Journal of Biomechanics* **15**(2), 91–98.

[231] Yang, F., Chong, A.C.M., Lam, D.C.C. and Tong, P. (2002): Couple stress based strain gradient theory for elasticity. *International Journal of Solids and Structures* **39**(10), 2731–2743.

[232] Yang, J. (2005): An introduction to theory of piezoelectricity, Springer, Boston, MA. DOI:10.1007/b101799

[233] Yang, J.S. (2000): Bleustein-Gulyaev waves in piezoelectromagnetic materials. *International Journal of Applied Electromagnetics and Mechanics* **12**(3), 235–240.

[234] Yang, J.S. (2001): Bleustein-Gulyaev waves in strained piezoelectric ceramics. *Mechanics Research Communications* **28**(6), 679–683.

[235] Yang, J.S. and Wang, J. (2008): Dynamic anti-plane problems of piezoceramics and applications in ultrasonics-a review. *Acta Mechanica Solida Sinica* **21**(3), 207–227.

[236] Yuan, X. and Zhu, Z.H. (2012): Reflection and refraction of plane waves at interface between two piezoelectric media. *Acta Mechanica* **223**(12), 2509–2521.

[237] Zaitsev, B.D., Kuznetsova, I.E., Joshi, S.G. and Borodina, I.A. (2001): Acoustic waves in piezoelectric plates bordered with viscous and conductive liquid. *Ultrasonics* **39**(1), 45–50.

[238] Zelentsov, V.B., Lapina, P.A., Mitrin, B.I. and Eremeyev, V.A. (2020): Characterization of the functionally graded shear modulus of a half-space. *Mathematics.* **8**(4), 640–658.

[239] Zhang, C., Caron, J.J. and Vetelino, J.F. (2001): The Bleustein-Gulyaev wave for liquid sensing applications. *Sensor and Actuators B Chemical* **76**(1–3), 64–68.

[240] Zhang, P., Wei, P. and Tang, Q. (2015): Reflection of micropolar elastic waves at the non-free surface of a micropolar elastic half-space. *Acta Mechanica* **226**, 2925–2937.

[241] Zhang, P., Wei, P. and Li, Y. (2016): Wave propagation through a micropolar slab sandwiched by two elastic half-spaces. *Journal of Vibration and Acoustics* **138**(4), 041008.

[242] Zhang, P., Wei, P. and Li, Y. (2017): Reflection of longitudinal displacement wave at the visco-elastically supported boundary of micropolar halfspace. *Meccanica* **52**, 1641–1654.

[243] Zhang, Q., Zhu, Z., Chen, J. and Zhao, H. (2020): A piezomagnetic composite material force-sensitive film with high force-sensitive properties. *Journal of Magnetism and Magnetic Materials* **512**(2), 166901.